POLITECNICO DI TORINO

DIMEAS – Dipartimento di Ingegneria Meccanica ed Aerospaziale

Thesis submitted for the
Master of Science in Aerospace Engineering

Interplanetary space geodesy study of the MMX project

Master Thesis

Supervisor:
Manuela BATTIPEDE
Politecnico di Torino

Co-supervisor:
Julien LAURENT-VARIN
CNES

Candidate:
Rebecca MARTINELLI

Academic Year 2019/2020

Per quel saluto, che non ci è stato concesso

Acknowledgements

I would like to express my special thanks of gratitude to my CNES tutors, Julien Laurent-Varin and Jean-Charles Marty, who supervised me all along my internship period, being always disposed to give me explications and making this experience turn into something exceptional. I would also like to thank the entire CNES GS team and groups working on the MMX project, they never hesitated to give me important advice and made me feel a real team member.

A very important thanks goes to my Master Thesis supervisor, Professoressa Manuela Battipede, not only for her support in this special occasion, but also for having given me a real passion for orbital mechanics: her course at Politecnico helped me understand what I would have like to do in my future.

Special thanks also go to my internship colleague, Anthony Clausse, for our tight-knit cooperation.

Un ringraziamento di vero cuore è rivolto a tutti i miei amici di Tolosa: Federico, Alessandro, Caterina, Filippo, Federico, Vincenzo, Giovanni, Enrico, Michael, Naomi, Nicolò, Federico, Andrea, Riccardo, Alessandro e Matteo. Avete reso speciali questi ultimi miei due anni, insieme abbiamo condiviso momenti unici e io porterò sia loro che voi, con me per tutta la vita. Un ringraziamento speciale va a Mylo e Sara, amiche eccezionali, nonché le coinquiline migliori che io potessi mai desiderare.
Un grazie particolare lo rivolgo anche a Tommaso, perché in fondo Tolosa non sarebbe stata la stessa senza te.
E per Chiara, senza la quale non sono mai stata per più di mezza giornata da due anni a questa parte, un grazie infinito. Si dice che in queste esperienze si possano conoscere persone speciali, con le quali poi si rimarrà legati per sempre. A me è successo: io ho conosciuto lei.

Un immenso ringraziamento è indirizzato anche ai miei amici del Politecnico: Sofia, Elena, Erika, Franceso, Marco, Ludovico, Nicolò, Tommaso, Edoardo, Federico, Salvatore, Andrea, Luca, Elia, Francesco, Marco e Davide. Insieme abbiamo passato momenti spettacolari, sia tra i banchi delle aule, sia fuori: io avrò per sempre un bellissimo ricordo dei miei anni da universitaria, ed è grazie a voi.

E ancora, grazie a voi, Irene e Deborah, che definirvi “amiche” mi suona quasi strano: siete molto di più, lo siete sempre stato ed in questi anni di distanza me lo state ulteriormente dimostrando. Non vi ringrazierò mai abbastanza.

Mille volte grazie a te, la mia Elisabetta, che sempre ci sei stata per me e so che sempre continuerai ad esserci. Nonostante i chilometri di lontananza, ti ho sempre avuta vicina, ed il fatto che questo mai cambierà è una vera certezza e gioia per me.

Per concludere, un grazie incommensurabile è per tutta la mia famiglia.
Grazie ai miei nonni, i miei zii e mio cugino, che mi seguono costantemente, passo a passo, e che sempre sono al settimo cielo per ogni mio traguardo raggiunto, piccolo o grande che sia. L’affetto che mi dimostrate non ha eguali.
Grazie ai miei genitori. Non basterebbero tutte le pagine scritte in questa Tesi per ringraziarli a sufficienza. La loro presenza ed il loro affetto sono i capi saldi della mia vita. Grazie a mia mamma, che sempre c’è per me e grazie a mio papà che sempre è dalla mia parte (e le cui frasi speciali mi hanno aiutata ad arrivare fino a questo punto della mia carriera universitaria). Vi sento spesso dire che io sono il vostro orgoglio, cosa che mi riempie il cuore di gioia. Ma la verità è che voi siete il mio: senza voi nulla di tutto ciò che ho compiuto finora sarebbe mai stato possibile. Grazie.

Abstract

Phobos and Deimos, the mythological twin sons of the Greek god of war, Ares, gave their names to the two Martian natural satellites. Discovered by the American astronomer Asaph Hall in 1877, within six days of each other, they are respectively orbiting about 6000km and 20070km around the red planet's surface ground.
However, still today their origin appears to be uncertain. Multiple theories have been developing during all these years, but no one has never been proved. Thus, the main issue remains: where do Phobos and Deimos really come from?

Perhaps, this question left unanswered for many years, could finally find a response: Japanese MMX (Martian Moons eXploration) mission planned by the JAXA for 2024 represents the world's first practical attempts to solve this mystery.
In fact, the Martian moon exploration had represented the main objective for no mission yet: only flybys and long-range observations have been realised up to now. On the contrary, MMX focuses its entire attention on this topic, planning flybys or rendezvous with Deimos, and orbits around Phobos leading the satellite to lend on its surface and collect samples, for the first time in the world. The mission outcome could inevitably provide useful information, getting closer to the truth about the Martian moon origin.
Nevertheless, Phobos ground samples could not afford complete answers. To unveil this mystery, wider understandings in its physical features are necessary: the gravitational field, the ephemeris around Mars and the rotation around its axis are Phobos geodesic parameters whose knowledge is sensed to be improved during the MMX mission.

Considering this purpose of detecting real Martian moon physics, this internship project is centred on Phobos gravity field analysis. Several existing models of this geodesic characteristic have been developed on the base of the latest Phobos shape model and assuming homogeneous density distribution. Three main modelling methods are being using [1]: the harmonic expansion approach (HEA), the mass elements approach (MEA), and the polyhedron approximation approach (PAA).
The study here presented, is built on the first methodology: the considered Phobos gravity model is conceived as a spherical harmonic expansion.
The latter can now relay on one of the most accurate shape models of Phobos to date, complete up to degree and order 20. Consequently, a set of spherical harmonic coefficients up to degree and order 20 describe one of the most realistic Phobos gravity models own at the present day.
However, its precision is still far from the necessary level for conducting exact analysis. Effectively, one scientific purpose of the MMX mission is exactly to increase this model accuracy. Throughout orbits in proximity of Phobos surface and employment of multiple measurement techniques, the satellite would be able to adjust this current model.

In this context, this internship project has been ideated to provide an estimation of the MMX capacity in recovering Phobos gravity field model, through the most realistic simulations possible.
Conducted with the up to 20 degree-gravitational model as a realistic reference and hypotheses on actual unknowledge of real Phobos gravity field, this study has enabled an approximation of the model upgrade obtainable at the end of the MMX mission. This is an absolutely useful result: it elucidates which are the effective MMX possibilities in recovering the Martian moon gravity field and allows the identification of which are the mission conditions in term of trajectories and measurements, allowing the best model adjustment.

Abstract (Italian version)

Phobos and Deimos, i due gemelli della Mitologia greca, figli del dio della guerra, Ares, danno il loro nome ai due satelliti naturali di Marte. Scoperti dall'astronomo americano Asaph Hall nel 1877, essi orbitano ad una distanza rispettivamente di circa 6000km e 20070km attorno alla superficie del pianeta rosso. Tuttavia, ancora al giorno d'oggi la loro origine appare incerta. Molteplici teorie sono state formulate durante il corso di questi anni, ma nessuna tra queste è mai stata provata. Dunque, la domanda tutt'ora rimane: come Phobos e Deimos si sono creati?

Tale questione rimasta a lungo irrisolta, potrebbe forse trovare ora una risposta: la missione giapponese MMX (Martian Moons eXploration), previsa dalla JAXA per il 2024, rappresenta il primo tentativo pratico al mondo di risolvere questo mistero. Infatti, la vera esplorazione delle lune di Marte non era ancora stata l'obiettivo principale di alcuna missione spaziale: solamente flyby ed osservazioni a lunga distanza sono state realizzate fino ad ora. Al contrario, la missione MMX concentra la sua attenzione sullo studio dettagliato di questi satelliti naturali, includendo flyby o rendez-vous con Deimos, orbite nelle strette vicinanze di Phobos e l'atterraggio sulla superficie di quest'ultimo, con il consecutivo prelevamento di campioni di terreno. Il successo di tale missione potrebbe fornire informazioni utili per avvicinarsi alla scoperta della verità sull'origine delle due lune marziane.
Ciononostante, per svelare il mistero una più ampia conoscenza dei parametri geodetici è anche necessaria. Per tale motivo, il campo gravitazionale, le effemeridi attorno a Marte e la rotazione attorno al suo asse sono caratteristiche fisiche di Phobos la cui conoscenza verrà ampliata nel coro della missione MMX.

Considerando questi obiettivi scientifici, il progetto svolto durante questo tirocinio è prettamente centrato sull'analisi del campo gravitazionale di Phobos. Diversi modelli già esistenti di tale caratteristica geodetica, sono stati matematicamente creati sulla base dell'ultima modellizzazione sviluppata per la forma di Phobos, considerando la presenza di una distribuzione omogenea di densità. Tre sono i più comuni modelli utilizzati al giorno d'oggi [1], sviluppati attraverso: il metodo dell'espansione armonica (HEA), il metodo degli elementi di massa (MEA) ed il metodo dell'approssimazione poliedrica (PAA).
Lo studio qui presentato è realizzato sulla base del primo metodo: il modello di campo gravitazionale considerato è concepito come un'espansione di armoniche sferiche.
Questa tecnica trova le sue fondamenta su uno dei più accurati modelli di forma di Phobos, anch'esso sviluppato attraverso l'uso delle armoniche sferiche, complete fino al grado e all'ordine 20. Di conseguenza, un insieme di coefficienti armonici dettagliati fino all'ordine 20 descrive uno dei più realistici modelli gravitazionali di Phobos, conosciuti attualmente. Tuttavia, la precisione di quest'ultimo lunge ancora dal livello necessario per condurre studi esatti. Per tale ragione, uno degli obiettivi scientifici della missione MMX è esattamente quello di migliorare l'accuratezza di tale modello: attraverso l'utilizzo di particolari orbite in prossimità di Phobos e specifiche tecniche di misura, il satellite dovrà essere in grado di correggere il modello gravitazionale attuale.

In questo contesto, tale progetto di tirocinio nasce con l'idea di realizzare simulazioni le più realistiche possibili, con l'obiettivo di fornire una stima dell'effettiva capacità della missione MMX di migliorare la conoscenza del reale campo gravitazionale di Phobos. Considerando il modello ad espansione di armoniche sferiche completo fino al grado 20 come referenza realistica e molteplici ipotesi sulla sua inaccuratezza, tale studio ha condotto ad un'approssimazione del possibile perfezionamento del modello gravitazionale attuale raggiungibile al termine della missione MMX. Questo risultato è utile non solo perché mostra le effettive potenzialità della missione, ma anche mette in evidenza quali sono le condizioni in termini di orbite e tecniche di misura, che possono condurre alla migliore ricostruzione possibile del vero campo gravitazionale di Phobos.

Table of Contents

List of Figures

List of Tables

Acronyms

MMX	Martian Moons eXploration
GRGS	Groupe de Recherche de Géodésie Spatiale (Space Geodesic Resarch Group)
QSO	Quasi-Satellite Orbit
GINS	Géodésie par Intégrations Numériques Simultanées (Geodesy with Simultaneus Numeric Integrations)
EPIC	Etablissement Public à Caractère Industriel Commercial (Public Establishment for Industrial Commericial Activities)
OMP	Observatoire Midi-Pyrénées (Midi-Pyrénées Observatory)
FD	Flight Dynamics
GS	Géodésie Spatiale (Space Geodesy)
MOI	Mars Orbit Insertion
MOE	Mars Orbit Escape
CR3BP	Circular Restricted Three-Body Problem
ER3BP	Elliptical Restricted Three-Body Problem
BCBF	Body Centred Body Fixed
SH	Spherical Harmonic
HEA	Harmonic Expansion Approach
MEA	Mass Element Approach
PAA	Polyhedron Approximation Approach
IS	International System
DSN	Deep Space Network
LIDAR	Light (or Laser Imaging) Detection And Ranging

1 Introduction

Interplanetary space geodesy study of the MMX project. This is the title of the internship, upon which this report is written. This headline encloses the main global topic of the entire project: the analysis of geodesic parameters within the context of the MMX mission.
This mission is envisaged by the Japanese space agency, the JAXA, but the collaboration with the French government space agency CNES has been demanded for specific operational sectors, as for orbital design and mission analysis.
One of the main mission scientific purpose is the most accurate evaluation possible of the geodesic features characterising the Martian moons. Particularly, concerning the primary MMX target, Phobos, the Japanese project plans to measure its gravitational field, its ephemeris in relation to Mars and its rotation parameter.

In this context, the internship has been realised in the CNES Space Geodesy DSO/DV/GS service, which takes part in the Groupe de Recherche de Géodésie Spatiale (GRGS, Space Geodesic Resarch Group).
The entire project is focused on MMX phases dedicated to Phobos exploration. This principal concern imposes the necessity of going through the analysis of the specific trajectories which will be covered by the MMX satellite near the target body: the QSOs (Quasi-Satellite Orbits).
Moreover, along its QSOs, the satellite will be sensed to use several measure techniques to get a complete Phobos observation. As regards geodesic parameter detection, DSN, LIDAR and Optical measurements will be adopted. This feature determines the main internship project procedure: the simulation and reinterpretation of these three MMX measures, for the purpose of evaluating the mission success in adjusting the actual Phobos gravity model.
The entire project analysis has been conducted through the employment of the accurate CNES software called GINS (Géodésie par Intégrations Numériques Simultanées), able to compute trajectories and return planetary physic parameters, with an extreme precision level.

Since the multiple aspects to be considered for a proper study development, an introduction about the global internship context and its detailed physic background is necessary.

1.1 CNES: a main component in Geodesic Science

Founded in 1961 the Centre National d’Etudes Spatiales (CNES, National Centre for Space Studies) is the French government spacy agency, responsible for shaping and implementing France’s space policy in all Europe.

CNES owns the “EPIC” (Etablissement Public à Caractère Industriel Commercial) title, meaning that it is a public state-owned company of commercial and industrial nature. It is now counting a more-than 2400-workforce, the biggest space budget in Europe and multiple collaborations with Arianespace and European Space Agency (ESA) on five main focusing sectors:

1. Science and Innovation
2. Space and Earth Observation
3. Telecommunications
4. Launchers
5. Defence and Security

CNES activities are distributed on four establishment centres:

1. The **Toulouse Space Centre**: it is the main CNES site, counting 1700 employees, most of whom are engineers and managers. It is responsible for project management, research and technology studies, operations for satellite station acquisition and orbital control, computer and mathematics technology, support activities such as administration, logistics and communication.
2. The **Launching site in the Guyana Space Centre**: settled in 1964, 250 employees work in this launch site for all the ESA launchers, Ariane, Soyouz and Vega. It is set in Kourou, an ideal geographical position, near the equator, which enables launches towards the East and the North in maximal security conditions.
3. The **Launcher Direction Centre**: created in 1974 in the town of Evry, this site counts 285 employees ensuring Arian launcher developments, Arianespace production phases and realisation of first Vega launcher stages and launch pads for Soyouz launchers;
4. The **Launcher Directorate**: settled in in Paris, 185 employees work there for Space policy direction and administration.

This internship project has been completely realised in the first listed CNES site, the Toulouse Space Centre. The latter represents the central point of a vast scientific and university space complex, including aerospace engineering schools (ISAE-Supaero, ENAC, INSA, etc.), laboratories (OMP, OERA, CESR, etc.) and companies (Airbus Defence and Space, Thales Alenia Space, Interspace, etc.).
In this technical and operational scientific centre led by CNES, this traineeship took specifically place in the Midi-Pyrénées Observatory (OMP) establishment, within the Space Geodesy service of the Toulouse Space Centre.
On one side, this service is one of CNES Science Laboratories, taking part in the GRGS, since 1971. This Space Geodesic Resarch Group is a consortium of French research institutes, which collaborate for the purpose of contributing to Space Geodesy analysis, Orbital Mechanics studies, Earth’s gravity field calculation, accurate Positioning and Reference Systems, etc.
On the other side, the OMP is a Universe Science Observatory, constituted of Space Science, Earth and Environment Laboratories, focused on research, observation, education and common international scientific cooperation.
The OMP counts 360 researchers, 325 engineers, 200 PhD students and postdocs, working in six different laboratories:

1. **GET**: Géoscience Environnement Toulouse (Toulouse Geoscience Environment)
2. **CESBIO**: Centre d’Etude Spatial de la BIOsphère (Biosphere Space Study Centre)
3. **IRAP**: Institut de Recherche en Astrophysique et Planétologie (Astrophysics and Planetology Research Institute)

4. **LEGOS**: Laboratoire d'Etudes en Géophysique et Océanographie Spatiales (Geophysical and Oceanographic Studies Laboratory)
5. **ECOLAB**: LABoratoire ECOlogie fonctionnelle et environnement (Functional Ecology and Environment Laboratory)
6. **LA**: Laboratoire d'Aérologie (Aerology Laboratory)

These laboratories cover wide scientific study domains, from deep space exploration and interplanetary research, to solar system planet study and Earth interior science. All these space branches are treated through laboratory analysis, instrumental results, theoretical approaches and numerical simulations.

This internship has been developed with the CNES Space Geodesy team, in GET laboratory, focusing on geodesic analysis in the context of the forthcoming MMX mission.

1.2 The MMX mission

As its title suggests, this internship project has completely been developed in the framework of the Martian Moons eXploration mission.
This mission is envisaged by the Japan Aerospace Exploration Agency, while the CNES collaboration is requested for orbital mechanic design and mission analysis.
The MMX mission in sensed to be launched in the second half of 2024 and realise the exploration of the two Martian moons, Deimos and Phobos. The latter corresponds to the primary focus of interest: the first landing on its surface, with a consequent ground sample collection, is the main purpose of the entire MMX project. The success in this objective would represent an extremely innovative result for all the Space scientific community.
Overall, the mission appears to have an elevate scientific interest, since it aims to elucidate the origin of both the Martian moons. This discovery would enable an important advancement in the knowledge of small celestial bodies and early solar system evolution process [2].

Because of the delicate tasks assigned to the MMX project, several investigations on satellite system configuration are being conducted, in order to fix satellite requirements for the mission realisation:

- The fixed propulsion system configuration consists in the employment of chemical propulsion, both for the outgoing and the return phases;
- The global spacecraft configuration individuates three separate modules: the Propulsion, the Exploration and the Return ones;
- The satellite launch will be realised in Summer 2024, from Tanegashima Space Center by an H3-24L rocket;
- The total mission life duration is programmed to be more than five years;
- The target satellite mass has been set at 3500kg;
- The global power consumption should stay approximately within 900W;
- The satellite orbital control will be performed by the generation of chemical speed variation $\boldsymbol{\Delta V \cong 5.0 km/s}$.

Moreover, different launch window constraints are being evaluated at the present moment:

- The nominal launch is supposed in 2024, while the backup one is fixed in 2026;

- At the launch date Earth C_3 should be within $18\mathrm{m}^2/s^2$;
- The launch asymptote declination should be within 30°, imposed by the launch site and the vehicle types;
- More than two consecutive weeks in succession should be available within the launch window;
- The time of flight to reach Mars should stay within one Earth year;
- Considering the nominal launch date and a 3-year stay for a sufficient exploration, the departure from Mars should be in 2028 and the return to Earth in 2029.

The global MMX orbital description is represented in the following figure:

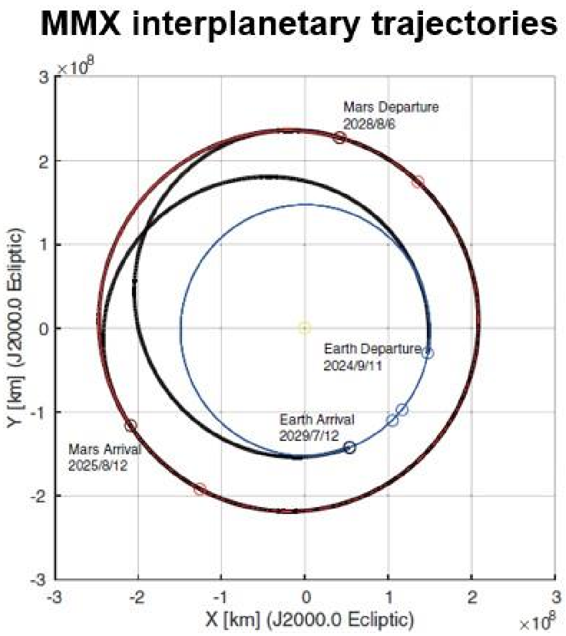

Figure 1 *- Representation of MMX nominal interplanetary trajectories, in J2000 inertial frame [2].*

The entire satellite flight within the mission has been divided into five main phases.
The first one considers the launch and the transfer toward Mars. The interplanetary trajectory is supposed to be a direct transfer orbit from Earth to Mars, where several correction manoeuvres and precise orbit determination (through two-way Doppler and delta-differential one-way ranging technique) will be adopted.

The second phase includes the satellite transfer to Phobos co-orbit. Since the latter is characterised by an about zero degree-inclination, it is impossible to reach it directly from the interplanetary trajectory. Consequently, a specific Mars Orbit Insertion (*MOI*) has been ideated: it consists in three different steps, globally demanding an approximately two week-duration and a maximum $\Delta\boldsymbol{V} \cong \mathbf{2000}\boldsymbol{m/s}$.
The following figure represents a 2-Dimensional composition of this consecutive three *MOI* trajectories:

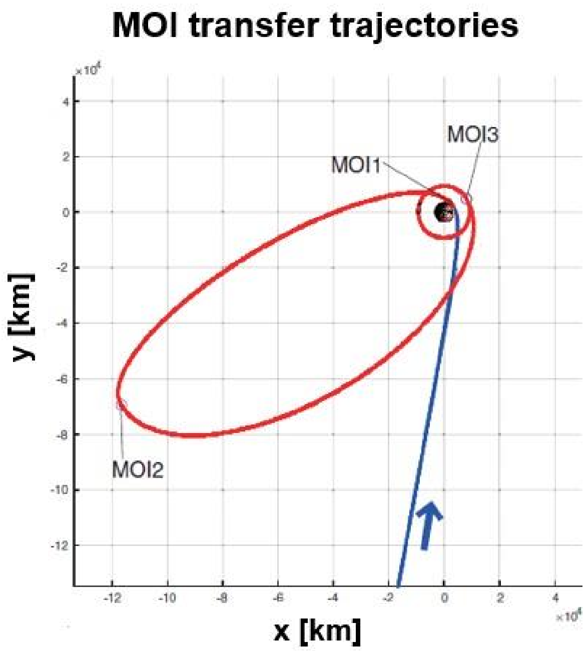

Figure 2 *- Representation of the three MOI manoeuvres employed to reach Phobos co-orbit [2].*

In the *MOI1*, the spacecraft will be first injected into an ellipsoidal orbit, defined by an apoapsis of about 40 times the Mars rayon (globally about 272200km), and a periapsis altitude of about 500km. The argument of periapsis has not been fixed yet. The most convenient choice would be to set it around 0° and 180°: the equatorial plane would thus contain the apoapsis, where the next manoeuvre for the inclination change could be realised, leading to a significant reduction in the fuel consumption.
The second transfer step constituted by the *MOI2*, will start about 3.5 days after the *MOI1* manoeuvre. It corresponds to an intermediate orbit characterised by the same periapsis and inclination of the Phobos co-orbit.
About 2.5 days after, the *MOI3* manoeuvre will be performed to lower the apoapsis to the Phobos co-orbit one and finally place the satellite on the real Phobos co-orbit around Mars.
Once reached Phobos, the satellite will begin to orbit on specific trajectories, designed for this particular orbital condition: the Quasi-Satellite Orbits, whose features will be detailed in the next paragraph.

After the completion of Phobos observation and sampling, the MMX program includes an additional third mission phase, consisting in several flybys around or rendez-vous with the second Martian moon, Deimos, in relation to the left fuel quantity: the rendez-vous operations would require about 500m/s excess compared to flybys.
In the first case, the satellite would be positioned into Deimos co-orbit through a Hohman transfer orbit, while a flyby would need an apoapsis displacement so that the satellite could intersect the Deimos trajectory, achieving the orbital resonance.

The fourth MMX phase is centred on the satellite operations for Mars escaping. Considering that at this point of the mission the satellite will be orbiting around Phobos or Deimos, the Mars Orbit Escape (*MOE*) consists in three control manoeuvres, representing the *MOI* reverse sequence. Therefore, the escape operations will again demand approximately two weeks and a maximum $\Delta \boldsymbol{V} \cong \mathbf{2000}\boldsymbol{m/s}$.
During the *MOE1* the spacecraft orbit apoapsis will be raised up to 40 times the Mars rayon.

In this specific orbital point, the *MOE2* manoeuvre will lower the periapsis altitude to 500km and turn the orbit inclination into the correct escaping one.
Finally, the *MOE3* will be again execute at the apoapsis in order to insert the satellite in the definitive interplanetary transfer orbit, escaping from Mars.

The fifth and last MMX phase concerns the satellite return on Earth, starting from the end of the last *MOE3* and finishing about one month before the capsule re-entry. As for the outgoing flight, a direct transfer orbit will be used.
In this situation, the employment of trajectory correction manoeuvres and precise orbital determination with two-way Doppler and delta-differential one-way ranging technique is requested again. In this way the satellite will be conducted to the accurate target point for the capsule separation. This capsule, containing Phobos ground samples, will be realised several hours before the re-entry in Earth atmosphere. It will then land using a parachute and be immediately recovered, while the spacecraft will be de-orbited thought the chemical propulsion system, escaping Earth gravity toward interplanetary space.

1.3 QSO trajectoires

As specified before, the MMX project is led by the JAXA, but since 2016 CNES is involved in its mission analysis and orbital mechanics aspects.
The latter are being treating by the CNES Flight Dynamics team, who collaborate in the definition of preliminary orbital design for the mission phases addressed to the close Phobos observation.
These orbital mechanics studies appear to be extremely delicate because of the particular physical conditions in which the satellite will realise its trajectories.

These conditions are the results of the specific Mars-Phobos system, defining the main MMX sphere of action.
Phobos is a Martian natural satellite, whose orbital plane roughly corresponds to both its equatorial plane and the Mars one. It is featured by a medium diameter of 22.2km, a surface of $1.5483 \cdot 10^9$ m² and a mass of $1.07 \cdot 10^{16}$kg. Its orbit around Mars is defined by a semi-mayor axis of 9375km, a period of 7.65h and an eccentricity of 0.015.
However, the Martian moon dimension and proximity in relation to its central body generate an unusual problematic gravitational environment for any transiting trajectory.
First of all, Phobos is characterised by a sphere of influence extremely close to its surface. The direct consequence is that any satellite orbiting in proximity this celestial body will be inevitably subjected not only its gravitational attraction, but also to the larger Martian influence. This means that the definition of the satellite motion through common Keplerian dynamics laws is forbidden.
It is thus mandatory to set this orbital analysis as a three body-problem, where the central body is Mars, the secondary is Phobos and the third is the satellite.
Moreover, neither the eccentricity of Phobos orbit around Mars, nor the non-uniformity characterising the moon gravitational field can be neglected in this artificial motion study.

In the special environment constituted by this unique Mars-Phobos couple, a kind of retrograde orbits have been identified as possible observation trajectories at distances of several dozens of kilometres from Phobos surface: the so called Quasi-Satellite Orbits [3].
These QSO trajectories are inspired by a particular formation flying of two satellites around a central body. In fact, a Quasi-Satellite is an object characterised by a specific co-orbital

configuration with a secondary planet to which the object stays close over several orbital periods.
This configuration is defined by a *1:1* orbital resonance. In orbital mechanics, a resonance occurs when two or more orbiting bodies reciprocally exert a periodic gravitational influence, usually due to their orbital period ratio, defined by small integer values ($\boldsymbol{n_i}$). As an example, considering two bodies orbiting respectively with orbital periods $\boldsymbol{T_1}$ and $\boldsymbol{T_2}$, their resonance configuration can be expressed as:

$$\frac{T_1}{T_2} = \frac{n_1}{n_2} \tag{1}$$

In this case, they are characterised by an $\boldsymbol{n_1: n_2}$ orbital resonance.
Consequently, such a resonance definition can be interpreted as the ratio between the number of orbits completed by two bodies in the same time interval.
This means that, with its *1:1* resonance with the secondary body, a QSO around a central body, takes the identical time to be completed than the orbit realised by the secondary around the same primary body. However, these two equal period-orbits are characterised by different eccentricities.
In the specific MMX case, the satellite realises its QSOs around Mars, in *1:1* resonance configuration with Phobos:

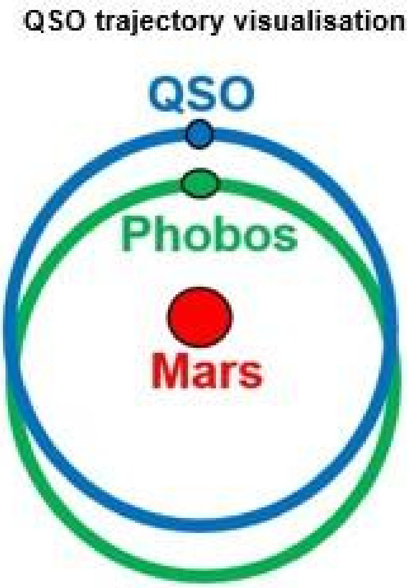

Figure 3 - *Schematic representation of QSO trajectories employed in the MMX mission.*

In this specific orbital configuration, the spacecraft realising a QSO trajectory follows a direct movement from the perspective of the central body, while if observed by the secondary, the satellite appears to travel in an oblong retrograde orbit.

For the MMX case, both 2 and 3-Dimensional QSO trajectories are being evaluating. In fact, even if orbits within the Phobos orbital plane appear to be easier to be controlled, the sake of complete surface mapping and precise gravity estimation leads to the need of QSOs with non-zero relative inclination with respect to Phobos equator, in order to fly over high latitude zones [4].

Because of this necessity, the methodology implemented for simulating them, is not limited to planar motions, but can be extended to inclined QSO, whose dimensions are only limited by the natural dynamics of the system.
Since the particularities defining the Mars-Phobos environment, this methodology is completely based on a three-body model.
The initial simplest model considered for describing QSOs is the Circular Restricted Three Body Problem (CR3BP), defined by the following dynamics equations:

$$\begin{cases} \ddot{x} - 2\dot{y} = \dfrac{\partial \Omega}{\partial x} \\ \ddot{y} + 2\dot{x} = \dfrac{\partial \Omega}{\partial y} \\ \ddot{z} = \dfrac{\partial \Omega}{\partial z} \end{cases} \tag{2}$$

where the potential function $\boldsymbol{\Omega}$ is define as:

$$\begin{cases} \Omega(x,y,z) = \frac{x^2+y^2+z^2}{2} + \frac{1-\mu}{r_1} + \frac{\mu}{r_2} \\ r_1 = \sqrt{(x-\mu)^2 + y^2 + z^2} \\ r_2 = \sqrt{(x+1-\mu)^2 + y^2 + z^2} \end{cases} \tag{3}$$

This set of equations is expressed in the barycentric synodic frame, rotating with Mars and Phobos. It adopts the normalised quantity for:

- the distance: the length unit corresponds to the Phobos orbit semi-major axis;
- the time: the time unit correspond to the Phobos orbital period around Mars and it is defined considering a constant angular velocity (*2π·time unit*);
- the mass: $\boldsymbol{\mu}$ is the mass parameter, assuming an approximate value of $1.66 \cdot 10^{-4}$, defined through Phobos (M_{Phobos}) and Mars (M_{Mars}) masses:

$$\mu = \frac{M_{Phobos}}{M_{Phobos} + M_{Mars}} \tag{4}$$

However, as expressed before, Phobos orbit eccentricity is not negligible since it also influences the satellite motion within this particular environment.
Consequently, it is necessary to pass to an Elliptical Restricted Three Body Problem (ER3BP), in order to compute more realistic QSO trajectories.
The dynamics equation system characterising this model, appears to be exactly the same as the (2), used for the CR3BP, with the only difference that the potential function has also to take into account Phobos eccentricity ($\boldsymbol{e}$):

$$\Omega_E(x,y,z) = \frac{1}{1+e \cdot cos(\nu)} \left(\frac{x^2+y^2+z^2}{2} + \frac{1-\mu}{r_1} + \frac{\mu}{r_2} \right) \tag{5}$$

This time, the potential function is also defined in function of the satellite true anomaly $\boldsymbol{\nu}$, the time dependent-orbital parameter. This element leads to the definition of normalised quantities also depending on time:

- the distance: the length unit corresponds to the actual orbital radius of Phobos for each value of $\boldsymbol{\nu}$;

- the time: since the angular velocity is no more constant on an elliptic orbit,the time unit is also time-dependent.

On the contrary, the mass parameter $\boldsymbol{\mu}$ always assumes the same time independent value.

However, the consideration of the only Phobos eccentricity is not sufficient to obtain realistic QSO trajectories. For this aim, a complex gravity characterization of Phobos needs to be used instead of the point mass approximation. In this context, a spherical harmonic (SH) expansion of Phobos gravity based on Chao-Rubincam model [5], has been taken into account.
The adoption of the spherical harmonic model enables to compute Phobos gravitational acceleration only within a reference frame cantered on its mass centre, and whose axes rotate with it. This specific reference frame is referred to as the Body Centred Body Fixed (BCBF) system.
The best solution found is thus the introduction of a new equation system, providing the full time-invariant differential equations of the Mars-Phobos ER3BP-SH in Phobos BCBF frame, with the fixed physical units of the CR3BP.
This new equation system consists in the description of the ER3BP dynamics with the mean anomaly (***M***) as independent variable.
Once again, the first three dynamics equation are the same as in system (2), but two elements make the main difference.
The first one is that a fourth equation is added:

$$\dot{\boldsymbol{\nu}} = \boldsymbol{\omega_z}(\boldsymbol{\nu}) \tag{6}$$

The second difference is that the potential function is now expressed as:

$$\boldsymbol{\Omega_M}(\boldsymbol{q}) = \boldsymbol{U_{G,1}}\left(\boldsymbol{q} - \frac{1-e^2}{1+e\cdot cos(\nu)}[1,0,0]^T\right) + \boldsymbol{U_{G,1}}(\boldsymbol{q}) - \frac{(1+e\cdot cos(\nu))^4}{(1-e^2)^3}\left(\frac{q^T p_q}{2} + (1-\mu)\frac{1-e^2}{(1+e\cdot cos(\nu))^2}x\right) \tag{7}$$

with:

$$\begin{cases} \boldsymbol{q} = (\boldsymbol{x}, \boldsymbol{y}, \boldsymbol{z}) \\ \boldsymbol{\omega}(\boldsymbol{\nu}) = \dfrac{(1+e\cdot cos(\nu))^2}{(1-e^2)^{\frac{3}{2}}}[1,0,0]^T \\ \boldsymbol{P}(\boldsymbol{\nu}) = (\boldsymbol{\omega}(\boldsymbol{\nu}) \wedge)^2 \end{cases} \tag{8}$$

where the $\boldsymbol{U_{G,i}}$ term represents the gravitational acceleration due to ***i*** body: for Phobos case, it includes the gravity Spherical Harmonic accelerations [6].

At the same time, it is also possible to use a method defining the satellite relative speed and position, in relation to Phobos.
The starting point is the study of the unperturbed Hill's relative motion equations for the elliptic case, assuming that the attraction of the secondary body is negligible ($\boldsymbol{\mu}$ = 0).
The consequent dynamics equations are the Tschauner-Hempel equations:

$$\begin{cases} \ddot{x} - 2\dot{y} - \dfrac{3x}{1+e\cdot cos(\nu)} = 0 \\ \ddot{y} + 2\dot{x} = 0 \\ \ddot{z} + z = 0 \end{cases} \tag{9}$$

The solution of this differential equation system can be written as a function of six parameters, referred to as the *Osculating Elements*, ***C*** = [***α***, ***φ***, ***δx***, ***δy***, ***γ***, ***ψ***]] [7], where:

- ***α*** and ***γ*** represent the amplitude of satellite motion in the in-plane and in the out-of-plane directions, respectively;
- ***φ*** and ***ψ*** represent the injection phases;
- (***δx***, ***δy***) represent displacement of the centre of motion in Phobos orbital plane, where (0, 0) corresponds to the Martian moon mass centre.

As a consequence, the equation solutions, defining the six components of the satellite state vector (position and speed), are expressed as follows:

$$
\begin{aligned}
&x = \alpha \cdot \big(1 + e \cdot cos(\nu)\big)\, cos(\nu + \varphi) + \delta x \\
&y = -\alpha \cdot \big(2 + e \cdot cos(\nu)\big)\, sin(\nu + \varphi) + \delta y \\
&z = \gamma \cdot cos(\nu + \psi) \\
&\dot{x} = -\alpha \cdot \big(sin(\nu + \varphi) + e \cdot sin(2\nu + \varphi)\big) \\
&\dot{y} = -\alpha \cdot \big(cos(\nu + \varphi) + e \cdot cos(2\nu + \varphi)\big) \\
&\dot{z} = -\gamma \cdot sin(\nu + \psi)
\end{aligned}
\tag{10}
$$

Successively, it is possible to set two realistic hypotheses:

1. The mass of the secondary body (Phobos) is much smaller than the primary (Mars) one: $\mu \ll 1$;
2. The satellite orbits in the proximity of the secondary body: $r_2 \ll 1$.

These considerations allow to eliminate from equation system (9) all the negligible terms, obtaining the simplified equation system:

$$
\begin{cases}
\ddot{x} - 2\dot{y} - \frac{3x}{1+e\cdot cos(\nu)} = -\frac{1}{1+e\cdot cos(\nu)} \cdot \left(\frac{\mu x}{r_2^3}\right) \\
\ddot{y} + 2\dot{x} = -\frac{1}{1+e\cdot cos(\nu)} \cdot \left(\frac{\mu y}{r_2^3}\right) \\
\ddot{z} + z = -\frac{1}{1+e\cdot cos(\nu)} \cdot \left(\frac{\mu z}{r_2^3}\right)
\end{cases}
\tag{11}
$$

Finally, this set of differential equations can be turned into an equation system of *Osculating Elements*, by the application pf the constant variation method to solutions (10).
The consequent resolution of the *Osculating Element* system, leads to compute satellite state vector components, expressed in the Cartesian coordinate system, at each step of the integration.

This QSO simulation methodology presents multiple advantages for the MMX mission analysis.
Firstly, thanks to the employment of the *Osculating Elements*, it enables a full control of trajectory design parameters, such as the amplitude, the phases and the displacement of the satellite motion centre.
Furthermore, this method can be applied to both planar and 3-Dimensional QSO trajectories, exactly in the same way, without any excessive computational time increase.

In fact, the most significant difference is that the calculation of 2-Dimensional orbits involves an out-of-plane amplitude $\boldsymbol{\gamma = 0}$, representing the null Cartesian z-dimension $\boldsymbol{z = \dot{z} = 0}$.
Since these QSOs are contained in the Phobos orbital plane around Mars, they can be represented through ***xy***-graphs:

EME2000 frame Mars-centred	EME2000 frame Phobos-centred	Phobos BCBF rotating frame
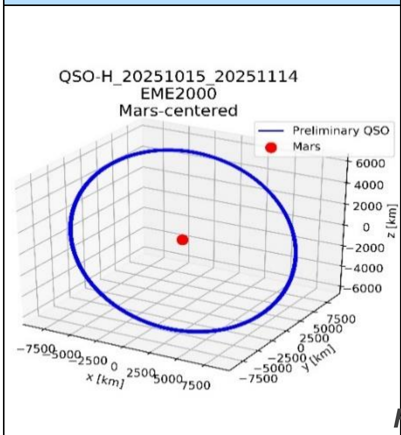	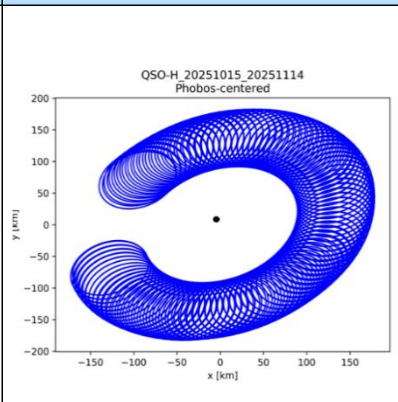	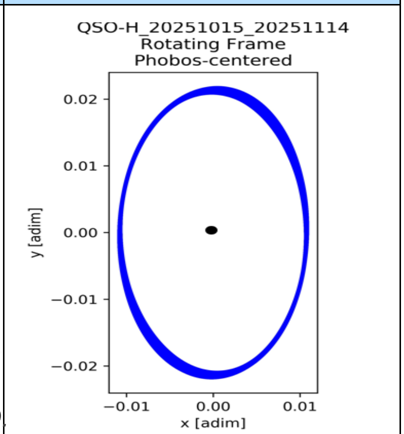
	Figure 4.a *- 2D high-altitude QSO*	
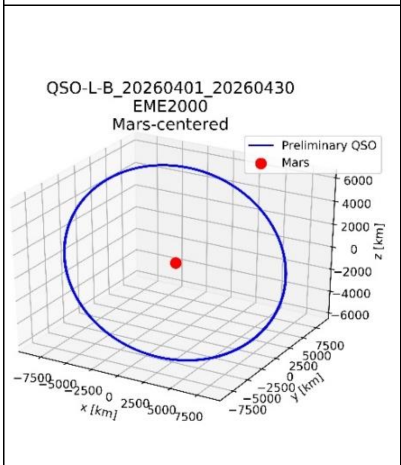	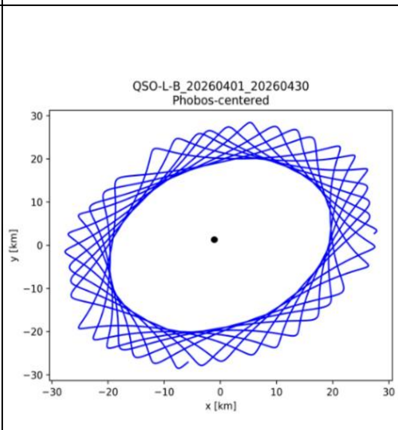	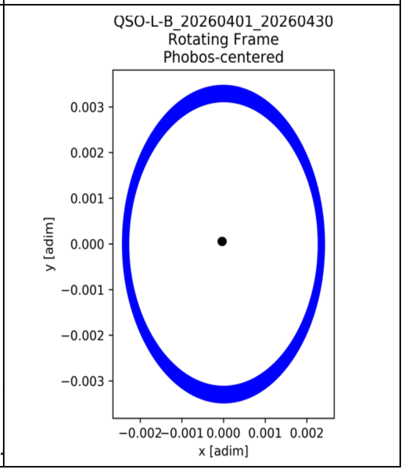
	Figure 4.b *- 2D low-altitude QSO*	

Figure 4 *- Representation of 2-Dimensional QSO trajectories.*

On the contrary, 3-Dimensional QSO trajectories are characterised by an out-of-plane amplitude $\boldsymbol{\gamma \neq 0}$. However, both the literature and orbit simulation prove that the consideration of $\boldsymbol{\gamma > 0.9\alpha}$ leads to trajectory instabilities. Consequently, it is necessary to individuate couples $(\boldsymbol{\gamma, \alpha})$ able to respect the QSO stability conditions, while maximising the reachable latitude over Phobos equator, in order to explore the largest portion possible of the target surface.
Effectively, the ideal purpose is to realise orbits characterised by a high inclination and close to the Martian moon, so that areas at high latitudes would be accessible with an excellent resolution.
However, the combination of decreasing the satellite altitude $(\boldsymbol{\alpha})$, while increasing the orbital inclination $(\boldsymbol{\gamma})$ inevitably causes instable QSO trajectories.
An example of a stable 3-Dimensional QSO is presented in the following figures:

EME2000 frame Mars-centred	EME2000 frame Phobos-centred	Phobos BCBF rotating frame
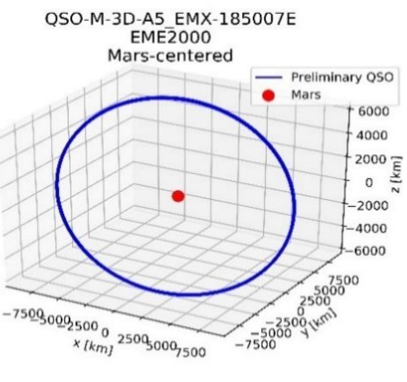	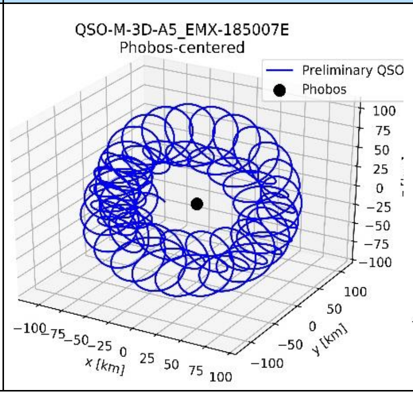	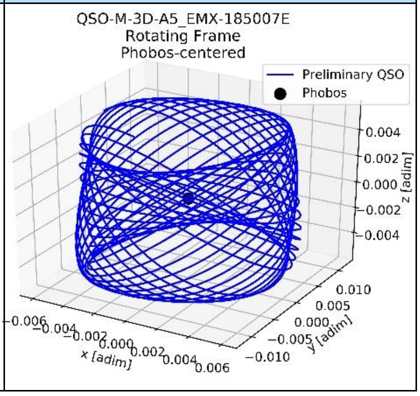

Figure 5 *- Representation of 3-Dimensional QSO trajectories.*

To conclude, this set of computed QSO trajectories not only enable the satellite to orbit in Phobos proximity and observe its surface, but also they allow the detection of its gravity field, whose accurate restitution represents one of the main scientific purpose of the MMX mission.

1.4 Gravity field model

As mentioned before, the main focus of this internship project is the analysis of MMX mission capability of recovering current Phobos gravity field model.

Effectively, at the present moment the knowledge of this Martian moon geodesic feature has not reached an excellent accuracy level yet. This means that nowadays Phobos gravity model is characterised by a certain imprecision.
Consequently, MMX will start its exploration, relying on this approximate target gravity awareness. However, during the mission phases centred on Phobos exploration, a continue, gradual update of Phobos model will be realised.
This procedure is based on the realistic concept that the closer the satellite will move towards the Martian moon and the more measurements it will make, the more it will be able to increase its precision in detecting gravity field, through the employment of specific measure techniques (such as Doppler, LIDAR and Optical navigation images).
This improvement in Phobos gravity restitution with the shorting of spacecraft altitude over Phobos surface and its observation operations, will be translated in an upgrade in the current gravity model available along the mission.
The final purpose is that, once the satellite will have completed its QSOs near the Martian moon, the new obtained Phobos gravity model will result much more accurate and closer to the real field, than the initial template used at the beginning of the mission.

Nevertheless, in order to understand the evaluation in this Phobos geodesic parameter, it is firstly necessary to know how its gravity field is modelled.
Firstly, its model takes origin from the body shape and gravity potential (***U***) model, developed as a series of spherical harmonics [8]. The latter can be expressed as:

$$\boldsymbol{U(r,\varphi,\lambda) = \frac{\mu}{r} \cdot \sum_{l=0}^{\infty} \left(\frac{R}{r}\right)^{l} \cdot \sum_{m=-l}^{l} K_{lm} Y_{lm}(\varphi,\lambda)} \tag{12}$$

where:

- $(\boldsymbol{r},\boldsymbol{\varphi},\boldsymbol{\lambda})$ are the spherical coordinates relative to the body, its radius vector latitude and longitude, respectively (Figure 6);
- ***R*** represents the reference length (normally the semi-mayor body axis);
- $\boldsymbol{K_{lm}}$ corresponds to the dimensionless coefficient of degree ***l*** and order ***m***;
- $\boldsymbol{Y_{lm}}$ is the complex surface harmonic function of degree ***l*** and order ***m***;
- $\boldsymbol{\mu}$ is the body standard gravitational parameter, defined by its gravitational constant ***G*** and its mass ***M***:

$$\boldsymbol{\mu = G \cdot M} \tag{13}$$

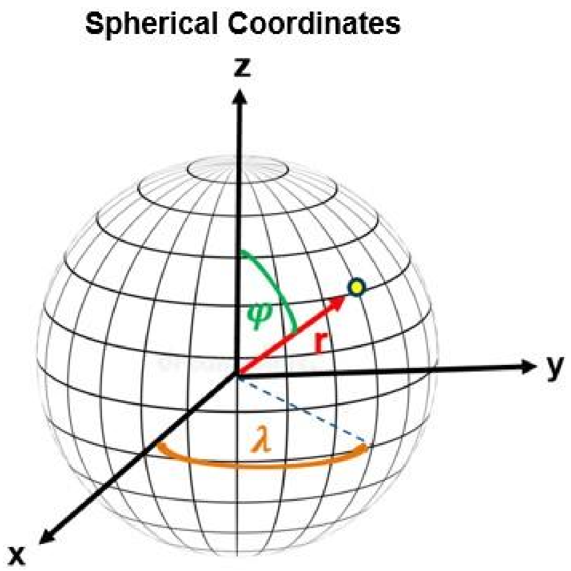

Figure 6 *- Spherical coordinate schematic representation.*

The $\boldsymbol{Y_{lm}}$ terms are strictly linked to the usual Legendre polynomials (order ***m*** = 0) and the relative functions (order ***m*** ≠ 0) $\boldsymbol{P_{lm}}$:

$$\boldsymbol{Y_{lm}(\varphi,\lambda) = P_{lm}(sin\varphi)e^{im\lambda}} \tag{14}$$

where, for orders ***m*** ≥ 0, and considering $\boldsymbol{u} = \boldsymbol{sin\varphi}$, the Legendre elements are defined as follows:

$$\begin{gathered} \boldsymbol{P_{lm}(u) = \frac{(1-u^2)^{\frac{m}{2}}}{2^l!} \cdot \frac{d^{l+m}}{du^{l+m}}[(u^2-1)^l]} \\ \boldsymbol{P_{l,-m}(u) = (-1)^m \cdot \frac{(l-m)!}{(l+m)!} P_{lm}(u)} \end{gathered} \tag{15}$$

These surface harmonic functions $\boldsymbol{Y_{lm}}$ can be graphically represented, in relation to different orders and degrees:

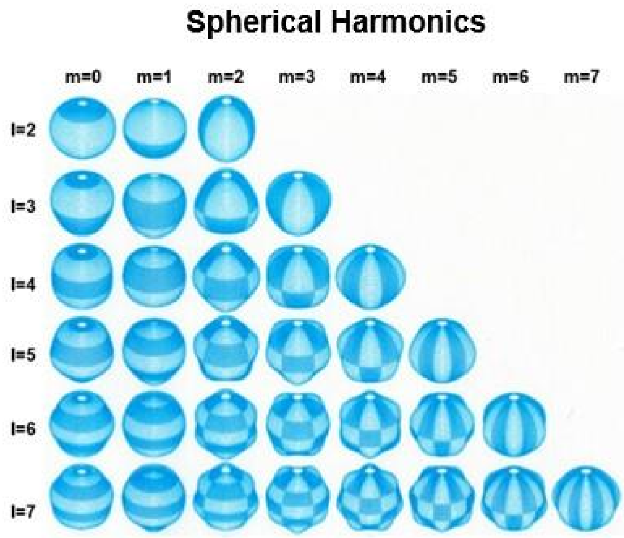

Figure 7 *- Spherical harmonic schematic representation.*

With this $\boldsymbol{Y_{lm}}$ definition, it is possible to express the $\boldsymbol{K_{lm}}$ terms as:

$$\boldsymbol{K_{lm}(\varphi,\lambda) = \frac{(-1)^m}{MR^l} \cdot \iiint r'^l\, Y_{l,-m}(\varphi',\lambda')dM'} \tag{16}$$

The previous expression relies on an integral extended to the entire body volume and on the current spherical coordinates ($\boldsymbol{r',\varphi',\lambda'}$) and mass element $\boldsymbol{dM'}$ of the considered point on the body surface.

Moreover, these complex spherical harmonic elements $\boldsymbol{K_{lm}}$ are normally related to the real Stokes coefficients $\boldsymbol{C_{lm}}$ and $\boldsymbol{S_{lm}}$ ($\boldsymbol{m} \geq 0$):

$$\begin{aligned} &\boldsymbol{(2-\delta_{0,m})K_{lm} = C_{lm} - iS_{lm}} \\ &\boldsymbol{(2-\delta_{0,m})K_{l,-m} = (C_{lm} + iS_{lm}) \cdot \frac{(l+m)!}{(l-m)!}(-1)^m} \end{aligned} \tag{17}$$

where $\boldsymbol{\delta}$ is the Kronecker symbol.
It is exactly this set of Stokes coefficients to be implemented in order to define a body gravity field model described as expansion of spherical harmonics.
They are completely related to the spherical harmonic functions and at the same time, to the body shape. In fact, they are defined as follows:

- **Zonal coefficients**: they are characterised by an order ***m=0***. If they assume a value different from zero, they represent a lack of symmetry along the body latitude ("North-South" direction), relative to its equatorial plane.
- **Sectorial coefficients**: they are characterised by the same degree and order value, ***l=m***. If they are different from zero, they represent a lack of rotational symmetry around the body polar axis, along its longitude.
- **Tesseral coefficients**: they are characterised by different degree and order values, ***l ≠ m* ≠ 0**. If they are different from zero, they represent a lack of rotational symmetry around the body polar axis, along both its longitude and latitude.

However, in geodesic analysis the normalised version of Stokes coefficients is usually adopted:

$$\overline{\boldsymbol{C}}_{\boldsymbol{lm}} = \frac{\boldsymbol{C}_{\boldsymbol{lm}}}{\boldsymbol{N}_{\boldsymbol{lm}}}$$
$$\overline{\boldsymbol{S}}_{\boldsymbol{lm}} = \frac{\boldsymbol{S}_{\boldsymbol{lm}}}{\boldsymbol{N}_{\boldsymbol{lm}}} \tag{18}$$

where the $\boldsymbol{N}_{\boldsymbol{lm}}$ term is defined as follow:

$$\boldsymbol{N}_{\boldsymbol{lm}} = \left[\frac{(2-\delta_{0,m})(2l+1)(l-m)!}{(l+m)!}\right]^{\frac{1}{2}} \tag{19}$$

In the context of this internship project, gravity filed models of both the central body, Mars, and its moon, Phobos, have been defined by ones of the respective most precise known set of normalised Stokes coefficients.

Consequently, this entire analysis aimed to simulate the restitution of the Martian moon gravity field, has been based on the capability of the MMX mission to return accurate $\overline{\boldsymbol{C}}_{\boldsymbol{lm}}$ and $\overline{\boldsymbol{S}}_{\boldsymbol{lm}}$ values.

2 Employed and implemented informatics tools

The main purpose of this internship project is the evaluation of the accuracy level reachable in Phobos gravity filed model recovery within the MMX mission. Consequently, this estimation has to take into consideration the mission phases strictly dedicated to the specific Martian moon exploration.
It has thus been necessary to simulate and analyse the satellite capability of returning a precise Phobos gravity field, while it is realising its QSO trajectories, considering the employment of measurement techniques fixed by the JAXA.

The search of this primary objective led to the necessity of three separate, but consecutive moments, within this project development:

1. A precise orbital analysis, addressed to the treatment of preliminary QSO trajectories computed by the JAXA and CNES Flight Dynamics teams;
2. An accurate evaluation of MMX mission effective possibilities in generating a reliable restitution of Phobos gravity filed;
3. A detailed study conducted on the obtained results: visual and graphical representations proved to be inevitable for accurate result interpretations.

It has been possible to complete the first two steps, throughout the employment of the powerful CNES GINS software, expressly designed for orbital and geodesic studies. Effectively, this tool enables both realistic orbital processing and planetary physical parameter correction.
Thus, GINS is able to provide all the demanded results.
However, for what concerns the consecutive analysis of these results, particular graphical tools have been needed.
Therefore, a specific Python module has been developed, for the visualisation of main GINS outputs: the ***Visualisation Module***.

The two following paragraphs will detail both these informatics tools, the GINS software and the Python module.

2.1 The GINS software

GINS is an orbitography software completely realised by the CNES Space Geodesy team. Its code writing started at the beginning of the 1970s, and from that moment on, it has known numerous evolutions, updates and improvements, constantly following the changes in international standards. Nowadays, it is constituted by 240000 Fortran90 code lines [9].
At first, GINS got born to process the available space geodesy data, taking into account only one satellite at a time.
In the early 1990s, the software became able to include more than one satellite: it was designed to consider GPS constellation satellites and to process data from their receivers, both on board and on the Earth ground.
A fundamental evolution arrived in 1999, when GINS turned into an “planetary” software, able to process DSN (Deep Space Network) tracking data of satellites orbiting around bodies other than the Earth (Mars, Venus, planetary satellites, asteroids).
In 2009, GINS was updated to also treat the multi-constellation cases of study.
From 2010 up to the present day, the software continues to be constantly updated in order to improve its reliability and calculation times for routine processes of space gravimetric missions (CHAMP, GRACE, GOCE) and DORIS, GNSS, LASER and VLBI ((Very Long Baseline Interferometry)) data processes for the kinematics and the terrestrial reference system as part of the GRGS's contribution to international services (IGS, IDS, ILRS, IVS).
The main applications of the GINS software can be classified in four macro categories:

1. Precise calculation of artificial satellite orbits around different celestial bodies in the solar system;
2. Determination, correction and restitution of geodesic features: gravitational field coefficients, rotation parameter, ground station position and speed, solid and oceanic tide model coefficients, mean oceanic surfaces, atmospheric model parameters, etc.;
3. Simulation of several measurement techniques;
4. Treatment of cases without any satellite (landers, VLBI).

As detailed below, all these software applications have to be developed following the same procedures, dictated by the GINS standard operating.

2.1.1 GINS Organigram

In order to clarify the GINS functioning, the following figure represents a detailed visual schema, showing the main software components.

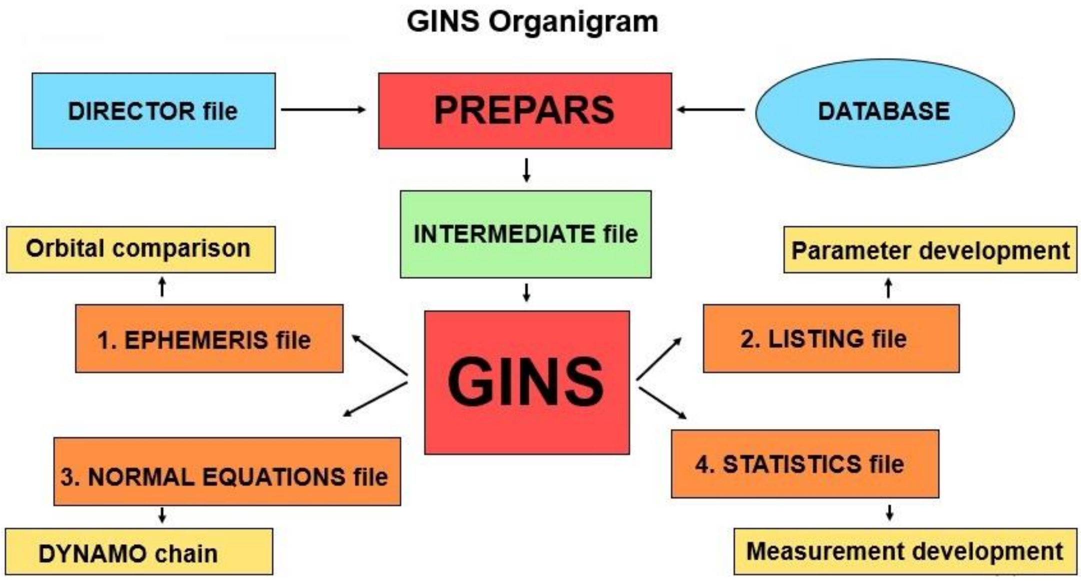

Figure 8 *- Schematic representation of the GINS software organigram.*

As underlined by this schema, the first necessary component for the GINS chain it is the so called "*Director*" input file. This element contains all the instructions the software needs to realise the desired procedure.
The "*Director*" file is characterised by the following structure:

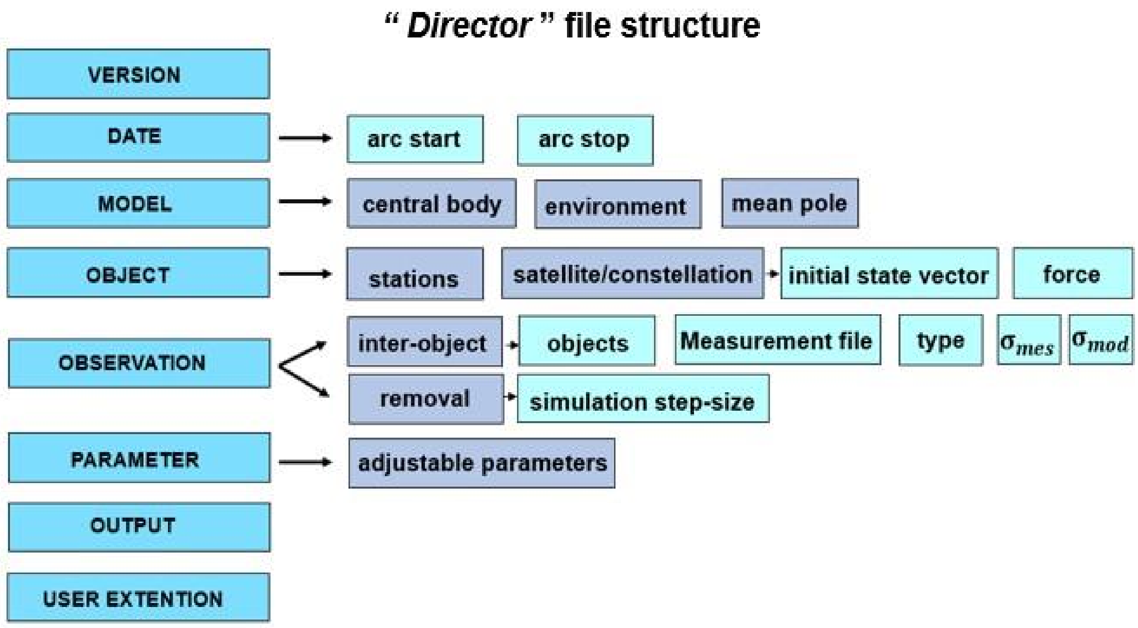

Figure 9 *- Schematic representation of the "Director" file structure.*

The elements present in this schema, are here described:

- The ***version*** specifies the GINS edition to be used for a specific study case.

- The ***date*** parameter identifies the interval time relative to the whole computation. The interval starting and the ending instants are defined by the values assumed by the *arc start* and *arc stop* parameters.
- The ***model*** section specifies which models are adopted for the computation, in terms of *central body*, *environment* (physical phenomena to be taken into account and natural satellite) and *mean pole* location.
- The ***object*** section lists all the elements involved in the computation: ground *stations*, *constellation* or *satellite(s)*, their *initial state vectors* and the *forces* acting on them, and, in the only case of VLBI computation, the *quasar* model.
- The ***observation*** section describes all the measurements realised between objects and the way they are taken into account. In its interior, the *inter-object data* subsection mainly defines between which *objects* these measurements are effectuated, the reference **"***Measurements***"** *file*, the measurement *type* (laser, Doppler, interferometer, ephemeris, inter-satellites, etc.), the a priori standard deviation on measurements ($\boldsymbol{\sigma_{mes}}$) and on adopted models ($\boldsymbol{\sigma_{mod}}$).
  In this context, it is important to underline that the quadratic mean of these two last parameters defines the white noise $\boldsymbol{W_n}$ characterising each type of measurements:

$$\boldsymbol{W_n} = \sqrt{\frac{1}{2} \cdot (\sigma_{mes}^2 + \sigma_{mod}{}^2)} \tag{20}$$

  Moreover, another remarkable parameter is defined in this section. In the *removal* subsection, the time *simulation step-size* between consecutive measurement simulations is here expressed in seconds.
- The ***parameter*** section describes all the elements of the specific study case, including the so defined *adjustable parameters*, which are set as free, so that GINS can modify and correct them, for the purpose of obtaining realistic and accurate results.
- The ***output*** section specifies which elements have to be inserted in the desired GINS outputs.
- The ***user extension*** section gathers various parameters used for extending GINS standard functionality.

Considering the GINS organigram in Figure 8, the second element necessary for the software operating is the "*Database*". It contains a list of specific files thoroughly describing every physical parameter relative to all the celestial bodies considered in GINS, callable from the "*Director*" file.

Both the "*Director*" file and the "*Database*" represent the input elements for the PREPARS module. This module constitutes a first important step in the complete GINS chain, since it allows to turn the input "*Director*" instructions into a precise formulation readable from the GINS software. In fact, the PREPARS output is an "*Intermediate*" file, which contains all the calculation directions, translated in GINS informatics language.
Thus, this "*Intermediate*" file represents the effective input element for the real software, which, in turn, gives birth to four main outputs:

1. "***Ephemeris***" file, containing the satellite tabulated orbits which have been adjusted during the process and their possible extrapolation. Various formats are possible for this file, but the standard counts:

   - the satellite identifying number
   - the exact integration instant, expressed in Julian Day and Second;
   - the time reference frame (TAI, TUC, TE, etc.)
   - the coordinate system (XYZ, RTN, AEI, etc.)

- the celestial reference frame (EME, etc.)
- the reference mean equator date (J2000, 1950.0, etc.)
- the three components of the satellite position (expressed in [m]) speed (in [m/s]) and acceleration (in [m/s²]) vectors in the integration reference frame;
- the three components of the satellite position (expressed in [m]) and speed (in [m/s]) vectors in the terrestrial reference frame;
- the eclipse index ranging from 0 to 1 expressing the satellite passage in the shade (index=0) or in the half-light (0<index<1) of a celestial body;
- the quality index, expression of the accuracy level.

This output file can be in turn, an input for GINS, as an ephemeris "*Measurement*" file to enter in the "*Director*" *observation* block, or as a bulletin source to insert in the *object* section, under heading *initial state vector*.

2. "***Listing***" file, the main software output, containing a list describing the performed calculations and parameters. It involves a global summary of all the main results: general statistics on measurement residuals for each iteration, adjusted parameter values and characteristics of input models and "*Director*" file.

3. "***Normal Equations***" file, written in a binary format and containing the set of *p* linear equations linking *p* unknown parameter values, which can be expressed in the form a symmetrical definite positive matrix. This file can be read and used by the various programs in the DYNAMO package, which leads to their resolution.

4. "***Statistics***" file, containing individual measurement residuals and all information useful to produce measure statistics, graphical representation and evolution in time control.

2.1.2 GINS software reference system

Before starting to talk about how effectively the GINS software works, it is preliminary important to know which are the possible reference frames it can use to realises all its data computations. It is therefore necessary to rapidly describe GINS time and space scales, both of which are defined by the International System (IS) units.

Concerning time references, *International Atomic Time* (IAT) is used in study cases where Earth represents the central body, while *Barycentric Dynamical Time* (BDT) is preferred for all other solar system bodies.
All dates involved in orbit descriptions, are expressed considering the *modified Julian date 1950.0* (01/01/1950) as the origin. Generally, the input data are converted to IS and IAT units when being read, along with result values reported in output files (orbits, normal equations, statistic files), which are also normally expressed in IS units.
However, input and output files can employ different date systems:

- Calendar dates: DD/MM/YYYY, DD/MM/YY or DOY/YYYY (Day of Year/Year);
- Julian dates 1950 (JUL50) = days after 01/01/1950 at 0h;
- Julian dates J2000 = days after 01/01/2000 at 12h;
- ***Julian/Gregorian dates = J2000 dates + 2451545*** days;
- Modified Julian dates ***(MJD) = J2000 date – 51544.5*** (days);

- GPS dates: WWWW/D = GPS week and day of the week (from 0=Sunday to 6=Saturday, week 1 = week starting 13/01/1980).

Moreovere, these files can use various time scales:

- IAT = International Atomic Time;
- UTC (Coordinated Universal Time). The relation between the UTC and the IAT depends on the date in question (***UTC = IAT – 34.0s*** at the start of 2011);
- GPS time (GPST = IAT-19 s);
- BDT = Barycentric Dynamical Time;
- TT = Terrestrial Time (***TT=IAT +32.184 s***).

In any case, if necessary, GINS is able to perform conversions between these several time scales and date systems.

As regard the space references, many different frames are again possible.
Anyway, it is always first necessary to fix the central body, around which all the orbits have to be calculated. This body can be chosen between the Earth and any other celestial body within the Solar System, implemented in the GINS software. The central body centre of mass represents the origin of the main coordinate reference system, whose axis orientation follows the usual international conventions.
However, in most cases, two main reference frames are adopted: a spatial system linked to the central body and the inertial EME2000 (Earth's Mean Equator, at 12:00 Terrestrial Time on 1 January 2000) reference system, in which the dynamical computations are made.
Moreover, for what concerns coordinates system, the standard employed for GINS calculations is the Cartesian one (***x,y,z***).
Nevertheless, for some input and output files, different coordinate and reference systems are available. In fact, in order to model the satellite motion, process particular data or realise specific calculations regarding the central and secondary bodies, GINS offers the possibility to choose between the most common frame systems employed in space geodesic studies:

- ***Ellipsoidal reference system***: it adopts ellipsoidal coordinates (***φ,λ,h***), describing the ellipsoidal longitude ***φ***, measured positively from South to North, the longitude ***λ***, measured positively from West to East**,** and the height ***h***, above the ellipsoid surface. It owes its name to the closest mathematical modelled surface to the real celestial rotating body one: a revolution ellipsoid or of a sphere flattened at its poles. These shapes are featured by the equatorial semi-mayor axis ***a*** and the polar semi-minor axis ***b***, defining their oblateness ***f = (a-b)/a***. In case of spherical surface shape (***f*=0,** rayon ***R***), these coordinates are referred to as *spherical coordinates*, and they can be linked to the *rectangular coordinates*, by the following geometrical relations:

$$\begin{cases} \boldsymbol{r = R + h} \\ \boldsymbol{x = r \cdot cos(\varphi) \cdot cos(\lambda)} \\ \boldsymbol{y = \ r \cdot cos(\varphi) \cdot sin(\lambda)} \\ \boldsymbol{z = \ r \cdot sin(\varphi)} \end{cases} \tag{21}$$

- ***Local ellipsoidal reference system***: it adopts two angles in order to individuate a specific point direction in relation to a particular observer or geodesic instrument. These angular coordinates are the *Elevation* (or *Altitude*) angle ***γ***, set between the local normal direction and the imaginary line linking the observer to the observed object, and the *Azimuth* angle ***θ***, between the projection of the observed object direction on the local horizontal plane and a system reference direction. This last direction is usually identified with the North or with the normal of the reference ellipsoid.

- ***Keplerian orbital elements***: this specific spatial system allows to describe any object orbit around the central body and it is constituted by the six following elements:

$$\begin{aligned} &\boldsymbol{a} : \text{ semi} - \text{mayor axis} \\ &\boldsymbol{e} : \text{ eccentricity} \\ &\boldsymbol{i} : \text{ inclination} \\ &\boldsymbol{\omega} : \text{ argument of periapsis} \\ &\boldsymbol{\Omega} : \text{ argument of ascending node} \\ &\boldsymbol{M} : \text{ mean anomaly} \end{aligned}$$

  The Keplerian elements are able to define the form of the tangential ellipse to an object orbit, its orientation in relation to the central body and the exact position of the studied object on the ellipse. Moreover, they conduce to the computation of the elliptical orbital period ($\boldsymbol{T} = \boldsymbol{2\pi} \cdot \sqrt{\frac{a^3}{\mu}}$).
  If the object in question realises an unperturbed motion along its trajectory, only subjected to the attractional forces exercised by the central body, all the Keplerian elements defining its orbit are constant, apart from the mean anomaly, which varies over time along with the object position. However, even if the orbiter is exposed to other perturbing forces, its Keplerian elements usually change slowly in time and it is always possible to define at any moment an osculating orbit, based on its instantaneous Keplerian elements.

- ***Satellite RTN local orbital coordinates***: this system has its origin in the satellite centre of mass and it is defined by three main directions. The radial direction ***R***, links the system origin to the central body centre of mass, the tangential direction ***T***, along the satellite track and parallel to its speed vector, and the normal direction ***N*** perpendicular to the orbit plane completing the right-hand orthogonal frame. This kind of coordinate system is especially appropriate for ephemeris analysis along the orbit.

- ***Coordinate systems linked to the satellite***: every satellite is characterised by its own coordinate system, which identifies the position of its various components. Its origin and mayor axis depend on the spacecraft and its attitude law, while its main coordinates have to be specified in the input file of the satellite macro-models.

Despite the various reference systems utilisable by GINS, the realisation of specific coordinate changes is within the software capabilities.
In fact, a given set of position and speed coordinates ($\boldsymbol{P_1}$, $\boldsymbol{V_1}$) expressed in a particular reference fame *1*, can always be expressed in another reference frame *2* by the correspondent coordinates ($\boldsymbol{P_2}$, $\boldsymbol{V_2}$), through the use of the transformation relations, containing the relative rotation matrix ***M(t)***:

$$\begin{cases} \boldsymbol{P_2 = M(t) \cdot P_1} \\ \boldsymbol{V_2 = M(t) \cdot V_1 + \frac{dM(t)}{dt} \cdot M(t)^{-1} \cdot P_2} \end{cases} \tag{22}$$

2.1.3 The GINS software structure

Once understood on which time and space reference frames GINS bases its calculations, it is possible to pass to the description of the real software structure. The latter is constituted by the concatenation of the steps represented in the figure below:

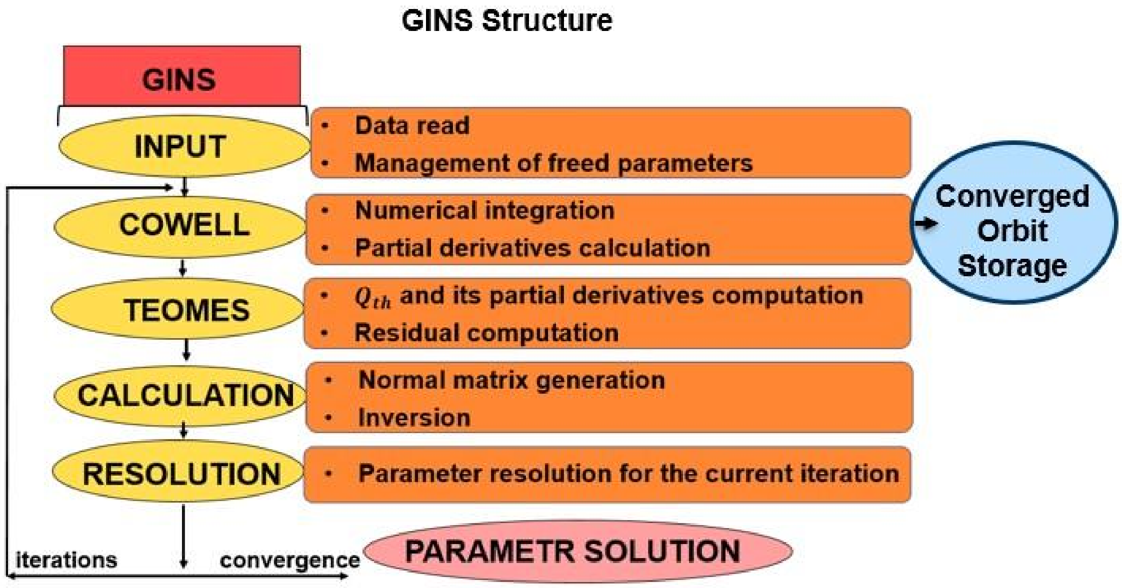

Figure 10 *- Schematic representation of the GINS software structure.*

A detailed description of each of the GINS step is reported below.

GINS first step: Data read and management

Starting from the beginning, the GINS software receives the "*Intermediate* file as input. It is so able to interpret all the instructions and data it needs to realise a specific calculation. Moreover, in this first step, GINS already starts to elaborate the freed parameters: the physical elements, whose initial a priori value can be adjusted by GINS in order to get closer to a more realistic condition.

GINS second step: Calculation of satellite orbits

Once GINS received the instructions for a specific study case and all the necessary data from the input file, it moves to the numerical computation of artificial satellite orbits. It consists of a dynamics equation integration between specific initial and final time instants, $[\boldsymbol{t_{in}}, \boldsymbol{t_{fin}}]$.

In order to realise this computation, the software necessitates two main pieces of information:

1. The satellite initial state vector at the time instant $\boldsymbol{t_0} = \boldsymbol{t_{in}}$, $[\,\bar{\boldsymbol{r}}_0, \dot{\bar{\boldsymbol{r}}}_0\,]$ (where $\bar{\boldsymbol{r}}_0 = (\boldsymbol{x_0}, \boldsymbol{y_0}, \boldsymbol{z_0})$ and $\dot{\bar{\boldsymbol{r}}}_0 = (\dot{\boldsymbol{x}}_0, \dot{\boldsymbol{y}}_0, \dot{\boldsymbol{z}}_0)$ are respectively its initial position and speed vectors, here written in Cartesian coordinates) or the relative Keplerian elements $(\boldsymbol{a_0}, \boldsymbol{e_0}, \boldsymbol{i_0}, \boldsymbol{\Omega_0}, \boldsymbol{\omega_0}, \boldsymbol{M_0})$;

2. Models of all the forces acting on the satellite along its orbit.

Starting from these elements, GINS calculates the numerical integration of the fundamental dynamics equation:

$$\ddot{\bar{r}} = \frac{d^2\bar{r}}{dt^2} = \sum_n \overline{F_i}\left(\bar{r}, \dot{\bar{r}}, \alpha_i\right) \tag{23}$$

where $\ddot{\bar{r}}$ is the satellite acceleration, $\sum_n \overline{F_i}$ the sum of the n forces acting on the orbiter and α_i the adjustable parameters on which the n forces depend. The integration of equation (23) conducts to the calculation of the desired orbit.
However, coupled with the trajectory computation, the adjustment of the initial state vector and of the adjustable dynamic parameters have also to be calculated. This step involves the derivation of the fundamental dynamics equation in relation to the respective elements ($\bar{r}_0$ and α_i) :

$$\frac{d^2}{dt^2}\left(\frac{\partial\bar{r}}{\partial\overline{r_0}}\right) = \frac{\partial\ddot{\bar{r}}}{\partial\overline{r_0}} = \sum_n \frac{\overline{\partial F}}{\partial\bar{r}} \cdot \frac{\partial\bar{r}}{\partial\overline{r_0}} + \sum_n \frac{\overline{\partial F}}{\partial\dot{\bar{r}}} \cdot \frac{d}{dt}\left(\frac{\partial\bar{r}}{\partial\overline{r_0}}\right) \tag{24}$$

$$\frac{d^2}{dt^2}\left(\frac{\partial\bar{r}}{\partial\alpha_i}\right) = \frac{\partial\ddot{\bar{r}}}{\partial\alpha_i} = \sum_n \frac{\overline{\partial F}}{\partial\bar{r}} \cdot \frac{\partial\bar{r}}{\partial\alpha_i} + \sum_n \frac{\overline{\partial F}}{\partial\dot{\bar{r}}} \cdot \frac{d}{dt}\left(\frac{\partial\bar{r}}{\partial\alpha_i}\right) + \sum_n \frac{\overline{\partial F}}{\partial\alpha_i} \tag{25}$$

All these three differential equations need to be solved with a very high precision, since GINS furnish results characterised by an excellent accuracy level. As a consequence, GINS adopts one of the actual most used integration method for orbitohraphy: the Cowell integration method [10].
This method was proposed in 19th century by Numerov and then developed by Cowell as a multistep "prediction-correction" method, which brings the resolution of differential equations. It proved to be particularly suitable for studies of orbital mechanics especially because:

- It allows to conserve in memory information relative to the previous steps (whose number depends on the integration degree), useful for interpolation at different dates from the current one;
- It requires less CPU time in comparison with direct integration methods.

Re-writing the dynamics fundamental equation in a more schematic form, it is possible to describe an artificial satellite motion as follows:

$$\ddot{\bar{y}}(t) = f\left(t,\ \bar{y}(t),\ \dot{\bar{y}}(t)\right) \tag{26}$$

This relation links the instantaneous satellite acceleration vector $\ddot{\bar{y}}(t)$ to the time instant t, the relative instantaneous position $\bar{y}(t)$ and speed $\dot{\bar{y}}(t)$ vectors, by a specific function f. As a consequence, elements $\ddot{\bar{y}}(t)$, $\dot{\bar{y}}(t)$ and $\bar{y}(t)$ correspond respectively to the $\ddot{r}$, $\dot{\bar{r}}$ and $\bar{r}$ terms used in equation (23), while the function f includes all the perturbing forces acting along the satellite orbit.
In order to resolve this vectorial differential equation, it is necessary to discretise the problem in a specific study interval time [t_0 , t_N], so that:

- $t_{n+1} = t_n + h$, where $n = 0, \dots, N-1$;

- $(\boldsymbol{N-1})$ is the number of time intervals discretizing the considered orbit arc;
- $\boldsymbol{h}$ is the discretization step.

At this point, the Cowell method searches for an approximation $\overline{\boldsymbol{y}}_{\boldsymbol{n}}$ of the equation (26) real solution $\overline{\boldsymbol{y}}$, at any instant $\boldsymbol{t_n}$ belonging to the study interval time [$\boldsymbol{t_0}, \boldsymbol{t_N}$], so that $\overline{\boldsymbol{y}}_{\boldsymbol{n}} \simeq \overline{\boldsymbol{y}}(\boldsymbol{t_n})$. Consequently, it is possible to consider the following approximations:

- $\overline{\boldsymbol{y}}_{\boldsymbol{n-i}} \simeq \overline{\boldsymbol{y}}(\boldsymbol{t_{n-i}})$;
- $\boldsymbol{f}(\boldsymbol{t_{n-i}}, \overline{\boldsymbol{y}}_{\boldsymbol{n-i}}, \dot{\overline{\boldsymbol{y}}}_{\boldsymbol{n-i}}) \simeq \boldsymbol{f}(\boldsymbol{t_{n-i}}, \overline{\boldsymbol{y}}(\boldsymbol{t_{n-i}}), \dot{\overline{\boldsymbol{y}}}(\boldsymbol{t_{n-i}}))$.

It is now possible to improperly adopt the following denomination: $\overline{\boldsymbol{y}} = \boldsymbol{y}$, $\dot{\overline{\boldsymbol{y}}} = \dot{\boldsymbol{y}}$ and $\ddot{\overline{\boldsymbol{y}}} = \ddot{\boldsymbol{y}}$. Moving on with the application of the finite difference method, it is possible to re-write the equation (26) in the following form:

$$\sum_{i=N}^{M} (\boldsymbol{a_{-i}} \cdot \boldsymbol{y_{n-i}}) = \boldsymbol{h}^2 \cdot \sum_{i=P}^{Q} (\boldsymbol{b_{-i}} \cdot \boldsymbol{f_{n-i}}) \qquad \textbf{(27)}$$

The first equation member is an $\ddot{\boldsymbol{y}}(\boldsymbol{t_n})$ approximation, resulting from Taylor's developments, while the second one is an $\boldsymbol{f}(\boldsymbol{t_{n-i}}, \boldsymbol{y_{n-i}}, \dot{\boldsymbol{y}}_{\boldsymbol{n-i}})$ approximation. In general, the inferior and superior limit values of the summations are set at: $\boldsymbol{N} = \boldsymbol{P} = -\boldsymbol{1}$, $\boldsymbol{M} = \boldsymbol{k}$ and $\boldsymbol{Q} = \boldsymbol{l}$, where $\boldsymbol{k}$ and $\boldsymbol{l}$ are the indexes we want to consider.

The following step is the $\boldsymbol{y}(\boldsymbol{t_{n-i}})$ development around $\boldsymbol{t_n}$, which allows to calculate $\dot{\boldsymbol{y}}_{\boldsymbol{n-i}}$ and $\ddot{\boldsymbol{y}}_{\boldsymbol{n-i}} = \boldsymbol{f_{n-i}}$. The numerical integration of these developments within equation (27), brings to:

$$\boldsymbol{a_1} \cdot \boldsymbol{y_{n+1}} + \boldsymbol{a_0} \cdot \boldsymbol{y_n} + \boldsymbol{a_{-1}} \cdot \boldsymbol{y_{n-1}} = \boldsymbol{h}^2 \cdot [\boldsymbol{b_1} \cdot \boldsymbol{f_{n+1}} + \boldsymbol{b_0} \cdot \boldsymbol{f_n} + \boldsymbol{b_{-1}} \cdot \boldsymbol{f_{n-1}}] \qquad \textbf{(28)}$$

After that, by identifying each member to its corresponding one, it is possible to find the appropriate values for coefficients $\boldsymbol{a_i}$ and $\boldsymbol{b_i}$:

$$\frac{1}{2}\boldsymbol{y_{n+1}} - \boldsymbol{y_n} + \frac{1}{2}\boldsymbol{y_{n-1}} = \boldsymbol{h}^2 \cdot [\frac{1}{24}\boldsymbol{f_{n+1}} + \frac{10}{24}\boldsymbol{f_n} + \frac{1}{24}\boldsymbol{f_{n-1}}] \qquad \textbf{(29)}$$

The $\boldsymbol{f_{n+1}}$ term intervenes in the previous equation, which shows that the descripted integration method is an implicit one, also defined as a correction method. It consequently means that it is necessary to preliminary use an explicit numeric integration method: a prediction method.

1. Prediction method: Firstly, this preliminary method allows to calculate a first $\boldsymbol{y_{n+1}}$ evaluation:

$$\sum_{i=-1}^{1} (\boldsymbol{a_{-i}} \cdot \boldsymbol{y_{n-i}}) = \boldsymbol{h}^2 \cdot \sum_{i=0}^{2} (\boldsymbol{b_{-i}} \cdot \boldsymbol{f_{n-i}}) \qquad \textbf{(30)}$$

This expression development brings to the following equation, expressed for instance, till the third order:

$$\boldsymbol{y_{n+1}} - \boldsymbol{2y_n} + \boldsymbol{y_{n-1}} = \frac{1}{12}\boldsymbol{h}^2 \cdot [\boldsymbol{13f_{n+1}} - \boldsymbol{2f_{n-1}} + \boldsymbol{f_{n-2}}] = \boldsymbol{h}^2 \cdot \boldsymbol{f_n} \qquad \textbf{(31)}$$

Its resolution enables the computation of the $\boldsymbol{y^{(0)}}_{\boldsymbol{n+1}}$ term, which will be the initial point in the correction method.

2. Correction method: Secondly, it is possible to pass to the correction step, using an iterative numeric method based on equations of the style of (29):

$$y^{(k+1)}{}_{n+1} - 2y_n + y_{n-1} = \frac{1}{12}h^2 \cdot \left[f\left(t_n, y^{(k)}{}_{n+1}\right) + 10f_n + f_{n-1}\right] \quad (32)$$

In such a way, it is now possible to define the y_{n+1} value:

$$y_{n+1} = \lim_{k \to \infty} y^{(k)}{}_{n+1} \quad (33)$$

Specifically, the GINS software uses this Cowell linked-step numeric integration method, adopting a constant integration step size and normally an 8 grade-integration, which consists in considering the actual state vector value, the three previous ones and the four following ones:

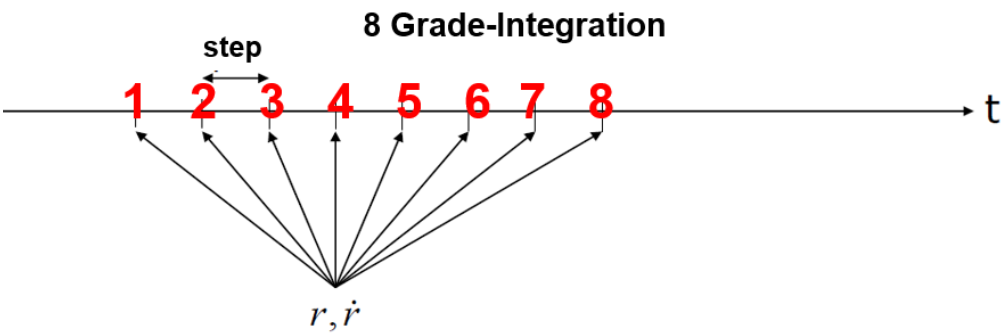

Figure 11 *- Schematic Cowell method representation.*

Now, coming back to the dynamics equation (23), it is also important to focus on which forces $\overline{F_i}$ the GINS software takes into account to compute the satellite acceleration along its orbit. GINS has the access to the detailed description of all the possible force and relative acceleration models it can uses, by the documentation contained in the "*Obelix*" numerical library [11].
Within all forces acting on satellites, it is possible to make a distinction between gravitational and non-gravitational ones.

1. Gravitational forces: their definition in GINS is based on calculation of the gravitational potential of the central and perturbing bodies, which cause satellite accelerations that can be expressed as spherical harmonic functions. Gravitational force origins are multiple:

- <u>Central body gravity potential</u>: the central body attraction acting on satellites, is due to its potential ***U***, conventionally expressed in a system of spherical coordinates (r, φ, λ):

$$U = \frac{\mu}{r} \cdot \sum_{l}^{l_{max}} \sum_{m=0}^{l} \left(\frac{a_e}{r}\right)^l \cdot \overline{P}_{lm}(\sin\varphi)\left[\overline{C}_{lm}\cos(m\lambda) + \overline{S}_{lm}\sin(m\lambda)\right] \quad (34)$$

This definition, almost equivalent to equation (12) and valid if the distance r from the central body centre of mass is larger than its semi-mayor axis a_e, contains the normalized Legendre function $\overline{P}_{lm}(\sin\varphi)$, the normalized Stokes coefficients $\overline{C}_{lm}$ and $\overline{S}_{lm}$, (equation (18)) and the standard gravitational parameter μ.
Once defined the gravitational potential, the acceleration $\overline{a}$ produced on the satellite by the central body is calculated in the rotating frame linked to this specific celestial body:

$$\overline{a} = \left(\frac{\partial U}{\partial x}, \frac{\partial U}{\partial y}, \frac{\partial U}{\partial z}\right) \tag{35}$$

Since the gravity field of a celestial body is completely defined by the μ and the a_e parameters, $\overline{C}_{lm}$ and $\overline{S}_{lm}$ coefficients are free. As a consequence, their partial derivatives are calculated:

$$\begin{aligned} \frac{\partial U}{\partial \overline{C}_{lm}} &= \frac{\mu}{r} \cdot \left(\frac{a_e}{r}\right)^l \cdot cos(m\varphi)\, \overline{H_l^m}(sin\varphi) cos(m\lambda) \\ \frac{\partial U}{\partial \overline{S}_{lm}} &= \frac{\mu}{r} \cdot \left(\frac{a_e}{r}\right)^l \cdot cos(m\varphi)\, \overline{H_l^m}(sin\varphi) sin(m\lambda) \end{aligned} \tag{36}$$

where $\overline{H_l^m}$ represent the Helmoltz polynomials.

- Perturbing body potentials: particularly interesting for this internship project, a perturbing object is any celestial body, other than the central one, which exercises a gravitational influence over the satellite motion. Effectively, gravitational accelerations generated by all the perturbing bodies, have to be added together, to compute their total action on the spacecraft orbit.
  In order to understand how these forces act, it is possible to consider an inertial system with origin in ***O***, where only one perturbing body $\boldsymbol{P}$, characterized by a mass $\boldsymbol{M_p}$ influences the motion of the spacecraft ***S*** around the central body ***C*** :

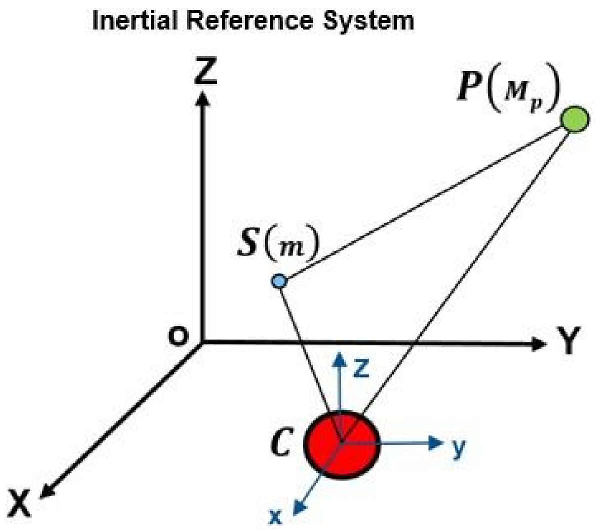

Figure 12 *- Representation of three-body reference frame.*

Now, it is possible to define two different acceleration terms. The first one is the *central term* of the perturbing body acceleration:

$$\overline{a_s}^{RC} = -G \cdot M_P \cdot \frac{\overrightarrow{PS}}{|\overrightarrow{PS}|^3} + \frac{\overrightarrow{CP}}{|\overrightarrow{CP}|^3} \tag{37}$$

In order to take into account of all the perturbations caused by secondary bodies, the celestial body point-mass hypothesis is not sufficient. Thus, it is necessary to add a specific second term, referred to as the *coupling term* of the perturbing body acceleration.

This term, limited to the $\boldsymbol{C_{20}}$ coefficient of the harmonic development of the potential of the central body, is expressed in the following form:

$$\overline{\boldsymbol{a_s}}^{\boldsymbol{Coupling}} = -\frac{3}{2}\sqrt{5}\ \frac{\boldsymbol{G \cdot M_C}}{\left|\overrightarrow{\boldsymbol{CP}}\right|^5} \cdot \boldsymbol{a_e}^2 \cdot \overline{\boldsymbol{C}}_{20} \left[\mathbf{5}\boldsymbol{sin}^2(\boldsymbol{\varphi_p}) - \mathbf{1} \begin{pmatrix} x_p \\ y_p \\ z_p \end{pmatrix} - \mathbf{2} \begin{pmatrix} 0 \\ 0 \\ z_p \end{pmatrix} \right] \quad \textit{(38)}$$

Moreover, it is important to underline that differently from the previous case, in this force model, no parameter is free.

- Surface masses: particular massive elements on central body surface can generate an acceleration $\overline{\boldsymbol{a}}$ on satellite motion. This acceleration, normally expressed in the primary body rotating frame, can be computed, knowing the main features of these surface elements: their mass, height and instantaneous distance from the satellite flying over them.

- Potential of Earth tides: Earth tides influence satellite orbit, by generating accelerations derived from the central body deformation potential, due to gravitational effects of perturbing bodies. This deformation potential is described by four different terms:
  - $\boldsymbol{U} = \boldsymbol{U_k}$: Earth tide potential
  - $+\Delta\boldsymbol{U_{\delta k}}$: frequency dependent correction of Love numbers $\boldsymbol{K_{lm}}$ of the deformation [12]
  - $+\Delta\boldsymbol{U_e}$: correction of ellipticity
  - $+\Delta\boldsymbol{U_p}$: correction of Earth polar tide

- Potential of fluid tides: it is induced by the water mass movement, caused by perturbing body the potential. This movement is not only radial and the horizontal displacement is highly perturbed by the presence of the continents. Generically, fluid waves are classified in long-period, diurnal and semi-diurnal waves, and they are divided into main (whose amplitude is defined by the model) and secondary (whose amplitude is computed by the admittance) waves.

- Potential of solid and ocean polar tides: this model enables the consideration of solid Earth response to the rotational movement. It is computed taking into account the rotation pole posting in relation to the mean pole and employing spherical harmonic coefficients.

- Potential of atmospheric pressure variations: this template considers the gravitational potential generated by the displacement of atmospheric masses.

- Relativistic forces: the relativistic effects are considered as second order perturbation within the non-relativistic mechanics adopted to integrate the satellite dynamics equations. The model considered in GINS comprises three terms: the Schwarzschild (the most significant), the Coriolis (or geodetic precession) and the Lense-Thirring (relativistic effects due to the rotation of the central body) terms.

2. Non-Gravitational forces: their definition in GINS is free from celestial body gravitational characteristics. The software takes into account the following Non-Gravitational acceleration origins:

- Atmospheric layers: the atmospheric friction generates a satellite acceleration, which is computed in GINS as the sum of frictional forces applied to every elementary spacecraft structural part (flat facets, cylinders, spheres or semi-spheres). In fact, each particular shape produces a drag and lift acceleration.

- Direct solar pressure: the solar radiation pressure causes a satellite acceleration because of the received solar flux action. GINS calculates it, by adding up all the elementary radiation influences over each satellite surface components. Moreover, the software is able to compute when the global received solar flux needs to be attenuated by the presence of one or more bodies between the Sun and the satellite (eclipse condition). In fact, a shadow function is introduced (between 0 and 1) to represent the effective solar flux received by the satellite.

- Re-diffused and infra-red radiation pressures: the re-diffused radiation pressure is the origin of a satellite acceleration, mainly caused by the action of the solar flux re-transmitted by the central body. However, if a part of this body is in a shadow condition, it does not transmit any albedo flux, exactly as for a satellite passing in an eclipse zone, it is considered not to receive any albedo effect. At the same time, the infra-red radiation pressure generates another satellite acceleration due to the action of the infra-red flux transmitted by the central body. Once again, GINS calculates both these influences through the addition of each elementary accelerations applying on every satellite exposed surface parts.

- Empirical accelerations: in order to decrease the effects of modelling faults, model imprecisions, poor knowledge of physical or thermo-optical satellite properties, a set of empirical accelerations is adopted by GINS. They can be added to the main acceleration total sum in the three directions, at each integration step.

GINS third step: Calculation of theoretical measurements and measure residuals

Normally, an artificial satellite is supposed to realise different kinds of measurements along its trajectory, in relation to the mission purposes.
The GINS software employs specific techniques in order to take into account this measuring capacity.

Firstly, theoretical quantities of measurements ($\boldsymbol{Q_{th}}$) are calculated, using if necessary, the very precise knowledge of the Earth ground station positions and of their movements due to plate tectonics and loading phenomena.
In this context, GINS is able to process several measure techniques: Laser Telemetry, VLBI, Optical, Altimetric, Crosspoint, Doppler (DSN or ESA network), PRARE, GNSS, inter-satellite (GRACE) and Gradiometric (GOCE) measurements can be directly treated by the software.
Despite the multiple measures, the most of them can be defined in GINS using two main modelled physical parameters, relative to optical and radio signal: the *travel time* $\boldsymbol{\tau}$ and the *geometric distance* $\boldsymbol{d}$.
The first one includes the signal geometric travel time ($\boldsymbol{\tau_{geom}}$), to be added to relativistic propagation corrections ($\boldsymbol{\tau_{rel}}$) and delays ($\boldsymbol{\tau_{del}}$) occurring when signals cross the atmosphere (for ground receivers), troposphere, ionosphere, interplanetary medium (plasma, for interplanetary measurements) and solar corona proximity. As a consequence, the travel time is considered to be composed of three terms:

$$\boldsymbol{\tau = \tau_{geom} + \tau_{rel} + \tau_{del}} \tag{39}$$

The first term, $\boldsymbol{\tau_{geom}}$, is obtained directly from geometric distance, which is calculated by a GINS specific *measurement function*. The latter returns the distance between any two objects (orbiters, stations, quasars) according to their positions $\vec{\boldsymbol{P}}$ at the time instant $\boldsymbol{t_1}$, corresponding to the signal emission from the emitter (object ***1***), and at the time instant $\boldsymbol{t_2}$, identifying the signal reception through the receiver (object ***2***):

$$d_{geom} = c \cdot \tau_{geom} = |\vec{P}_2(t_2) - \vec{P}_1(t_1)| \tag{40}$$

Once GINS computed the desired measurement theoretical quantities (Q_{th}), the next step is the measurement adjustment. This action consists in the comparison between theoretical quantities and actual measurements (Q_{obs}) of the measure type ***i***, in order to find its residual R_i :

$$R_i = Q_{obs,i} - Q_{th,i} \tag{41}$$

This residual quantity contains both the probable measurement instrumental noise and the inaccuracy contribution caused by errors in theoretical quantity modelling.
The process to establish the best measure value possible, continues with the minimization of the deviations between actual and theoretical measurements. In fact, the global residuals are gradually reduced in GINS iterations until convergence is achieved, by adjusting physical and empirical parameters set as adjustable (free) in a specific study case.

GINS fourth step: Numeric calculation of normal equations

As expressed before, at each iteration GINS computes the residual R_i of all the *n* types of measurement taken into account in a specific study case. Moreover, each of these types is associated with a particular weight π_i, specified in the "*Director*" file *measurement* section. Therefore, the following expression is considered for each measure i $(= 1, 2, \ldots, n)$:

$$\begin{cases} R_i = Q_{obs,i} - Q_{th,i}(\vec{X}) \quad (\pi_i) \\ \quad \vec{X} = (X_1, X_2, \ldots, X_p) \end{cases} \tag{42}$$

As this expression shows, every theoretical measurement is a non-linear function of the parameters X_j (***j*** = 1, 2, …, p), which take part in its calculation. All or part of these parameters are refined by writing the linearization in the first order of the measurement equations according to the following general expression:

$$Q_{th,i}(\vec{X} + \Delta\vec{X}) = Q_{th,i}(\vec{X}) + \sum_k \frac{\partial Q_i}{\partial X_k} \Delta X_k \quad (\pi_i) \tag{43}$$

where the X_k variable represents the a priori (or current) value of a parameter, the ΔX_k term is the correction to this X_k value and it is a component of the parameter correction vector $\Delta\vec{X}$, and the $\frac{\partial Q_i}{\partial X_k}$ terms correspond to the partial derivatives of the theoretical quantities computed by the *measurement function*.
At this point, considering the set of ***p*** parameters $\vec{X} = (X_1, X_2, \ldots, X_p)$ and the residuals of the set of ***n*** weighted measurements $\vec{R} = (R_1, R_2, \ldots, R_n)$ GINS is able to generate the matrix system of the linear observation equation (43), linked to each type of measures:

$$A_{n,p} \Delta\vec{X} = \vec{R} + \vec{\varepsilon} \quad (\pi_{n,n}) \tag{44}$$

where $\vec{\varepsilon}$ is the residual error between theoretical $Q_{th,i}(\vec{X} + \Delta\vec{X})$ and actual $Q_{obs,i}$, $A_{n,p}$ is the ***n***x***p*** partial derivative matrix, while $\pi_{n,n}$ is the ***n***x***n*** measurement weight square matrix. The latter is a diagonal matrix if all the considered measurement types are independent, but it may contain non-diagonal elements in case of measurements correlated with one another.
The GINS objective is to minimize the residual error $\vec{\varepsilon}$, using the conventional least square method. This resolution method allows to demonstrate that:

$$\boldsymbol{A^T \pi \vec{\varepsilon} = \vec{O}} \tag{45}$$

Consequently, by multiplying all members of matrix system (44) by the $\boldsymbol{A^T \pi}$ term, it is possible to obtain the corresponding normal equations:

$$\boldsymbol{A^T \pi A \Delta \vec{X} = A^T \pi \vec{R}} \tag{46}$$

The latter represents the standard ***normal equation***. However, in "degraded" cases, in which a low number of measurements in relation to the considered parameters generates an under-determined system, it may be useful to add to the (46) a set of $\boldsymbol{n_c}$ equations of constraints applying to all or part of the parameters. These constraint equations are generated in a second phase, by the DYNAMO chain (directly connected with GINS) and they can be expressed in the following form:

$$\boldsymbol{C_{p,p} \Delta \vec{X} = \vec{O}} \tag{47}$$

where the $\boldsymbol{C_{p,p}}$ term represents the matrix of constraints on parameters, which has to be added to the standard normal equation matrix $\boldsymbol{A^T \pi A}$, in order to generate the normal constrained system:

$$\boldsymbol{(A^T \pi A + C) \Delta \vec{X} = A^T \pi \vec{R}} \tag{48}$$

The term on the right is referred to as the *second term* of the normal equation: $\boldsymbol{\vec{D}} = \boldsymbol{A^T \pi \vec{R}}$. The complete system matrix $\boldsymbol{\vec{N}} = \boldsymbol{A^T \pi A + C}$ is called *normal matrix*, and it is defined as *constrained* if the $\boldsymbol{C}$ matrix is non-zero.

Once the process reached the convergence, GINS stores the normal equation relative to each types of measurement in the output file *"Normal Equations".*

Moreover, another index is calculated by GINS: the a priori standard residual variation, before the resolution:

$$\boldsymbol{\sigma^2 = \frac{\vec{R}^T \pi \vec{R}}{n}} \tag{49}$$

<u>GINS fifth step: Resolution of the parameters</u>

Once collected all the normal equations, GINS pass to their numerical resolution by an inversion method:

$$\boldsymbol{\Delta \vec{X} = (A^T \pi A + C)^{-1} A^T \pi \vec{R}} \tag{50}$$

Using this invers equation, it is possible to calculate the measurement residuals and their a posteriori variance:

$$\boldsymbol{\vec{R}' = \vec{R} - A \Delta \vec{X}} \tag{51}$$

$$\boldsymbol{\sigma'^2 = \frac{\vec{R}'^T \pi \vec{R}'}{n - p + n_{cont}} = \frac{n\sigma^2 - \Delta \vec{X}^T D}{n - p + n_{cont}}} \tag{52}$$

At the same time, the formal uncertainty is given by the diagonal terms of the variance-covariance matrix:

$$\boldsymbol{C_{ov} = \sigma'^2 (A^T \pi A + C)^{-1}} \tag{53}$$

<u>GINS Iterations:</u> As shown in Figure 10, GINS adopts an iterative approach: once generated the normal equations, the software repeats all its steps starting from the numerical integration for the orbit computation.

In the first iteration, the parameters are initialized at their a priori value, depending on the selecting model, and the software calculates the measurement residuals and their partial derivatives, building the normal equation system for the first time and invers it to find a first solution.
Then, in each iteration, the obtained correction $\Delta\vec{X}$ is added to the current value $\vec{X}$, which is taken into consideration for computing theoretical measurement quantities and their residuals. These iterations continue until convergence is reached, this means when global residual variation assumes a lower value then the desired convergence criterion ε_{conv}, according to the following expression:

$$\frac{[\sum_n R_i^2]_{iter} - [\sum_n R_i^2]_{iter-1}}{[\sum_n R_i^2]_{iter-1}} < \varepsilon_{conv} \tag{54}$$

Both the convergence criterion and the maximal number possible of iterations can be chosen by the user, who has to express them in the "*Director*" file.
The set of normal equations can be saved on demand once the convergence is achieved or after an additional iteration. This particular iteration starts from the beginning of the orbit numeric integration, but continues only until the generation of the normal equation matrix, which in this case is stocked in the "*Normal Equations*" output file. If this last iteration is requested, the final value of the parameters (sum of a priori values and successive corrections obtained in the iterations, is used for the additional iteration, in which the residuals of the retained measurements and the partial derivatives are recalculated. If an additional iteration is imposed, residuals of the retained measurements and their partial derivatives are recalculated. In this case, normal systems without constraints are then rebuilt and stored in "*Normal Equations*" output files, which are ready for use by the programs in the DYNAMO chain.

2.1.4 DYNAMO chain

The DYNAMO chain consists in a series of programs which uses the furnished normal equations and performs usual linear algebra operations:

1. DYNAMO-D: this program allows to resolve a normal equation, using three possible inversion techniques: the Cholesky method, the conjugate gradient method or the specific value and vector method. As before, resolving normal equations in DYNAMO consists in inverting the normal matrix ***N*** (with possible constraints), in order to obtain the solutions:

$$\vec{X} = \vec{X}_0 + \Delta\vec{X} = \vec{X}_0 + N^{-1}\vec{D} \tag{55}$$

where $\vec{X}_0$ represents the a priori values of the parameters.
Again, the a posteriori residual variance σ'^2 is computed through the a priori value σ^2, by the following expression:

$$\sigma'^2 = \sigma^2 + \frac{\vec{D}^T \Delta\vec{X}}{n-p} \tag{56}$$

Its output consists in a file containing solutions, possibly with the variances or the complete covariance matrix of the parameters, according to the selected inversion method. Before the inversion, it is also possible to add a predefined constraint equation (Kaula's law for gravity field coefficients, the minimum constraints for station network solutions or a set of constraint values specified by the user).

2. DYNAMO-B: this DYNAMO tool leads to normal equation reduction. By reducing a normal equation, only its most useful parameters are retained. This operation is essential when working with equations containing a very high number of parameters: they are determined by combining the observations over several months or years. This operation consists in excluding from the equation those parameters which do not need to be solved. The latter can either be completely eliminated (fixed to their initial values and ignored) or reduced (resolved and reinjected in the normal equation system).

3. DYNAMO-C: this DYNAMO module allows the combination of several normal equations (which may be weighted) in a single equation by summing the various contributions on the common parameters. Considering two normal equations, weighted by $\boldsymbol{\pi_1}$ and $\boldsymbol{\pi_2}$, the following operations are performed:

$$\begin{cases} \boldsymbol{\pi_1} \cdot \left(\boldsymbol{N_1}\Delta\overrightarrow{\boldsymbol{X}} = \boldsymbol{D_1}\right) \\ \\ \boldsymbol{\pi_2} \cdot \left(\boldsymbol{N_2}\Delta\overrightarrow{\boldsymbol{X}} = \boldsymbol{D_2}\right) \end{cases} \rightarrow \quad (\boldsymbol{\pi_1 N_1} + \boldsymbol{\pi_2 N_2})\Delta\overrightarrow{\boldsymbol{X}} = (\boldsymbol{\pi_1 D_1} + \boldsymbol{\pi_2 D_2}) \qquad \textbf{\textit{(57)}}$$

In this case, the variance is defined as:

$$\boldsymbol{\sigma^2} = \sum_{\boldsymbol{i}} \pi_i \, \boldsymbol{\sigma_i}^{\boldsymbol{2}} \qquad \textbf{\textit{(58)}}$$

4. DYNAMO-P: this program is useful to act the permutation of a normal equation. In fact, it places the equation unknowns in a predefined sequence by permuting the order of lines and columns of the matrix and of the second member. After the permutation, if two or more identical unknowns are detected, they are compacted into a single unknown.

5. DYNAMO-W: this module applies the research for optimal weighting. This aspect is important, since it is often needed to combine normal equations derived from observation of different tracking systems, natures, precisions, etc. This search aims to estimate the weight of each equation set, in order to obtain the optimal combination of the various measurements, thereby producing the most accurate solution of parameters to be determined.

2.2 Python *Visualisation Module*

As mentioned before, in the context of this internship, GINS outputs needed to be treated by a visualisation tool, which enables an intuitive an immediate interpretation of the obtained results. This particular need led to the generation of a specific informatics module, coded in Python language and able to simplify the result comprehension.
Since the multiple quantity of result types to be analysed within this project, several functions have progressively become part of the Python ***Visualisation Module***.

Firstly, this project has required an orbital study, focused on QSO trajectories realised by the satellite around Mars, in constant proximity to its main target, Phobos.

Considering this orbital design, as explained in paragraph 2.1.1, GINS gives birth to "*Ephemeris*" output files, mainly containing the satellite state vector components et every demanded time instant, in relation to the central body (Mars, in this case).
This aspect resulted in the creation of several specific Python functions, designed to deal with this output kind:

- "***Trace_Orbits_GINS***" function: its primary input is exactly an "*Ephemeris*" file resulting from GINS, and its output is a 3-Dimensional representation of the described orbit trace, within a Cartesian coordinate system (***x***,***y***,***z***). Moreover, if the user desires, it is also able to create the graph relative to the evolution in time of satellite speed. Furthermore, this function (along with all the next ones) has the possibility to take into account the presence of a multi-satellite situation.
  In the specific MMX study case, this function has been employed for tracing satellite QSO trajectories around Mars. Examples of the derived orbit visualisation are presented in the first column of Figure 4 and Figure 5.

- "***Trace_Orbits_Phobos_Centered***" function: its main input is again represented by the GINS "*Ephemeris*" output file, relative to the satellite orbits around the primary body. However, if requested by the user, it can also receive two of these inputs, since it is able to treat two orbits together, while comparing them. Its second input type is newly an "*Ephemeris*" file, but relative to the secondary body ephemeris around the primary. This function realises an interpolation (whose function is detailed below) of the secondary ephemeris, in relation to the satellite time vector containing all its integration instant. In this way, the position vectors of both the satellite and the secondary body are obtained at the same time moments. Consequently, a displacement of the reference system origin is applied. The latter consists in the subtraction between position components of the satellite and the secondary body, leading to the computation of satellite trajectory expressed in the reference system centred on the secondary object. Finally, its 3-Dimensional representation in the Cartesian coordinate system is provided as output. Moreover, if demanded, this function can apply the same procedure to speed vectors.
  Within the MMX context, this function enables to pass from satellite QSO centred on Mars, to trajectories expressed in Phobos-centred frame. Visual examples are shown in the second column of Figure 4 and Figure 5.

- "***Trace_Dist_Eph***" function: its input can still be an "*Ephemeris*" GINS file expressed in the central body reference frame, or the trajectory file generated by the previous "*Trace_Orbits_Phobos_Centered*" function, cantered on the secondary body. It is able to trace the time evolution of several distance parameters, in relation to user's need: the satellite position vector modules or only its three Cartesian components, separately.
  In the MMX mission study, this function enables the trace these satellite position distances, in relation to Mars or Phobos centre of mass.

- "***Trace_Dist_Multi_Eph***" function: as its name suggests, it is similar to the previously described function "*Trace_Dist_Eph*". In fact, it considers exactly the same input types, but it needs two of these files. The direct consequence is that, according to user's request, this function can trace on the same graph the distance parameter time evolution of both the orbits defined in the two inputs. Moreover, it also enables the visualisation of relative differences between the two trajectories, considering again the position vector modules and/or each of their components.
  Within the internship project, this function has turned out to be useful for visualising relative distances between two QSO trajectories around Phobos. Resulting examples are presented in graphs in Figure 20.

- "***Interp_Ephem***" function: it is the ephemeris interpolation function, employed by the previous ones. Its inputs are the time vectors of both the trajectory to be interpolated and to be used as reference, and the corresponding series of one position coordinate, to be interpolated. In this way, using this function on all the three position coordinates, separately, the complete interpolated satellite position vector is obtainable. This orbital interpolation is computed by a Lagrange function of order 8. This specific order has been chosen in order to be consistent with the Cowell grade 8 integration method employed by GINS.

Secondly, as specified before, during Phobos exploration phase of the MMX mission, several measurement types will be employed. The measure techniques here taken into account for the geodesic analysis are the Doppler DSN, the LIDAR and the Optical navigation images.
While the latter two can be represented as particular type of ephemeris measurements, Doppler captures provide completely different results. Consequently, they need separate functions, allowing their visual representation:

- "***Trace_Dop_Mesure***" function: its input is the DSN "*Measurements*" GINS output file, which provides the measure values and their time instants, employed for tracing Doppler measurement evolution in time. Examples of this representation are reported in Figure 24 and Figure 25.

- "***Trace_Point_Mesure***" function: its first input is an "*Ephemeris*" file, describing the orbit along which the satellite realises Doppler captures, whose "*Measurements*" file constitutes the second input. It traces the positions where these measurements are taken, along a specific orbit.
  Within the MMX mission analysis, this function is a significant tool for visualising the QSO sections covered by DSN captures. Examples of these traces are reported in Figure 27.

Finally, throughout QSO trajectories and specific measurement techniques, the MMX satellite is sensed to return the most precise Phobos gravity field possible. The evaluation of the accuracy level obtainable by the MMX mission in recovering this geodesic parameter has been realised by the GINS adjustment (paragraph 2.1.3) of Phobos gravity Stokes coefficients (detailed in the following chapters).
A visual representation of this adjustment capacity is thus necessary in order to immediately interpret the results. This graphical expression has been obtained through the development of a specific function:

- "***Coeff_Grav***" function: its main inputs are two files containing the normalised Stokes coefficients, defining two different Phobos gravity models. The first one represents the most accurate model of this project, employed as reference realistic template, while the second one corresponds to the corrected gravity model, returned after the GINS adjustment procedure. All these coefficients are graphically represented by rectangular blocks, composing the typical pyramidal shape of spherical harmonic representation, relying on degrees $\boldsymbol{l}$ and orders $\boldsymbol{m}$ (Figure 7).
  In order to estimate the reached adjustment precision level, the percentage difference is computed between every corresponding $\overline{\boldsymbol{C}}_{\boldsymbol{lm}}$ and $\overline{\boldsymbol{S}}_{\boldsymbol{lm}}$ belonging to the two different models. A special colour scale is used to underline this difference: the more the adjusted coefficients are similar to the reference ones, the more their block assumes a colour close to the blue. On the contrary, if this difference increases, they tend to a reddish colour.
  In this MMX analysis, this function has resulted to be a powerful tool, able to elucidate the Phobos gravity recovery performances both of each QSO trajectory and of the entire mission. Examples of resulting graphs are presented in Figure 38.

3 Internship project development

As expressed before, the main internship objective is the analysis of Phobos geodesic features, especially its gravity field.
In order to reach this target, multiple development steps had been necessary. This step chain is represented in the following schema:

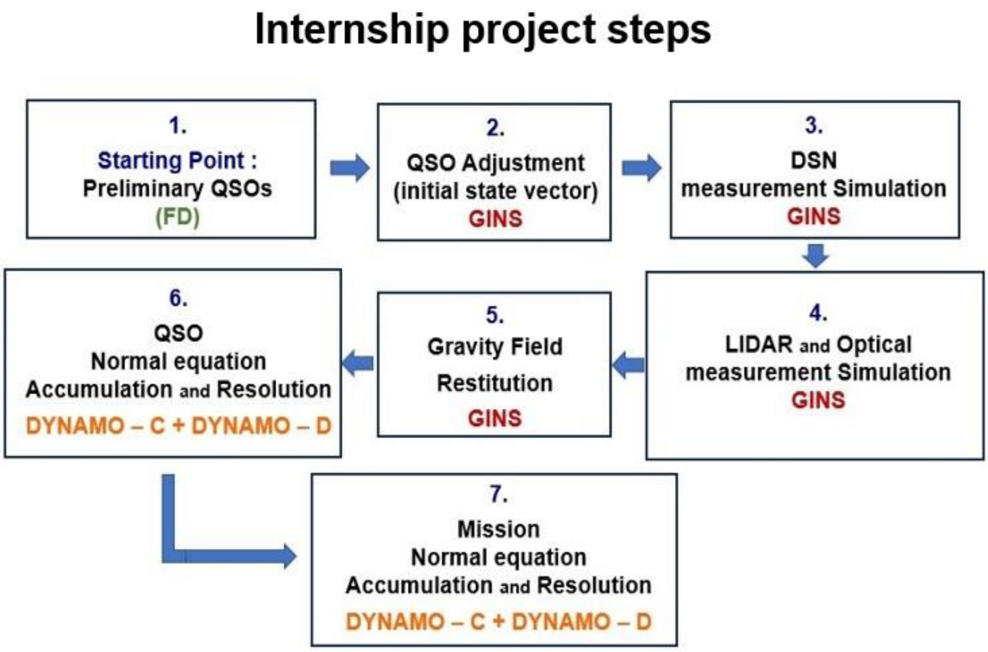

Figure 13 *- Schema representing the step series followed to develop the internship project.*

Each of these development steps has required the coding of specific scripts in Bash and Fortran languages, aimed at generating and treating the needed input and output files for the GINS software and its DYNAMO chain.
A detailed description of each project step is reported in the following paragraphs.

3.1 Starting point: preliminary QSO trajectories

During the MMX phases designed for Phobos exploration, the satellite will realise several QSO trajectories, allowing it to stay in near proximity to the Martian moon.
The JAXA FD team has already simulate these orbits: they represent the preliminary QSOs for the CNES Space Geodesic group.
Primarily, in order to employ these simulated trajectories for a realistic mission analysis throughout the GINS software, they have to be adjusted to get the same GINS high precision level. Successively, multiple procedures can be applied over the corrected trajectories, for the purpose of realising the desired geodesic analysis.

Thus, the starting point of this internship project is exactly represented by the set of preliminary QSO trajectories simulated by the FD teams.
Effectively, all the QSOs necessary to complete the MMX mission part relative to Phobos, have already been fixed by the JAXA. The last update to this specific set of trajectories was established by the Japanese Space Agency in May 2020, and it represents the QSO database used to develop the internship project.
Each of these orbits is characterized by three size parameters ***X***, ***Y*** and ***Z***, where the latter is different from zero for only 3-Dymensioanl orbits. This specific identification is adopted because of the impossibility of describing QSOs through the common orbital parameters: as detailed in paragraph 1.3, these trajectories are not Keplerian movements, consequently a characterisation different from the six Keplerian orbital elements (paragraph 2.1.2) has to be used.
Moreover, they are also defined by an approximate revolution period around Mars and fixed initial and final dates (all the considered QSOs last between 14 and 35 days).
The list of the thirty-three selected QSO in the following table:

Name	Type	X [km]	Y [km]	Z [km]	Pseudo period [h]	Start (TDB)	End (TDB)	CNES ref
QSO-H	2D High altitude	100	200	0	7.6	2025 OCT 15 2025 DEC 15 2026 JAN 15	2025 NOV 14 2026 JAN 15 2026 FEB 14	10_H_2D
QSO-M	2D Medium altitude	50	96	0	7.1	2025 NOV 15 2026 FEB 15 2026 JUL 15 2026 AUG 15 2026 SEP 15 2026 OCT 15 2026 NOV 15 2027 JAN 15 2027 FEB 15 2027 MAR 15 2027 MAY 15 2027 JUIN 15 2027 AUG 15 2027 SEP 15 2027 OCT 15 2027 NOV 15 2027 DEC 15	2025 DEC 14 2026 MAR 02 2026 AUG 13 2026 SEP 13 2026 OCT 14 2026 NOV 13 2026 DEC 14 2027 FEB 13 2027 MAR 16 2027 APR 13 2027 JUIN 13 2027 JUL 14 2027 SEP 13 2027 OCT 14 2027 NOV 13 2027 DEC 14 2028 JAN 13	11_M_2D
QSO-L-A	2D Low altitude	30	50	0	5.8	2026 MAR 01 2026 DEC 01 2027 JAN 01 2027 APR 01 2027 MAY 01 2028 JAN 15	2026 MAR 30 2026 DEC 30 2027 JAN 15 2027 APR 30 2027 MAY 15 2028 JAN 13	12_L_2D
QSO-L-B	2D Low altitude	22	32	0	4.4	2026 APR 01 2026 MAY 01 2026 JUIN 01 2026 JUL 01	2026 APR 30 2026 MAY 30 2026 JUIN 30 2026 JUL 16	12_Lb_2D
QSO-L-C	2D Low altitude	20	27	0	3.8	2026 JUIN 01 2026 JUL 01	2026 JUL 01 2026 JUL 14	12_Lc_2D
QSO-M-3D	3D Medium altitude	50	100	25		2027 JUL 15	2027 AUG 14	

Table 1 *- Table containing all the QSO trajectories, which will be used in the MMX mission.*

At the same time, all the QSO trajectories appearing in the table below, are organised in four different MMX mission phases, in order to reach the prefixed objectives in the best way possible:

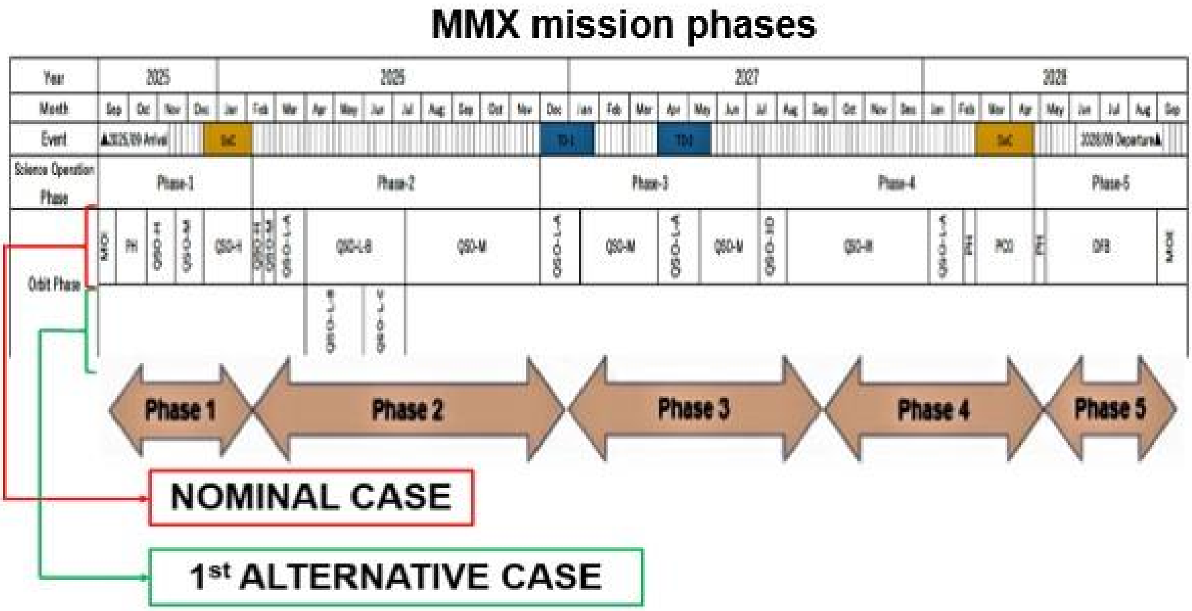

Figure 14 *- QSO repartition between the MMX mission phases, in nominal and first alternative cases.*

Each particular combination of QSO trajectories is recognized to be the best one to fulfil the purpose of every phase:

- ***Phase 1***: referred to as LSS phase, it consists in a first Phobos observation, leading to the Landing Site Selection.
- ***Phase 2***: referred to as LSS-MEGANE phase. MEGANE stands for "Mars-moon Exploration with GAmma rays and NEutrons". This is a gamma ray and neutron observation instrument to clarify the characteristics of chemical elements constituting Phobos ground. It allows the observation of the major elements and hydrogen composing the global target surface, which can be used for selecting the sampling location.
- ***Phase 3***: it represents the spacecraft landing moment on Phobos surface.
- ***Phase 4***: it consists in a series of trajectories leading the satellite to escape from Phobos.
- ***Phase 5***: it represents the moment of the possible flyby or rendez-vous with the second Martian moon, Deimos. Since Phobos is no more the main target in this mission phase, the latter has not been considered within the internship project.

As Table 1 shows, QSO trajectories are characterized by different designations, depending on their orbital size and the altitude ***h*** they reach over Phobos surface:

- **QSO-H**: they are 2-Dimensional orbits, reaching high altitudes over Phobos surface (***h*** ≥ 100km) and characterised by a revolution period of about 7.6h. This trajectory class is exclusively adopted during the initial MMX phase, when the satellite is still quite distant from the Martian moon, but starts to move nearer.
- **QSO-M**: they are 2-Dimensional orbits, reaching medium altitudes (100km ≤ ***h*** < 50km) and characterised by a revolution period of about 7.1h. This class of orbits is adopted in all the MMX phases.
- **QSO-M-3D**: as specified by its name, it is a 3-Dymensional orbit class, characterized by a medium size, as the QSO-M trajectories, and used in the first period of the fourth mission phase.

- **QSO-L**: they are 2-Dimensional orbits, reaching low altitudes (***h*** ≤ 50km). Within this trajectory class, there are three different subgroups. The QSO-L-A are characterised by a revolution period of about 5.8h and they have a role in the second, third and fourth mission phases. The QSO-L-B and the QSO-L-C are smaller than the previous one: with a period of 4.4h and 3.8h respectively, they are used in the second MMX phase.

For what concerns the last mentioned second phase, it is important to point out a particular aspect. As exposed in Figure 14, the JAXA not only has already fixed a nominal combination of QSO trajectories composing the second MMX phase, but also a first alternative case. In the standard situation, the QSO-L-B trajectory is covered by the satellite for a period starting on the 01/04/2026 and finishing on the 15/07/2026. The possible alternative is bringing the QSO-L-B final date forward to the 01/06/2026 and adding a consecutive QSO-L-C trajectory, continuing until the 15/07/2026. Both this study cases have been analysed in this project.

However, as Table 1 and Figure 14 underline, the nominal and first alternative sets of QSOs manly consist in 2-Dimensional orbits, with the only exception of one 3-Dymensional trajectory. Nevertheless, as explained before, orbits passing out Phobos orbital plane, are useful to reach the observation of a larger part of the target surface: their presence would be important to get better scientific objectives. As a consequence, a second alternative orbit set counting more 3-Dimensional QSOs, is being taking into account as a possible orbital solution. The table below lists different versions of the two QSO-M-3D groups considered for this second supplemental case:

Name	Type	X [km]	Y [km]	Z [km]	Pseudo period [h]	Start (TDB)	End (TDB)	CNES ref
QSO-M-3D-A	3D medium altitude	49.6 48.8 47.2 49.9 50.0	93.8 92.3 89.6 95.8 96.7	10.5 19.6 30.3 39.4 50.3		2026 SEP 01 2026 SEP 01 2026 SEP 01 2026 SEP 01 2026 SEP 01	2026 OCT 02 2026 OCT 02 2026 OCT 02 2026 OCT 02 2026 OCT 06	13_M_3D
QSO-M-3D-B	3D medium altitude	49.6 48.8 47.2 49.9 50.0	93.8 92.3 89.6 95.8 96.7	10.5 19.6 30.3 39.4 50.3		2027 JUL 15 2027 JUL 15 2027 JUL 15 2027 JUL 15 2027 JUL 15	2027 AUG 15 2027 AUG 15 2027 AUG 15 2027 AUG 15 2027 AUG 19	

Table 2 *- Table containing two possible groups (and different versions of them) of 3-Dimensional QSO trajectories.*

These 3-Dimensional QSO classes are referred to as QSO-M-3D-A and QSO-M-3D-B. Both them are medium-altitude orbits and five their versions characterized by different ***Z***-dimensions are being analysing at the moment. In the context of this project, only the two versions reaching the lower (QSO-M-3D-A1 and QSO-M-3D-B1) and the higher (QSO-M-3D-A5 and QSO-M-3D-B5) latitudes over Phobos surface, have been considered in order to analyse this third alternative case.
The latter thus differs from the nominal situation in the definition of the second and the fourth mission phases. In the second alternative phase, the period between the 01/09/2026 and the 02/10/2026 is covered by one of the first four versions of the QSO-3D-M-A trajectory, instead of the nominal QSO-M one. A second possible option is the use of the most inclined QSO-3D-M-A5, finishing on the 06/10/2026.

Instead, the fourth phase presents a substitution of the initial nominal QSO-3D-M trajectory with one of the first four versions of the QSO-3D-M-B, both ending on the 14/08/2027. Again, a second solution is the employment of the most inclined QSO-3D-M-B5, continuing until the 19/08/2027:

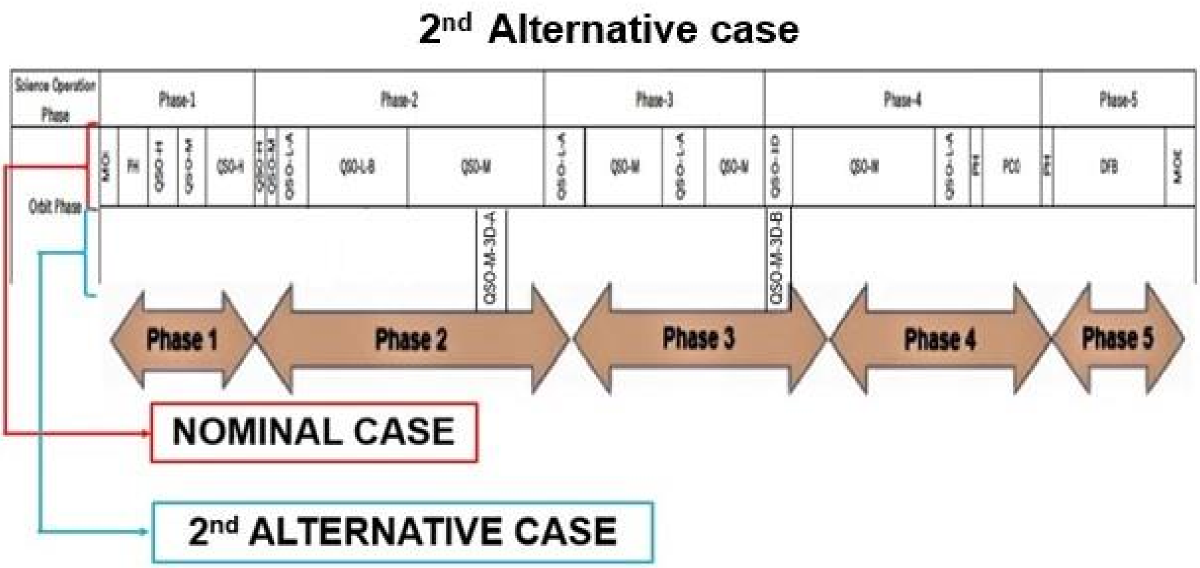

Figure 15 *- QSO repartition between the MMX phases, in nominal and second alternative cases.*

Thereby, these lists of 2 and 3-Dimensional QSO trajectories, represent the basis of this internship project.
Starting by the FD preliminary simulations of these orbits, all the project steps have been developed in order to adapt these trajectories to GINS precision level and treat them for the purpose of reaching the prefixed objective: the analysis of Phobos gravity field model.

However, a preparatory step is necessary. In fact, since the entire project method is based on the use of the GINS software, it is mandatory that all the input files describing the QSO sets are in the correct GINS format.
Effectively, the FD team adopts its own specific software for orbital simulation. This means that the preliminary QSO files arrive to the CNES Space Geodesy group in a particular format, containing:

- The time passed from an orbit initial date, expressed in [s]. An integration step size of 120s have been used;
- The three components of satellite position (expressed [m]) and speed (in [m/s]) vectors, in Phobos centred EME2000 reference frame;
- The three components of satellite position (expressed [m]) and speed (in [m/s]) vectors, in in Mars centred EME2000 reference frame;
- The dimensionless satellite position and speed vectors in Phobos rotating frame.

As a consequence, the first action to do on preliminary QSO trajectory files, is their conversion into the correct ephemeris GINS format, detailed in section 2.1.1.
At the same time, also Phobos ephemeris around Mars have to be computed. Relying on FD files, a simple subtraction is calculated between satellite state vector components expressed in the two different reference systems centred respectively on Mars and Phobos. In this way, the Martian moon motion relative to its central body, Mars, is thus calculated. This operation is

realised using the only preliminary orbital data, so that exactly the same FD hypotheses have been here considered for Phobos ephemeris.

3.2 QSO trajectory adjustment

Once obtained the preliminary QSO trajectories in the GINS format, it is necessary to apply an orbital adjustment, in order to provide them with the same precision level adopted in the CNES Space Geodesy software.
This aim is reached by using really precise full dynamical force models to make the desired corrections to the preliminary orbits. Effectively, GINS is perfectly adapted to this purpose. In the specific case of the MMX mission analysis, its utilisation allows to take into account [13]:

- The real celestial body ephemeris, instead of the Keplerian approximation to their orbital motions;
- The Mars gravitational attraction, computed with the accurate JPL Mars gravity field model, derived from the MRO mission and developed up to degree/order 120 [14]. Mars gravity spherical harmonics up to degree 10 have been taken into account within this project;
- The Mars tidal effects, which are taken into account through the $\boldsymbol{k_2}$ coefficient;
- The perturbing third body attraction of the Sun and the planets (Earth, Jupiter, Saturn, Uranus and Neptune);
- The solar radiation pressure effecting the spacecraft, considering the following set of assumption:

$$\begin{cases} Spacecraf\ surface = 52m^2 \\ Spacecraf\ mass = 1000kg \\ Spacecraft\ C_r = 1.3 \end{cases}$$

  where the C_r term represents the satellite reflectivity coefficient.
  The force exercised by the solar pressure is considered to be zero when the satellite transits in an eclipse condition in relation with the Sun: when the Sun is behind Mars or Phobos. Instead, this solar action is considered to grow as gradually as the satellite passes from an eclipse condition, to a half-light situation, to a complete visibility state. In order to take into account this solar pressure variation along the satellite orbits, the eclipse index described in section 2.1.1 is employed;
- The relativistic effects generated by the most important of the three terms GINS can take into account: the Schwarzschild term;
- The Phobos gravitational attraction, calculated using a specific model. Normalized gravity Stokes coefficients of the Martian moon can be computed under the assumption of a homogeneous mass distribution, considering Phobos equatorial radius $\boldsymbol{a_e} = \mathbf{11000.0}\ \boldsymbol{m}$ and its gravitational parameter $\boldsymbol{\mu} = \boldsymbol{G} \cdot \boldsymbol{M} = \mathbf{711381.66}\ \boldsymbol{Nm^2/kg^2}$. Firstly, Phobos polyhedron shape is converted into a series of spherical harmonics (Figure 16.a), secondly this series is used to compute the target gravity field in each point of its modelled shape (Figure 16.b):

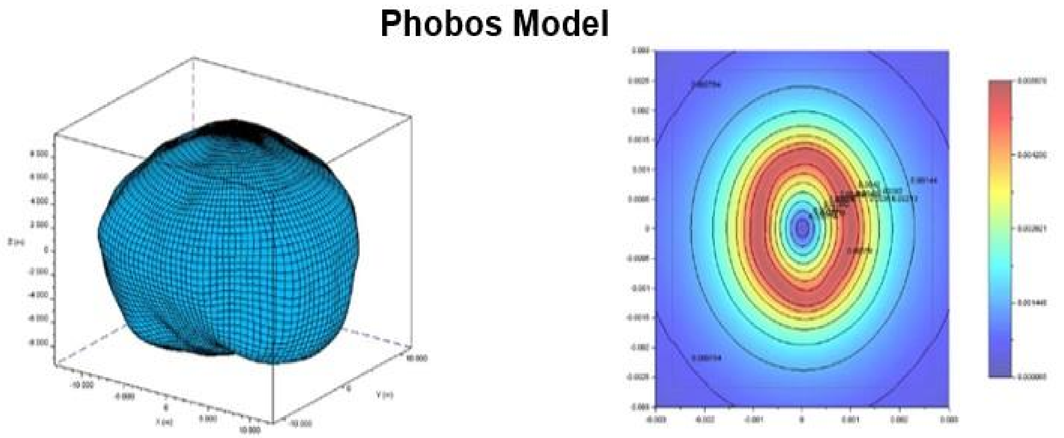

Figure 16.a – *3D visualization of Phobos spherical harmonic shape model.*

Figure 16.b – *2D representation of internal Phobos gravity model.*

Figure 16 - *Phobos shape and gravity modelling through spherical harmonic expansion.*

On the base of this shape model, Phobos external gravity filed can be expressed by a set of Stokes coefficients (paragraph 1.4).
In this internship project, the reference model is represented by gravity spherical harmonics up to the degree 20 (whose respective normalised coefficient values are reported in Annex A): one of the most precise Phobos gravitational model available nowadays. Consequently, this reference gravitational field has been used as "*natural satellite gravity*" in the "*model*" section of the *Adjustment* "*Director*" GINS file.

With this precise force model, it is possible to proceed with the adjustment of all the QSO trajectories needed in the MMX mission and listed in Table 1 and Table 2. The same procedure detailed in the following, is applied to every orbit, one by one, within the *Adjustment* project step.
The *Adjustment* step consists in adopting the format corrected-preliminary orbits as measurements of ephemeris type, within the GINS software. This means that the approximate QSO trajectory files are employed as "*inter-object data – file*" in the "*observation*" section of the *Adjustment* "*Director*" input file.
Moreover, a smaller integration step-size is here considered, in comparison to the 120.0s employed by the JAXA FD team. With the aim of having more adjusted ephemeris information, a value of 60.0s has been inserted under heading "*integration step-size*" in the "*parameter*" section of the *Adjustment* "*Director*".
GINS execution of instructions contained in this "*Director*" file, leads to the correction of satellite initial state vectors (initial position and speed) on each QSO. The adjustment criterion is the minimization of the 3-Dimensional residuals computed along the entire orbits, which means the distance between the dynamically QSOs simulated by GINS and the FD team preliminary orbits.

The first tested approach for QSO adjustment, was composed by the following two moments:

1. Inserting the preliminary QSO trajectory files under heading "*satellite – initial state vector*" in the "*object*" section of the *Adjustment* "*Director*" input file, the adjustment was conducted only over the first 6-hour orbit arc of each orbit. These corrected arcs were then described in the "*Ephemeris*" output files, whose post-treatment through the Python *Visualisation Module*, allowed their graphical representation. One of these visualisations is observable in the figure below, where an adjusted QSO-L-A arc is considered as an example:

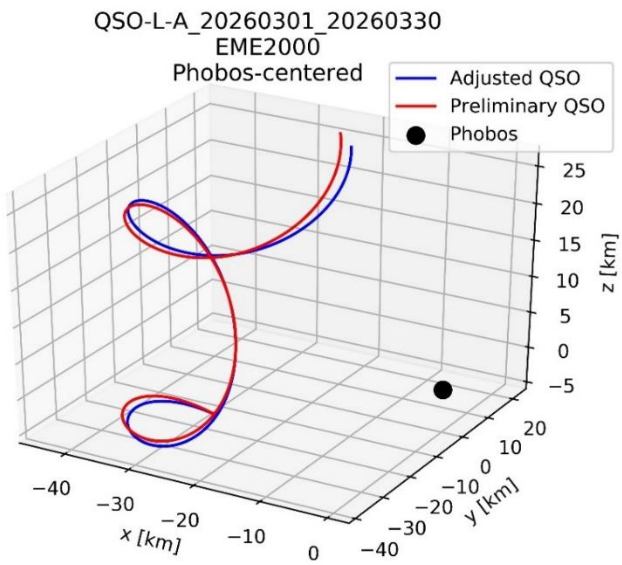

Figure 17 *- Adjustment example over a 6-hour QSO-L-A orbit arc.*

2. This adjusted initial 6-hour arc of each trajectory was then propagated over all the orbit duration, for the purpose of generating complete adjusted QSOs. In this case, an additional *Propagation* "*Director*" file was thus necessary. Its entry "*satellite – initial state vector*" in the "*object*" section was dedicated to the adjusted 6-hour QSO arc files, created by GINS in the previous moment.

Fortunately, this adjustment technique brought to light two important aspects.
First of all, GINS adjustment procedure failed in several QSO cases. This feature is due to the fact that on these particular orbits, even a little error on satellite initial state vector is able to propagate and grow out of all proportion along a period of 6 hours. This element caused the uncorrected GINS adjustment execution or the absence of the adjustment procedure convergence, for several considered trajectories.
Secondly, even when certain orbits succeeded in their 6-hour adjustment, the moment of their propagation highlighted a second problem. The propagation of a QSO trajectory over a period between 14 and 35 days, generates an excessive propagation of the probable initial state vector error, remaining from the previous GINS orbit arc adjustment.

A perfect graphical representation of this error increase in time, is shown in the figure below, reporting as an example the same QSO-L-A trajectory than Figure 17.

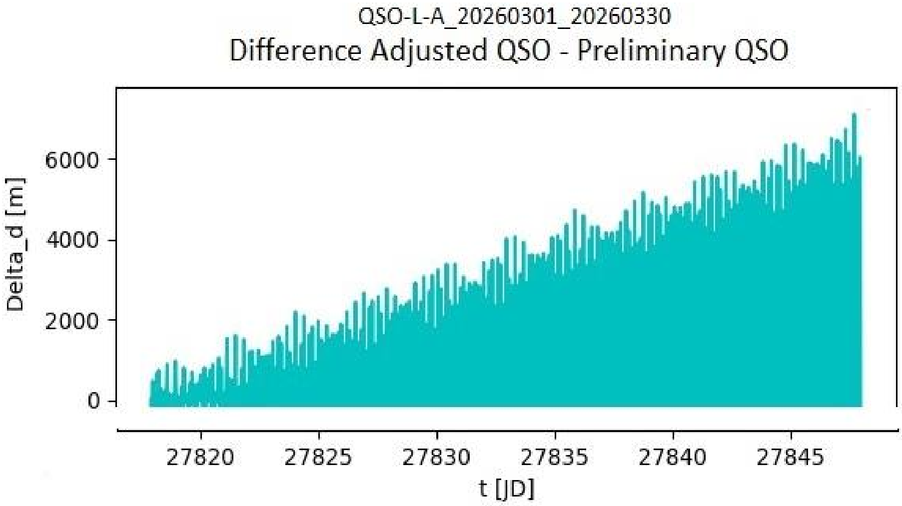

Figure 18 *- Position difference between an original preliminary QSO-L-A and its propagated orbit starting from a 6-hour adjusted arc.*

This figure represents the module of the difference between the position vectors on the preliminary QSO trajectory and its initial adjusted and propagated version. As it is clear from this graph, the starting difference between the two orbits is almost null, while it gradually keeps growing until the final date. This position discrepancy evolution in time perfectly confirms the propagated growth to excess of an initial position and speed error.

Because of these constraints in QSO behaviour, another adjustment process has thus been ideated. Taking into account the failure of some trajectories in being adjusted over a period of 6 hours, the strong error rise in time and the necessity of correcting orbits along their entire duration, a gradual adjustment has been developed.
Thus, the procedure has been split into five *Adjustment* sub-steps:

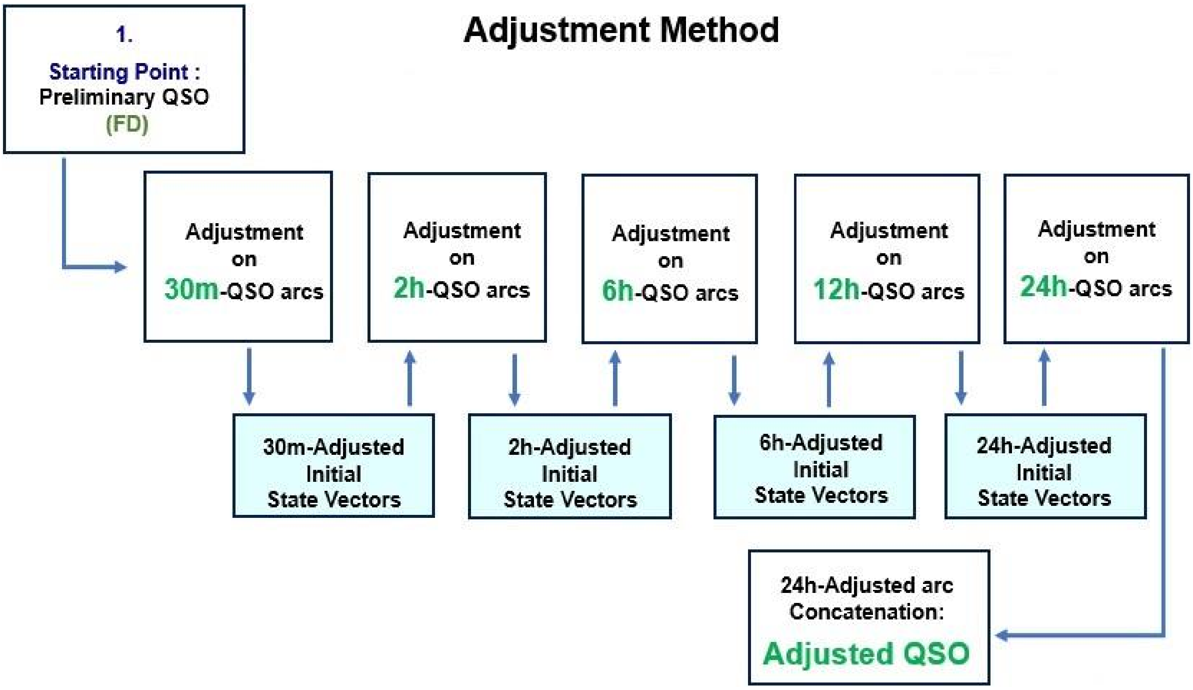

Figure 19 *- Shema representing the adjustment procedure developed in this internship project.*

Each *Adjustment* sub-step is detailed below:

1. All the entire QSO trajectories are firstly divided into **30 minute**-orbit arcs. Considering that it is the satellite initial state vector to be corrected, only one in every forty-eight arcs is adjusted using GINS. In this way, the correction is applied at the beginning of each day taking part in a QSO. As it represents the first orbital adjustment, again the preliminary QSO trajectory files correspond to the "*satellite – initial state vector*" in the "*object*" section of the *Adjustment* "*Director*".
   This method allows to eliminate all problems in adjustment execution and convergence, since considering only half an hour, the remaining initial state vector errors cannot excessively propagate.
2. The complete QSO trajectories are successively split into **2-hour** orbit arcs. The files containing the previously adjusted orbit arcs of thirty minutes is now used as "*satellite – initial state vector*" in the *Adjustment* "*Director*". In this case, one every twelve arcs is adjusted, in order to get one corrected arc at the beginning of each QSO day.
3. The whole QSO trajectories are then decomposed in **6-hour** orbit arcs. One every four of these arcs is effectively adjusted, using the previous 2-hour corrected arc files as "*satellite – initial state vector*" in the *Adjustment* "*Director*". Consequently, the first six hours of each QSO day are corrected.
4. The entire QSO time periods are now split into **12-hour** orbit sections. In order to correct the initial state vector at the beginning of each day composing the trajectories, one every two arcs is adjusted. This time, the entry "*satellite – initial state vector*" in the *Adjustment* "*Director*" is reserved for the adjusted 6-hour QSO arc files.
5. The entire QSOs are finally parted into **24-hour** orbit arcs. Adopting the adjusted 12-hour arc files as "*satellite – initial state vector*" in the *Adjustment* "*Director*", each of these arcs is really adjusted and concatenated to each other, in order to cover all the QSO durations.

It is possible to realise this global adjustment since a gradual operation is employed. In every sub-step, the adjustment period increases, but at the same time, an always more precise corrected initial state vector is provided. Consequently, even with a strong initial error propagation in time, this method enables to obtain complete adjusted QSO trajectories, similar to the preliminary ones.

As all GINS "*Ephemeri*s output files, these adjusted orbits are expressed in the central body (Mars) centred reference system. With the purpose of better observing the results, they can be treated with the Python *Visualisation Module*, to turn their reference coordinate system into the Phobos centred one. The following figures, representing one orbit for each QSO class as an example, show the satisfying results for the *Adjustment* step.

Adjusted QSO – Preliminary QSO

<table>
<tr><th>Trajectories</th><th>Position Difference</th></tr>
<tr><td>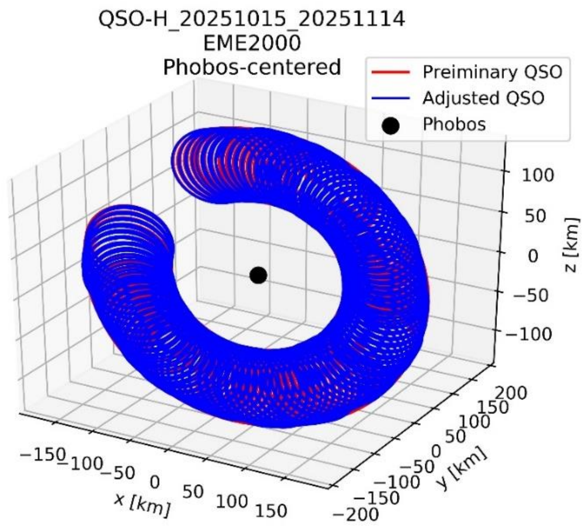
</td><td>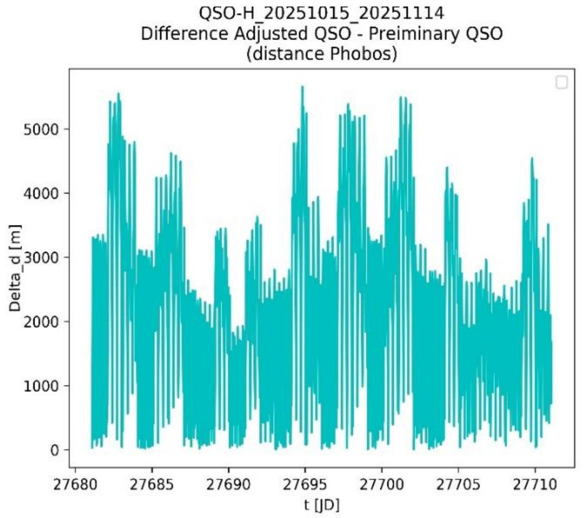
</td></tr>
<tr><td colspan="2">Figure 20.a – QSO-H class example.</td></tr>
<tr><td>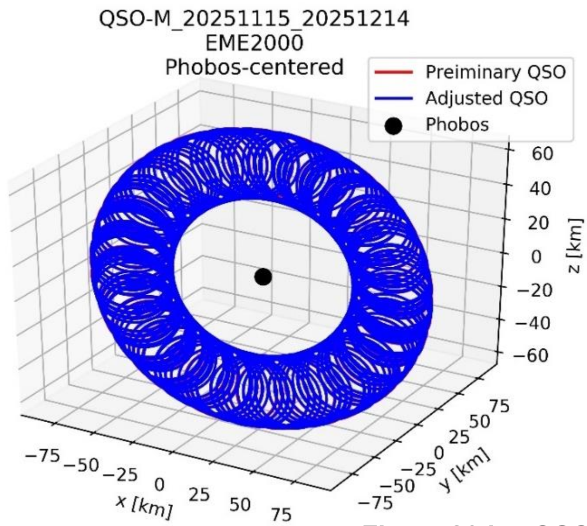
</td><td>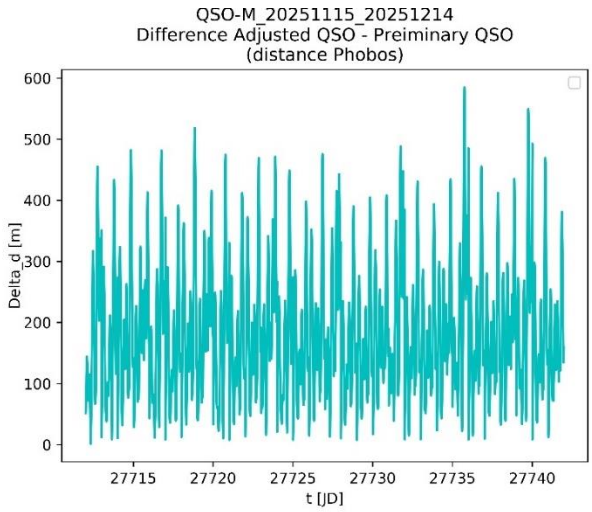
</td></tr>
<tr><td colspan="2">Figure 20.b – QSO-M class example.</td></tr>
</table>

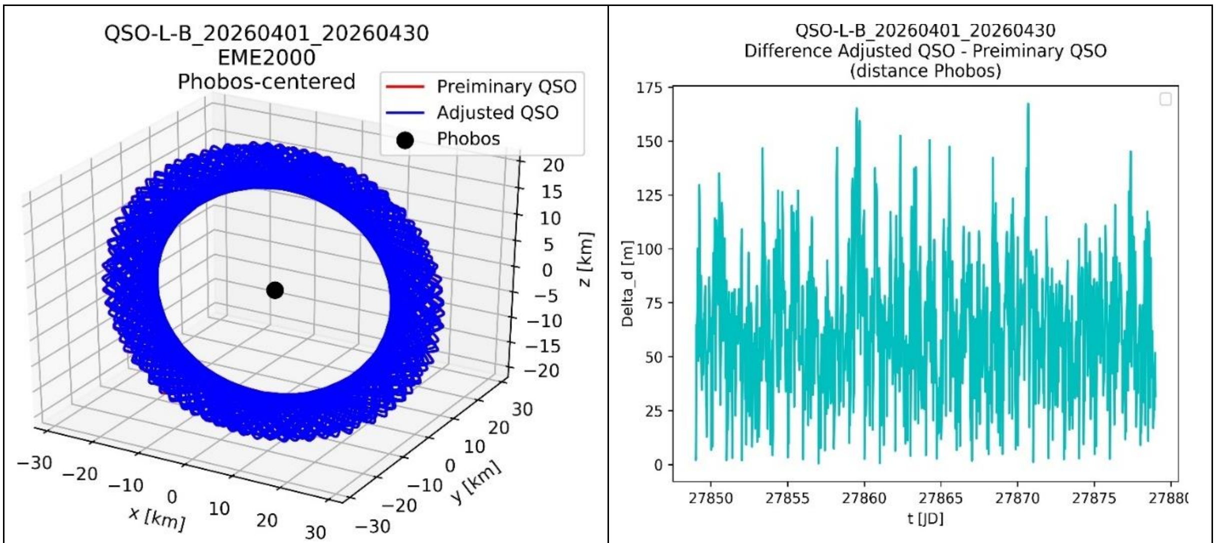

Figure 20.c *– QSO-L class example.*

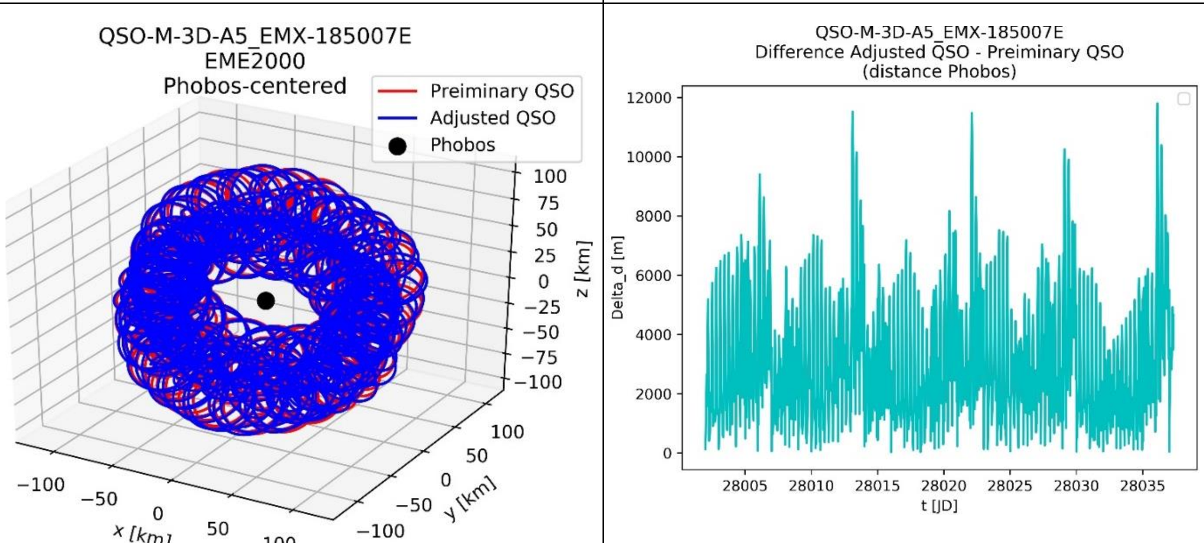

Figure 20.d *– QSO-M-3D class example.*

Figure 20 *- Adjustment examples over 24-hour arcs, covering the complete QSO trajectories.*

The trajectory representations on the left of the figure, prove that all the QSO classes allow a satisfactory orbital adjustment: the corrected orbit traces appear not to be that far from the preliminary ones.
Moreover, a significant remark stands from the observation of graphs on the right, reporting the evaluation in time of satellite-Phobos distance difference between the corrected and the preliminary trajectories. Generically, the higher diversities correspond to the conjunction instants between consecutive 24-hour orbit arcs. Again, this aspect does not represent a problem: the adoption of this QSO partition method in all the project steps, allows anyway an accurate geodesic analysis.
Furthermore, the difference increases with the 2-Dimensional QSO dimensions, while the highest value is reached with the 3-Dimensional cases. This aspect is highlighted in the following table, showing the maximal difference and final ***r.m.s.*** (between all the 24h-arcs composing these orbits) values of every QSO class (in relation to the orbits employed as examples):

Orbit class	Maximal difference [km]	Maximal r.m.s. [km]
QSO-H	5.45	2.35
QSO-M	0.585	0.155
QSO-L	0.165	0.051
QSO-M-3D	11.8	3.77

Table 3 *- Maximal differences in satellite position along adjusted and preliminary orbits.*

Both this difference values and graphs in Figure 20.d lead to understand that the QSO-M-3D represents the most difficult class to be treated and adjusted. In fact, even if these 3-Dimensional orbits reach only medium altitudes over Phobos surface, their adjusted versions appear to be farther from their respective preliminary trajectories, than the 2-Dimensional QSO-M orbits. However, their adjustments result to get an acceptable accuracy level.

To conclude, it is possible to supposed that the larger a QSO is, the higher are the relative maximal preliminary-adjusted position distances and the adjustment ***r.m.s.*** values, probable because of a difference in Mars gravity models used for the preliminary simulations and the GINS adjustment. Nevertheless, all the adjusted QSOs conserve their orbital features, dimensions, stability, and distances from Phobos. Thus, the primary adjustment purpose is reached: the obtainment of reference orbits on which apply all the necessary procedures to return the target gravity filed.
Finally, it is important to underline that an orbital adjustment over consecutive 24-hour arcs, concatenated over the entire period of a QSO, may generate a gap between state vectors at the last instant of an arc and at first instant of the consecutive one. In any case, this possibility does not represent a problem for this specific internship project. In fact, its final scientific purpose is the analysis of Phobos physical parameters and not the perfect reconstruction of the MMX orbital evolution.
This means that, once chosen to adopt this partition method of QSO trajectories in 24-hour orbit arcs, it is sufficient to apply it in all the following project steps. In this way, this splitting procedure cannot damage the final geodesic analysis results.

3.3 DSN measurement simulation and QSO extrapolation

Once adjusted the necessary QSO trajectories, the second project step is the simulation of the desired measurements along these orbits.
As announced before, measures concerning Phobos geodesic analysis are the DSN, LIDAR and Optical navigation ones.

The initial measure *Simulation* step deals with the first group of measurements, the Doppler DSN type.
DSN measurements represent an important component in the MMX mission, since they provide Doppler and Range information in the spacecraft line of sight, in deep space.
The method selected to capture these measurements is the *2-Way Doppler* approach. It consists in the transmission of a signal by an Earth station, with a frequency $\boldsymbol{f_T}$ (usually in the *S* or *X* band) during an interval $[\boldsymbol{t_{1,s}}, \boldsymbol{t_{1,e}}]$. Normally, this frequency can be controlled: by changing it in a linear manner in each time interval, an optimisation of the final signal reception

on Earth is possible. The signal transmitted by the station is then received on-board by the satellite transponder, which multiplies it by a specific frequency factor $\boldsymbol{M_2}$ and re-transmits it during a time interval [$\boldsymbol{t_{2,s}}$, $\boldsymbol{t_{2,e}}$], with a frequency $\boldsymbol{f_R}$.
This signal is successively received by a ground station on Earth, during a time interval [$\boldsymbol{t_{3,s}}$, $\boldsymbol{t_{3,e}}$], referred to as the counting time $\boldsymbol{T_c}$. Finally, this received signal frequency is then compared with a reference frequency $\boldsymbol{f_{ref}}$, calculated by multiplying the originally transmitted $\boldsymbol{f_T}$ with a frequency factor $\boldsymbol{M_{2,R}}$.

A visual representation of a *2-Way Doppler* method is given by the following figure:

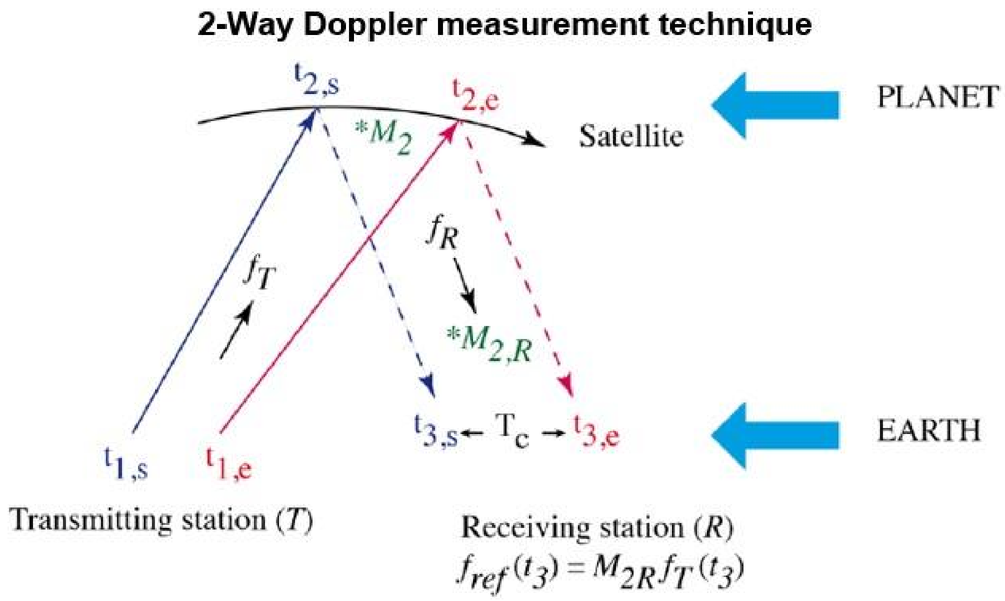

Figure 21 *- Schematic representation of the 2-Way Doppler technique [9].*

On the basis of this *2-Way Doppler* approach, the measured quantity is expressed and calculated by the GINS software as follows [13]:

$$\boldsymbol{q_{obs} = \frac{M_{2R}}{T_c}\int_{t_{3,s}(ST)}^{t_{3,e}(ST)} f_T(t_3)dt_3 - \frac{M_2}{T_c}\int_{t_{1,s}(ST)}^{t_{1,e}(ST)} f_t(t_1)dt_1 + corrections} \quad \textit{(59)}$$

where $\boldsymbol{ST}$ represents the Earth station time and the $\boldsymbol{corrections}$ term includes all the necessary adjustments for signal propagation in Earth atmosphere, interplanetary environment (plasma) and Sun proximity (corrections due to the solar corona).
In reality, modelling these propagation effects over an electromagnetic signal, results to be quite difficult. Models used in the GINS software are accurate, but their precision level does not allow to calculate absolutely exact values. Consequently, the wider are the DSN signal passages through these delicate space environments, the more the simulated Doppler values are compromised by the $\boldsymbol{corrections}$ model inaccuracies.
In the specific MMX study case, a particular expedient has been adopted to reduce this Doppler measurement imprecision. In fact, the GINS software enables to fix a limit for Earth atmosphere portion to be crossed by the electromagnetic signal.

As the following figure shows, this crossed atmosphere layer almost depends on the ground DSN antenna observation angle.

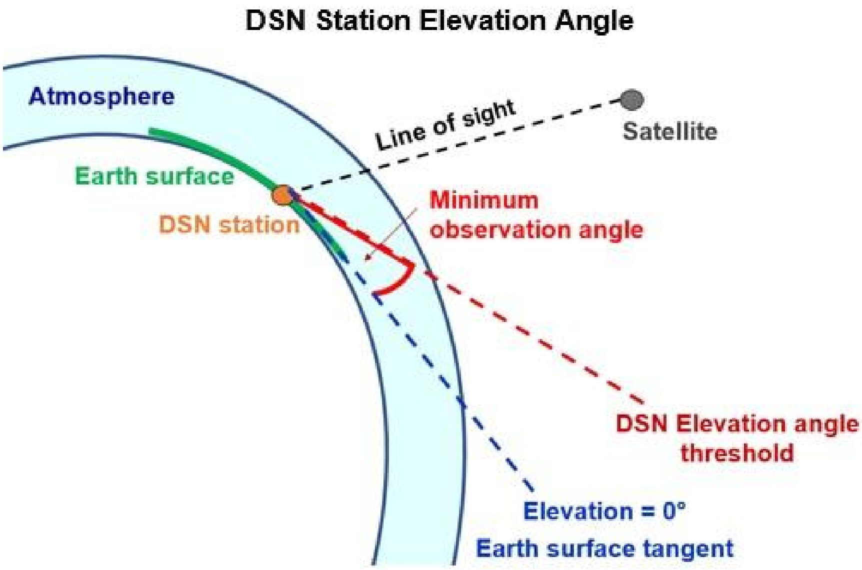

Figure 22 *- Effects of the DSN antenna observation angle on the crossed atmosphere layer.*

This figure highlights that the smaller is the ground antenna minimum Elevation angle, the thicker is the Earth atmosphere layer which DSN signals have to cross. However, a higher minimum observation angle provides a low number of Doppler captures, since resulting the area covered by the DSN station turns out to be reduced.
Because of this aspect, the antenna Elevation parameter has to be fixed for an accurate Doppler measurement simulation. For the purpose of finding a compromise between the necessity of minimizing the crossed atmosphere width and the need of getting the maximum quantity of DSN measurements possible, the optimised minimum antenna Elevation angle has been fixed at 15.0°.

Apart from the thus set antenna observation angle, the JAXA has already imposed many other parameters and constraints, relative to the caption of DSN measurements during the MMX mission:

- Normally, DSN measurements will be realised using Madrid (Spain) and Usuda (Japan) ground stations;
- The possibility of employing only Usuda station is taken into account (this hypothesis represents an additional study case analysed in this project);
- In these station-covered areas, one DSN measurement will be taken every minute;
- The Doppler noise standard deviation (σ_{DSN}) is fixed at 3.75mHz, corresponding to a speed error of 0.2 mm/s in the satellite line of sight.

Taking into account these hypotheses, the procedure followed in the *DSN Simulation* step is reported in schema below:

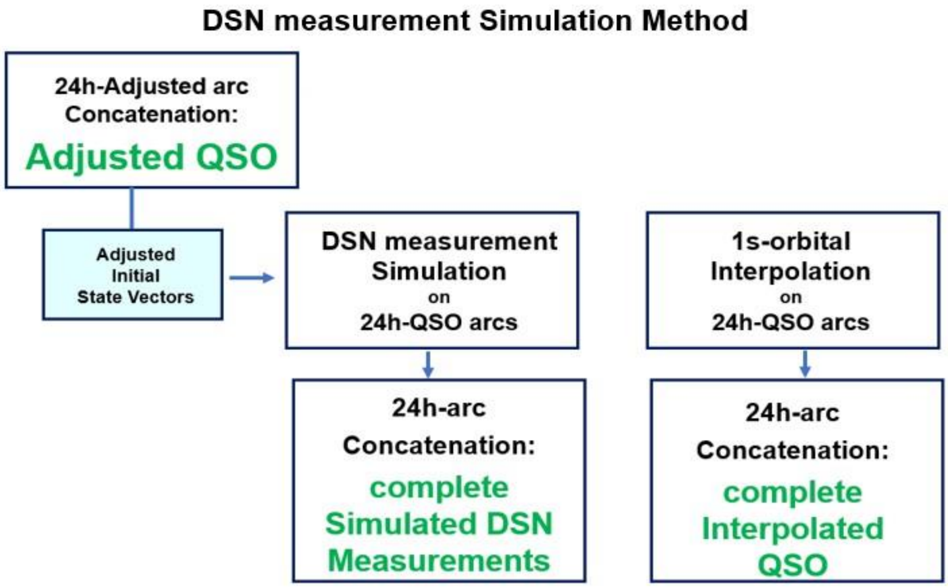

Figure 23 *- Schematic representation of the DSN simulation approach.*

The aim of this project step is to follow the method represented in the schema, in order to simulate Doppler measurements along all the adjusted QSO trajectories.
Since the latter have been realised as a concatenation of corrected 24-hour orbit arcs, also in the *DSN Simulation* step it is necessary to treat each entire orbit by splitting it into 1 day-portions. These orbit arcs have then to be newly concatenated at the end of the simulation procedure.
Once again, the GINS software is perfectly adapted for this DSN measurement simulation. The specific *DSN Simulation* "*Director*" input file to be used is mainly composed by:

- The same reference Phobos gravity field, modelled by spherical harmonics up to the degree 20, under heading "*natural satellite gravity*" in the "*model*" section;
- The "*Ephemeris*" files defining the complete adjusted QSOs (generated in the previous step), as "*satellite – initial state vector*" in the "*object*" section;
- The *station* file containing the detailed positions of Madrid and Usuda DSN ground antennas (for the nominal case), under heading "*inter-object data – objects" in the "observation"* section;
- The key word "*DSN Doppler 2*", defining the *2-Way Doppler* technique, as "*inter-object data – simulation"* in the "*observation*" section. The same section included the minimum antenna elevation angle, fixed at 15.0°, under heading "*removal – minimum elevation threshold"*;
- The Doppler white noise to be simulated along with DSN measurements, in order to represent possible errors in the generated values. The white noise is calculated by GINS with equation (20). Consequently, it can be defined in the "*Director*" file through the measurement noise standard deviation $\boldsymbol{\sigma_{DSN}}$, fixed at 3.75mHz by the JAXA.

In addition to these main *DSN Simulation "Director"* instructions, two different measurement time steps need to be set, in order to respect all JAXA constraints.
Specifically, as preannounced before, DSN measurement type requires a simulation time step of 60.0s.
However, this value would not be appropriate for the next *LIDAR Simulation* step. In fact, the time step between two consecutive LIDAR measures is fixed by the JAXA at 1.0s. The problem is that, as the next paragraph will detail, LIDAR (and Optical) measurements are simulated as

ephemeris measure types. This means that their simulation has to be based on QSO trajectory files generated as "*Ephemeri*s" outputs from the *DSN Simulation* step.
Therefore, because of the 1 second-time step imposed for LIDAR measures, output QSO "*Ephemeris*" characterised by an integration time step of 60.0s would not be utilisable for the next LIDAR simulation.
Consequently, it is necessary to fix two different time steps in the *DSN Simulation "Director*" file:

1. A "*simulation step size*" of 60.0s in its "*observation*" section, relative to the Doppler measurement simulation;
2. An "*integration step size*" of 1.0s in its "*parameter*" section, relative to the integration time step for the output "*Ephemeris*" files. This element involves a GINS orbit interpolation, needed to pass from the previous adjusted QSO files, integrated every 60.0s, to the new 1.0s-integrated ones.

In this way, once GINS realised the entire *DSN Simulation* procedure over all the 24-hour orbit arcs, two main types of output are generated:

1. The Doppler "*Measurements*" file, containing the measures stimulated every 60.0s, in time intervals corresponding to areas not covered by the DSN Earth stations;
2. The "*Ephemeris*" file, containing the adjusted QSO arcs, interpolated every 1.0s.

Finally, as for the *Adjustment* step, all the simulated DSN measurements and the interpolated QSO ephemeris on 24-hour orbit arcs, have then to be concatenated.
In this way, the entire Doppler "*Measurements*" and interpolated QSO "*Ephemeris*" output files are obtained.

Beginning with the first of these GINS outputs, its treatment with the Python *Visualisation Module* leads to generate a representation of Doppler measurements captured during the entire orbit durations.
A QSO-L-A trajectory is here considered as an example, in order to show DSN measure evolution in time. For the purpose of a clear representation, a period of only five days has been considered to generate the following graphs.

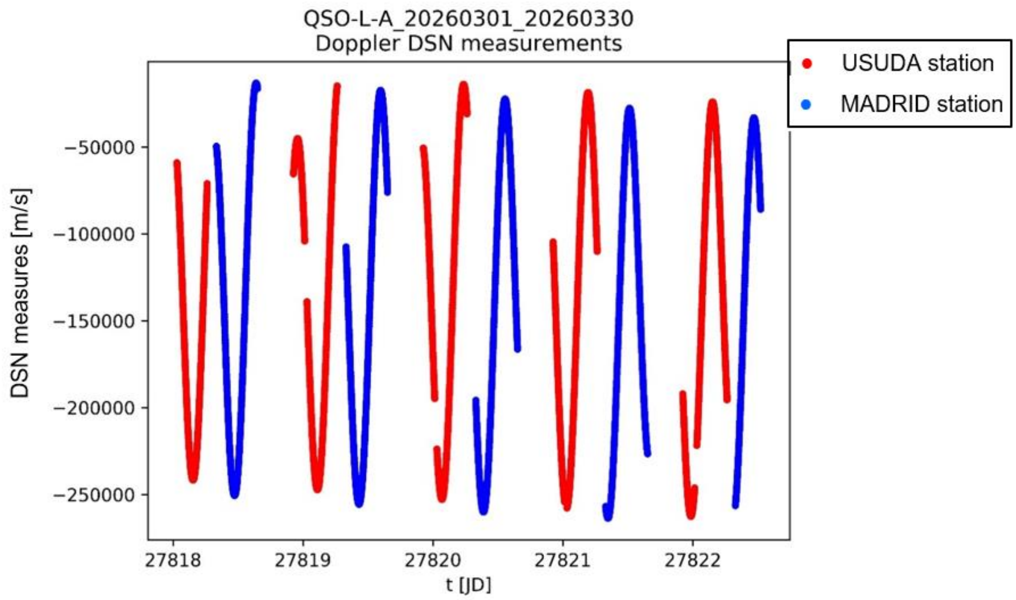

Figure 24 - *Example of DSN measurements evolution in time along a 5-day period of a QSO-L-A.*

This figure perfectly proves the sinusoidal time progress of Doppler measurements. This temporal evolution is due to constant relative motion between Earth and Mars (and Phobos).
Moreover, this graph underlines the lack of measurements in some time intervals. This aspect witnesses an important consequence of the JAXA hypothesis over the DSN captures.
Since each ground station covers a time of about 8.0h per day, the employment of two DSN antennas leads to Doppler measures available only for 16.0h every 24.0h. This causes visibility interruptions along QSO trajectories, between the Madrid and the Usuda covered areas.
Obviously, this situation got worst if considering only the Japanese antenna.
The analysis of this additional study case starts with the generation of a new complete Doppler *"Measurement"* file for each QSO, containing the only information relaying on the Japanese ground station. It is not necessary to repeat all the GINS simulation procedure: a simple extraction of Usuda measures from the original files is sufficient.
Once again, the employment of the proper Python *Visualisation Module* function, leads to the following result, relative to the same QSO-L-A trajectory taken as an example in the previous figure:

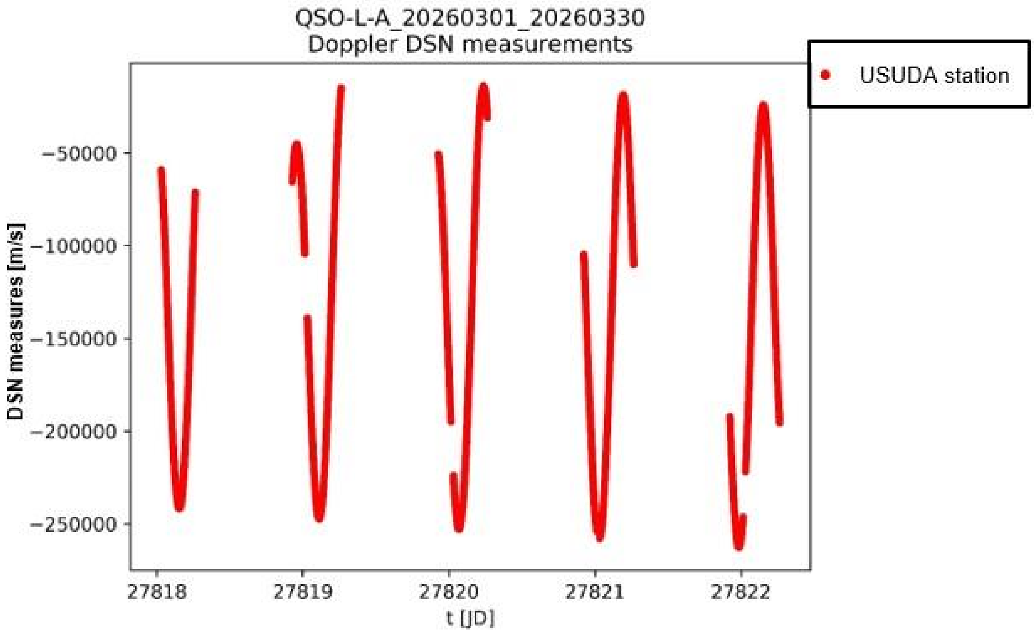

Figure 25 *- Example of DSN measurements along a 5-day period of a QSO-L-A, simulated with the only Usuda ground station.*

In comparison with Figure 24, this graph presents the only red curves corresponding to the Usuda captures. These remaining DSN traces highlight the larger time intervals without any Doppler measurements. This bigger lack of measures causes a lower accuracy level in the DSN data treatment realised in the next project step, detailed in the following.

Passing now to the second fundamental *DSN Simulation* output, it is possible to visualise the orbital traces described in the "*Ephemeris*" file, defining the entire 1 second-interpolated QSO trajectories.
In fact, once again the Python *Visualisation Module* allows the representation of these trajectories and their differences in relation to the simply adjusted ones. The same trajectories reported in Figure 20, are used here as examples again:

Interpolated QSO – Adjusted QSO

Trajectories	Position Difference
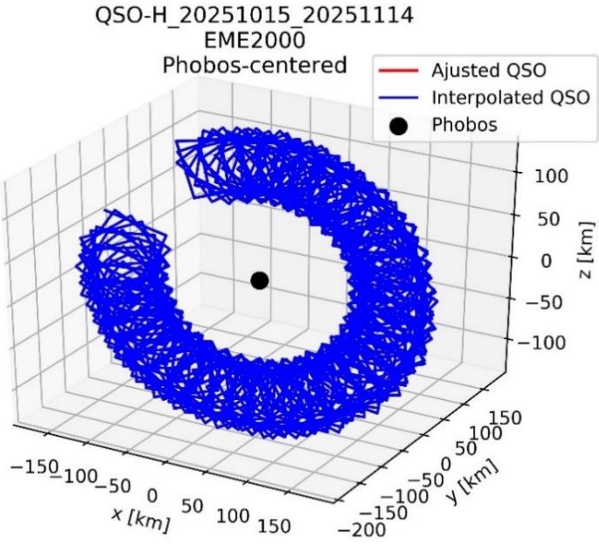	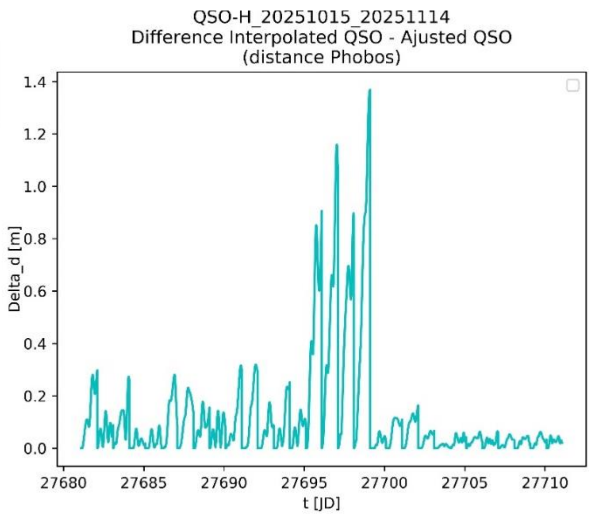

***Figure 26.a** – QSO-H class example.*

Trajectories	Position Difference
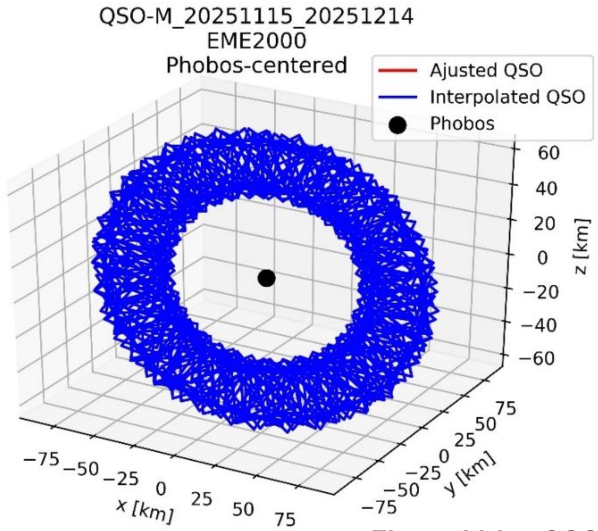	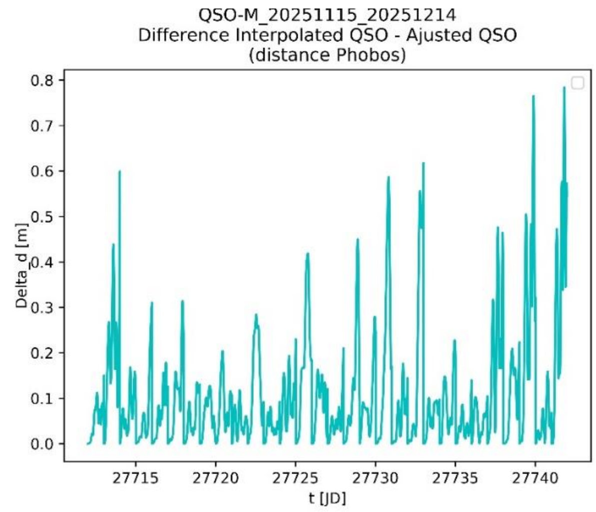

***Figure 26.b** – QSO-M class example.*

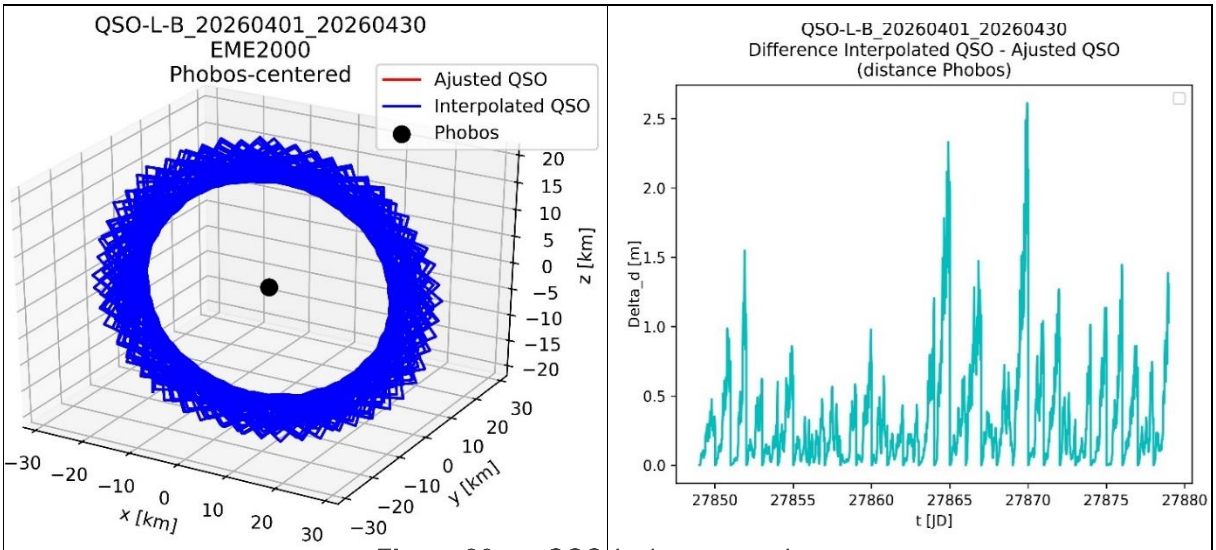

Figure 26.c *– QSO-L class example.*

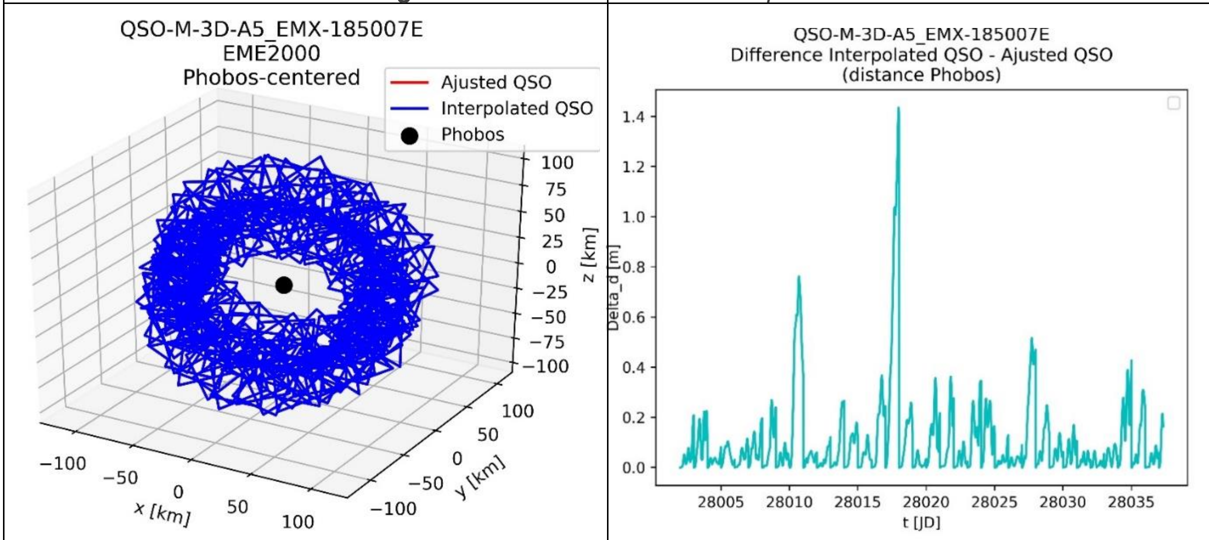

Figure 26.d *– QSO-M-3D class example.*

Figure 26 *- Examples of interpolated trajectories belonging to the four QSO classes.*

These figures prove the accuracy level of GINS interpolation procedure. Effectively, for all the QSO classes, the satellite position difference between the adjusted and the interpolated trajectories is minimal.

Moreover, the combination of both Doppler "*Measurements*" and interpolated QSO "*Ephemeris*" files, enables the visualisation of areas covered by DSN measures along satellite orbits:

DSN measurement position

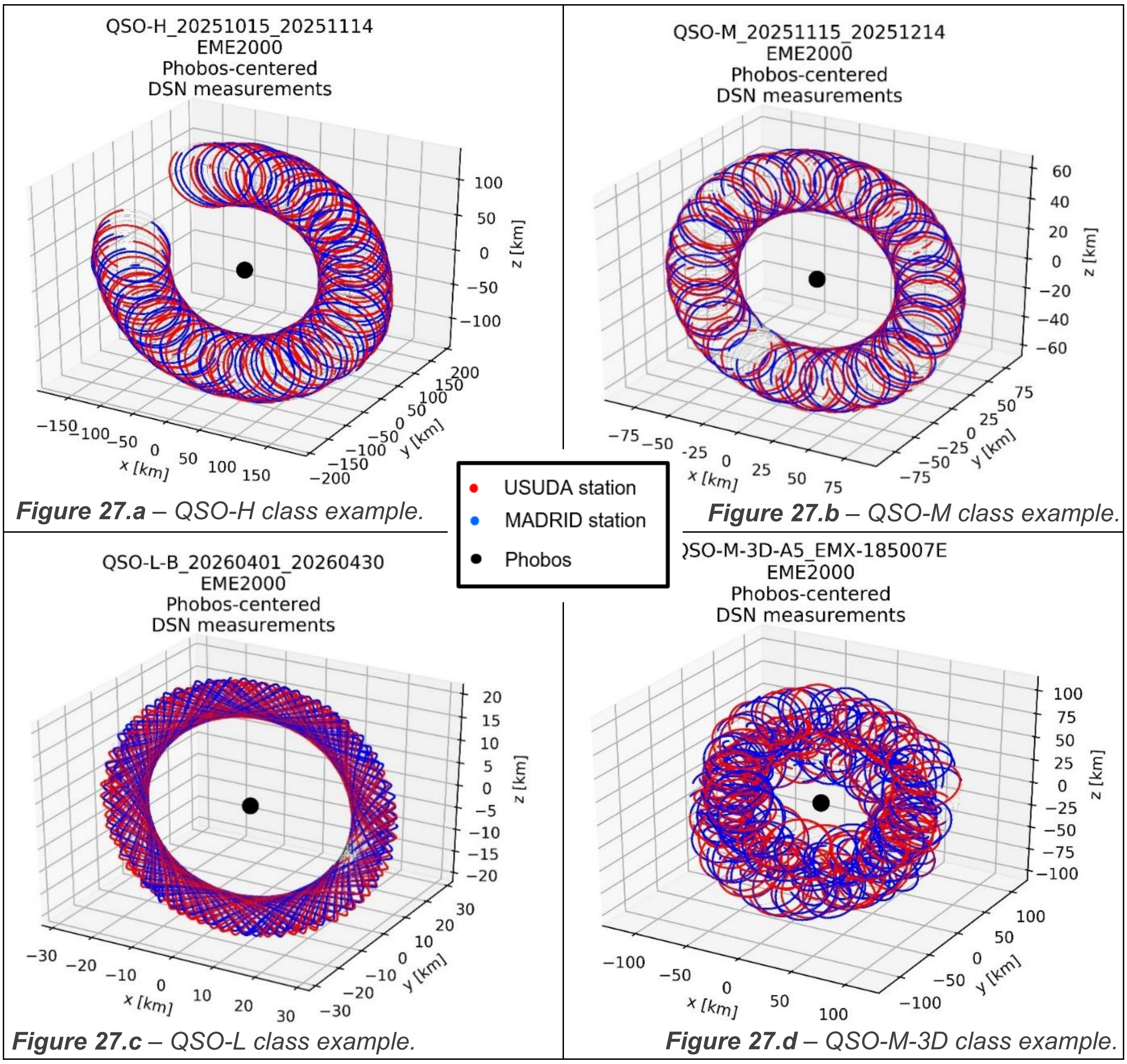

Figure 27.a *– QSO-H class example.*

Figure 27.b *– QSO-M class example.*

Figure 27.c *– QSO-L class example.*

Figure 27.d *– QSO-M-3D class example.*

Figure 27 *- Areas covered by DSN measures along trajectories belonging to the four QSO classes.*

These graphs prove the presence of certain QSO portions not covered by DSN measurements. This feature appears no to be so evident in lower trajectory cases (Figure 27.c), because of the multiple complete orbits realised by the satellite within the entire QSO durations.
In any case, there are little Doppler-free sections in all these orbits, corresponding to the about 8.0h per day not covered by Madrid and Usuda DSN antennas (or the 16h not covered by the only Usuda ground station).

To conclude, along with DSN measurement and trajectory graphical visualisation, both the Doppler "*Measurements*" and the interpolated QSO "*Ephemeris*" output files constitute the basis for the next project step: the ephemeris measurement simulation.

3.4 Ephemeris measurement simulation

Apart from DSN, the other important MMX measurements for Phobos geodesic analysis are the LIDAR and Optical ones.
Respectively useful for detecting satellite altitude and its motion within its tangential plane, they both directly give information about the spacecraft position over its orbits. Consequently, the model developed for their simulation, treats both LIDAR and Optical measures as ephemeris measurement types.
Therefore, the best coordinate reference frame where to simulate them, has been individuated in the strictly linked to the satellite-RTN system:

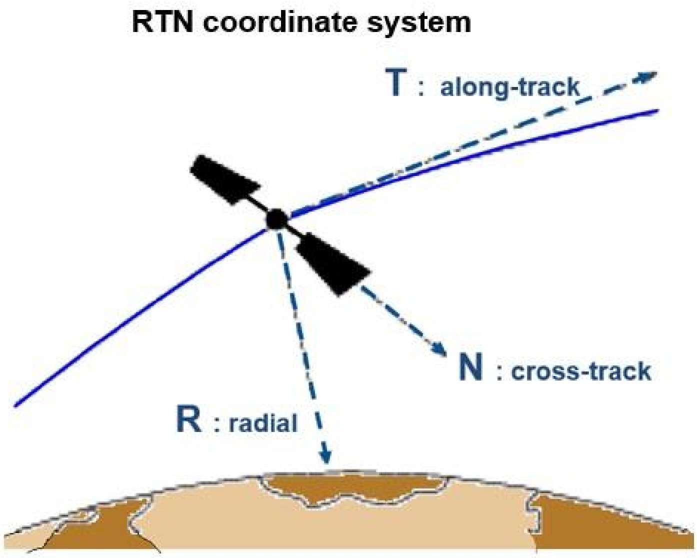

Figure 28 *- Satellite RTN coordinate system, used for LIDAR and Optical measure simulation.*

In the MMX context, the RTN system has its centre in the satellite centre of mass, its radial direction ***R*** pointing Phobos mass centre, its tangential direction ***T*** along the satellite QSO track, and its normal direction ***N*** perpendicular to the other two, oriented for respecting the right hand rule.
This coordinate system selection defines the first preliminary action to do in the *Ephemeris Simulation* step. Since the previously interpolated QSO trajectories are expressed in the GINS standard Cartesian (***x,y,z***) coordinate system centred on Mars, they firstly need to be converted in the satellite (***R,T,N***) system.

However, as for the DSN case, before starting with LIDAR and Optical simulation, it is necessary to take into account the constraints fixed by the JAXA:

- LIDAR and Optical measurements will be taken only when the satellite will pass in areas not covered by the DSN antennas;
- In these parts of QSO trajectories, the satellite will capture one LIDAR measurement every second and only one Optical measurement every hour;
- The satellite will be always able to take Optical captures, independently from its altitude, while LIDAR technique will be employed only in case of distance between satellite and Phobos surface equal or lower than 50.0km. This means that only along orbits belonging to QSO-L class, LIDAR measurements will be considered;

- LIDAR noise standard deviation ($\boldsymbol{\sigma_L}$) is set at 2.0m if satellite altitude over the target surface is equal or lower than 100.0m, while it assumes a value of 22.0m if this distance is equal or higher than 100.0km.
  Instead, the Optical noise standard deviation ($\boldsymbol{\sigma_O}$) is defined as an angular error in relation to Phobos centroid and it is fixed at 0.1°.

Respecting all these JAXA hypotheses, the ephemeris measure simulation method is completely built on results of the previous *DSN Simulation* step. In fact, its two outputs, the Doppler "*Measurements*" and the 1 second-interpolated QSO "*Ephemeris*" files, are the starting points for this *Ephemeris Simulation* project phase.
This direct dependence on the preceding step is highlighted by the schema below, showing the procedure followed for the treatment of LIDAR and Optical measures.

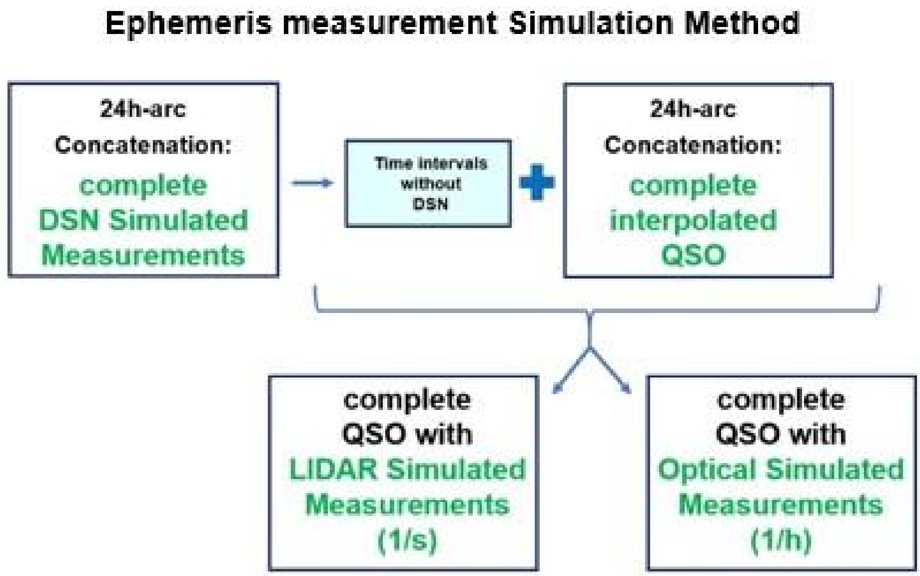

Figure 29 *- Schematic representation of LIDAR and Optical measure simulation approach.*

The approach reported in this schema has been developed coding a Fortran programme able to:

1. Reading the complete simulated DSN "*Measurements*" files (with Madrid and Usuda captures and with the only Usuda ones) relative to each QSO trajectory.
   This leads to establish which are the time intervals within the orbit total durations, without Doppler measures. As imposed by the JAXA constraints, these intervals represent the ranges where LIDAR and Optical measurements can be taken, thus simulated.

2. Reading the complete 1 second-interpolated QSO "*Ephemeris*" files, which provide all the necessary data on which LIDAR and Optical measure simulation is developed.
   Firstly, these QSO trajectories are treated with the same technique used in the *"Trace_Orbits_Phobos_Centered"* function of the Python *Visualisation Module*: their reference system origin is displaced from Mars to Phobos and they are expressed in relation to the Martian moon position.
   Secondly, once obtained the spacecraft position ($\vec{\boldsymbol{P}}_{xyz}$) and speed ($\vec{\boldsymbol{V}}_{xyz}$) vectors in relation to Phobos mass centre, they are converted in (***R**,**T**,**N***) coordinates, adopting the following rotation method [15]:

$$\vec{\boldsymbol{P}}_{\boldsymbol{RTN}} = \begin{pmatrix} \boldsymbol{R} \\ \boldsymbol{T} \\ \boldsymbol{N} \end{pmatrix}_{\boldsymbol{sc}} = \boldsymbol{\Gamma} \cdot \begin{pmatrix} \boldsymbol{x} \\ \boldsymbol{y} \\ \boldsymbol{z} \end{pmatrix}_{\boldsymbol{sc}} = \boldsymbol{\Gamma} \cdot \vec{\boldsymbol{P}}_{\boldsymbol{xyz}} \quad \textit{(60)}$$

where $\boldsymbol{\Gamma}$ is the (***x***,***y***,***z***) to (***R***,***T***,***N***) rotation matrix. It is an orthonormal matrix defined as:

$$\boldsymbol{\Gamma} = \begin{pmatrix} \hat{\boldsymbol{S}}^{\boldsymbol{T}} \\ \hat{\boldsymbol{I}}^{\boldsymbol{T}} \\ \hat{\boldsymbol{C}}^{\boldsymbol{T}} \end{pmatrix} \quad \textit{(61)}$$

where:

$$\begin{cases} \hat{\boldsymbol{S}} = \dfrac{\vec{\boldsymbol{P}}_{\boldsymbol{xyz}}}{|\vec{\boldsymbol{P}}_{\boldsymbol{xyz}}|} \\ \hat{\boldsymbol{C}} = \dfrac{\vec{\boldsymbol{P}}_{\boldsymbol{xyz}}\ \boldsymbol{x}\ \vec{\boldsymbol{V}}_{\boldsymbol{xyz}}}{|\vec{\boldsymbol{P}}_{\boldsymbol{xyz}}\ \boldsymbol{x}\ \vec{\boldsymbol{V}}_{\boldsymbol{xyz}}|} \\ \hat{\boldsymbol{I}} = \boldsymbol{C}\ \boldsymbol{x}\ \boldsymbol{R} \end{cases} \quad \textit{(62)}$$

3. Simulating the two ephemeris measurement types. After getting satellite position vectors $\vec{\boldsymbol{P}}_{\boldsymbol{RTN}}$ in the (***R***,***T***,***N***) coordinate system, it is possible to proceed with the real simulation of LIDAR and Optical measurements, which will be detail in the next two paragraphs.
   It leads to the computation of satellite simulated position vectors $(\vec{\boldsymbol{P}}_{\boldsymbol{RTN}})'$ in the (***R***,***T***,***N***).

4. Re-converting these simulated $(\vec{\boldsymbol{P}}_{\boldsymbol{RTN}})'$ vectors in the Cartesian (***x***,***y***,***z***) coordinate system, using the inverse formula of the equation (60):

$$(\vec{\boldsymbol{P}}_{\boldsymbol{xyz}})' = \boldsymbol{\Gamma}^{-\boldsymbol{1}} \cdot (\vec{\boldsymbol{P}}_{\boldsymbol{RTN}})' \quad \textit{(63)}$$

   Considering the orthonormal propriety characterizing the rotation matrix $\boldsymbol{\Gamma}$, this equation can be simplified in:

$$(\vec{\boldsymbol{P}}_{\boldsymbol{xyz}})' = \boldsymbol{\Gamma}^{\boldsymbol{T}} \cdot (\vec{\boldsymbol{P}}_{\boldsymbol{RTN}})' \quad \textit{(64)}$$

   The obtained $(\vec{\boldsymbol{P}}_{\boldsymbol{xyz}})'$ vectors have then to be expressed in relation to the Mars mass centre, by a reverse displacement of the reference frame origin from Phobos to its central body.
   This last action is mandatory, since "*Ephemeris*" files (for both QSO trajectories and simulated ephemeris measurements) must be expressed in a coordinate system centred on the central body, if they represent input files for the GINS software.

5. Writing at most four output files for each QSO, containing the simulated ephemeris measurements:

QSO class	Simulated ephemeris measurement file
QSO-H QSO-M QSO-L	1. Optical simulated $(\vec{\boldsymbol{P}}_{xyz})'$ vectors: one every hour, only in time intervals not covered by Madrid and Usuda DSN measurements
	2. Optical simulated $(\vec{\boldsymbol{P}}_{xyz})'$ vectors: one every hour, only in time intervals not covered by Usuda DSN measurements
QSO-L	3. LIDAR simulated $(\vec{\boldsymbol{P}}_{xyz})'$ vectors: one every second, only in time intervals not covered by Madrid and Usuda DSN measurements
	4. LIDAR simulated $(\vec{\boldsymbol{P}}_{xyz})'$ vectors: one every second, only in time intervals not covered by Usuda DSN measurements

Table 4 *- Possible simulated "Ephemeris" measurement output files.*

All these simulated ephemeris measure files are suitable for being used in GINS "*Director*" as "*Measurements"* input, for the next project steps.

The next two paragraphs will go into the details of the third action realised by the Fortran programme: LIDAR and Optical measurement effective simulation.

3.4.1 LIDAR measurement simulation

Following the project chronological order, the first ephemeris measures to be modelled have been the LIDAR ones.
LIDAR stands for "Light Detection And Ranging". Effectively, this is a ranging instrument, which will be positioned on-board the satellite and whose project is now headed by the JAXA member Dr. Hiroki Senshu as a PI (Principal Investigator) of LIDAR in MMX mission.
On one side, LIDAR instrument will be useful to detect information on shape of the Martian moon surface. This is a fundamental element for MMX scientific purposes, such as the creation of shape models and the investigation of the surface conditions [16].
However, LIDAR technique will be primarily indispensable for spacecraft operations thanks to its ranging detection capability. In fact, this instrument will be able to measure distances (ranging) by irradiating a laser light which will illuminate parts of the target surface and will be then reflected towards a specific LIDAR sensor on-board the satellite.
Moreover, it will be possible to derive Phobos surface altitude and albedo distribution, from measuring time taken for the laser reflected light to return to the sensor and its reflection energy.

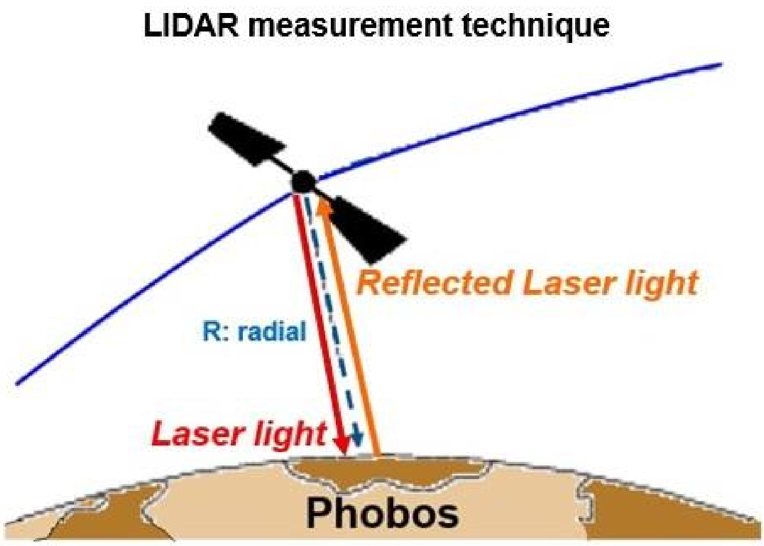

Figure 30 *- Schematic representation of LIDAR technique.*

Since this laser instrument deals with distance evaluations, in this internship project LIDAR captures are simulated as altimetric measurements, in a simplified model. The definition "simplified" is referred to the fact that the laser simulation method has been developed taking into account the instantaneous distances between the satellite and Phobos mass centre, while in the reality, LIDAR laser light will reach the target surface.
However, this approach enables to get an initial LIDAR measurement approximation, which appears to be sufficiently accurate (especially considering the limited Phobos dimensions).
In accordance with this altimetric concept, the simulation model defines LIDAR measurement error as an inaccuracy on the altitude reached by the satellite over the centre of Phobos.
This distance imprecision leads to an ephemeris uncertainty along the radial direction ***R*** of the instantaneous spacecraft positions on its QSO trajectories.
Evidently, LIDAR inaccuracy level increases with the satellite altitude: this aspect justifies JAXA constraint of using LIDAR instrument only within a distance of 50.0km from Phobos.
All these altimetric considerations lead to a LIDAR measurement simulation model consisting in the addition of a perturbation $(\vec{\boldsymbol{\delta}}_{RTN})_L$ along the radial direction of the satellite position vector $\vec{\boldsymbol{P}}_{RTN}$, during time intervals without DSN measures, along the only QSO-L trajectories.
The consequent simulated position vector is:

$$(\vec{\boldsymbol{P}}_{RTN})'_L = \vec{\boldsymbol{P}}_{RTN} + (\vec{\boldsymbol{\delta}}_{RTN})_L \qquad \textbf{\textit{(65)}}$$

Taking into account that LIDAR perturbation involves the only radial direction, the previous relation can be expressed as:

$$(\vec{\boldsymbol{\delta}}_{RTN})_L = \begin{pmatrix} \delta R \\ \delta T \\ \delta N \end{pmatrix}_L = \begin{pmatrix} \delta R_L \\ 0 \\ 0 \end{pmatrix} \qquad \textbf{\textit{(66)}}$$

The quantification of this additional radial perturbation $\boldsymbol{\delta R_L}$ depends on LIDAR measurement error, defined by the relative noise standard deviation ($\boldsymbol{\sigma_L}$).
In fact, in this ephemeris measurement model, the $\boldsymbol{\sigma_L}$ element corresponds to an error standard deviation ($\boldsymbol{\sigma_R}$) over the satellite radial position in relation to Phobos mass centre:

$$\sigma_L = \sigma_R \tag{67}$$

The figure below shows a graphical interpretation of the σ_R element.

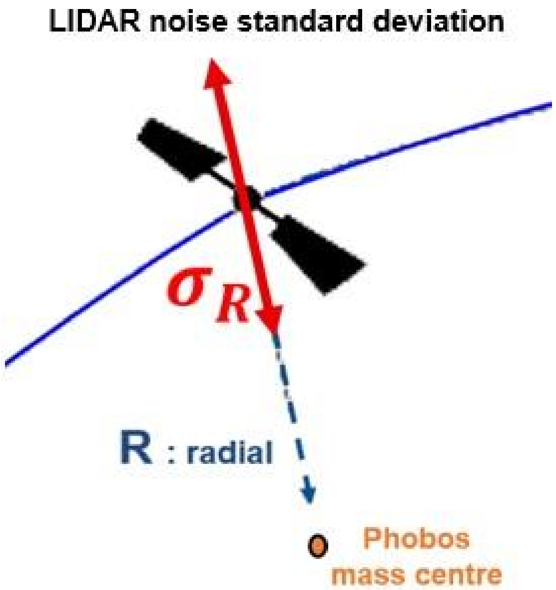

Figure 31 *- Schematic representation of LIDAR measurement noise standard deviation* $\sigma_L = \sigma_R$.

As announced before, the σ_L value is fixed by the JAXA at:

- $\sigma_L = 2.0m$ if the satellite reaches an altitude equal or lower than 100.0m over Phobos surface;
- $\sigma_L = 22.0m$ if the satellite reaches an altitude equal or higher than 100.0km over Phobos surface

This JAXA hypothesis suggests that, starting from an error standard deviation of 2.0m characterising an altitude of 100.0m, every increase of 99.9km in satellite distance from the Phobos surface generates an augmentation in the σ_L value of 20.0m.
As a consequence, in order to compute an appropriate LIDAR noise standard deviation for each spacecraft radial distance (R) from the Martian moon, a mathematic linear proportion is used:

$$99.9km : 20m = (R - 0.1km) : (\sigma_L - 2.0m) \tag{68}$$

The resolution of this linear proportion between satellite altitude and LIDAR noise element σ_L, leads to the definition of the standard deviation to be used to compute the radial position perturbation:

$$\sigma_R = \sigma_L = \frac{20m \cdot (R - 0.1km)}{99.9km} + 2.0m \tag{69}$$

Naturally, this expression involves a linear increase in LIDAR noise standard deviation with the distance reached by the satellite from Phobos mass centre.
Effectively, this feature is coherent with LIDAR technique, considering that the longer is the path to be cross by the laser light and its reflected ray, the larger its measuring inaccuracy is.
Once the σ_R value is computed, it is used to generate LIDAR radial perturbation over satellite positions on its QSO trajectories: $\delta R_L = \delta R_L(\sigma_R)$.

In fact, this perturbation is numerically calculated throughout a random normal Gaussian distribution function, characterized by mean value $\boldsymbol{\mu = 0}$, a standard deviation equal to $\boldsymbol{\sigma_R}$ and a probability density function expressible as follows:

$$\boldsymbol{f(x) = \frac{1}{\sigma_R\sqrt{2\pi}} e^{-\frac{1}{2}\left(\frac{x-\mu}{\sigma_R}\right)^2}} \qquad \textbf{\textit{(70)}}$$

This radial perturbation created in function of the LIDAR noise standard deviation $\boldsymbol{\delta R_L(\sigma_R)}$, is then added to the first component of satellite position vector, expressed in the (***R**,**T**,**N***) coordinate system.
Consequently, the effective LIDAR measurement simulation consists in the following perturbation of the only radial component of the $\vec{\boldsymbol{P}}_{\boldsymbol{RTN}}$ satellite vectors, expressed in the Phobos centred reference frame:

$$\boldsymbol{R' = R + \delta R_L(\sigma_R)} \qquad \textbf{\textit{(71)}}$$

As explained in the previous paragraph, the consequent perturbed satellite position vector $\left(\vec{\boldsymbol{P}}'_{\boldsymbol{RTN}}\right)_{\boldsymbol{L}}$ is then rotate in the Cartesian coordinates system $\left(\vec{\boldsymbol{P}}'_{\boldsymbol{xyz}}\right)_{\boldsymbol{L}}$ and expressed in relation to Mars mass centre. Finally, these $\left(\vec{\boldsymbol{P}}'_{\boldsymbol{xyz}}\right)_{\boldsymbol{L}}$ vectors are used to generate the resulting measure simulation outputs. Each QSO-L trajectory is thus characterized by two simulated LIDAR measurement files, containing:

1. the $\left(\vec{\boldsymbol{P}}'_{\boldsymbol{xyz}}\right)_{\boldsymbol{L}}$ vectors calculated every second, within time intervals without Madrid and Usuda DSN measurements;
2. the $\left(\vec{\boldsymbol{P}}'_{\boldsymbol{xyz}}\right)_{\boldsymbol{L}}$ vectors calculated every second, within time intervals without Usuda DSN measurements.

These two simulated measure files represent the basis for the next Phobos gravity field *Restitution* project step.
Moreover, the treatment of the first of these resulting files with the Python *Visualisation Module*, enables the graphical representation of simulated ephemeris LIDAR measurements and the relative satellite position differences in relation to the interpolated QSOs:

LIDAR ephemeris measurements – Interpolated QSO

Trajectories	Position Difference
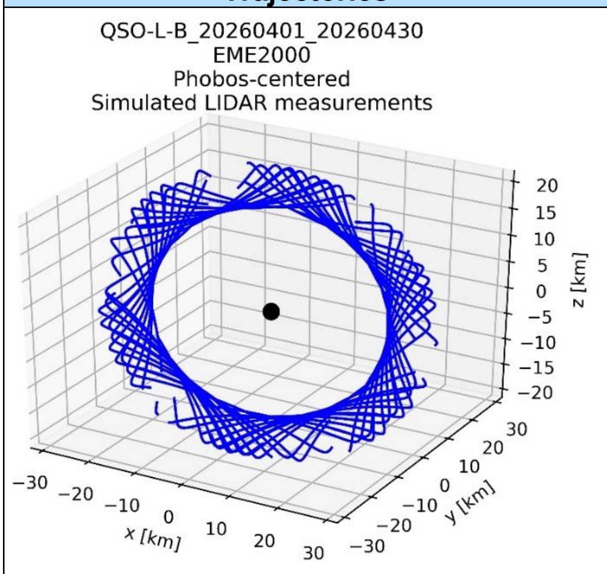	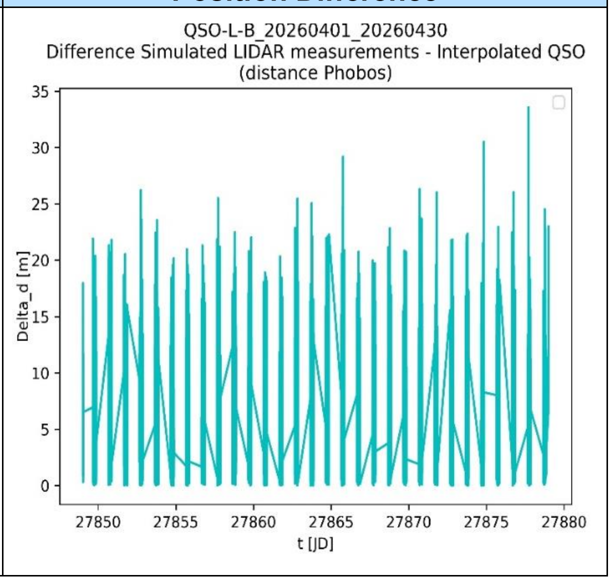

***Figure 32** - Example of simulated LIDAR measurements along a QSO-L trajectory.*

The ephemeris representation on the left underlines that LIDAR measurements are only considered in some portions of QSO-L trajectories. More precisely, laser captures are realised in only the DSN measurement-free orbit sections, complementary to areas represented in Figure 27.

3.4.2 Optical measurement simulation

On-board the satellite designed for the MMX mission, not only DSN sensors and LIDAR instrument will be present, but also specialised optical navigation cameras.
For instance, there will be the OROCHI. This name stands for “Optical RadiOmeter composed of CHromatic Imagers”. It is a wide-angle camera, suitable for observation of topography and material compositions of Phobos surface. This instrument is able to take images in the visible light reflected by the Martian moon surface at multiple wavelengths, and it can be employed for the identification of organic and inorganic materials.
A second conceived navigation camera is the so called TENGOO. TENGOO stands for “TElescopic Nadir imager for GeOmOrphology”. It is a telescopic camera, characterized by a narrow observation angle, useful for analysing the terrain details on Phobos surface. In fact, TENGO is able to capture surface images with a resolution of about 40.0cm and obtain information about the distribution of different materials, corresponding to the Martian moon samples which will be collected. Moreover, it can also be employed for checking safety at the planned landing site [17].

Such on-board cameras are a fundamental presence for the MMX mission: they allow the capture of navigation images, which not only are important for the target surface exploration, but also enable Optical navigation measurements.
The latter represent the complement to LIDAR measures and again, they are useful for detecting satellite motion along its orbits. In fact, Optical measurements provide information about satellite position within the normal plane to its radial direction pointing Phobos. This means that, considering the satellite (***R***,***T***,***N***) coordinate system, Optical captures are referred to the ***T-N*** plane, tangential to the spacecraft orbital track:

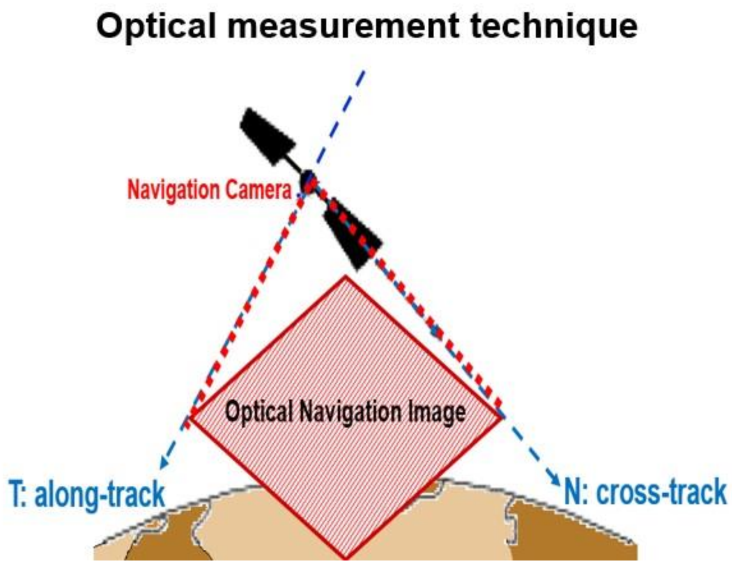

Figure 33 *Schematic representation of Optical navigation image technique.*

Because of their nature, Optical images provide direct information on satellite position vector ($\vec{\boldsymbol{P}}_{\boldsymbol{RTN}}$), exactly as the LIDAR laser. This leads to treat also the Optical as ephemeris measurement types, within this internship project.

However, differently from LIDAR measures, the Optical are modelled as *angular* measurements. This modelling approach is due to the fact that their capture and accuracy level strictly depend on the camera observation angle and its centring in relation to Phobos centroid. This characteristic imposes on the simulation model to define the Optical measurement error as an angular inaccuracy. Consequently, this time the measure inaccuracy leads to an ephemeris uncertainty along the tangential (***T***) and the normal (***N***) directions of instantaneous spacecraft positions on its QSO trajectories.
Therefore, the model developed for simulating Optical measurements consists in the addition of a perturbation $\left(\vec{\boldsymbol{\delta}}_{\boldsymbol{RTN}}\right)_{\boldsymbol{O}}$ along the tangential and normal directions of satellite position vectors $\vec{\boldsymbol{P}}_{\boldsymbol{RTN}}$, during time intervals without DSN captures. The consequent simulated position is defined as:

$$\left(\vec{\boldsymbol{P}}_{\boldsymbol{RTN}}\right)'_{\boldsymbol{O}} = \vec{\boldsymbol{P}}_{\boldsymbol{RTN}} + \left(\vec{\boldsymbol{\delta}}_{\boldsymbol{RTN}}\right)_{\boldsymbol{O}} \tag{72}$$

Considering that Optical perturbation involves only the tangential and normal directions, the previous relation can be expressed as:

$$\left(\vec{\boldsymbol{\delta}}_{\boldsymbol{RTN}}\right)_{\boldsymbol{O}} = \begin{pmatrix} \delta R \\ \delta T \\ \delta N \end{pmatrix}_{\boldsymbol{O}} = \begin{pmatrix} 0 \\ \delta T_{\boldsymbol{O}} \\ \delta N_{\boldsymbol{O}} \end{pmatrix} \tag{73}$$

The quantification of this additional tangential and normal perturbations, $\boldsymbol{\delta T_O}$ and $\boldsymbol{\delta N_O}$, depends on the Optical measurement error, defined by the relative noise standard deviation ($\boldsymbol{\sigma_O}$).
In fact, in this simulation model, the navigation image noise relays exactly on the error standard deviation of the camera centring, imposed by the JAXA to be $\boldsymbol{\sigma_O}$ **= 0.1°**.
As a consequence, the relative tangential ($\boldsymbol{\sigma_T}$) and normal ($\boldsymbol{\sigma_N}$) perturbation standard deviations are modelled through the following relation, linking the $\boldsymbol{\sigma_O}$ term to the spacecraft radial distance ($\boldsymbol{R}$) from Phobos mass centre:

$$\boldsymbol{\sigma_T} = \boldsymbol{\sigma_N} = \boldsymbol{R_{sc}} \cdot \boldsymbol{sin(\sigma_O)} \tag{74}$$

The figure below shows a graphical interpretation of the $\boldsymbol{\sigma_O}$, $\boldsymbol{\sigma_T}$ and $\boldsymbol{\sigma_N}$ elements.

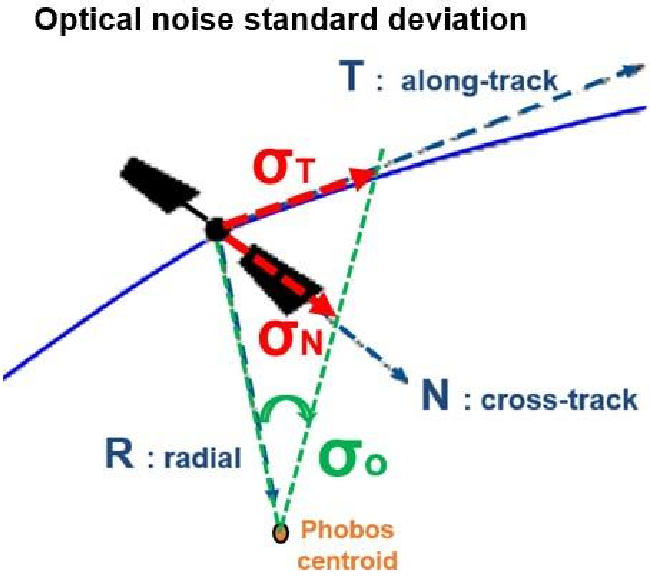

Figure 34 *- Schematic representation of Optical measurement noise standard deviation.*

This figure, along with equation (74), highlights the inevitable increase in Optical noise standard deviation with the altitude reached by the satellite over the target body. However, different form the LIDAR case, this augmentation is reduced by the sinusoidal presence.

Once computed the $\boldsymbol{\sigma_T}$ and $\boldsymbol{\sigma_N}$ values, they are used to generate the Optical ephemeris perturbations over satellite positions along its QSO trajectories: $\boldsymbol{\delta T_O = \delta T_O(\sigma_O)}$ and $\boldsymbol{\delta N_O(\sigma_O) = \delta N_O}$.
In fact, as for the LIDAR situation, these perturbations are numerically calculated through a random normal Gaussian distribution function, characterized by a mean value $\boldsymbol{\mu = 0}$, a standard deviation equal to $\boldsymbol{\sigma_T}$ (= $\boldsymbol{\sigma_N}$) and the same probability density function expressed in equation (70).
Consequently, both tangential and normal perturbations are modelled in function of the $\boldsymbol{\sigma_O}$ term, which is equivalent to mean that they are created in function of the derived tangential and normal error standard deviations: $\boldsymbol{\delta T_O(\sigma_T)}$ and $\boldsymbol{\delta N_O(\sigma_N)}$.
These two Optical perturbations are then added to the second and third components of satellite position vectors, expressed in the (***R,T,N***) coordinate system.
Therefore, Optical navigation measurement simulation consists in the following perturbation of the only tangential and normal components of $\boldsymbol{\vec{P}_{RTN}}$ satellite vectors, expressed in the Phobos centred reference frame:

$$\begin{cases} \boldsymbol{T_{sat}}' = \boldsymbol{T_{sat}} + \boldsymbol{\delta T_O(\sigma_T)} \\ \boldsymbol{N_{sat}}' = \boldsymbol{N_{sat}} + \boldsymbol{\delta N_O(\sigma_N)} \end{cases} \tag{75}$$

As explained in the previous chapter, perturbed satellite position vector $\boldsymbol{(\vec{P}'_{RTN})_O}$ is then rotate in the Cartesian coordinates system $\boldsymbol{(\vec{P}'_{xyz})_O}$ and expressed in relation to Mars mass centre.
Therefore, each QSO trajectory is characterized by two simulated Optical navigation measurement files, containing:

1. The $\boldsymbol{(\vec{P}'_{xyz})_O}$ vectors calculated every hour, within time intervals without Madrid and Usuda DSN measurements;

2. The $\left(\vec{P}'_{xyz}\right)_{0}$ vectors calculated every hour, within time intervals without Usuda DSN measurements.

Along with LIDAR ones, these two simulated measurement files constituted the basis for the immediately following Phobos gravity field *Restitution* project step.
Moreover, the treatment of the first of these resulting files with the Python *Visualisation Module*, enables the graphical representation of simulated ephemeris Optical measurements and the relative satellite position differences in relation to the interpolated QSOs:

Optical ephemeris measurements – Interpolated QSO

<table>
<tr><th>Trajectories</th><th>Position Difference</th></tr>
<tr><td>
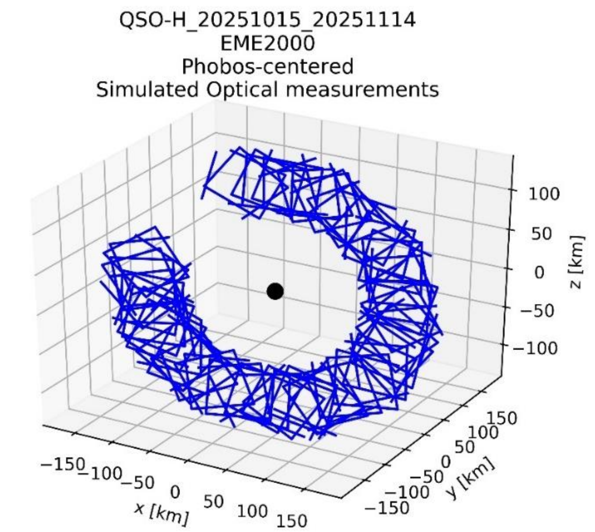

</td><td>
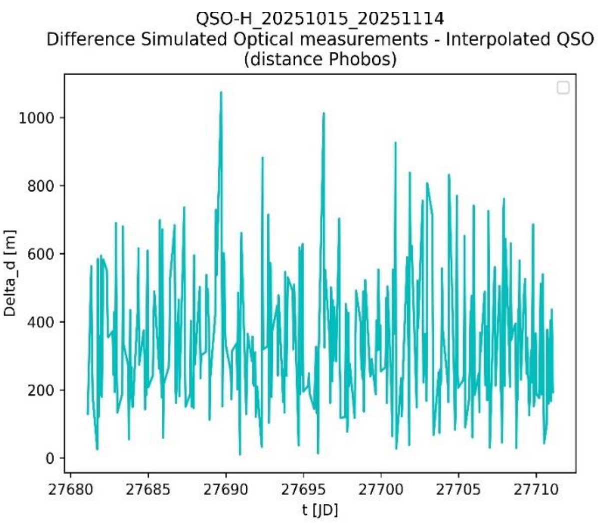

</td></tr>
<tr><td colspan="2">Figure 35.a – QSO-H class example.</td></tr>
<tr><td>
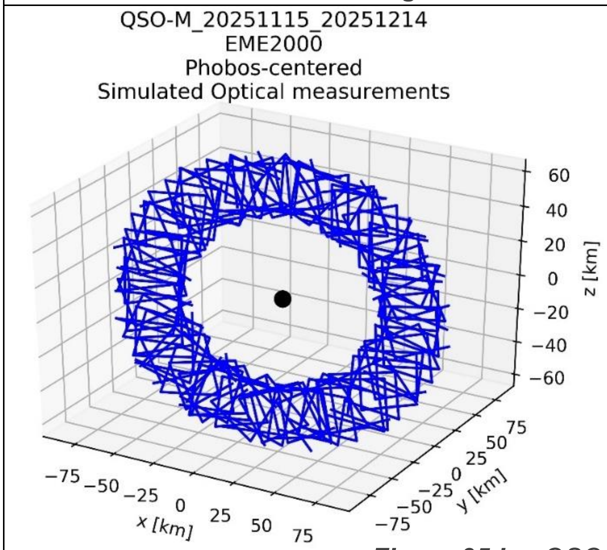

</td><td>
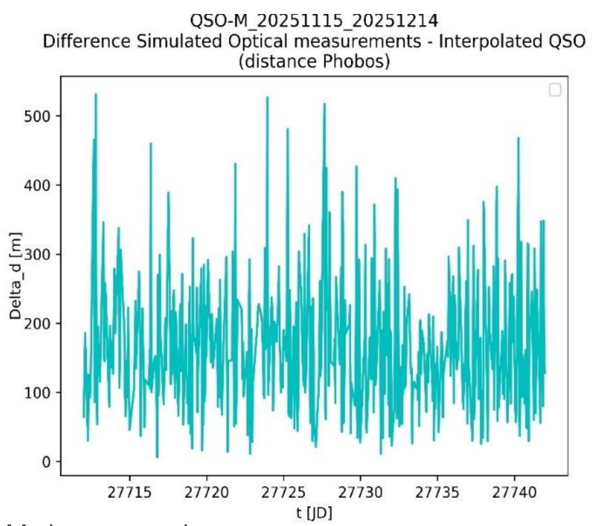

</td></tr>
<tr><td colspan="2">Figure 35.b – QSO-M class example.</td></tr>
</table>

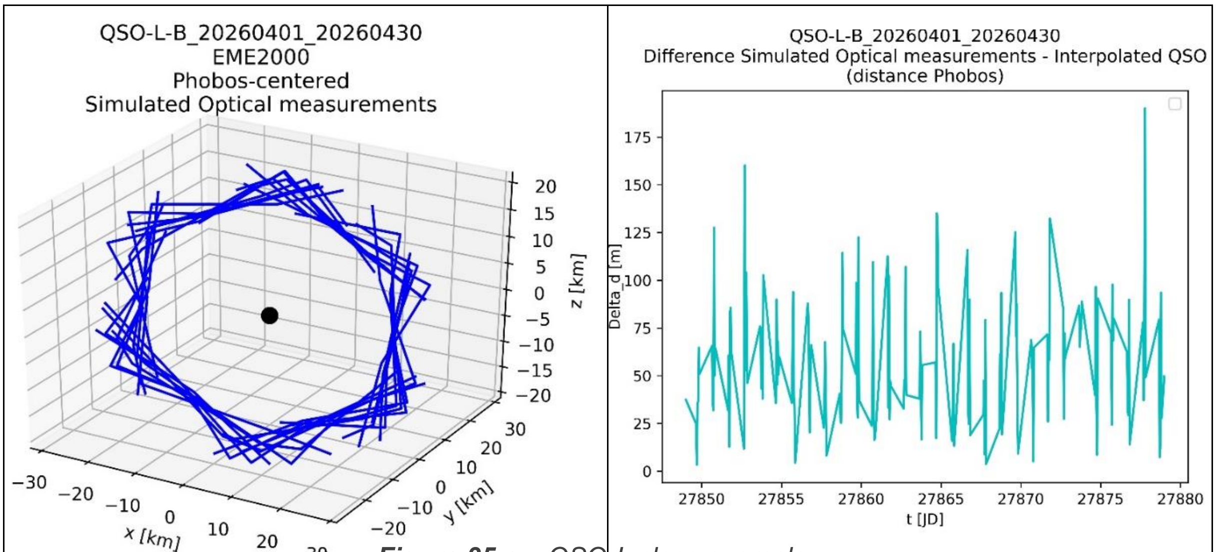

Figure 35.c *– QSO-L class example.*

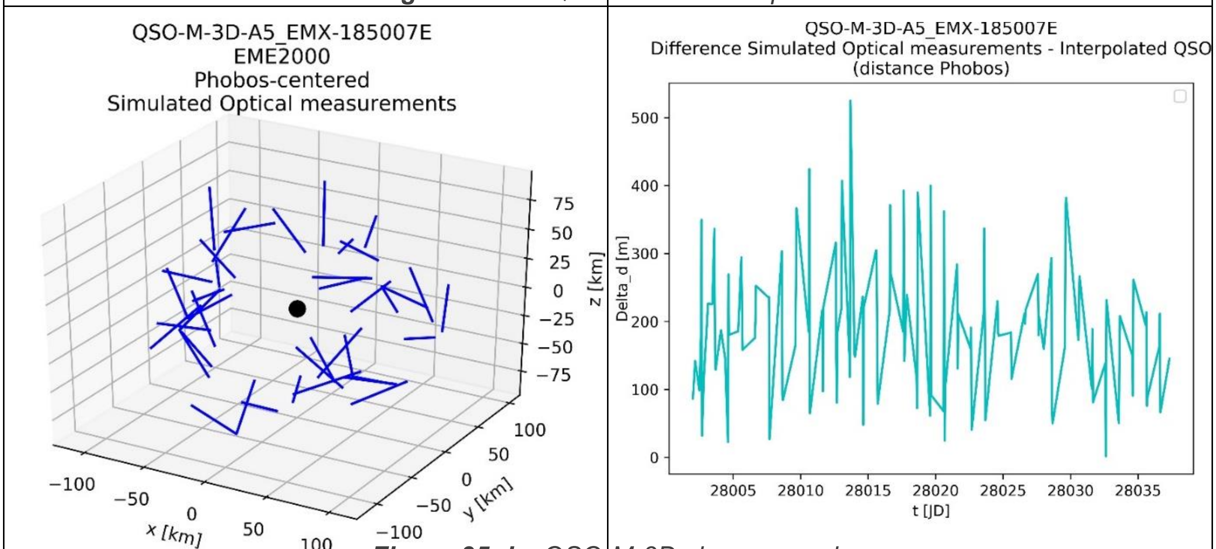

Figure 35.d *– QSO-M-3D class example.*

Figure 35 *- Examples of simulated Optical measurements along one trajectory for each QSO class.*

These graphs prove that, despite the small amount of Optical measurements, the latter represent an additional contribution in providing spacecraft position along its orbits. Effectively, the comparison between Figures 32 and Figure 35.c relative to the QSO-L trajectory, underlines the lower presence of Optical captures (one every hour) in relation to LIDAR ones (one every second). However, this aspect does not preclude the Optical navigation images to furnish quite precise position measures.

Moreover, the graphs on the right, reporting the module of the difference between position vectors relative to the interpolated QSO and the Optical simulation, highlights the increase in Optical measurement inaccuracy with the dimensions characterising a specific trajectory:

Orbit class	Maximal difference
QSO-H	1 km
QSO-M	0.5 km
QSO-L	0.175 km
QSO-3D-M	0.5 km

Table 5 *- Maximal differences in satellite position along simulated Optical ephemeris and interpolated orbits.*

3.5 Phobos gravity field restitution

At this point of the project, all measurement types requested from the JAXA for Phobos geodesic analysis, have been simulated.
As specified before, the simulation of all the DSN, LIDAR and Optical measures, is realised considering the project reference Phobos gravity model, defined by gravity spherical harmonics up to degree 20. This means that the simulated values represent the most realistic measurements possible within this study. Consequently, the latter are traded as precise measures to be used as reference in this gravity field *Restitution* project step.

Overall, a GINS parameter restitution procedure is able to estimate what could happen in a real mission. At the same time, it is useful at the moment when physical parameters need to be evaluated and adjusted, in case of non-perfectly accurate a priori values.
For instance, in the MMX case, the mission will start with a lack of knowledge of real Phobos gravity field: one of its objectives will be to correct the Martian moon gravitation model and finally return the most truthful version possible.
GINS restitution can emulate this process. Using both the initial unknowledge of some physical features and the reference measurements, GINS operates the correction of parameters set as adjustable in a specific study case.
This adjustment is realised by the software through a specific technique. During the restitution procedure, a new set of desired measurements is generated: GINS corrects the adjustable parameters, so that these new measures are forced to be as similar as possible to the reference ones. In this way, free parameters are conducted towards the values they would have within an accurate realistic geodesic model.

Specifically, in this internship context, the reference measurements are represented by the simulated DSN (with Madrid and Usuda stations and with the only Usuda one), LIDAR and Optical “*Measurements*” files:

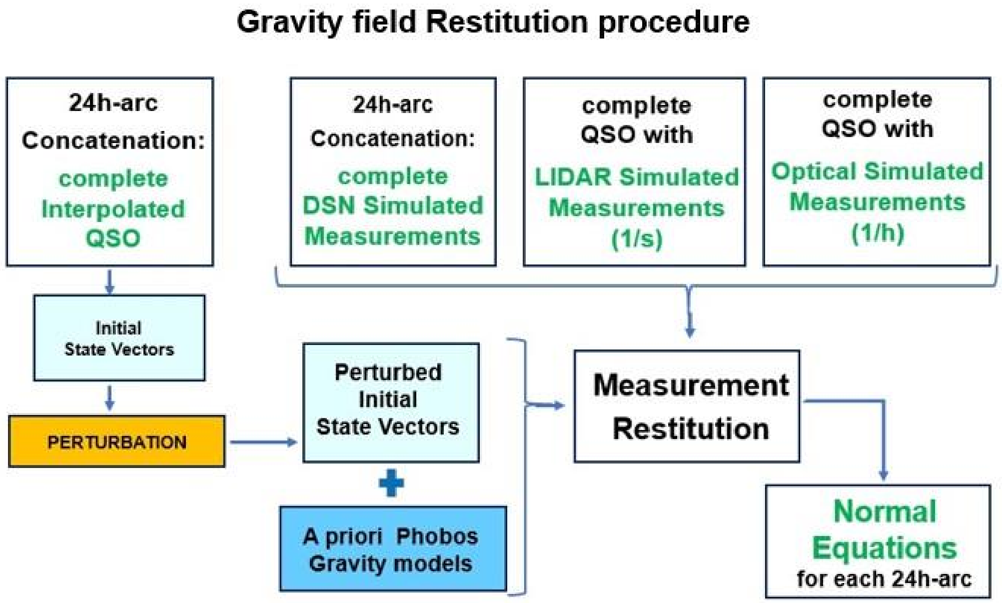

Figure 36 *- Schematic representation of the restitution procedure.*

In this MMX analysis, the initial imprecise geodesic knowledge concerns Phobos gravity field: the mission is supposed to recover as precisely as possible this parameter model. Consequently, in order to simulate the inaccuracy level of the target gravity model at the beginning of the mission, four different precise (the first) and non-accurate (the other three) a priori spherical harmonic templates are adopted:

1. "**Gravity model 1**": the first a priori Phobos gravity template is equivalent to the reference up-to-degree-20 model, used for QSO adjustment and measurement simulation;
2. "**Gravity model 2**": the second a priori Phobos gravity model contains the same reference Stokes coefficient values, but only up to degree 2. It is the less accurate template of the four used in this project;
3. "**Gravity model 3**": the third a priori Phobos gravity model includes the same Stokes coefficient values of the reference model, but only up to degree 3. This means that it is a little more accurate than the second template;
4. "**Gravity model 4**": the fourth a priori Phobos gravity filed template contains again gravitational spherical harmonics up to degree 20, but its Stokes coefficient numerical values are truncated at the third decimal place. Consequently, it is less precise than the reference model.

The first a priori Phobos gravity field model has been chosen in order to verify the influence of the simulated measurement noises on the restitution of gravitational Stokes coefficients. Instead, the other three inaccurate models are useful to test if an initial non-precise knowledge of real Martian moon gravity parameter, could preclude the correct model adjustment.

At the same time, exactly as for the Phobos gravitational field, the interest is also to understand if less precise satellite initial state vectors $[\vec{r}_0, \dot{\vec{r}}_0]$ can be adjusted into their correct values, leading to a proper gravity model recovery.
Basically, the most accurate initial state vectors of each 24-hour orbit arc are expressed in the complete interpolated QSO "*Ephemeris*" files. In fact, the latter are the outputs generated in the *DSN Simulation* step, where all trajectory arcs are interpolated taking into consideration the reference Phobos gravity model.

Thus, an a priori imprecise version of initial state vectors is used. Their noised version is calculated though the addition of a vectorial perturbation, including:

- a module position noise of ***200.0m***
- a module speed noise of ***0.8m/s***

The perturbed initial state vectors [$\vec{r'}_0$, $\vec{\dot{r'}}_0$] are set as QSO arc *initial state vectors* in GINS *Restitution* "*Director*" file, in order to discover if their perturbation can preclude the target gravity model adjustment.

Taking into account all these considerations, Phobos gravity Stokes coefficients up to degree 4 and satellite initial state vectors have been set as adjustable parameters.
It indicates that these two parameter groups can be corrected by GINS in order to conduct the newly simulated DSN, LIDAR and Optical measurements to be as close as possible to the reference ones.
However, the parameter adjustment method followed is not the same for both the groups.
For satellite initial state vectors, the correction procedure is completely solved within the GINS restitution procedure. On the contrary, for Phobos gravity field a supplemental iteration is imposed (paragraph 2.1.3). This means that the up to 4 degree-normalised Stokes coefficients are not directly adjusted during the restitution phase: their partial derivatives are computed and their normal systems without constraints rebuilt during the requested additional iteration.
This approach leads to generate "*Normal Equations*" output files, available for use by DYNAMO chain, where normal equation resolution could furnish the corrected up to 4-degree normalised Stokes coefficients.

As for the previous project steps, all the considerations expressed so far, have to be turned into GINS instructions in the *Restitution* "*Director*" file.
Moreover, since both DSN "*Measurements*" and interpolated QSO "*Ephemeris*" (which gave birth to the simulated LIDAR and Optical files) files are generated as a concatenation of 24-hour orbit arcs, it is again necessary to execute the GINS restitution procedure over each 1 day- QSO section, separately.
Therefore, every orbit arc is finally characterized by multiple *Restitution* "*Director*" files, in order to considerate all the various combinations of a priori Phobos gravity models and measurement types (DSN, LIDAR, Optical). The latter are represented in the following table:

QSO arc type	Initial state vector	A priori gravity model	Measurement restitution	Imprecision weight
QSO-H QSO-M QSO-L	[$\vec{r'}_0$, $\vec{\dot{r'}}_0$]	1 2 3 4	DSN (Madrid + Usuda) + Optical	σ_{DSN} , $\sigma_{T_{max}}$
			DSN (Usuda) + Optical	
QSO-L	[$\vec{r'}_0$, $\vec{\dot{r'}}_0$]	1 2 3 4	DSN (Madrid + Usuda) + LIDAR	σ_{DSN} , $\sigma_{R_{max}}$
			DSN (Usuda) + LIDAR	

Table 6 *– Phobos a priori gravity model and measurement combinations used in the Restitution step.*

This table reports in its last column another important parameter, linked to measurement types to be returned in the restitution procedure: the measurement imprecision weight.

This value represents the accuracy characterising a specific measure. More precisely, the higher a measurement type imprecision weight is, the lower its accuracy level results to be and the less it affects the parameter restitution. Put differently, the GINS restitution tends to rest more confident in reference measure types characterised by a lower imprecision weight parameter.
In this project, the accuracy of a measurement type is considered as inversely proportional to its error standard deviation. This leads to match the imprecision weight with the error standard deviation $\boldsymbol{\sigma_{DSN}}$ for DSN, $\boldsymbol{\sigma_R}$ for IDAR and $\boldsymbol{\sigma_T}$ $(= \boldsymbol{\sigma_N})$ for Optical captures.
In DSN case, there is no doubts that the imprecision weight is equal to $\boldsymbol{\sigma_{DSN} = 0.2mm/s}$.
On the contrary, in LIDAR and Optical measure simulation, these standard deviation values are calculated for each satellite position vector, with a time step of 1.0s. It is thus necessary to fix one single $\boldsymbol{\sigma_R}$ and $\boldsymbol{\sigma_T}$ for each QSO, individuated in the maximum values reached by LIDAR ($\boldsymbol{\sigma_{R_{max}}}$) and the Optical ($\boldsymbol{\sigma_{T_{max}} = \sigma_{N_{max}}}$) standard deviations on every entire orbit.

Once executed the entire GINS restitution procedure, the most significant outputs are the "*Listing*" and the "*Normal Equations*" files.
The "*Listing*" allows to discover which combinations of QSO arcs, measurements and a priori Phobos gravity models enable the GINS restitution to get the convergence at the correct measure residuals (***r.m.s.***), computed by equation (41). In this case, the correct measurement residual value corresponds to the measurement error standard deviation, since GINS uses these $\boldsymbol{\sigma}$ elements to calculate the relative measure white noise (equation (20)). Consequently, it is possible to conclude that correct ***r.m.s.*** values are:

- $\boldsymbol{rms \cong \sigma_{DSN} = 0.2mm/s}$ for DSN measurements;
- $\boldsymbol{rms \cong \sigma_{R_{max}}}$ for LIDAR measurements;
- $\boldsymbol{rms \cong \sigma_{T_{max}} = \sigma_{N_{max}}}$ for Optical measurements.

Therefore, the "*Listing*" files provide information about Phobos gravity filed restitution capability of each QSO, considering all measurement and Phobos gravity model combinations.
Thus, it is firstly possible to determinate which orbits are the more suitable for restitution convergence. Secondly, within all the convergent cases, an estimation of which QSOs are favoured in reaching correct final measurement residuals, appears to be useful.
This analysis over "*Listing*" data leads to the global percentage quantifications expressed in the table below, for each QSO group:

QSO Class	A priori gravity model	% Convergence over all the cases	% Correct r.m.s. over the converged cases
QSO-H	1	99.44	100.0
	2	99.44	100.0
	3	99.44	100.0
	4	99.44	100.0
QSO-M	1	98.39	99.80
	2	98.48	99.38
	3	98.28	99.90
	4	98.39	99.80
QSO-L	1	75.67	98.46
	2	76.49	5.320
	3	77.41	61.16
	4	75.67	96.82
QSO-M-3D	1	97.90	100.0
	2	98.20	100.0
	3	97.90	100.0
	4	97.90	100.0

Table 7 *- Global gravity field restitution capability of each QSO class.*

This table highlights the strong impact of the a priori Phobos gravitational field model on Stokes coefficient restitution.
Effectively, the least accurate a priori Phobos “Gravity model 2” can cause a low number of converged cases to proper **r.m.s**, especially considering QSO-L trajectories. The latter are the most affected by a large lack of knowledge of real Martian moon gravitational field. This aspect is made evident by their inferior percentages of correct final **r.m.s.**, when both Phobos “Gravity model 2” and “Gravity model 3” are considered.
This QSO-L higher sensitivity is coherent with their smaller dimensions, in comparison with QSO-H and QSO-M. In fact, the more a satellite transits in proximity of Phobos (or generically of every celestial body) the more it is influenced by the target gravity field. Consequently, these orbits are more impacted by the effects of higher degree-gravity coefficients. Since the a priori “Gravity model 2” and “Gravity model 3” count normalised Stokes coefficients only up to degree 2 and 3, respectively, the low-altitude QSOs suffer from their excessive inaccuracy.

The mathematical translation of these restitution data is represented by the second important output file: the “*Normal Equations*”.
In fact, as imposed by instructions set for GINS in the *Restitution* “*Director*”, one “*Normal Equations*” output file is written for every combination of arcs, measurement types and a priori Phobos gravity model, having reached the convergence in the restitution procedure.
In all these combining cases, one normal equation is created for every single measure kind. This leads to the generation of all the following possible normal equations, for each 24-hour orbit arc:

QSO arc type	A priori gravity model	Measurement combination	Normal equation relative to:
QSO-H QSO-M QSO-L	1 2 3 4	DSN (Madrid + Usuda) + Optical	**Ephemeris Optical** measurements
			Doppler DSN measurements
		DSN (Usuda) + Optical	**Ephemeris Optical** measurements
			Doppler DSN measurements
QSO-L	1 2 3 4	DSN (Madrid + Usuda) + LIDAR	**Ephemeris LIDAR** measurements
			Ephemeris DSN measurements
		DSN (Usuda) + LIDAR	**Ephemeris LIDAR** measurements
			Ephemeris DSN measurements

Table 8 *- Possible normal equation types, for each QSO and a priori model combination, reaching the restitution procedure convergence.*

These normal equations are written in a binary format in their relative output files and they express the linear systems corresponding to the parameters set as adjustable in the *Restitution* "*Director*": satellite initial state vectors and Phobos gravity normalised Stokes coefficients up to degree 4.
As explained before, position and speed vectors at the beginning of each QSO arc, are corrected within the restitution procedure. On the contrary, Phobos gravity coefficient correction is completely left to the DYNAMO chain.
Therefore, DYNAMO represented the main tool of the next project step, aimed to resolve harmonic Stokes coefficient normal equations.

3.6 Phobos gravity field resolution over each QSO

The preceding parameter *Restitution* phase provides the necessary results, upon which to base the development of the *Resolution* project step. In fact, each "*Normal Equations*" file contains one normal equation for each measure type considered in single 24-hour orbit arcs, characterised by every converged combination of Phobos gravity models and measurement kinds (Table 8).
Therefore, it is now necessary to resolve all these equation linear systems, in order to know in which way each QSO could contribute at the target gravity model recovery.
This leads to individuate the first action to be realised in this step: the accumulation of all the normal equations characterising each 24-hour orbit arc, for the purpose of generating single equations describing the entire QSOs.

However, as explained before, every trajectory is featured by a multiple series of normal equation types, corresponding to different measurements and a priori gravity models. Thus, it is fundamental to distinguish and collect properly al the possible kinds of information. Especially, it results particularly useful to combine all the normalised Stokes coefficient equations in relation to different types of measurements. In this way, it is possible to understand which measures really allow a precise reconstruction of Phobos gravity field.
Finally, the resolution of these clustered linear systems enables the computation of corrected normalised Stokes coefficients for every measurement combination, along each QSO.

A visual representation of this step approach, is represented in the following schema:

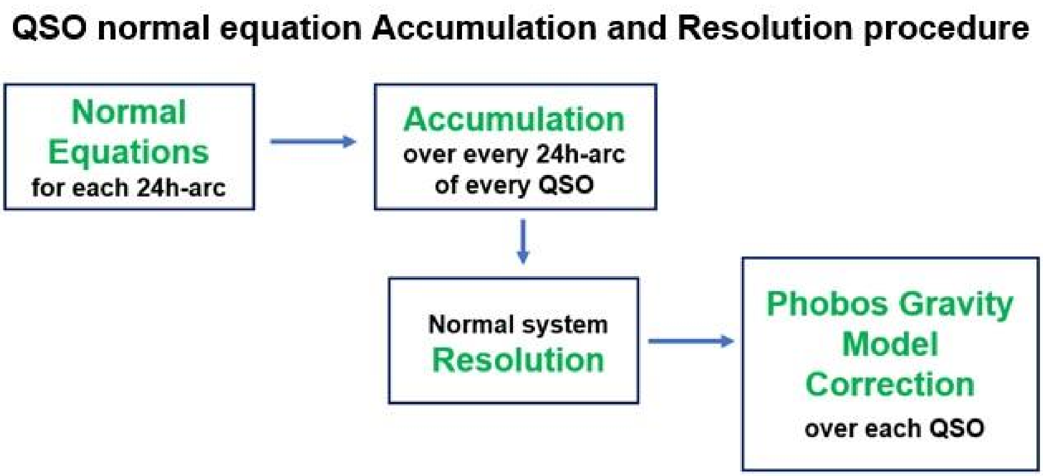

Figure 37 *- Schematic representation of the Resolution project step.*

The next two paragraphs detail normal equation accumulation and the resolution phases.

3.6.1 Normal equation accumulation

The phase of normal equation accumulation is necessary to collect information coming from the different measurement and a priori model conditions, expressed in Table 8.
In practical terms, for each of the four a priori Phobos gravity field models and for every single QSO, normal equations of the 24-hour orbit arcs are cumulated, according to the following measure combinations:

QSO arc type	A priori gravity model	Accumulation of normal equations relative to measurements:
QSO-H QSO-M QSO-L	1 2 3 4	**Doppler DSN** (Madrid+Usuda) only
		Normal equations relative to **Doppler DSN** (Usuda) only
		Doppler DSN (Madrid+Usuda) + **Ephemeris Optical**
QSO-L	1 2 3 4	**Doppler DSN** (Madrid+Usuda) + **Ephemeris LIDAR**
		Ephemeris Optical + **LIDAR** measurements
		Doppler DSN (Madrid+Usuda) + **Ephemeris Optical** + **LIDAR**

Table 9 *- Possible normal equation accumulation, for each converged combination of 24-hour QSO arcs, a priori Phobos gravity models and measurement types.*

This specific accumulation is conducted for the purpose of understanding which combinations of measurements are the most suitable for the detection of a precise Phobos gravity field, considering every QSO separately.

At a practical level, the numerical accumulation is realised by the DYNAMO-C program, which is specialised in this normal equation treatment. It directly works on normal linear systems, expressed in equation (46), where in this case the normal matrix is defined as:

$$\boldsymbol{A^T \pi A} \cdot \Delta\vec{\boldsymbol{X}} = \begin{bmatrix} \left[\frac{\partial Q_1}{\partial \vec{r'}_0}\right] & \left[\frac{\partial Q_1}{\partial \dot{\vec{r'}}_0}\right] & \left[\frac{\partial Q_1}{\partial \bar{C}}\right] & \left[\frac{\partial Q_1}{\partial \bar{S}}\right] \\ \vdots & \ddots & & \vdots \\ \vdots & & \ddots & \vdots \\ \left[\frac{\partial Q_M}{\partial \vec{r'}_0}\right] & \left[\frac{\partial Q_M}{\partial \dot{\vec{r'}}_0}\right] & \left[\frac{\partial Q_M}{\partial \bar{C}}\right] & \left[\frac{\partial Q_M}{\partial \bar{C}}\right] \end{bmatrix} \cdot \begin{pmatrix} \Delta\vec{r'}_0 \\ \Delta\dot{\vec{r'}}_0 \\ [\Delta\bar{C}] \\ [\Delta\bar{S}] \end{pmatrix} = \boldsymbol{A^T \pi \vec{R}} \qquad \textit{(76)}$$

This matrix is constituted by the partial derivatives of all the measurement types considered (Doppler and/or ephemeris) in relation to the physical parameters set as free in the *Restitution* procedure. The latter are thus the six state vector components $\vec{r'}_{0,i}$, $\dot{\vec{r'}}_{0,i}$ and the normalised Stokes coefficients $\bar{C}_{lm}$ and $\bar{S}_{lm}$ up to degree 4, represented by vectorial terms $\bar{C}$ and $\bar{S}$.
DYNAMO-C operates the accumulation of all the considered normal equations, by summing the various contributions on common parameters, both in the normal matrix and in the second member. This action leads to generate one single global equation, representing all cumulated information.

3.6.2 Normal equations resolution: result analysis

Once realised the desired normal equation accumulation over each QSO, numerical resolution is possible.
This action is charged for DYNAMO-D program. Employing equation (55), it realises the normal system inversion, leading to the calculation of the desired corrected parameters.
Final results relative to every entire QSO are thus obtained: the adjusted Phobos gravity coefficients up to degree 4, along with the value of their effective correction (equation (50)) and their standard deviation (equation (56)).

Successively, the "***Coeff_Grav***" function of Python ***Visualisation Module*** allows a visual representation of these results. In fact, the latter are here presented in form of graphs, showing the differences percentages between GINS adjusted coefficients and the most accurate ones, belonging to Phobos reference gravity model (20x20 spherical harmonic terms).
By the utilisation of this function, multiple result analyses are possible.

First result analysis: A first global result analysis enables to compare the capability of each QSO trajectory to adjust Phobos gravity field model.
In this context, results relative to the only combination of the DSN and Optical measurements are presented, as an example.
This analysis is here exposed following the accuracy level of the a priori gravitational templates employed in this project, but in a reverse order.
Therefore, the first exposed case involves results obtained with the a priori Phobos "Gravity model 1", which immediately appears interesting. In fact, since it perfectly corresponds to the most precise template used as a reference, it is inevitable to think that coefficient adjustment

should be excellent for all degrees. However, this is not what happens in 2-Dimensional QSO classes:

$\bar{C}_{lm}$	$\bar{S}_{lm}$
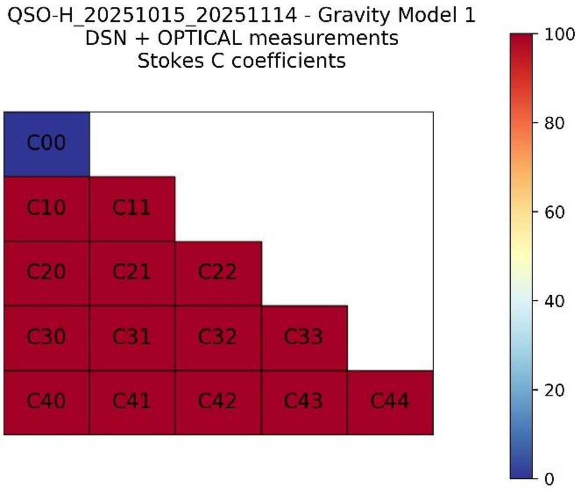	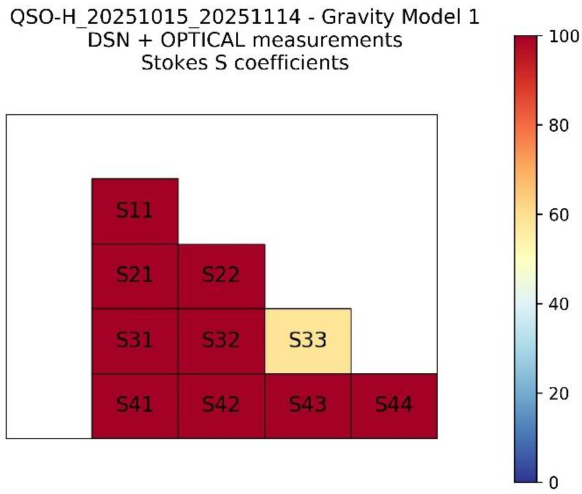

Figure 38.a *– QSO-H class example.*

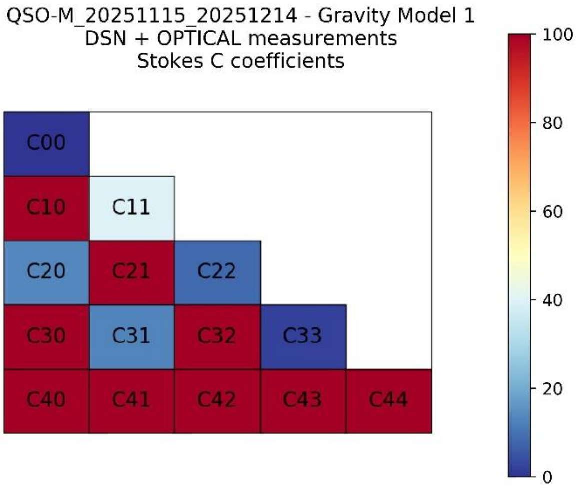	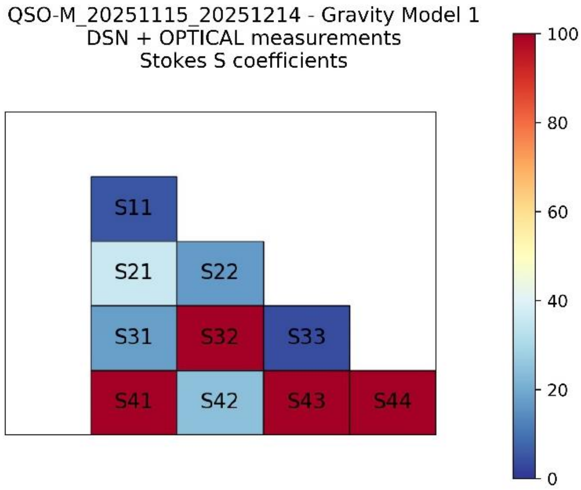

Figure 38.b *– QSO-M class example.*

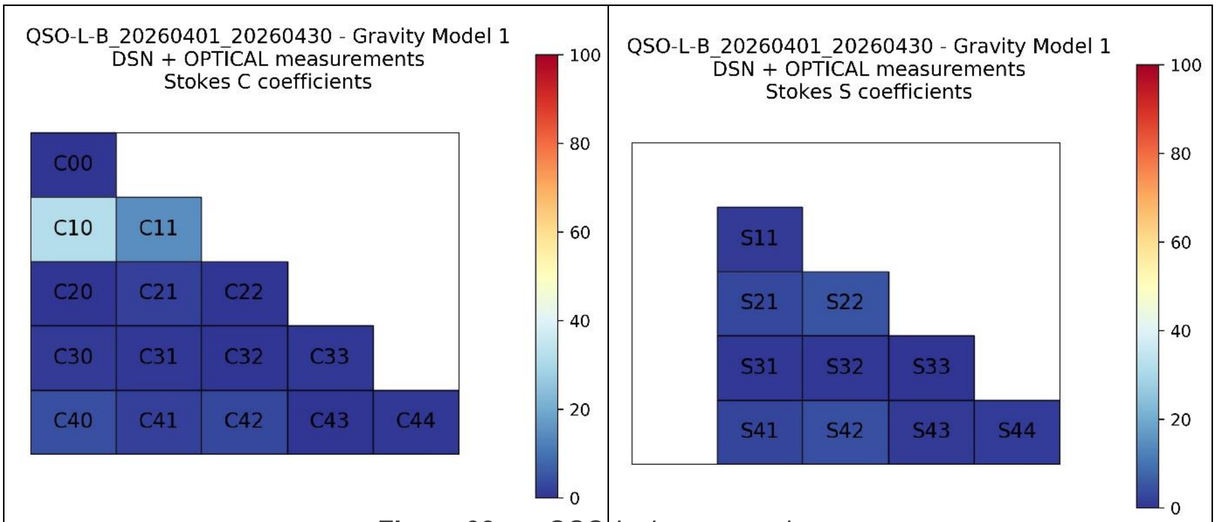

Figure 38.c *– QSO-L class example.*

Figure 38 *- Stokes coefficients adjusted from a priori Phobos "Gravity model 1", considering the DSN and Optical measurement combination along 2D QSOs.*

These graphs show results obtained with three different orbits, taken as examples to represent the general behaviour of the three 2-Dimensional QSO classes.
As they bring to light, the low-altitude orbits manage to return a sufficiently precise Phobos gravity version. On the contrary, the largest QSO-H trajectories are unable to correctly adjust normalised Stokes coefficients, apart from the perfect recover of the $\boldsymbol{C_{00}}$ term, corresponding to the Martian moon standard gravitational parameter $\boldsymbol{\mu = GM}$. At the same time, the QSO-M class results the get a better restitution of few gravity coefficients, almost up to the degree 3, but they are still far from a realistic representation of Phobos reality.

In the particular case of "Gravity model 1", this general inability is strictly linked to the high sensitivity to measurement noise and initial state vector perturbation. Effectively, in the measure *Simulation* step, a white noise has been considered for all the simulated measurement types. Moreover, a noised initial position and speed vector version has been adopted in the *Restitution* phase. Consequently, this missed correct reconstruction of Phobos gravity is a consequence of these two noise considerations.
This aspect proves that high and medium QSOs result to be more influenced by measurement and initial state vector noise then QSO-L trajectories. However, the same cannot be said for the 3-Dimensional QSO-M class, whose higher latitudes reached over Phobos surface allows them to recover almost all the Stokes coefficients:

$\overline{C}_{lm}$	$\overline{S}_{lm}$

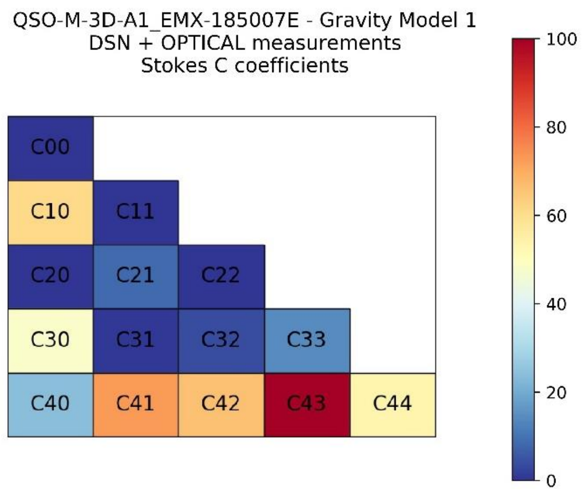

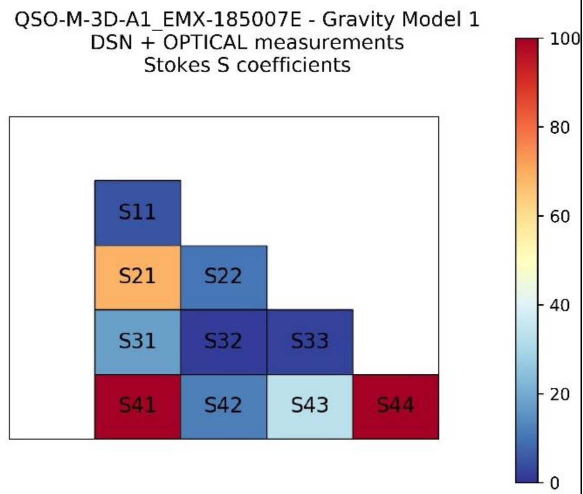

***Figure 39.a** – QSO-M-3D-A1.*

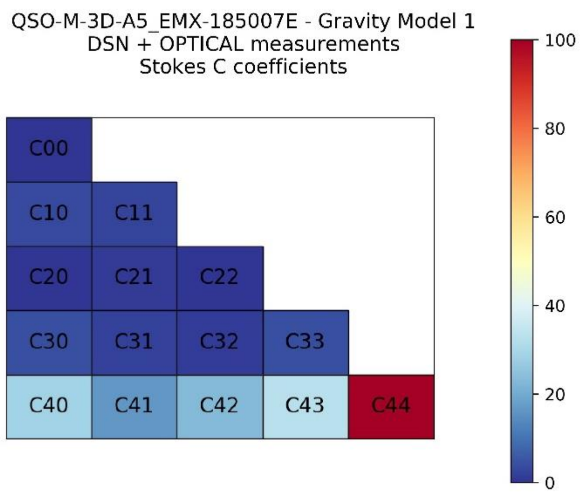

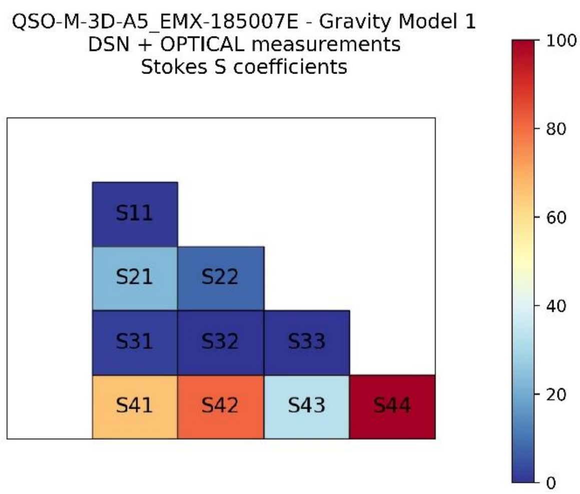

***Figure 39.b** – QSO-M-3D-A5.*

***Figure 39** - Stokes coefficients adjusted from a priori Phobos "Gravity model 1", considering the DSN and Optical measurement combination along QSO-M-3D trajectories.*

The previous graphs correspond to two 3D-QSO trajectories, respectively characterised by a lower (Figure 39.a) and a higher (Figure 39.b) latitude reachable over the target body.
These figures not only highlight the more precise restitution of Phobos gravity field afforded by the 3-Dimensional trajectories, but also prove that the more elevate is their *Z*-dimension, the more their capacity in Stokes coefficient reconstruction increases.

Continuing this analysis with the coefficient correction resulting from the adoption of the quite precise "Gravity model 4", the following graphs correspond again to the same 2-Dimensional trajectories taken as examples before:

$\overline{C}_{lm}$	$\overline{S}_{lm}$

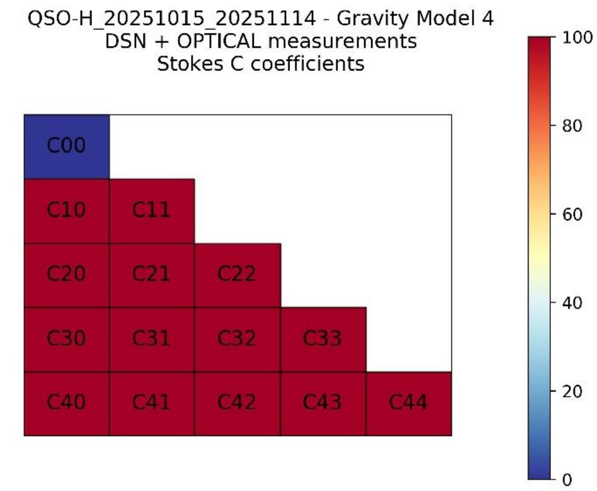

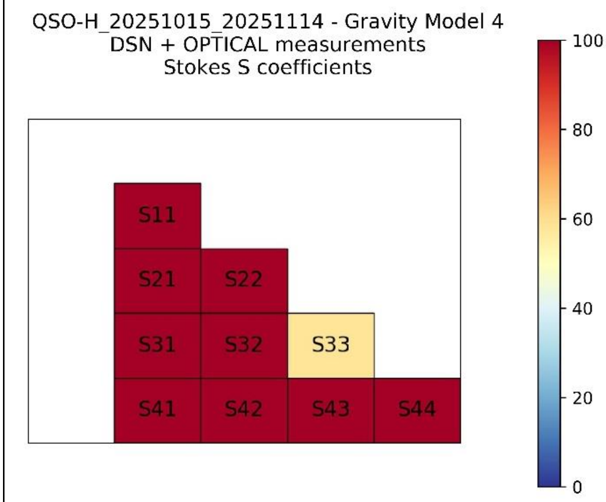

Figure 40.a *– QSO-H class example.*

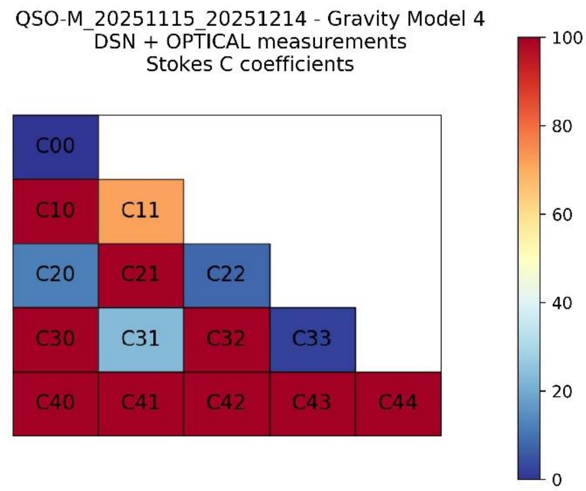

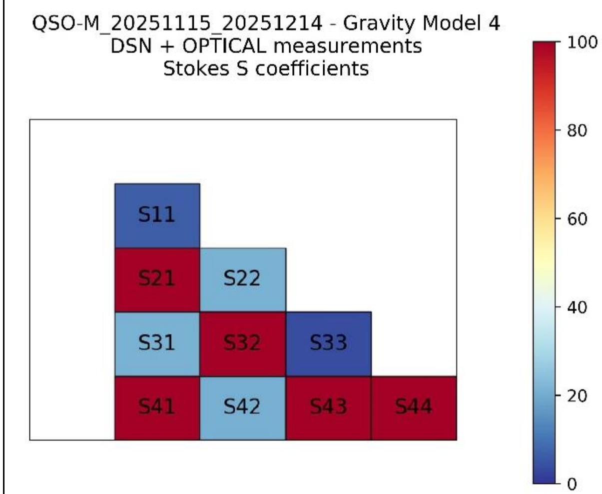

Figure 40.b *– QSO-M class example.*

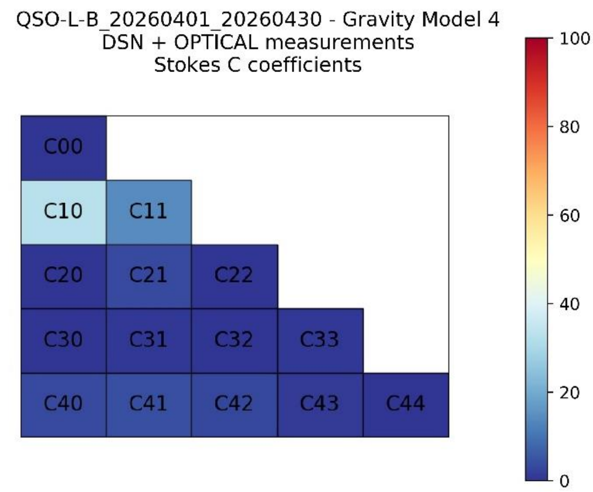

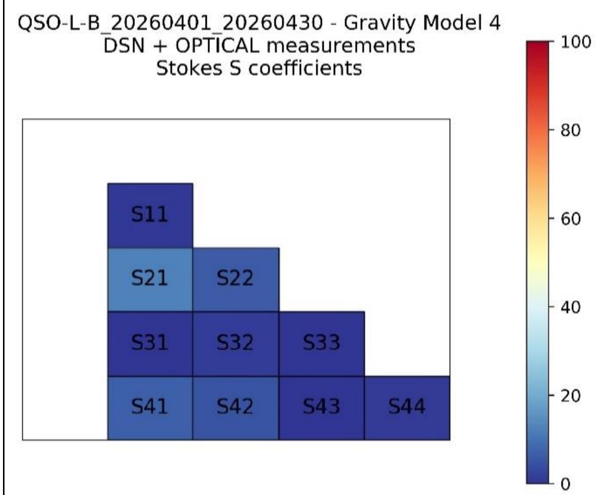

Figure 40.c *– QSO-L class example.*

Figure 40 *- Stokes coefficients adjusted from a priori Phobos "Gravity model 4", considering the DSN and Optical measurement combination along 2D QSOs.*

These graphs allow to understand that even adopting a Phobos gravity model not that different form the precise reference one, not all the orbits are able to correctly adjust all the normalised Stokes coefficients up to degree 4.
Without any doubts, the best gravity model adjustment is again realised by the low-altitude trajectories. In fact, they prove to be sufficiently near Phobos surface to be able to entirely return its up-to-degree-4-gravitational coefficients, corrected in a very precise way. In relation to the a priori "Gravity model 1" results, here a light worsening can be observed especially on $\bar{S}_{lm}$ coefficients, but it is absolutely negligible
Exactly as for the previous case, the largest QSO-H trajectories only manage to perfectly recover the $C_{00} = \mu = GM$. Unfortunately, for what concerns the correction of all the others Stokes harmonic elements, these orbits result to be too far from the target body.
The medium size-QSOs manifest again a proper correction of some of the coefficients, but they still result in not that proximity to Phobos in order to completely adjust its gravity model. Moreover, since in this case not only the measurement noises and the initial state vector perturbations, but also the inferior a priori model accuracy influences the results, the latter turn out to be slightly less precise than the "Gravity model 1" ones.
However, the adjustment capability of the 3-Dimensional QSO-M trajectories is newly different:

$\bar{C}_{lm}$	$\bar{S}_{lm}$

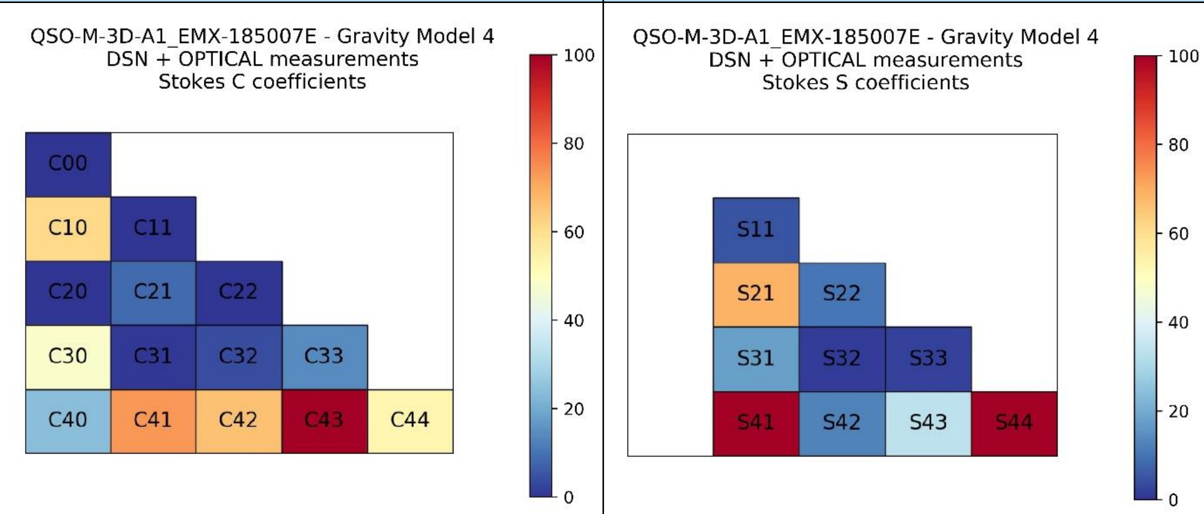

***Figure 41.a** – QSO-M-3D-A1.*

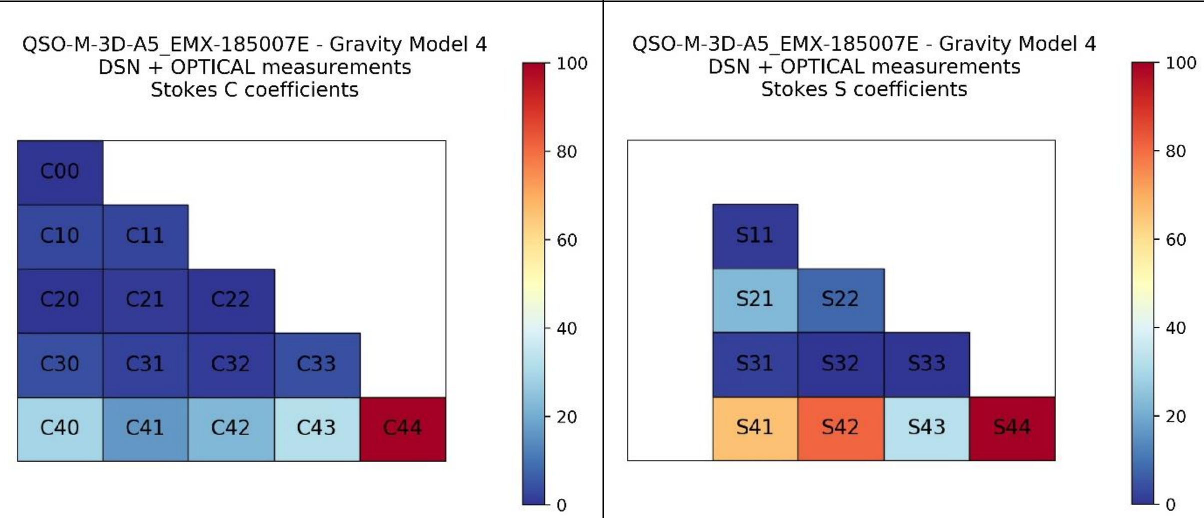

***Figure 41.b** – QSO-M-3D-A5.*

***Figure 41** - Stokes coefficients adjusted from a priori Phobos "Gravity model 4", considering the DSN and Optical measurement combination along QSO-M-3D trajectories.*

These graphs perfectly confirm that thanks to their passage in higher latitudes over Phobos body, the 3-Dimensional orbits allow a better restitution of the Martian moon gravity field, even starting with a slightly perturbed a priori model.
Moreover, these trajectories appear to be almost insensitive to moderate inaccuracy in the a priori knowledge of Phobos real gravity field: these graphs perfectly correspond to the ones in Figure 39, obtained with the a priori “Gravity model 1”.

Passing now to the analysis of results achieved conisdering a compltelly inacurate a priori template, as the “Gravity model 2”, it is possible to observe different behaviours. Employing again the same 2-Dimensional trajectories as examples, the resulting normalised Stokes coefficient graphs are the following:

$\overline{C}_{lm}$	$\overline{S}_{lm}$

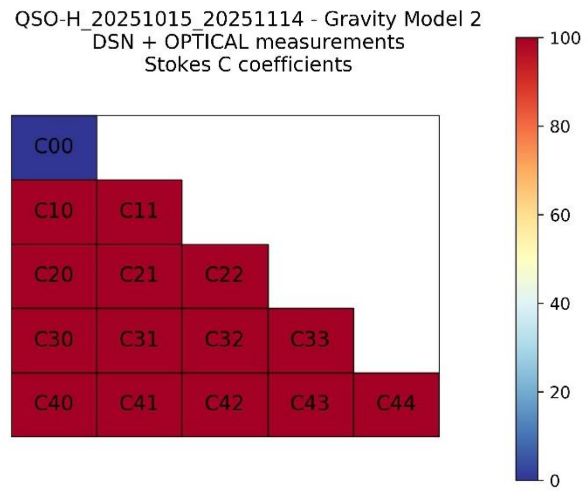

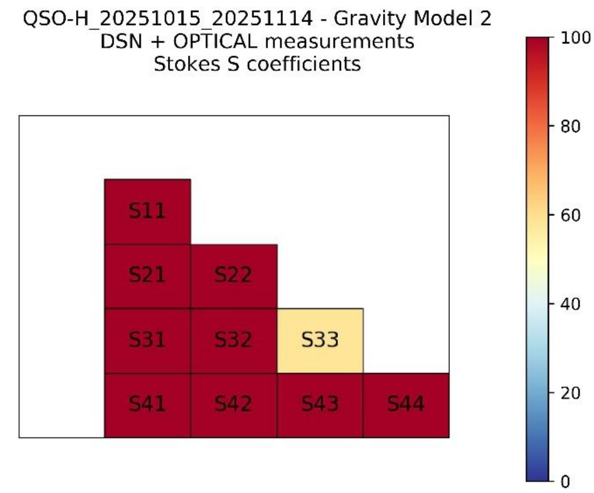

***Figure 42.a** – QSO-H class example.*

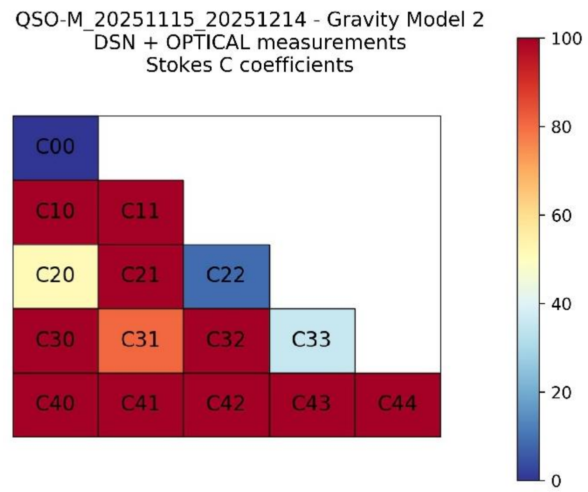

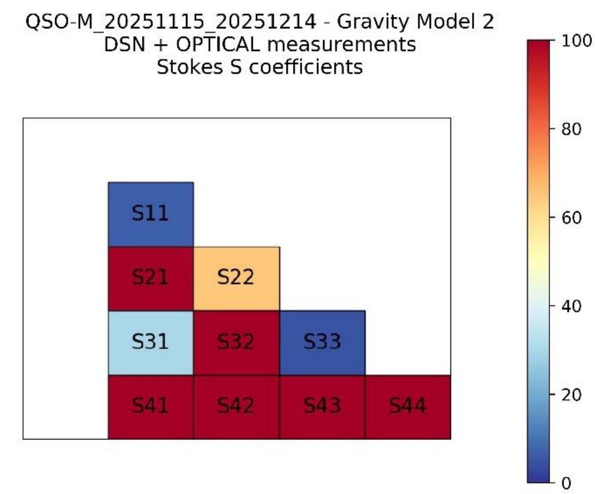

***Figure 42.b** – QSO-M class example.*

***Figure 42** - Stokes coefficients adjusted from a priori Phobos “Gravity model 2”, considering the DSN and Optical measurement combination along 2D QSO-H and QSO-M examples.*

The first remarkable aspect is that, even starting with an inaccurate a priory Phobos gravity model, both the QSO-H and the QSO-M classes turn out to have similar predisposition to adjust Stokes harmonic coefficients than the previous case, even if with a lower accurate level.

However, the most important result to highlight, concerns the QSO-L trajectories. In fact, this orbit class does not appear in Figure 42: the number of low-altitude-orbit arcs converged to a proper ***r.m.s.*** value within the restitution procedure is too small for ad adequate gravity recover. In fact, most of the QSO-L normal equations relative to the worst a priori "Gravity model 2", have been discarded because of their inaccuracy level (Table 7).
Consequently, since this extreme lack of information, it is impossible to generate a correction of Martian moon gravity coefficients. This impossibility is again linked to the fact that the low-altitude QSOs are the most affected by a gravity model inaccuracy. This is the reason why, in case of an excessive lack of the a priori knowledge of Phobos gravity field, the latter cannot be directly improved through the employment of QSO-L trajectories.
Nevertheless, this is not a motive to exclude this QSO class from the MMX orbital design. On the contrary, they represent a real strong element for the entire mission success, on condition that their employment occurs when a quite accurate Phobos gravity model is already available (Figure 38.c and Figure 40.c).
Because of this characteristic, the satellite will realise these smallest dimensioned orbits only starting from the second mission phase. The objective is to get a first target model correction during the initial Phobos mission phase, where only QSO-H and QSO-M are used. Successively, only when the Martian moon geodesic parameters will have been already updated, the satellite will begin its QSO-L trajectories. At that moment, Phobos gravity model will be sensed not to be that inaccurate: even the most sensitive orbits, will be able to calculate, partially correct and return the desired gravitational parameters.

In addition to this, another significant remark can be expressed in relation to 3-Dimensional QSOs. Effectively, these particularly trajectories result again to be sufficiently able to correct a strongly imprecise a priori Phobos gravity model:

$\overline{C}_{lm}$	$\overline{S}_{lm}$

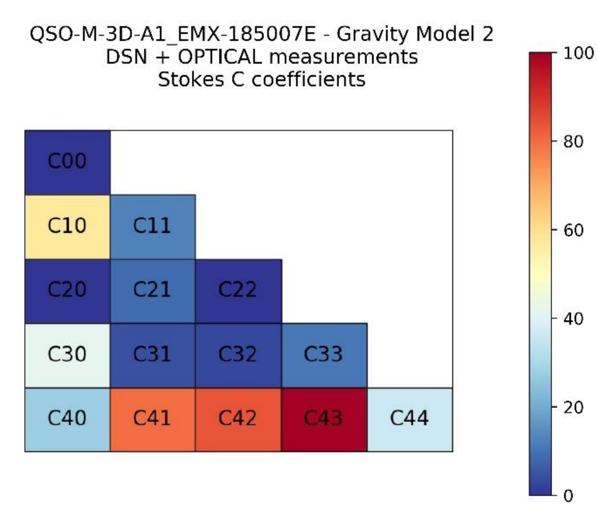

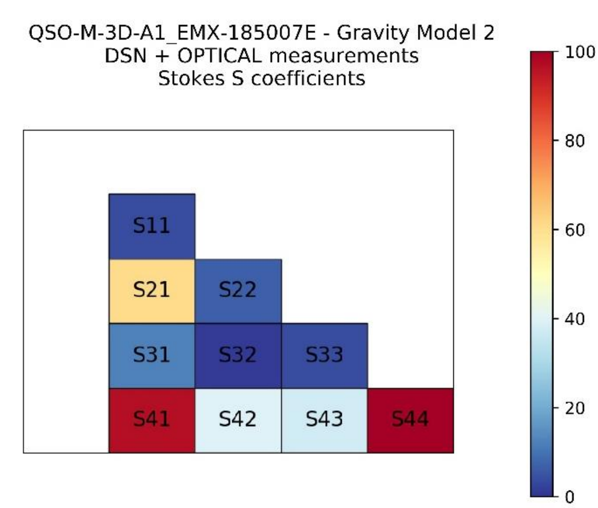

Figure 43.a *– QSO-M-3D-A1.*

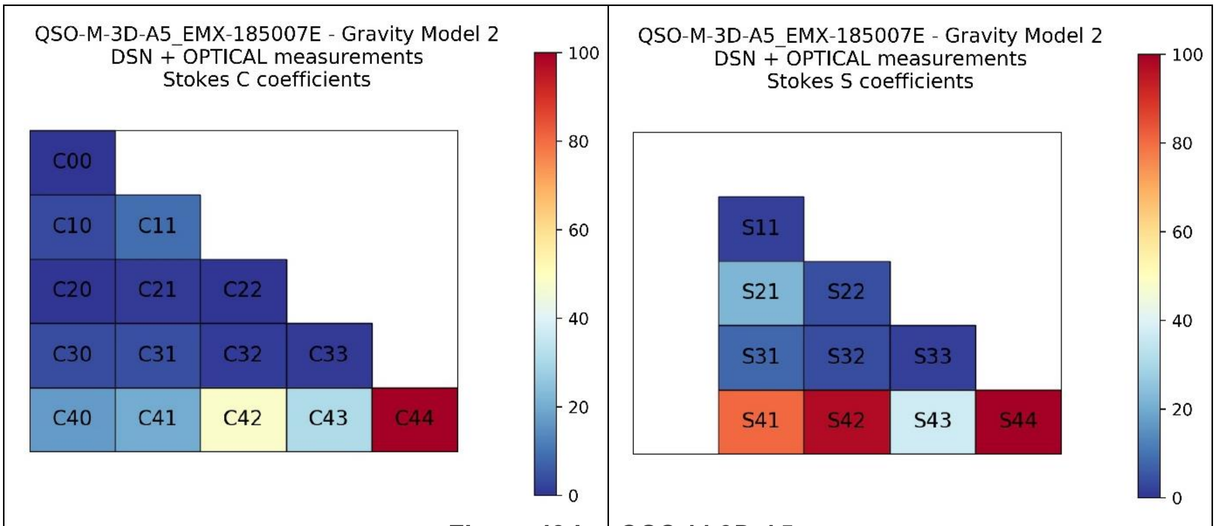

Figure 43.b *– QSO-M-3D-A5.*

Figure 43 *- Stokes coefficients adjusted from a priori Phobos “Gravity model 2”, considering the DSN and Optical measurement combination along QSO-M-3D trajectories.*

These graphs confirm that both the 3-Dimensional QSOs here presented as examples, are suitable for the reconstruction of Phobos gravity coefficients, even in initial conditions of a severely incomplete a priori model.
Moreover, even in this hardest case, it is newly clear that the more an orbit reaches elevate latitudes over the target surface, the higher is its capability of correctly adjusting a larger number of Stokes coefficients.
To conclude, the QSO-M-3D proved to be the least sensitive to any perturbation in the a priori gravity models. It is thus already possible to understand that the employment of these 3-Dimensional trajectories could represent a strength within the MMX mission.

<u>Second result analysis</u>: A second type of result analysis allows to compare the influence of different measurement combinations on QSO ability to correct a priori Phobos gravity field models. For this study, it is useful to consider an orbit belonging to the QSO-L class: in this way all the six computed measure combinations (Table 9) are available.
The choice of a low altitude trajectory leads to taking mainly into account results calculated with a sufficiently precise a priori Phobos gravity model. Effectively, as figured out in the previous analysis, these smaller orbits will be presumably employed only when the knowledge of target geodesic parameters will have already been improved. Consequently, an appropriate example can be individuated in the set of results relative to a QSO-L trajectory, with the a priori “Gravity model 4” (resulting graphs relative to the DSN and Optical measurement combination is available in Figure 40.c):

$\bar{C}_{lm}$	$\bar{S}_{lm}$

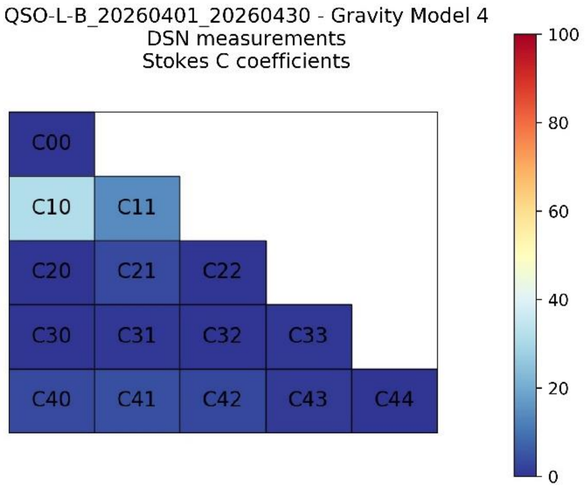

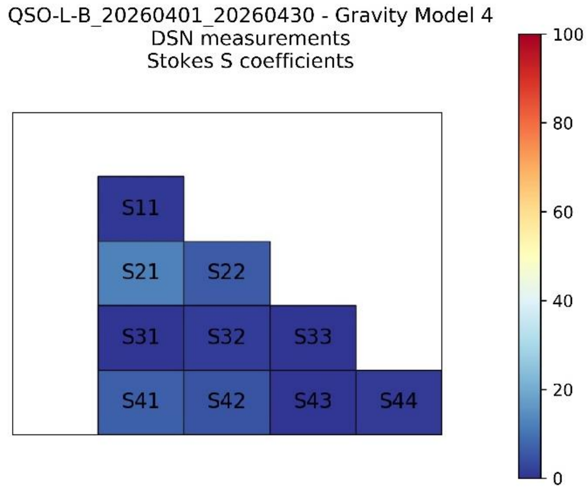

***Figure 44.a** – DSN measurements.*

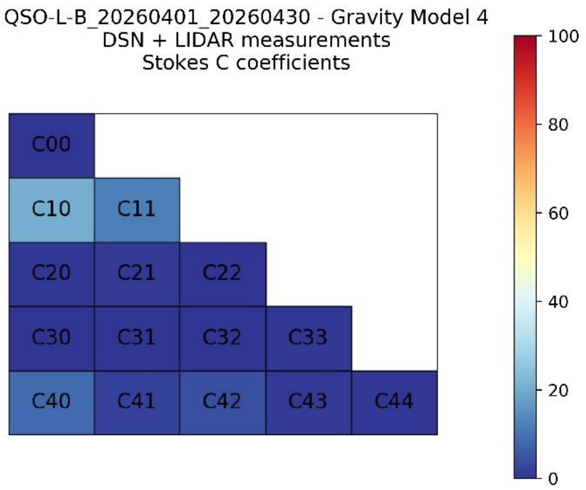

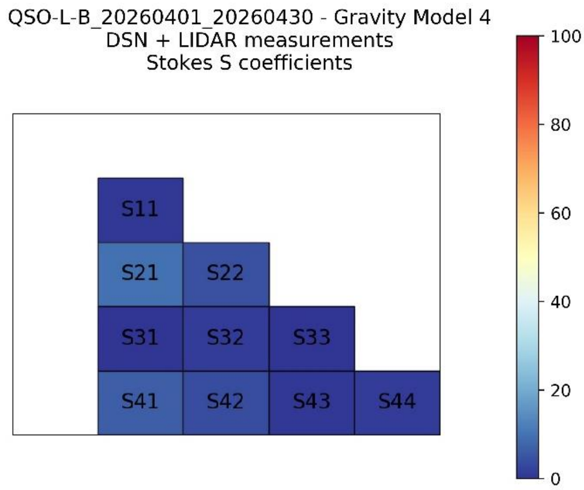

***Figure 44.b** – DSN and LIDAR measurement combination.*

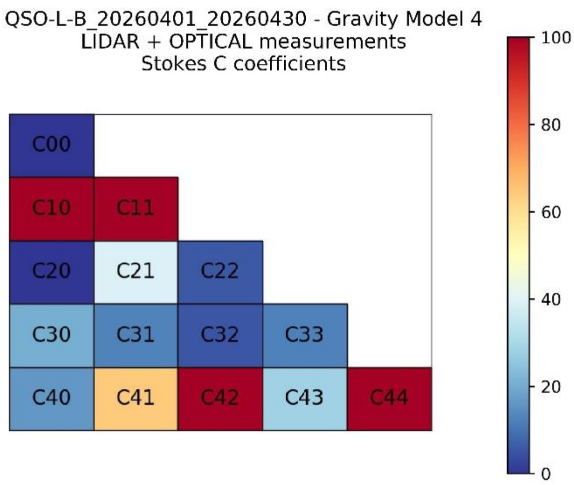

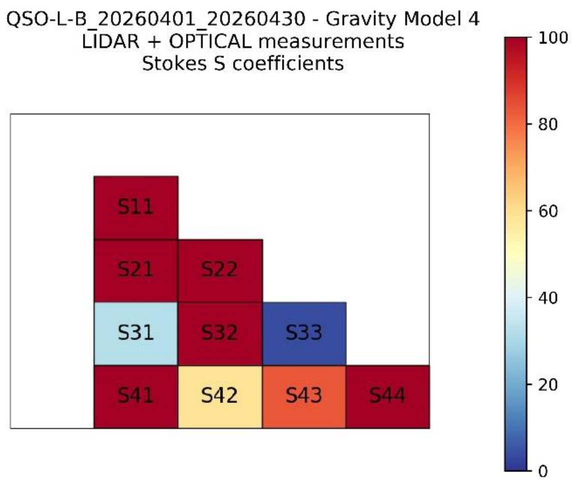

***Figure 44.c** – LIDAR and Optical measurement combination.*

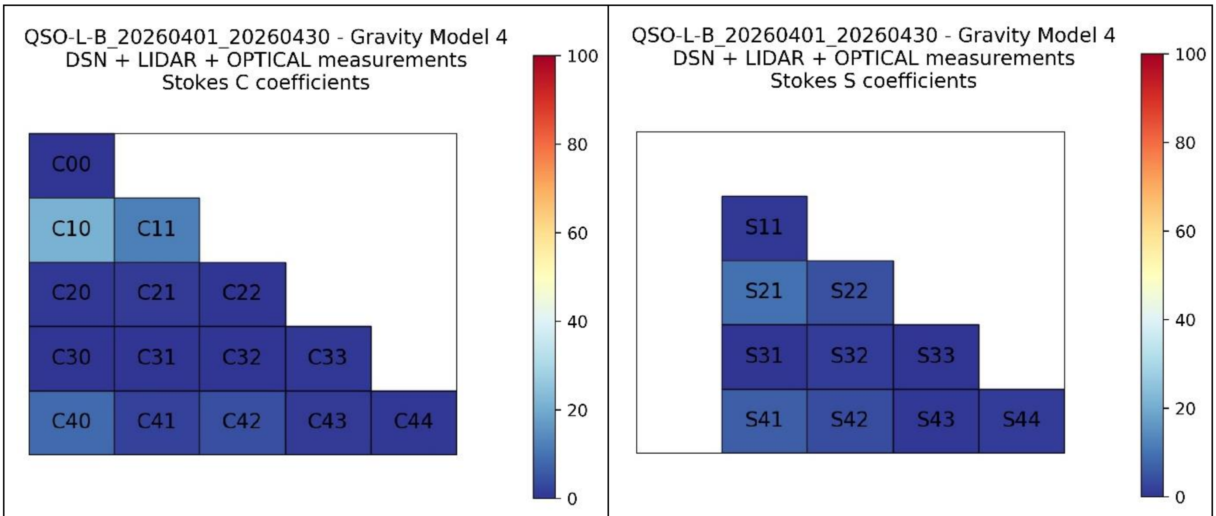

Figure 44.d *– DSN, LIDAR and Optical measurement combination.*

Figure 44 *- Stokes coefficients adjusted from a priori Phobos "Gravity model 4", considering all the five remaining combinations of measurements. Graphs relative to a QSO-L trajectory.*

Summarily, these graphs report satisfying adjusted gravity coefficients.
This aspect is another prove of the fact that QSO-L trajectories are perfect tools for improving the current knowledge of Phobos gravity field. Effectively, almost all the six combinations of measurements turn out to be sufficiently suitable for the scientific purposes of the MMX mission.

However, the most remarkable case which stands immediately out, is the combination of the two ephemeris measurement types, LIDAR and Optical ones (Figure 44.c). The adoption of only these two measures would not afford a perfect reconstruction of the realistic target gravity field: their final results are not that precise, despite the elevate quantity of LIDAR measurements. In the relative graph it is possible to observe the presence of some incorrect or only partially adequately adjusted normalised coefficients. More precisely, the ephemeris measurements here considered appear to be more sensitive to $\boldsymbol{C_{1m}}$ (both the zonal and sectorial terms), $\boldsymbol{C_{4m}}$ (the sectorial and some tesseral terms) and $\boldsymbol{S_{lm}}$ Stokes elements.
Instead, if DSN measurements are considered too, precise model recovery is reachable (Figure 44.d).
In conclusion, LIDAR and Optical techniques are not able to perfectly return real Phobos gravity field, alone: for higher accuracy levels, Doppler measures are necessary.

<u>Third result analysis</u>: A third type of result analysis allows the comparison between the employment of complete Doppler measurements, captured with both Madrid and Usuda DSN Earth stations, and Doppler information available with only the Japanese ground antenna.
In order to explain the different impact on results generated by these two Doppler approaches, it is useful to take as an example the same QSO trajectories as before, and the quite precise a priori Phobos "Gravity model 4".
The following figures represent $\boldsymbol{\bar{C}_{lm}}$ coefficients adjusted by the two different Doppler method. Relative $\boldsymbol{\bar{S}_{lm}}$ coefficient correction is impacted in the same way and its graphs are observable in Figure 57 in Annex B.

$\overline{C}_{lm}$ – DSN (Madrid + Usuda)	$\overline{C}_{lm}$ – (DSN Usuda)

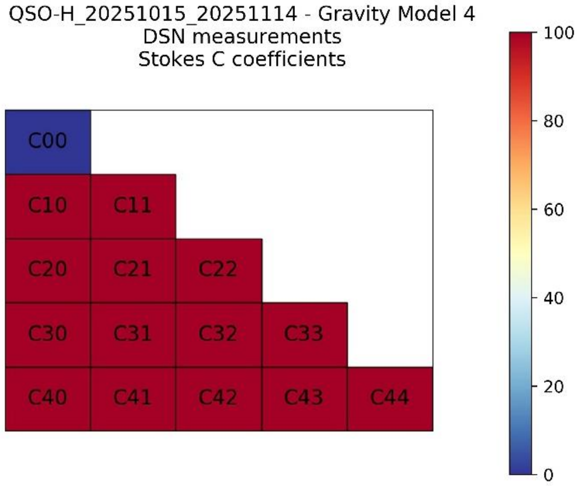

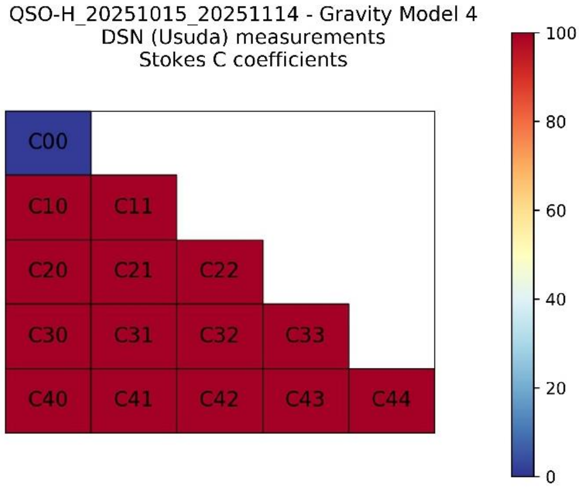

***Figure 45.a** – QSO-H class example.*

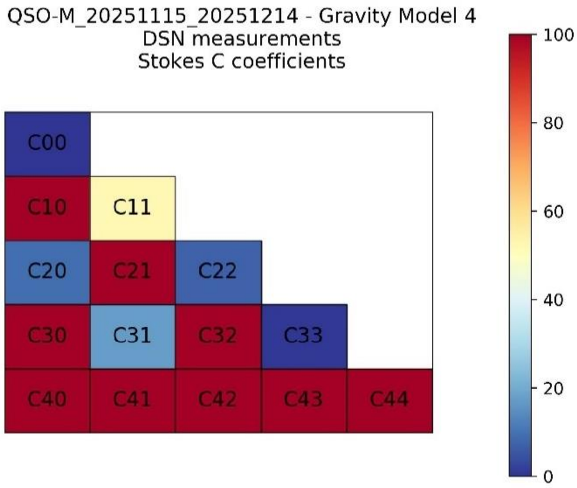

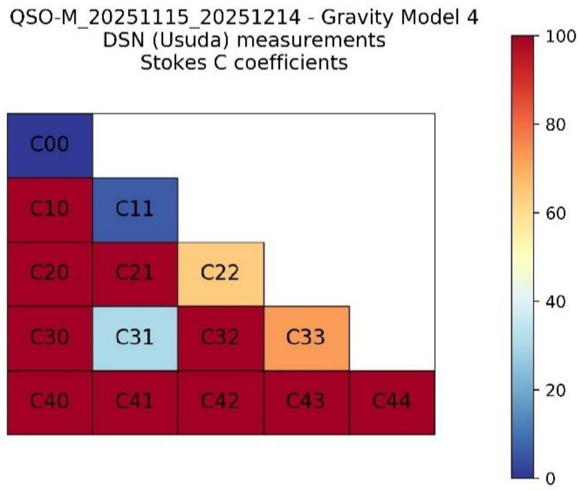

***Figure 45.b** – QSO-M class example.*

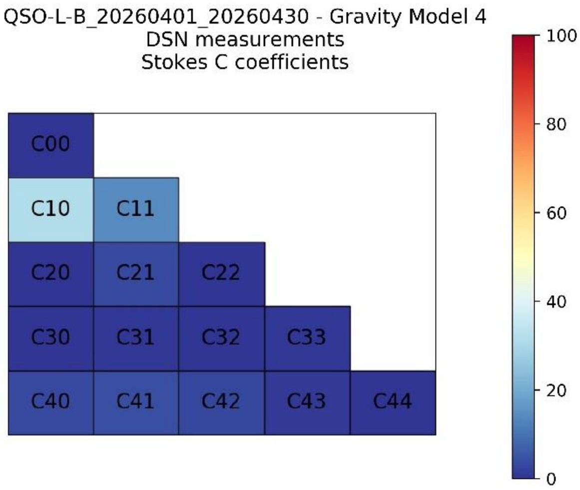

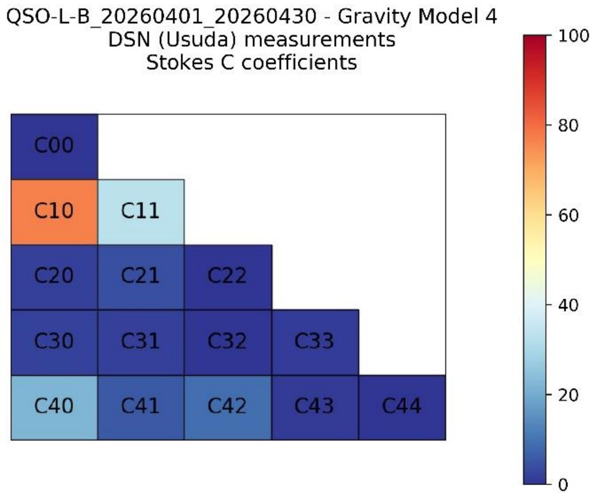

***Figure 45.c** – QSO-L class example.*

***Figure 45** - Stokes $\overline{C}_{lm}$ coefficients adjusted from a priori Phobos "Gravity model 4", considering DSN measurements realised with both Madrid and Usuda stations and with only Usuda antenna.*

These graphs prove that exactly the same feature is repeated in all the 2-Dimensional QSO classes: the employment of the only Usuda ground station, would lead inevitably to a slightly less accurate reconstruction of Phobos gravity field. This aspect is linked to the fact that the adoption of one single DSN antenna would clearly conduct to the collection of an inferior quantity of Doppler measurements. This reduction of information would translate in a lower capability of computing a completely precise adjustment of Martian moon gravity coefficients.
However, this accuracy loss appears not to be that significant, especially in terms of global mission results.
Therefore, it is possible to conclude that the use of both the DSN Earth stations would allow a better success as regard the MMX scientific objectives. Nevertheless, taking into account the entire mission, the imprecision caused by the use of one single DSN station is not excessive, thus acceptable.

The analyses carried out on every single QSO trajectory taking part in MMX orbital design, have been replicated on all the mission phases, in the next and last project step. As paragraph 3.7 will detail, all remarks and conclusions reached by studying results characterising each orbit separately, have then been found the same in mission phase analysis.

3.6.3 Parametric sensitivity

The detailed analysis over each QSO trajectory designed for the MMX phases focused on Phobos exploration, have been concluded with a parametric sensitivity study. Effectively, it appears useful to understand in which way and proportion these orbits are influenced by certain parameters and how the latter impact the QSO capability in recovering Phobos gravity model.
Thus, the sensitivity of previous described results has been tested to two different parameters: LIDAR measurement noise and Phobos ephemeris uncertainty.

1. <u>LIDAR measurement noise</u>: As equation (69) underlines in paragraph 3.4.1, LIDAR measure noise standard deviation $\boldsymbol{\sigma_L}(\mathbf{R})$ $(= \boldsymbol{\sigma_R}(\mathbf{R}))$ linearly changes with the instantaneous satellite radial position $\mathbf{R}$, in relation to Phobos mass centre.
This means that the noise considered for LIDAR simulation varies with the frequency of laser captures, fixed by the JAXA at 1.0s.
Consequently, an interesting analysis has been conducted throughout maintaining constant the $\boldsymbol{\sigma_R}$ value over a time interval of five minutes.
LIDAR simulation has been exactly the same, except for the noise standard deviation calculation: the total QSO-L periods have been divided into five-minute sections, whose first-second $\boldsymbol{\sigma_R}$ values calculated with equation (69) have been employed as a constant during the entire sections. Once gotten these five-minute constant $\boldsymbol{\sigma_R}$, formula (71) has been normally applied for simulating satellite radial position perturbation, due to LIDAR measurements.
In order to show the consequent effects, next figure reports the gravity model adjustment obtained with this LIDAR noise simulation method, along the QSO-L here taken as an example, considering LIDAR-Optical measure combination and Phobos a priori “Gravity model 4”:

$\overline{C}_{lm}$	$\overline{S}_{lm}$
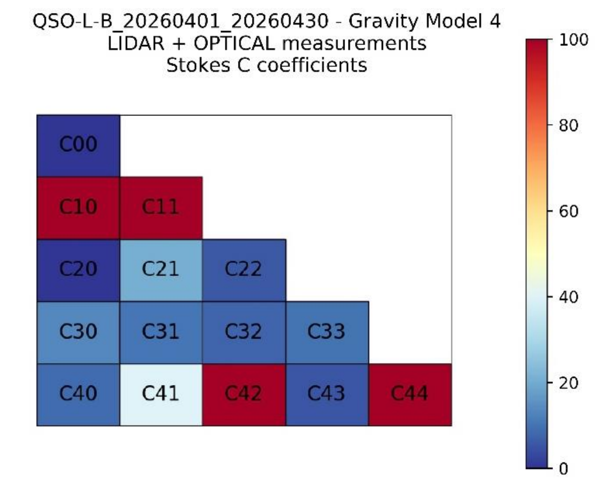	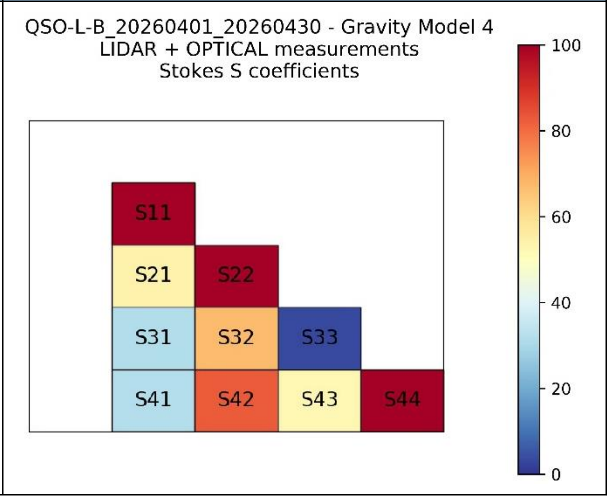

***Figure 46** - Stokes coefficients adjusted from a priori Phobos "Gravity model 4", considering a five-minute constant $\boldsymbol{\sigma_R}$ for LIDAR measurement simulation.*

These Stokes coefficient graphs have to be compared with the corresponding nominal ones in Figure 44.c.
It is possible to notice that the maintenance of LIDAR noise standard deviation constant over five-minute sections leads to slightly improved Phobos gravity model correction, in relation to the standard case, where $\boldsymbol{\sigma_R}$ changes every second. For both $\overline{C}_{lm}$ and $\overline{S}_{lm}$ groups, an increasement in the model recovery precision level is here visible.
However, result sensitivity to the change frequency of LIDAR measure noise appears to be not that high.
This aspect is probably due to the fact that along a QSO-L, satellite-Phobos radial distance $\mathbf{R}$ does not undergo drastic changes, and the same applies for LIDAR $\boldsymbol{\sigma_R}$ parameter. The direct consequence is that even keeping constant LIDAR noise standard deviation for a set period, final Phobos gravity model reconstruction improves, but not that much.

2. Phobos ephemeris uncertainty: As expressed in paragraph 3.1, the same hypotheses employed by the FD groups have been considered in this internship project for Phobos ephemeris.
Nevertheless, it is worthwhile knowing how this Martian moon ephemeris and a not perfect awareness of them can influence QSO behaviour in detecting the real gravitational field.
This interest has conducted to the study of Phobos gravity model adjustment sensitivity to a particular uncertainty over Phobos ephemeris.
Therefore, a displacement of 50.0m along Phobos speed direction has been simulated on the Martian moon position along its ephemeris around Mars. The perturbed Phobos ephemeris have then been used to describe the natural satellite motion in the *Restitution* "*Director*" file.
The influence of this parameter has been tested to increase with the reduction in QSO dimensions:

- The Phobos furthest QSO-H trajectories appear to be almost not impacted from a Martian moon position uncertainty. They proved to be still able to recovery the only Stokes $\boldsymbol{C_{00}}$ term, but in a lightly less accurate way than the original case.
- The QSO-M class starts to be influenced by a 50-meter Phobos displacement: its gravity model recovery is amply worse than the original case (Figure 47).

- The QSO-L are the most influenced by Phobos ephemeris parameter. Since they are the closest to the target surface, a not sufficiently accurate knowledge in its correct position, not allow the low-altitude QSO to generate a precise Phobos gravity model reconstruction. In fact, this analysis has brought to light that the largest part of QSO-L arcs is not able to get the convergence in GINS restitution procedure nor to converge to the correct ***r.m.s.*** value (paragraph 3.5). Consequently, the probability of obtaining accurate Phobos model recovery turns out to be extremely low, considering QSO-L trajectories and target ephemeris uncertainties.

Since all these consideration over QSO sensitivity to this Phobos geodesic parameter, the most significant graphs to report in this context, are relative to the medium-altitude-orbit class. Thus, the following figure presents results obtained with the QSO-M here taken as an example, considering DSN measurements and the a priori target "Gravity model 4":

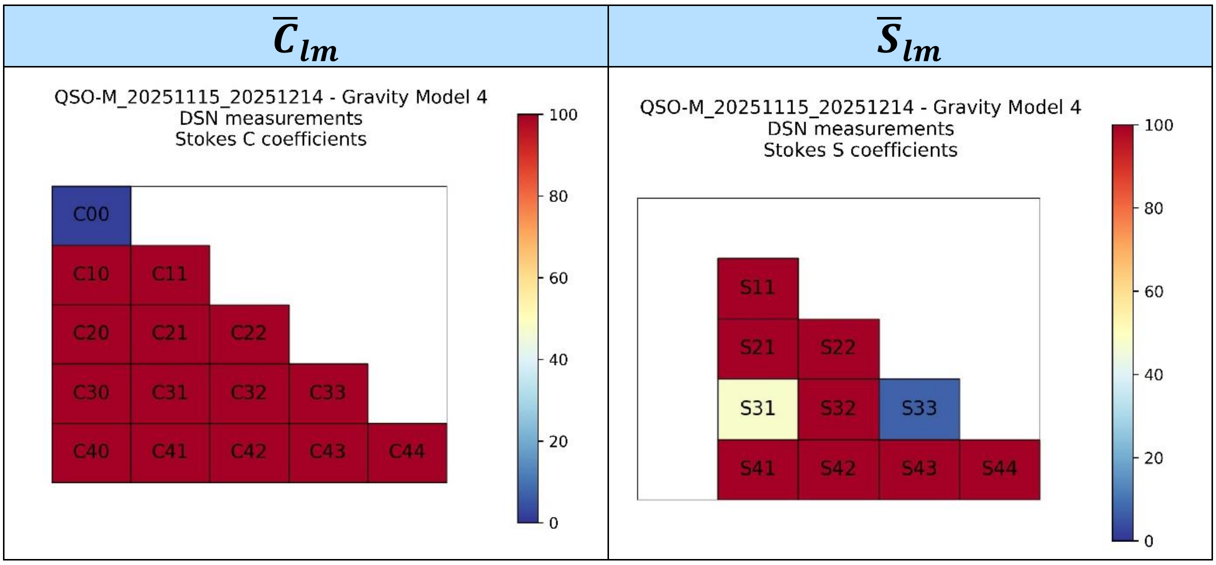

Figure 47 *- Stokes coefficients adjusted from a priori Phobos "Gravity model 4", considering a 50-meter displacement in Phobos position along its ephemeris around Mars.*

Correspondent $\bar{C}_{lm}$ and $\bar{S}_{lm}$ graphs obtained with nominal Phobos ephemeris, are respectively reported in Figure 45.b and Figure 57.b. The comparison between these results highlights the large QSO-L sensitivity to this Martian moon parameters. A 50-meter perturbation of Phobos position leads the medium-dimensioned trajectories to succeed in recovering only Stokes C_{00} coefficient and few S_{lm} terms: the global worsening in comparison to nominal results is evident.

3.7 Phobos gravity field resolution over the entire MMX mission

The final purpose is now to obtain Phobos gravity model correction results, relative to the complete MMX mission.
The method here employed is perfectly similar to the one adopted for the analysis over each trajectory, separately. The main difference resides in the process used for cumulating the

normal equations through the DYNAMO-C program, while their resolution by the use of DYNAMO-D, is exactly the same.

3.7.1 Normal equation accumulation and resolution

This second normal equation accumulation is based on outputs of the first one. In fact, the latter combines all the normal equations describing each 24-hour orbit arcs, giving birth to one single normal equation with inside global Phobos gravity information of the entire QSO trajectory. This approach is applied on every converged combination of a priori Phobos gravity models and measurement types, for every single MMX orbit.
Consequently, in this second accumulation step the collection is realised within the previously created normal equations, defining each complete QSO trajectory.
More precisely, it consists in a gradual accumulation over the four MMX mission phases (Figure 14 and Figure 15):

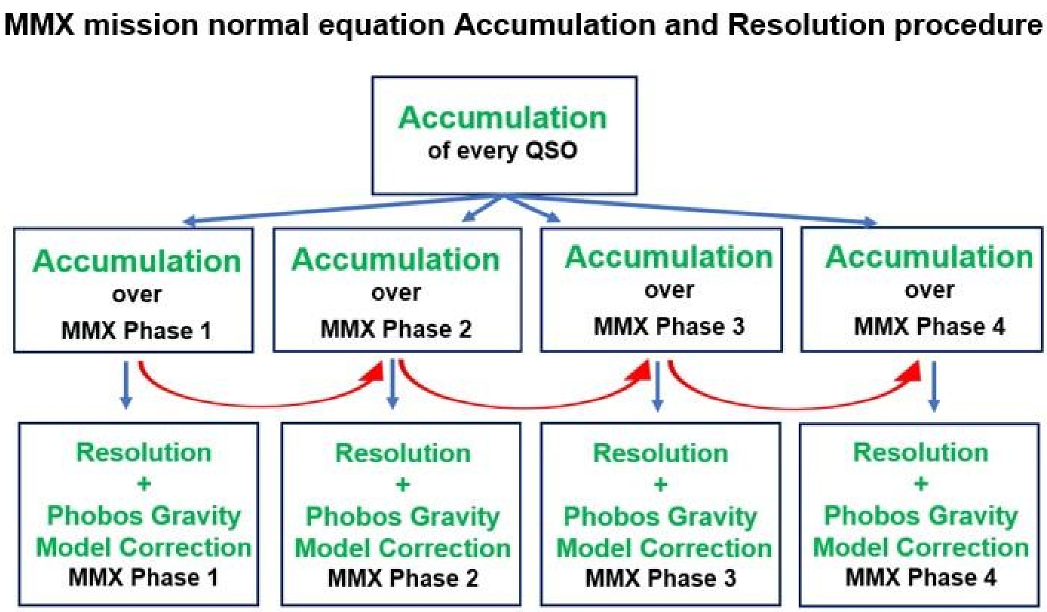

Figure 48 *- Schematic representation of the gradual normal equation accumulation and resolution over the entire MMX mission.*

These gradual accumulation and resolution enable an approximate simulation of what effectively will happen in the real mission:

1. Normal equations of each QSO trajectories composing the first mission phase are combined in one single linear system, whose resolution leads to a first global correction of Phobos gravity coefficients. This represents one of the first updates of the Martian moon gravity model reachable during the MMX mission. The latter will thus be able to continue its operations with a better knowledge of the target.
2. Normal equations of all the QSOs taking part in the second phase of the mission are cumulated with the equation characterising the entire first phase, by generating another single equation. The resolution of such a normal system provides a new adjustment of

Stokes harmonic coefficients. This is a representation of what will be the second probable Phobos gravity model update in the real MMX mission.

3. Normal equations characterising every QSO trajectory realised by the satellite during the third mission phase, are combined with the previous created equation containing information of the first two phases. One new global linear system is computed and solved, leading to an always better correction of the target gravity coefficients. At this point of the real MMX mission, the knowledge of Phobos gravity model should be farther increased.
4. Finally, normal equations of each QSO constituting the fourth mission phase, are combined with the equation computed before, with inside the complete information reached in the first three phases. This last accumulation provides a final linear normal system which allows the computation of furtherly adjusted Stokes coefficients. Therefore, at the end of the fourth phase, the real MMX mission is supposed to ensure the most accurate Phobos gravity field model possible, much more precise than the initial one.

3.7.2 Global result analysis

The gradual accumulation and resolution process detailed before, is applied on previously generated normal equations, relative to all the twenty-four possible combinations of a priori Phobos gravity models and measurement types (expressed in Table 9). Consequently, results relative to all these combinations, are available for a global analysis involving the entire MMX mission.
Specifically, this analysis has been conducted over all the three MMX study cases proposed by the JAXA: the nominal and the two alternative QSO scenarios (Figure 14 and Figure 15) have been studied within this internship project.
Once again, results obtained with exclusively DSN and Optical measurements are represented.

Nominal case: Nominal trajectory composition fixed by the JAXA for the MMX mission, consists in the following series of consecutive orbit classes:

- Phase 1: QSO-H → QSO-M → QSO-H
- Phase 2: QSO-M → QSO-L-A → QSO-L-B → QSO-M
- Phase 3: QSO-L-A → QSO-M → QSO-L-A → QSO-M
- Phase 4: QSO-3D-M → QSO-M → QSO-L-A

Since the first mission phase is constituted exclusively by high and medium altitude QSO trajectories, the only measurements available will be the DSN and the Optical ones. Effectively, during this initial part of the mission, the satellite will not be sufficiently near the target to be able to take accurate LIDAR measurements. Consequently, it will be allowed to use the only Doppler sensors and navigation camera, while it will exploit this phase to move closer to the Martian moon surface. The first Stokes coefficient adjustment is here represented, in relation to the four different a priori Phobos gravity:

$\overline{C}_{lm}$	$\overline{S}_{lm}$

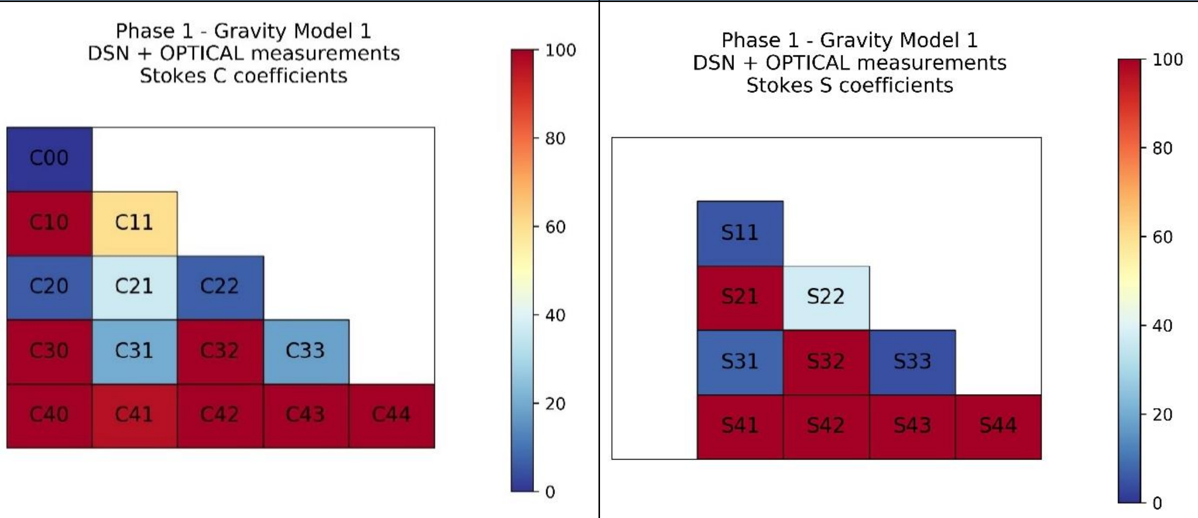

***Figure 49.a** – A priori Phobos "Gravity model 1".*

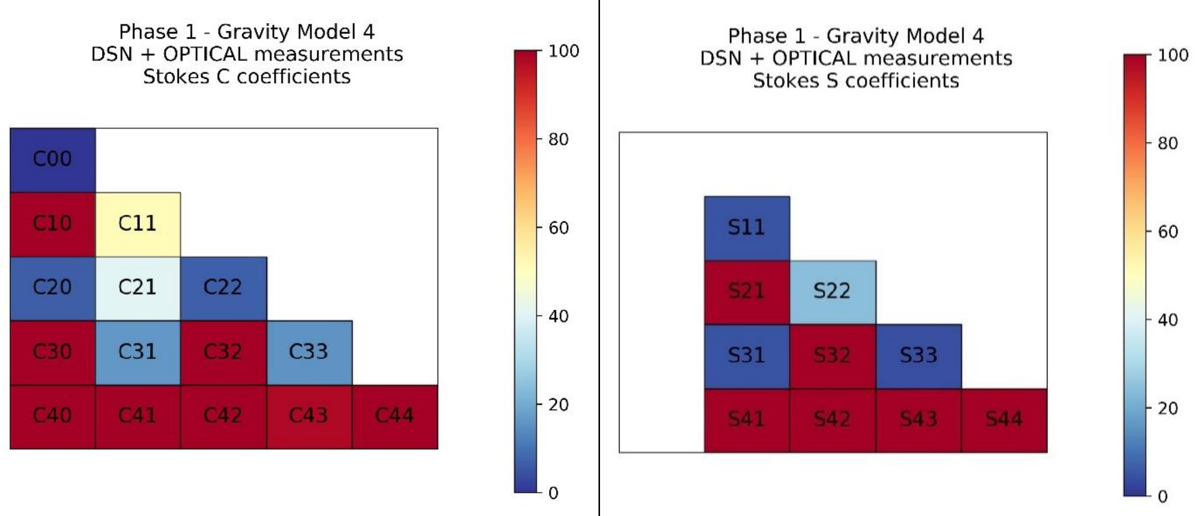

***Figure 49.b** – A priori Phobos "Gravity model 4".*

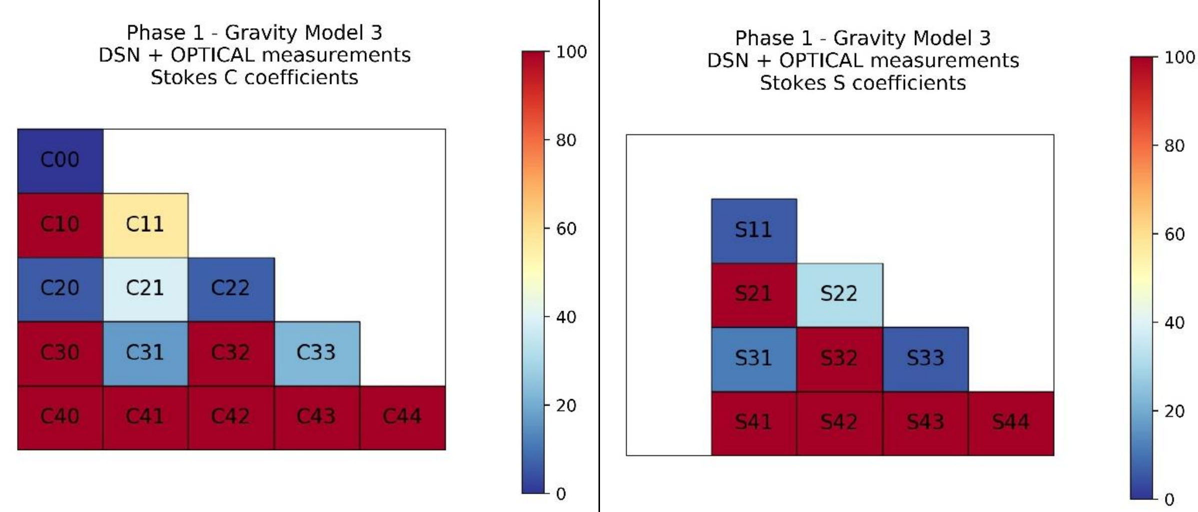

***Figure 49.c** – A priori Phobos "Gravity model 3".*

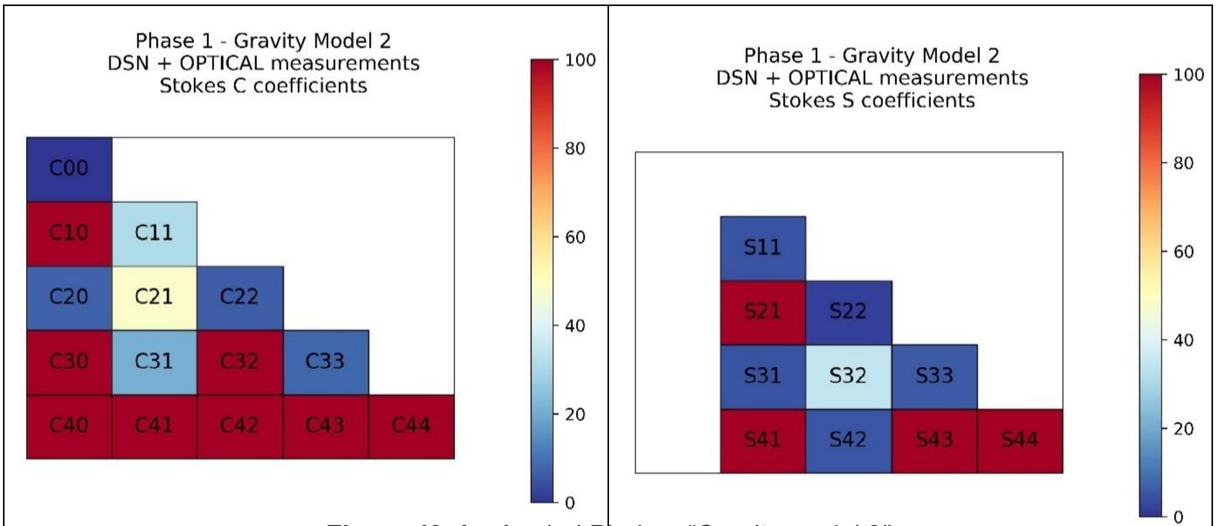

Figure 49.d *– A priori Phobos "Gravity model 2".*

Figure 49 *- Phobos gravity coefficient adjustment at the end of the first MMX Phobos phase.*

These results confirm an important conclusion, already stood out during the analysis of each QSO separately. The adoption of all the four a priori models proves that QSO-H and QSO-M trajectories composing the first mission phase, could afford an adequate correction of few gravity coefficients, especially up to the degree 3.
This means that, even if it is still far from a realistic restitution of Phobos reality, an initial slightly improved update of the Martian moon geodesic model can be reached at the end of the first MMX phase. Once terminated the initial phase, the satellite will already have reached a sufficient proximity to the target body to afford the realisation of its first low altitude trajectories. This means that also LIDAR measurements will be now available.

Considering now all the combinations of a priori Phobos gravity models and measurement types, the evaluation of Stokes coefficient adjustment at the end of the second mission phase has been realised. The followed procedure involves the accumulation of normal equations defining every orbit taking part in this phase, with the normal system generated at the end of the first phase. The resulting graphs are the following:

$\overline{C}_{lm}$	$\overline{S}_{lm}$

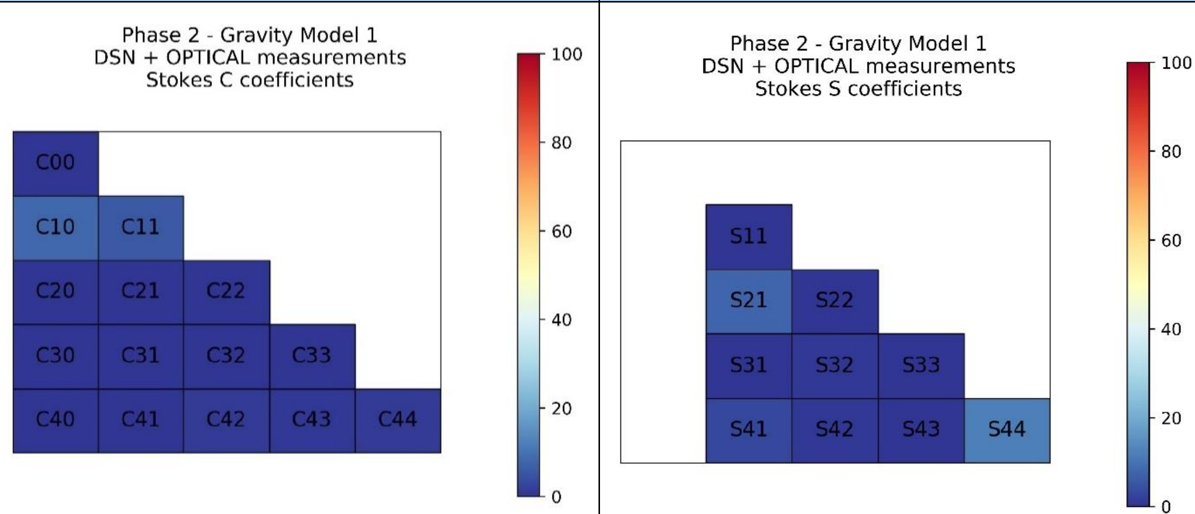

Figure 50.a *– A priori Phobos "Gravity Model 1".*

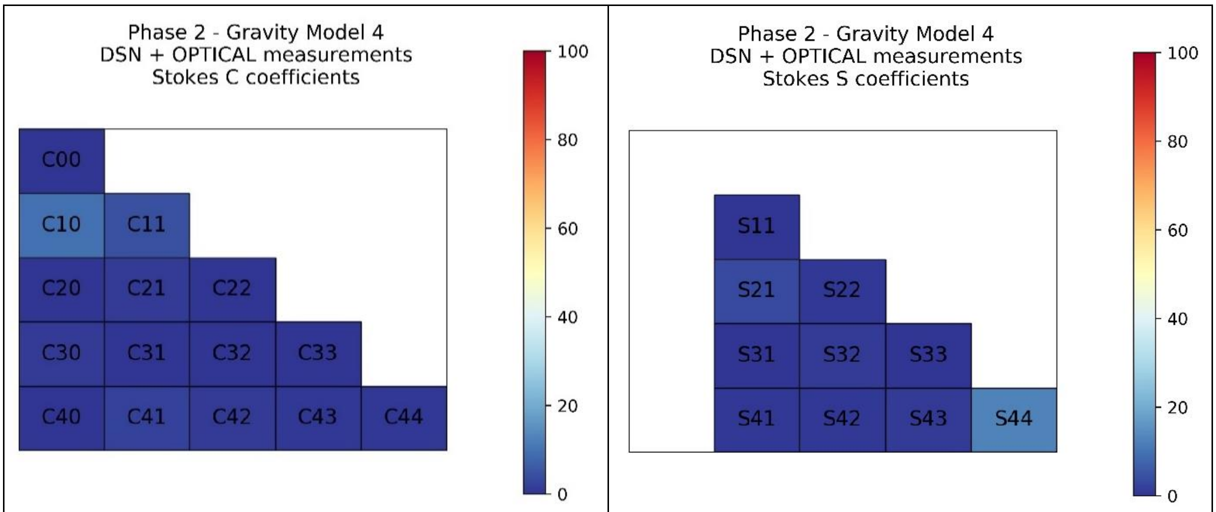

Figure 50.b *– A priori Phobos "Gravity model 4".*

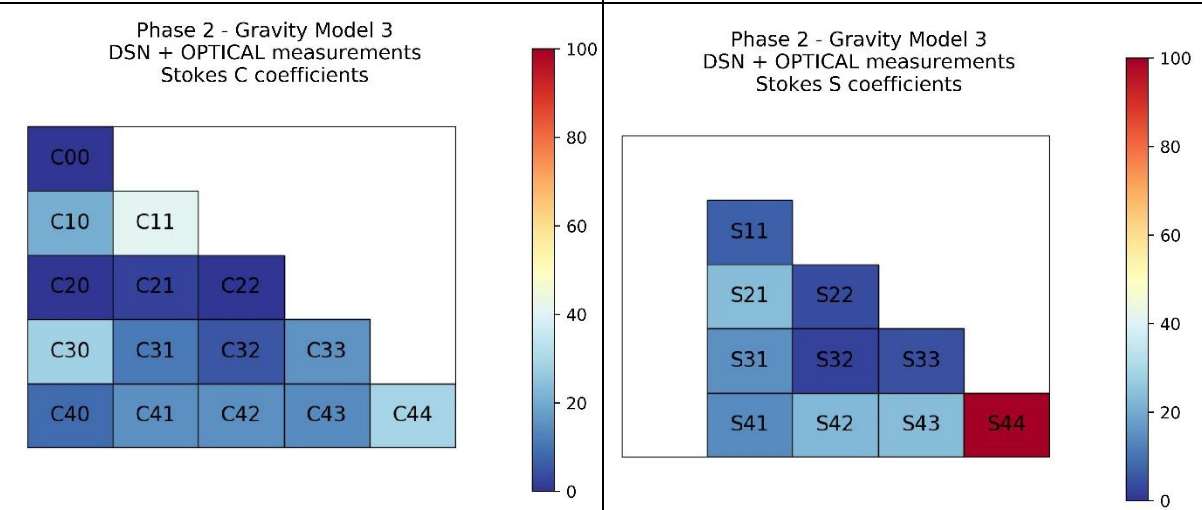

Figure 50.c *– A priori Phobos "Gravity model 3".*

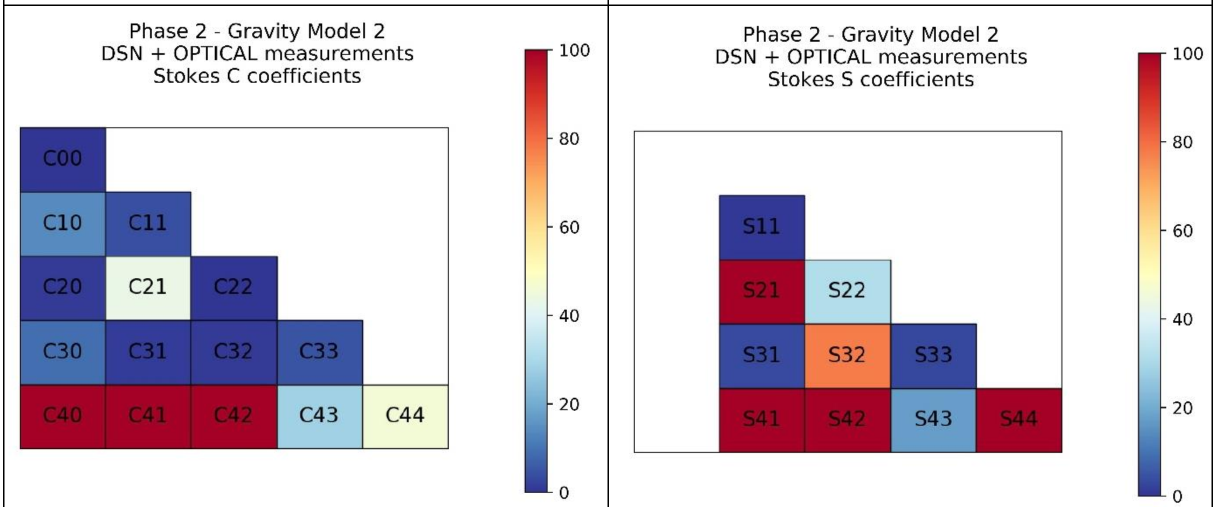

Figure 50.d *– A priori Phobos "Gravity model 2".*

Figure 50 *- Phobos gravity coefficient adjustment at the end of the second MMX Phobos phase.*

These graphs prove that at this point of the mission, the knowledge of Phobos real gravity field could already have significantly improved, especially in relation to the initial model employed at the beginning of the first phase. This model amelioration is particularly evident throughout the consideration of the two most precise a priori models (Figure 50.a and Figure 50.b), where all Stokes coefficients up to degree 4 manage to be properly adjusted. This high precision level gradually decreases with the worst a priori “Gravity model 3” and “Gravity model 2”. Particularly, the latter turns out to cause particularly difficulties in the restitution of proper degree 4-$\overline{C}_{4m}$ and $\overline{S}_{4m}$.
Generically, it is possible to affirm that the accuracy level reachable at the end of the second MMX phase, could allow a much more precise update of Phobos gravity model. The third MMX phase will thus have the possibility to begin with a higher detailed awareness the of Martian moon real gravity field.

The same approach has been used for the treatment of the third phase. By cumulating normal equations relative to this mission part, with the normal system generated by the two previous phase information, the reached coefficient correction level is presented in the following graphs:

$\overline{C}_{lm}$	$\overline{S}_{lm}$

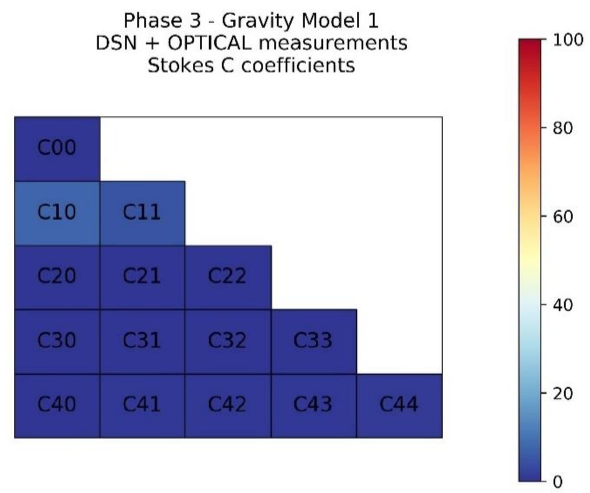

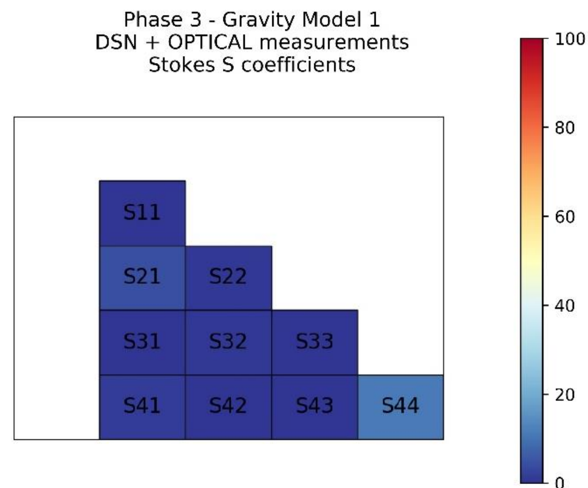

***Figure 51.a** – A priori Phobos “Gravity model 1”.*

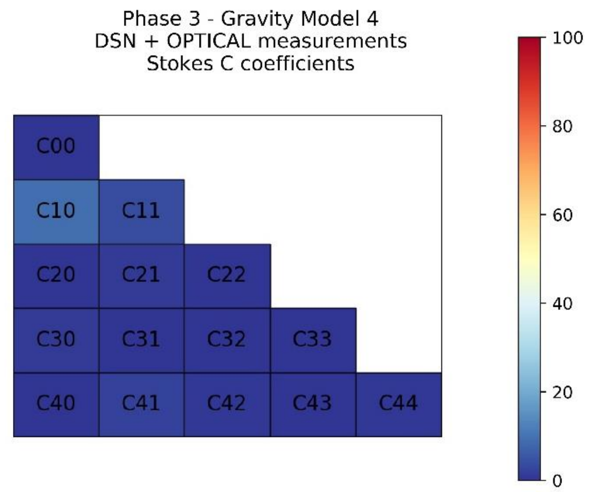

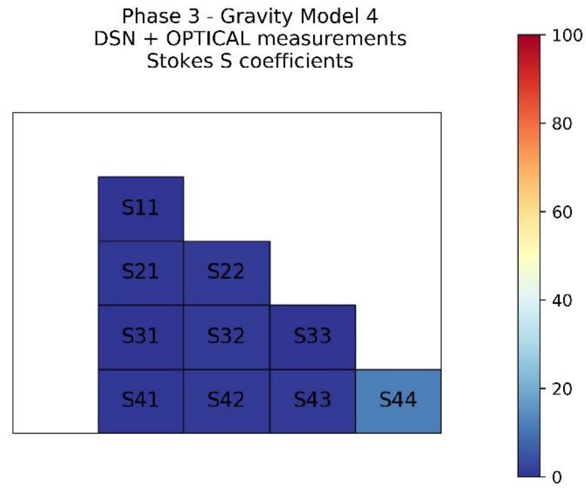

***Figure 51.b** – A priori Phobos “Gravity model 4”.*

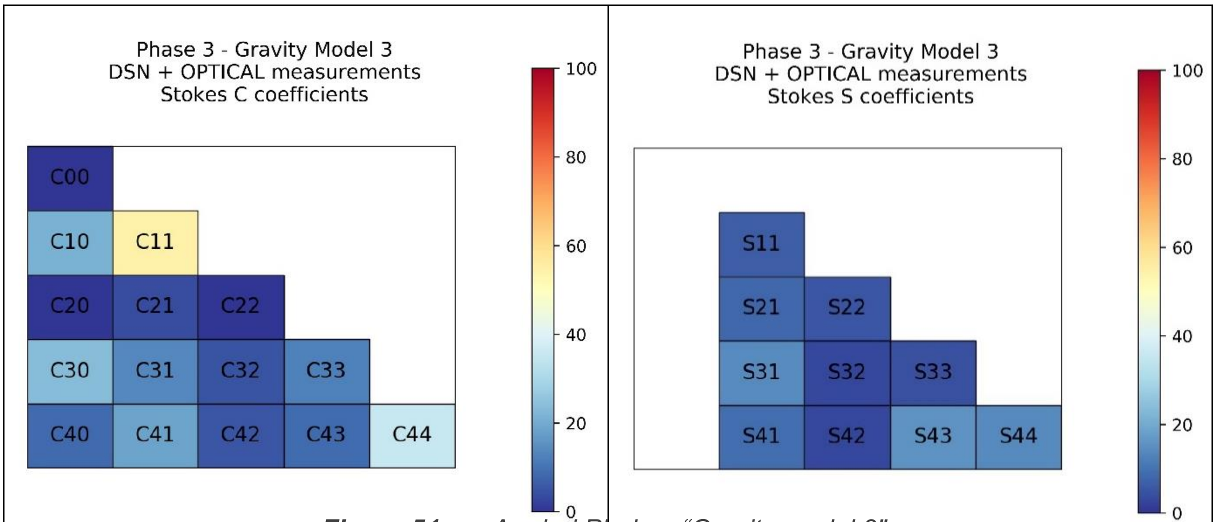

Figure 51.c *– A priori Phobos "Gravity model 3".*

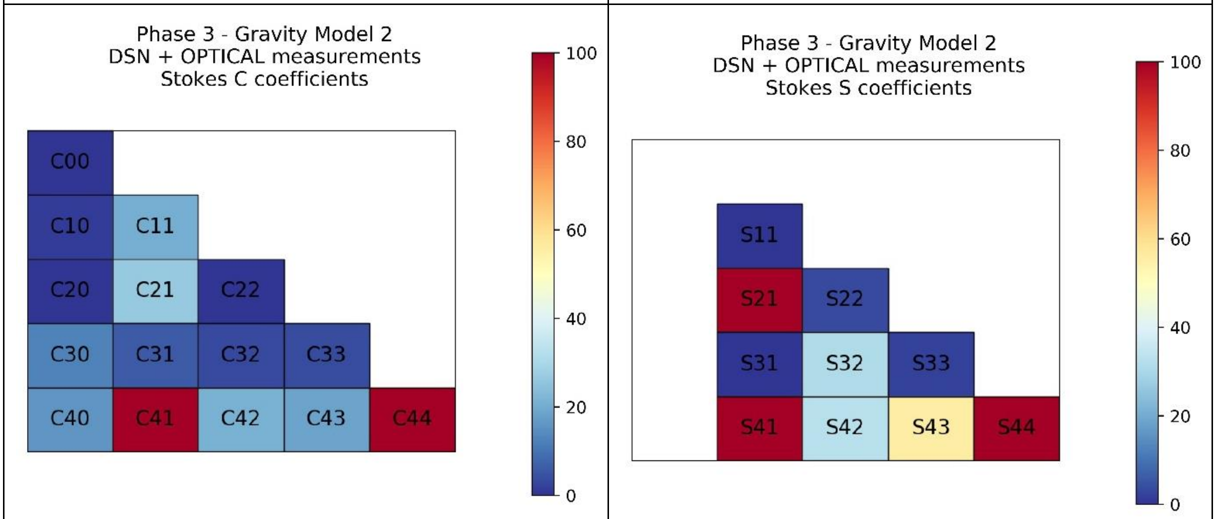

Figure 51.d *– A priori Phobos "Gravity model 2".*

Figure 51 *- Phobos gravity coefficient adjustment at the end of the third MMX Phobos phase.*

This result representation makes clear the fact that at the end of the third phase, the MMX mission would have the potential for providing a quite precise evaluation of Phobos gravity field. Again, the best model correction arrives from the employment of the most accurate a priori "Gravity model 1" and "Gravity model 4": all the coefficients are successfully adjusted.
Moreover, this time also the other less precise a priori templates afford a consistent model improvement. In fact, with the a priori "Gravity model 3", no more difficulties are detected for the return of correct order 4-Stokes coefficients, while "Gravity model 2" now allows the adjustment of a larger number of terms than at the end of the second phase.
In conclusion, at this point of the mission, an accurate update of the target gravity model could be affordable. Consequently, the beginning of last Phobos mission phase could rely on a sufficiently corrected gravity model.

Finally, the fourth phase have been treated. The accumulation of normal equations characterising every QSO composing this MMX part, has been combined with the collected information resulting from the previous three mission phases. The reached final normalised Stokes coefficient adjustment is presented below:

$\bar{C}_{lm}$	$\bar{S}_{lm}$

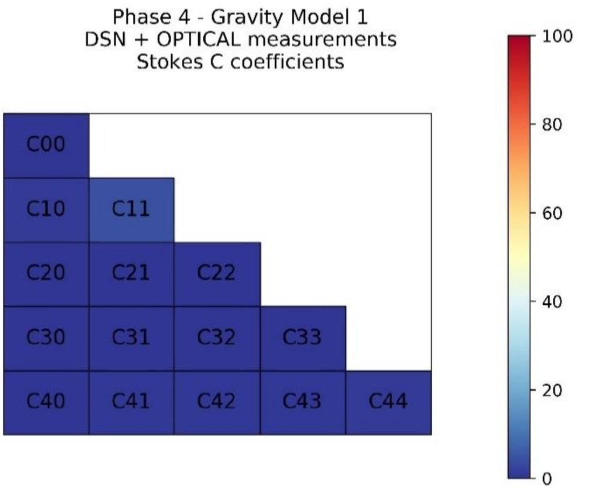

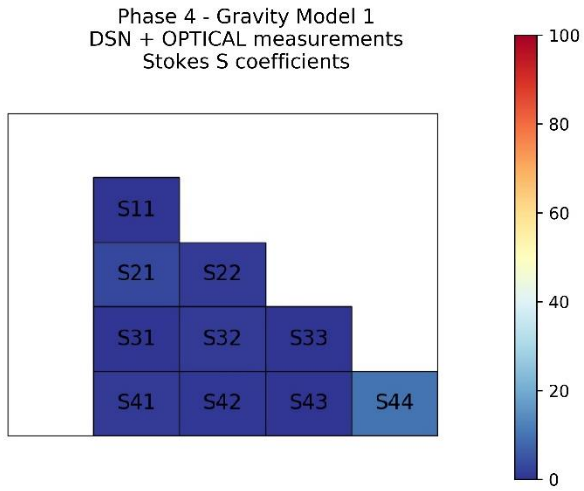

***Figure 52.a** – A priori Phobos "Gravity model 1".*

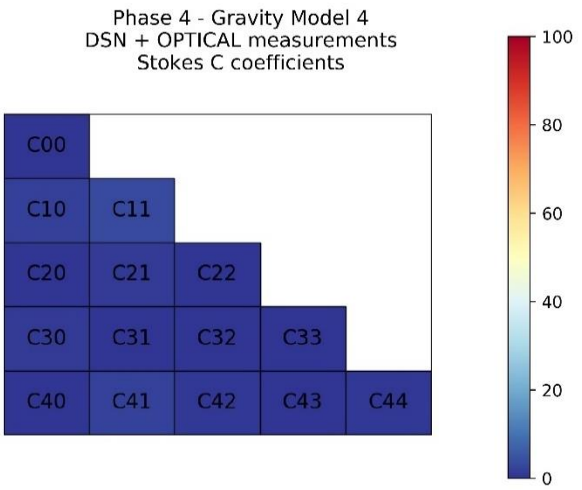

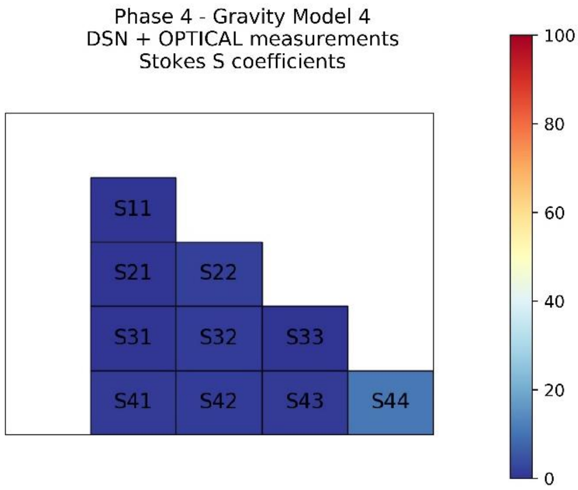

***Figure 52.b** – A priori Phobos "Gravity model 4".*

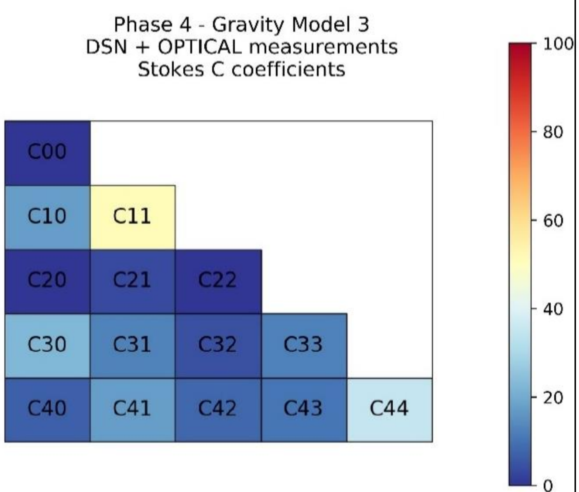

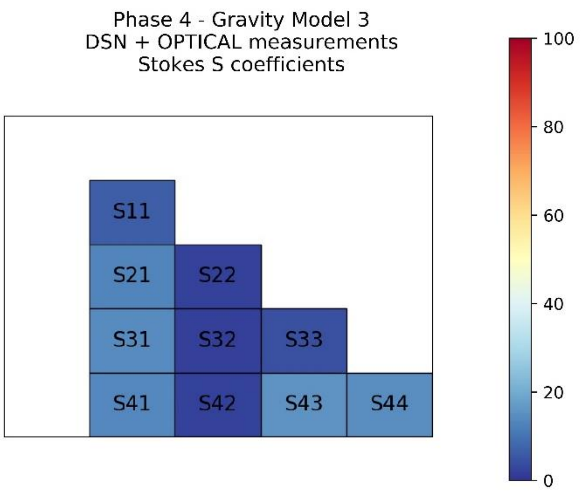

***Figure 52.c** – A priori Phobos "Gravity model 3".*

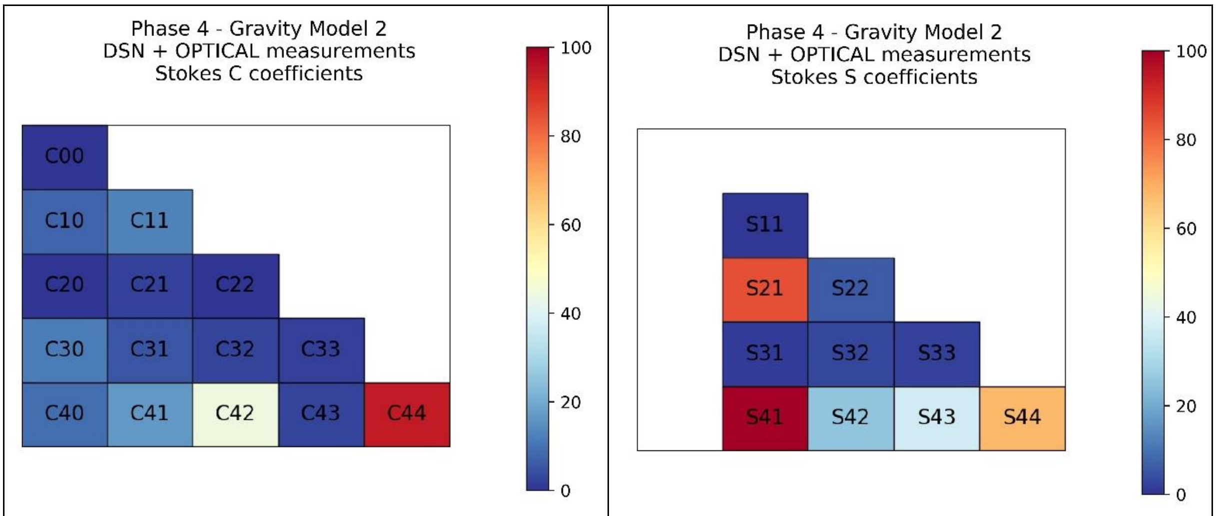

***Figure 52.d** – A priori Phobos "Gravity model 2".*

***Figure 52** - Phobos gravity coefficient adjustment at the end of the fourth MMX Phobos phase.*

The most of these final results appear to be entirely satisfactory. Phobos gravity model turns out to be sufficiently improved through this numerical computation.
In fact, the biggest part of all degrees and orders of both $\overline{C}_{lm}$ and $\overline{S}_{lm}$ coefficients results to get almost the same value of their counterparts in the target reference gravity model.
This result analysis leads to the conclusion that the MMX mission have the potential to carry out an accurate recovery of Phobos gravitational field model. Thus, the probable final update achievable by MMX could turn out to be much more accurate and closer to the real gravity field of the Martian moon.

In addition to this first conclusion, it is useful to exploit results obtained and the end of the fourth phase, in order to underline a relevant aspect. This remark concerns ephemeris measurements: LIDAR and Optical. As already stood out during the analysis of each single QSO, the combination of only these two measurement types provides the worst coefficient adjustment also in global mission results.
This feature is particularly evident with low precision-a priori models. Therefore, for the purpose of underlining the difference relative to results obtained with DSN and Optical combination, the graphs here presented correspond to the second worse a priori Phobos "Gravity model 3":

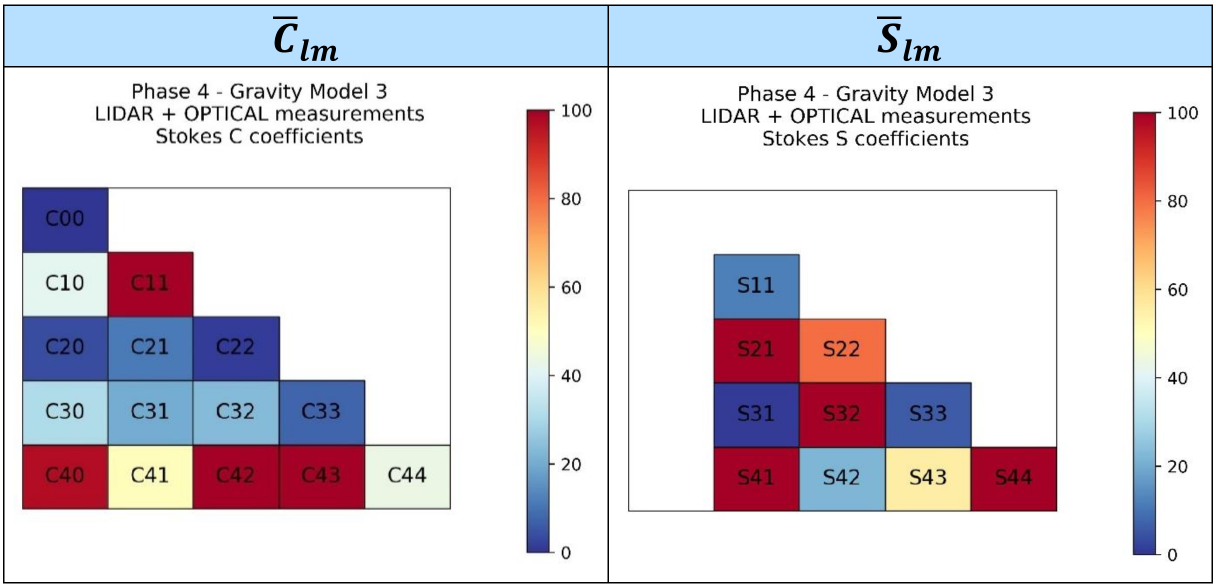

Figure 53 *- LIDAR and Optical measurement influence over the global Phobos gravity coefficient adjustment at the end of the fourth MMX Phobos phase. A priori Phobos "Gravity model 3".*

The comparison between these graphs and the corresponding in Figure 52.c, highlights the disparity in results obtainable with DSN-Optical and LIDAR-Optical measurement combination. The latter appears to have a lower ability to precisely adjust a perturbed initial gravity model. While the presence of Doppler measuring technique allows an almost perfect correction of all the normalised Stokes coefficients up to degree 4, the employment of only measurements of ephemeris type leaves many adjustment inaccuracies.
This feature is probably linked to the fact LIDAR and Optical measurements are characterised by a more significant white noise, in relation to DSN captures. The direct consequence is that Doppler measures are defined by a higher precision level, which leads them to reach better results and to prevail over the other measurement types.

Finally, a relevant remark concerning all the four MMX phases can be added. This analysis over the entire mission furtherly proves that the adjustment of a too inaccurate a priori Phobos gravity model, results to be impossible throughout the employment of the only low altitude trajectories.
This aspect is coherent with the typical attitude of QSO-L, already stood out by the previous steps of gravity field *Restitution* and normal equation *Resolution* for each trajectory, separately. In fact, this global accumulation over the phases proves again that the QSO-L class appears to be too sensitive to an excessive lack of precision in the a priori gravitational model.
The consequence is that the most imprecise a priori "Gravity model 2" does not allow QSO-L trajectories to be involved in normalised Stokes coefficient adjustment.
Thus, no measure combinations including LIDAR technique is able to furnish final results, for this a priori template. This situation reoccurs for all the four mission phases analysed: gravity model recovery from the a priori "Gravity model 2", is exclusively realised by QSO-M and QSO-H measurements.

Next chapter proposes possible solutions designed to avoid this inconvenience. The simulation of more realistic situations could enable not to consider any QSO-L trajectories for Phobos model correction with the imprecise a priori "Gravity model 2".

First alternative study case: The first alternative case differs from the nominal one exclusively in the definition of QSO trajectories composing the second phase:

- Phase 2: QSO-M → QSO-L-A → QSO-L-B → QSO-L-C → QSO-M

Consequently, the study of this first alternative case has been conducted exclusively up to the end of the second mission phase, where the difference with the nominal case should already be observable.
Moreover, since these two study cases differ from a various employment of QSO-L trajectories, the most useful comparison is between results obtained with measurement combination including LIDAR technique. A good example can thus be the accumulation of all ephemeris measures, whose graphs relative to $\overline{C}_{lm}$ coefficients are here presented (while the respective $\overline{S}_{lm}$ are reported in Figure 58 in Annex C):

$\overline{C}_{lm}$ - Nominal Case	$\overline{C}_{lm}$– 1st Alternative Case

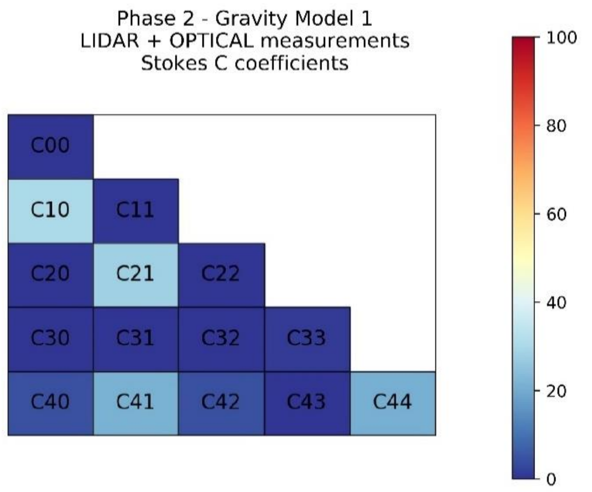

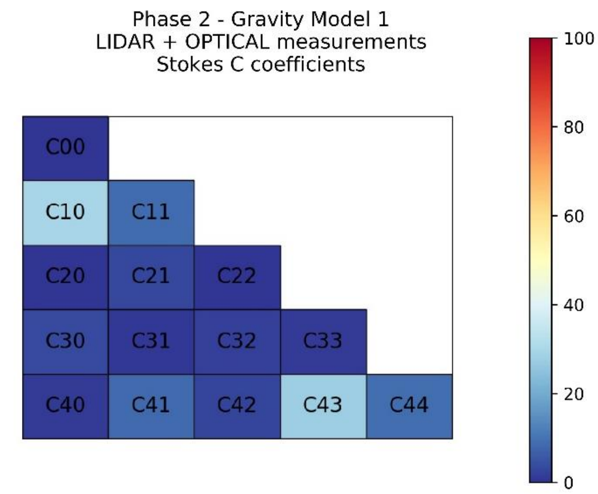

***Figure 54.a** – a priori Phobos "Gravity model 1".*

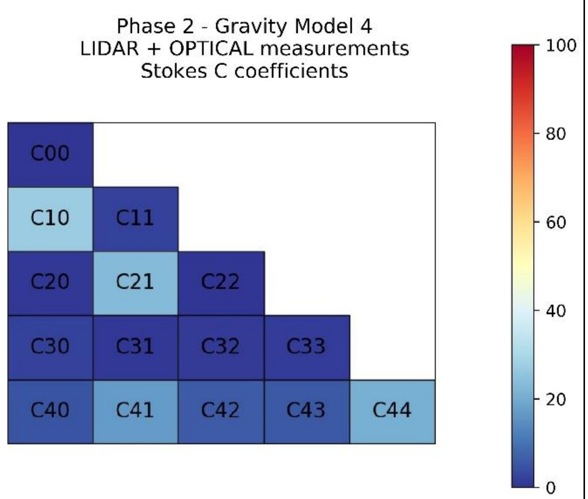

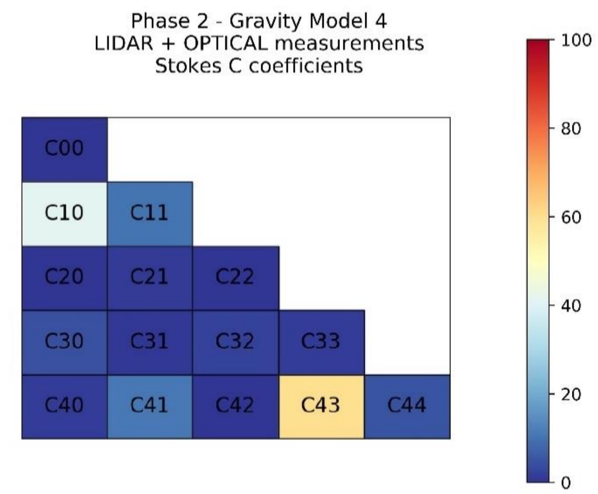

***Figure 54.b** – a priori Phobos "Gravity model 4".*

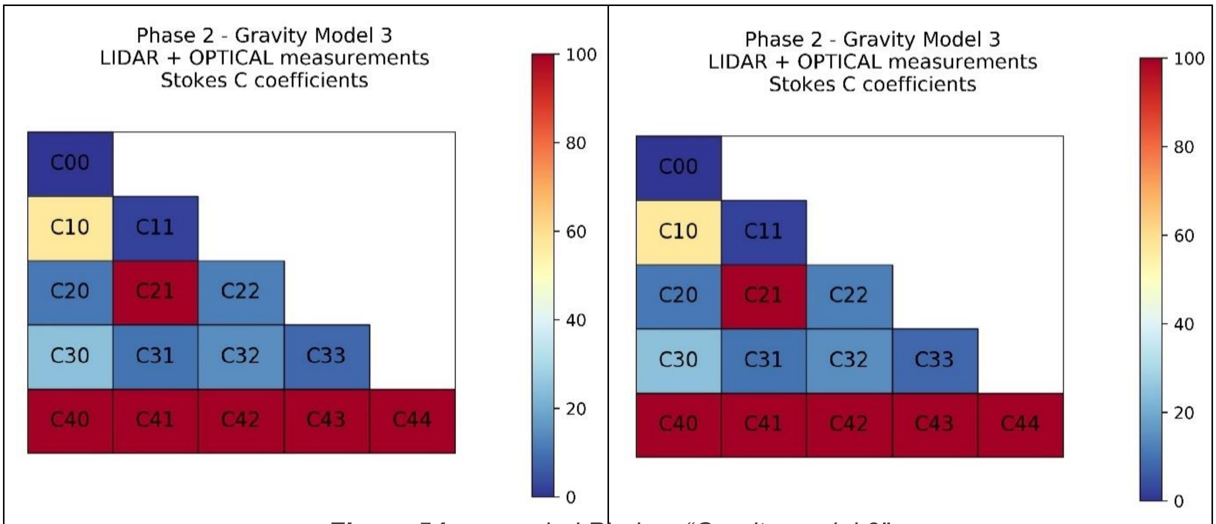

Figure 54.c *– a priori Phobos "Gravity model 3".*

Figure 54 *- Phobos gravity $\overline{C}_{lm}$ coefficient adjustment at the end of the second nominal and alternative MMX Phobos phase, considering the LIDAR and Optical measurement combination.*

The first remarkable aspect is that no results are presented for the a priori Phobos "Gravity model 2". Now, this lack appears clear: as confirmed by the conclusion stood out before, this gravity model is too inaccurate for its recovery by LIDAR measurements and any of their combinations.
Secondly, an attentive observation enables to confirm that in both nominal and first alternative cases, the adoption of the a priori "Gravity model 3" (Figure 54.c) leads to an absolutely equivalent correction of Stokes coefficients.
This feature is due to the fact that within a quite imprecise a priori Phobos gravity model, the same behaviour corresponds to both the QSO-L-B and the QSO-L-C sub-classes: the only two trajectory types defining the diversity between the nominal and this alternative case. In fact, the a priori "Gravity model 3" turns out to be still too inaccurate for allowing all the QSO-L trajectories to succeed in a proper geodesic parameter restitution and correction.
Especially, these QSO-L-B and QSO-L-C prove to be too sensitive to a lack of precision in the a priori gravitational model, so that both of them result to have very low effects on Stokes coefficient adjustment in the second mission phase. Effectively, at the end of this MMX phase, all model corrections based on LIDAR measurements arrive from the slightly larger and less sensitive QSO-L-A.
However, considering that at the end of the first phase, the MMX mission could already have reached a better resolution of the Martian moon field, the situation may appear different. In fact, the use of the more accurate a priori "Gravity model 4", evidences a light difference between the two study cases (Figure 54.b). This time, the employment of the QSO-L-B and QSO-L-C combination (first alternative case) provides a globally more complete resolution over all the coefficient degrees, except for the C_{43} term,. This marginally better adjustment also recurs with the a priori "Gravity model 1" (Figure 54.a)

<u>Second alternative case</u>*:* The second alternative case proposed by the JAXA, is the richest in 3-Dimensional QSO trajectories. It differs from the nominal one in the definition of the second and the fourth phases:

- Phase 2: QSO-M → QSO-L-A → QSO-L-B → QSO-M → QSO-3D-M-A → QSO-M
- Phase 4: QSO-3D-M-B → QSO-M → QSO-L-A

In this project context, only the alternative QSO-3D-M trajectories reaching the lowest (A1 and B1) and the highest (A5 and B5) latitude over Phobos surface have been analysed.
Consequently, this case comparison has been conducted over results obtained at the end of the second and the fourth mission phases, taking into account the QSO-3D-M- A1, B1, A5 and B5.

First of all, it is immediately possible to make a remark. As brought out by the analysis of each single orbit, 3-Dimensional QSOs result to be more suitable for better Phobos model correction, especially with less accurate a priori conditions.
Effectively, the employment of sufficiently accurate gravity models allows also the 2-Dimensional medium-altitude orbits to get precise geodesic parameter adjustment. On the contrary, an adequate improvement in Phobos gravity knowledge, starting from less precise initial templates, is affordable only by 3-Dimensional QSO-M trajectories (Figure 39, Figure 41 and Figure 43).
This consideration is furtherly proved by the fact that, using the a priori Phobos “Gravity model 1” and “Gravity model 4”, results reached by the nominal and the second alternative cases are basically the same (Figure 59 and Figure 60 in the Annex C).
For such reason, $\bar{C}_{lm}$ coefficient results here presented, correspond to the most imprecise a priori Phobos “Gravity model 2”. The same combination of DSN and Optical measurements is taken as an example, as for nominal case graphs relative to the second (Figure 50.d) and fourth (Figure 52.d) phases. Relative $\bar{S}_{lm}$ graphs are in Figure 61 in Annex C.

$\bar{C}_{lm}$ – Lower inclination (A1,B1)	$\bar{C}_{lm}$ – Higher inclination (A5,B5)
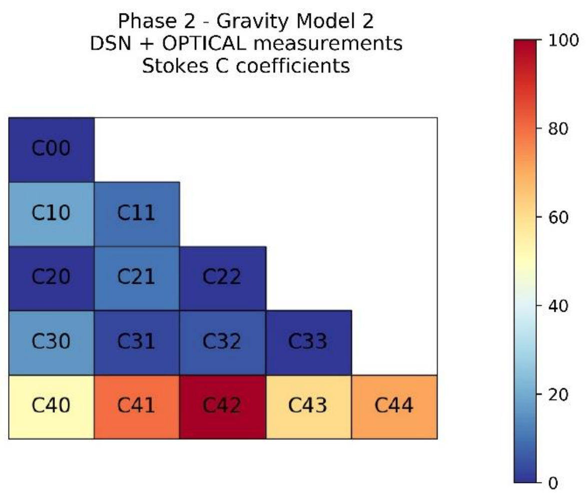	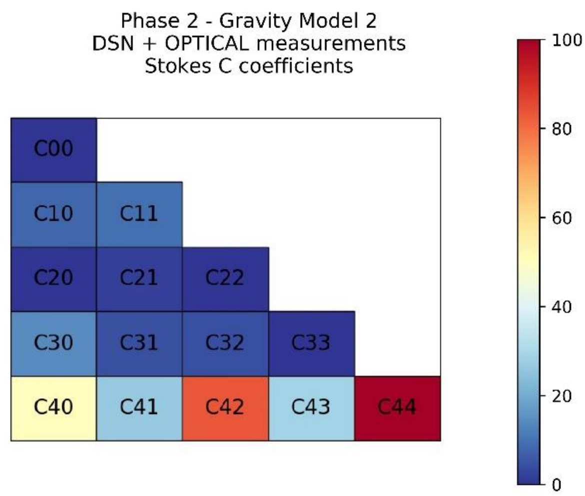

***Figure 55.a** – End of the second mission phase.*

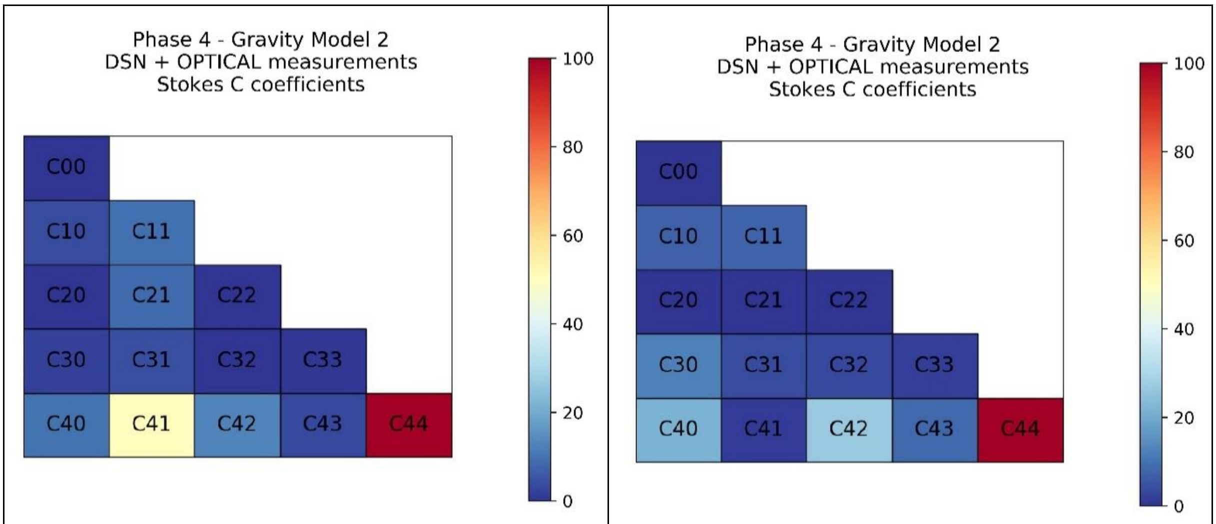

***Figure 55.b** – End of the fourth mission phase.*

***Figure 55** - $\overline{C}_{lm}$ adjustment from "Gravity model 2" at the end of the second and fourth phases, considering DSN-Optical measurement combination, along the least and the most inclined 3D orbits.*

If compared with the corresponding nominal case results, these graphs highlight a more precise Phobos gravity model correction, at the end of both the mission phases taking into account. However, this better resolution is particularly evident in the second phase. In fact, here a part of the nominal 2-Dimensional QSO-M trajectory is substituted by a QSO-M-3D-A: the consequent improvement in the accuracy level is more pronounced.
Instead, in the last phase, the exchange is between the nominal QSO-M-3D and a QSO-M-3D-B, both 3-Dimensional orbits. The resulted improving impact is thus present, but less marked.

Moreover, it is possible to conclude that the employment of the 3D-QSO versions reaching higher *z*-dimensions, could lead to an even better recovery of global Phobos gravity model. This is made evident by the supplemental comparison between graphs reported in the two columns of Figure 55. The ones on the right, showing a slightly more accurate gravity filed reconstruction, have been obtained with the consideration of the QSO-M-3D-A5 and the QSO-M-3D-B5. Effectively, both these orbits achieve higher latitudes over the Phobos surface than the QSO-M-3D-A1 and the QSO-M-3D-B1, whose marginally less precise results are presented on the left. Particularly, the more a 3-Dimensional orbit is inclined, the more its ability in adjusting $\overline{\boldsymbol{C}}_{\boldsymbol{4m}}$ Stokes elements increases.

4 Conclusions and possible prospects

This internship project has turned out to produce suitable results for the evaluation of which could be the real Phobos gravity model correction reachable by the MMX mission.
First of all, this analysis allows to understand the contribution of each 2 and 3-Dimensional QSO to the MMX success. In fact, results here presented, highlight that:

- The QSO-H trajectories, reaching exclusively higher altitudes over the Martian moon surface, are suitable for the perfect return of only the $\boldsymbol{C_{00}}$ Stokes element, thus the real Phobos standard gravitational constant $\boldsymbol{\mu}$.

- The QSO-M trajectories allow an incomplete reconstruction of the target gravity field: they enable the partial correction of up-to-2/3-degree-normalised Stokes coefficients. Consequently, they result to be suitable for the initial mission phases. Not being excessively sensitive to a large real field unknowledge, they allow first model corrections.
- The QSO-3D-M trajectories always manage to get a larger improvement in the actual knowledge of Phobos gravity model, in relation to their counterpart 2-Dimensional medium-altitude orbits. The higher is the latitude they can reach over the target body, the more accurate their gravity field detection can be.

- The QSO-L trajectories, reaching the closest proximities to Phobos surface, proved to be the most sensitive to the body gravity field. This feature implies two complementary aspects. Firstly, the low-altitude orbits are not able to correct a gravity model too imprecise in relation to the real field. Secondly, they amply proved to have the largest ability to precisely correct a not excessively perturbed a priori gravity model. The employment of these orbits in mission phases succeeding the first one, is a strong point for the entire MMX success in its geodesic objectives. In fact, they allow the recovery of Phobos gravity coefficients up to degree 4, the maximal degree analysed within this internship project.

Moreover, this project enables an evaluation of the influence relative to every considered measurement combination:

- DSN measurements appear to be fundamental for a complete and accurate restitution of Phobos gravity field. They are characterised by a high precision level, which is able to lead to an excellent correction of normalised Stokes coefficients (up to degree 4).

- Doppler measurements captured with the only DSN Usuda ground station, result in a loss of precision in Phobos gravitational field evaluation. In fact, this technique implies less DSN captures, thus less accurate gravity coefficient reconstruction. However, this loss of precision turned out to be rather limited, especially considering its slight effects on the entire mission. Consequently, it is possible to conclude that global model adjustment can still be sufficiently accurate, with the employment of the single Usuda antenna.

- The combination of only LIDAR and Optical measures is not able to rich the perfect correction of Phobos gravity model, especially considering a quite imprecise initial a priori knowledge. Consequently, DSN captures are necessary for reaching the best model recovery possible.

To sum it up, the global evaluation of all these results allows to get an important conclusion. They prove that using appropriate combinations of QSO trajectories and measurement techniques, the MMX mission has the potential to reach one of its main scientific purpose: the improvement in the knowledge of Phobos gravity field.

Furthermore, these first important results can represent the basis for a possible even more detailed analysis: the MMX mission study could proceed in many different directions. Thus, multiple are the prospects for the future:

- This internship study has been conducted considering all the four a priori Phobos gravity models separately, within the analysis of each MMX phase. This procedure allows to get a first interesting version of the probable target gravity restitution reachable by the mission. However, a more realistic case could be analysed. In fact, as detailed before, during the MMX process, a gradual correction will be applied over the actual Martian moon gravity model. While the satellite will move nearer the target body, the knowledge in its gravitational field will increase, so that a constant update of the relative model will be possible. As a consequence, it would be useful to proceed in a realistic gradual way within the last project steps of the *Restitution*, *Accumulation* and *Resolution*:

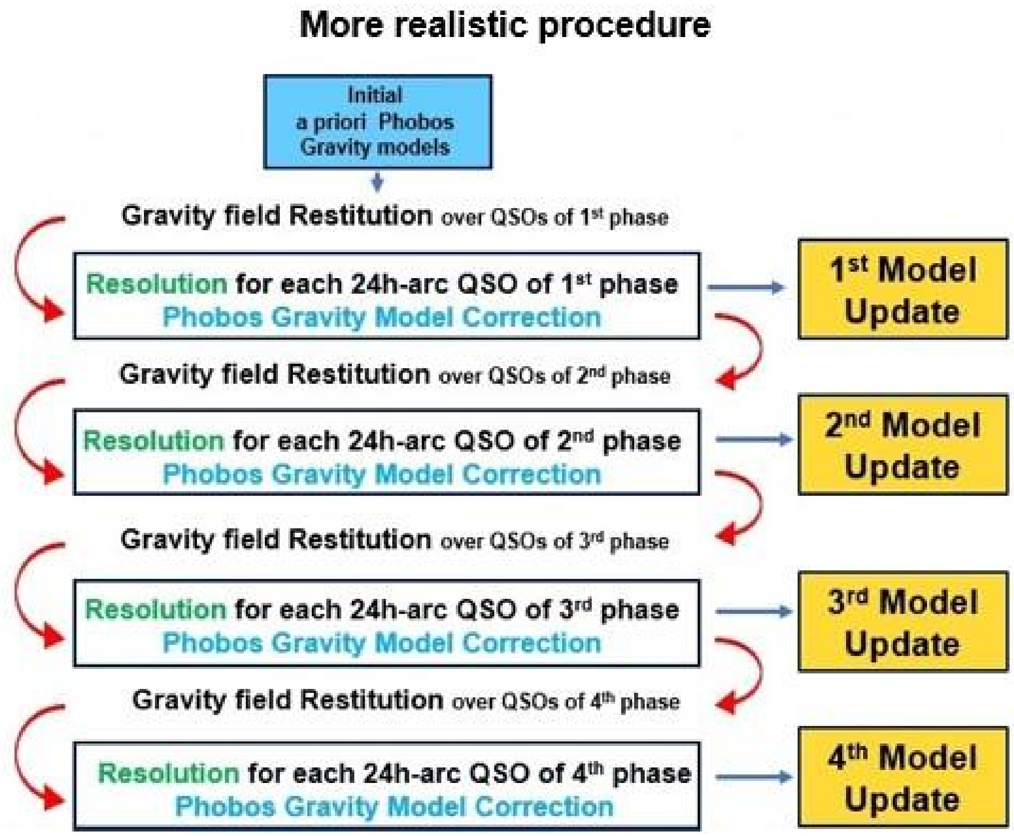

***Figure 56** - Possible more realistic and gradual Restitution-Accumulation-Resolution method.*

It would thus be possible to realise an initial gravity filed restitution over only the QSO trajectories taking part in the first mission phase, considering the desired a priori Phobos gravitational models.
Subsequently, their relative normal equations could be accumulated and resolved in order to get a first adjustment of Stokes coefficients. This would correspond to the earliest update reachable by the MMX mission of the knowledge in this target geodesic parameter.
These corrected gravity coefficients would then constitute the new a priori model, to be used in the *Restitution* procedure for QSO trajectories belonging to the second phase. It would lead to another normal equation accumulation and resolution in a new set of adjusted gravity coefficients. The latter would represent the second Phobos gravity update available in the MMX mission.
This second corrected model would also appear as a priori reference, in the gravitational field restitution in QSO trajectories of the third mission phase. Newly, the *Accumulation* and *Resolution* steps would give birth to an always more precise update in the actual a priori gravity model.
Finally, the latter would be employed in the *Restitution* step concerning the remaining QSOs, taking part in the fourth mission phase. The last normal equation accumulation and resolution would generate the final correction results, representing the definitive Phobos gravity model update accessible from the MMX mission.

- In the context of this internship project, only Stokes coefficients up to degree 4 have been set as free parameters, so that results here obtained are representative of only this limited group.
  It would be useful to extend the maximal adjustable degree of harminic gravity coefficients. In this way, it would be possible to understand which are the QSO trajectories and the measurement combinations more suitable for the reconstruction of higher degree-coefficients.
  At the same time, it would be clear the comprehension of how far the entire MMX mission would be able to recover Phobos gravity field model.

- This internship study has been completely focused on Phobos gravity filed study. However, the MMX mission has among its scientific objectives, the correct evaluation of the Martian moon ephemeris in relation to Mars and its rotation around its spin axis.
  Consequently, it would be possible to complete this space geodesy analysis with the addition of these two Phobos physical parameters, both treatable by the GINS software.

Annexes

Annex A: Normalised Stokes coefficients from Phobos shape model

The following two tables show normalised Stokes coefficients $\overline{C}_{\mathrm{lm}}$ and $\overline{S}_{\mathrm{lm}}$ numerical values**,** computed from Phobos shape model. These up-to-20-degree coefficients represent the Phobos gravity filed model used as realistic reference in this internship project.

l \ m	0	1	2	3	4	5	6	7	8	9	10	11	12	13	14	15	16	17	18	19	20
0	1																				
1	-1,99E-04	-7,94E-05																			
2	-4,76E-02	1,27E-03	2,47E-02																		
3	3,03E-03	-4,52E-03	-9,02E-03	1,62E-03																	
4	6,83E-03	3,21E-03	-2,54E-03	-3,22E-03	9,30E-04																
5	2,22E-03	-1,61E-03	1,55E-03	4,91E-04	-1,60E-03	-9,04E-04															
6	-1,23E-03	-1,89E-03	5,70E-04	1,55E-03	-5,27E-04	-6,23E-04	-3,81E-03														
7	-2,19E-03	2,61E-03	3,97E-04	-3,40E-04	4,36E-04	1,12E-03	2,98E-04	-3,10E-03													
8	2,97E-04	3,32E-04	-7,23E-04	-2,65E-04	3,97E-04	6,82E-05	1,16E-03	-1,21E-03	-1,98E-03												
9	1,55E-03	-1,55E-03	-6,89E-04	1,49E-04	-1,11E-04	-2,49E-04	1,45E-04	1,36E-03	2,65E-04	-5,84E-04											
10	-7,26E-05	-2,13E-04	4,46E-04	-5,69E-05	-5,80E-04	-1,67E-04	-4,07E-04	5,85E-04	1,34E-03	-1,88E-04	1,33E-03										
11	-8,84E-04	6,53E-04	6,01E-04	8,79E-05	-5,76E-05	3,32E-05	-7,87E-05	-5,01E-04	-3,56E-04	6,24E-04	2,82E-04	1,31E-03									
12	1,03E-04	2,97E-04	-2,57E-04	1,64E-05	3,83E-04	1,91E-04	-7,61E-05	-4,87E-04	-4,77E-04	3,03E-04	1,52E-04	1,03E-04	1,92E-03								
13	4,69E-04	-2,84E-04	-4,02E-04	8,91E-06	6,55E-05	-1,23E-05	2,04E-04	1,23E-04	1,14E-04	-7,42E-04	-5,19E-04	-1,75E-04	-4,78E-05	1,69E-03							
14	-1,03E-04	-3,62E-04	1,12E-04	8,25E-05	-2,41E-04	-1,56E-04	1,96E-04	2,55E-04	-2,78E-05	-2,65E-04	-2,42E-04	-5,87E-06	-7,25E-04	3,38E-04	1,30E-03						
15	-3,29E-04	9,13E-05	2,55E-04	-1,31E-04	2,40E-06	1,11E-04	-3,11E-04	1,26E-04	7,29E-05	6,16E-04	4,37E-04	-3,30E-04	-3,50E-04	-1,15E-03	-4,43E-04	3,62E-04					
16	7,77E-05	3,50E-04	-1,76E-05	-1,10E-04	8,89E-05	8,85E-05	-1,89E-04	-1,30E-04	1,85E-04	1,71E-04	1,44E-04	1,16E-05	8,12E-05	-2,65E-04	-1,24E-03	5,86E-04	-9,30E-04				
17	3,17E-04	3,20E-05	-2,28E-04	1,37E-04	-1,26E-04	-1,54E-04	4,05E-04	-1,81E-04	-3,97E-05	-2,71E-04	-4,01E-04	4,99E-04	6,49E-04	5,04E-04	1,88E-04	-1,05E-03	-3,32E-04	-1,96E-03			
18	-7,38E-05	-2,72E-04	-2,88E-05	1,33E-04	7,88E-05	-4,31E-05	8,75E-05	5,23E-05	-2,78E-04	-2,13E-04	1,55E-05	-9,57E-05	9,61E-05	2,36E-04	7,10E-04	-2,92E-04	-3,62E-04	3,33E-04	-2,99E-03		
19	-3,25E-04	-1,37E-04	2,43E-04	-5,61E-05	1,71E-04	1,45E-04	-4,31E-04	9,09E-05	4,00E-05	3,16E-05	4,20E-04	-3,15E-04	-7,41E-04	1,30E-04	2,36E-04	8,49E-04	5,90E-04	-5,01E-05	-1,17E-04	-2,68E-03	
20	7,09E-05	1,80E-04	3,11E-05	-1,40E-04	-1,63E-04	6,48E-05	6,87E-05	-4,65E-05	2,60E-04	2,63E-04	-2,56E-04	6,03E-05	-2,87E-05	-3,23E-04	-3,27E-04	1,39E-04	5,06E-04	1,62E-04	9,64E-04	5,43E-04	-2,62E-03

Table 10 *- Computed normalized Stokes $\overline{C}_{lm}$ coefficients from Phobos shape model.*

l \ m	0	1	2	3	4	5	6	7	8	9	10	11	12	13	14	15	16	17	18	19	20
0																					
1		-3,10E-04																			
2		1,41E-04	3,24E-04																		
3		2,16E-03	7,52E-04	-1,36E-02																	
4		-1,12E-03	-1,61E-03	2,79E-03	5,96E-05																
5		-9,74E-04	1,19E-04	2,76E-03	4,62E-04	-3,84E-03															
6		6,87E-04	1,21E-03	-1,60E-03	3,39E-04	2,85E-04	-8,11E-04														
7		2,36E-04	5,74E-06	-4,33E-04	9,88E-06	2,17E-03	7,83E-04	2,92E-04													
8		-2,71E-05	-1,06E-03	6,59E-06	-8,09E-05	-2,37E-04	3,47E-04	-2,42E-04	2,26E-03												
9		-1,45E-04	-3,37E-05	2,18E-04	-1,14E-04	-7,36E-04	7,36E-05	8,38E-04	2,34E-04	2,05E-03											
10		-5,87E-05	7,68E-04	4,33E-04	-2,49E-04	-1,12E-04	-6,33E-04	-4,49E-04	-7,17E-04	-4,32E-04	2,32E-03										
11		1,35E-04	-3,02E-05	-2,32E-04	7,18E-05	3,50E-04	-1,29E-04	-5,08E-04	-9,47E-05	-4,74E-04	1,97E-04	9,25E-04									
12		8,15E-05	-3,60E-04	-4,22E-04	3,38E-04	3,64E-04	3,59E-04	1,51E-04	-7,84E-06	-4,51E-05	-8,79E-04	-8,85E-04	4,41E-04								
13		-1,69E-04	-6,06E-05	1,26E-04	-1,15E-04	-7,83E-05	9,59E-05	4,14E-04	2,43E-04	-1,43E-05	-4,94E-04	-7,13E-04	2,05E-04	-1,30E-03							
14		-1,69E-04	1,43E-04	4,52E-04	-3,15E-04	-2,95E-04	-2,86E-05	-6,31E-05	8,33E-05	2,62E-04	4,32E-04	7,36E-04	-6,54E-04	-6,14E-04	-1,10E-03						
15		1,64E-04	1,20E-04	-9,57E-05	9,68E-05	-1,51E-04	-1,82E-04	-2,69E-04	-1,64E-04	3,37E-04	3,06E-04	2,00E-04	-4,50E-04	3,37E-05	1,55E-04	-2,64E-03					
16		2,64E-04	3,69E-06	-5,24E-04	2,42E-04	2,72E-04	-1,42E-04	1,47E-04	-7,73E-05	-4,55E-04	3,82E-05	-2,39E-04	9,10E-04	8,49E-04	-1,11E-04	-1,78E-04	-2,10E-03				
17		-1,28E-04	-1,04E-04	1,20E-04	-8,74E-05	2,36E-04	1,63E-04	6,77E-05	4,55E-05	-3,71E-04	-1,35E-04	-2,80E-05	2,16E-04	1,02E-04	-1,86E-04	1,03E-03	1,63E-04	-2,15E-03			
18		-3,25E-04	-1,31E-04	5,98E-04	-8,69E-05	-2,57E-04	1,48E-04	-1,71E-04	5,54E-05	5,06E-04	-2,92E-04	5,35E-05	-4,05E-04	-7,06E-04	6,50E-04	7,20E-04	1,11E-03	3,90E-04	-4,54E-04		
19		1,18E-04	7,20E-05	-1,67E-04	5,78E-05	-1,78E-04	-1,22E-04	6,34E-05	1,52E-05	2,22E-04	1,09E-04	-1,51E-04	-2,57E-04	-1,24E-04	-1,86E-05	-3,72E-04	1,82E-05	1,38E-03	3,74E-04	3,94E-04	
20		3,26E-04	2,00E-04	-5,93E-04	-8,82E-05	2,19E-04	-6,15E-05	1,66E-04	3,52E-05	-4,76E-04	2,92E-04	7,25E-05	1,78E-06	6,75E-04	-5,79E-04	-1,02E-03	-2,92E-04	1,96E-04	9,35E-04	7,61E-04	2,23E-03

Table 11 *- Computed normalized Stokes $\overline{S}_{lm}$ coefficients from Phobos shape model.*

Annex B: Phobos gravity field model adjustment along each QSO

$\overline{S}_{lm}$ – DSN (Madrid + Usuda)	$\overline{S}_{lm}$ – DSN (Usuda only)

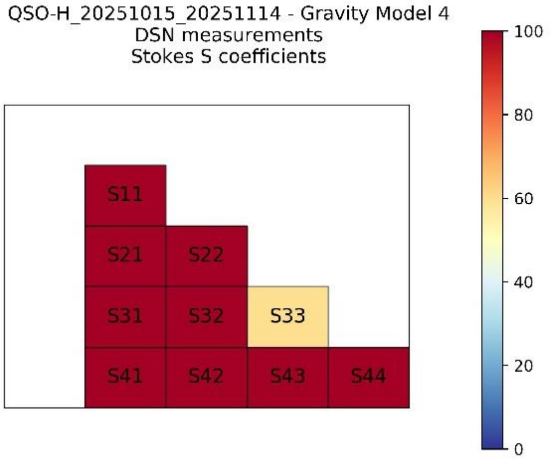

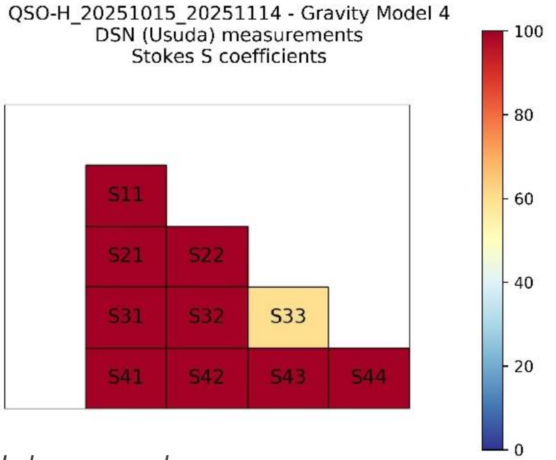

Figure 57.a *– QSO-H class example.*

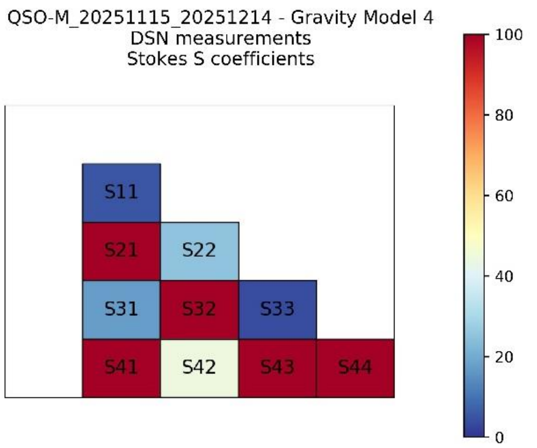

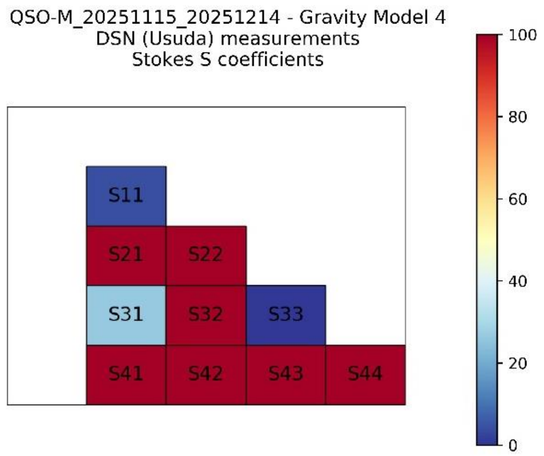

Figure 57.b *– QSO-M class example.*

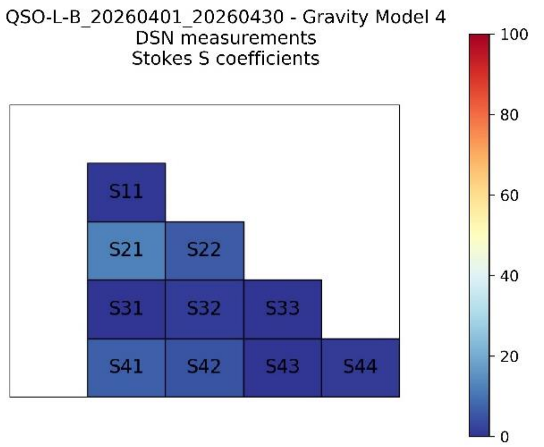

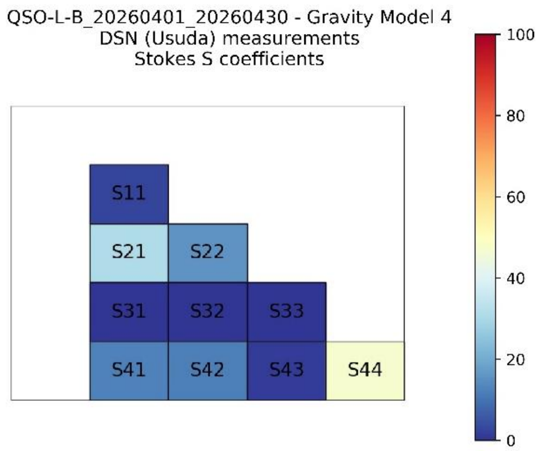

Figure 57.c *– QSO-L class example.*

Figure 57 *- Stokes $\overline{S}_{lm}$ coefficients adjusted from a priori Phobos "Gravity model 4", considering DSN measurements realised with both Madrid and Usuda stations and with only Usuda antenna.*

Annex C: Phobos gravity field model adjustment along the entire MMX mission

$\overline{S}_{lm}$ – Nominal Case	$\overline{S}_{lm}$ – 1st Alternative Case

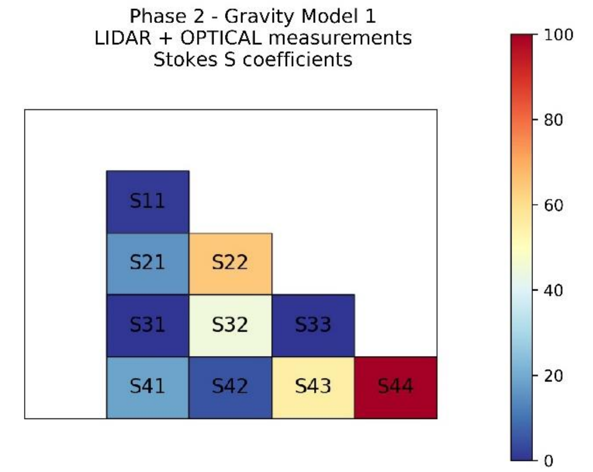

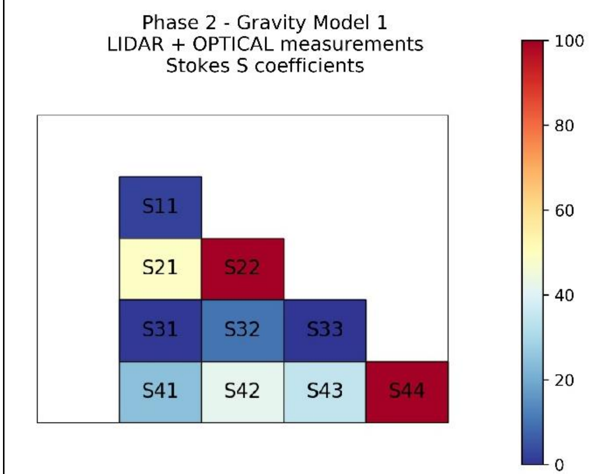

Figure 58.a *– a priori Phobos "Gravity model 1".*

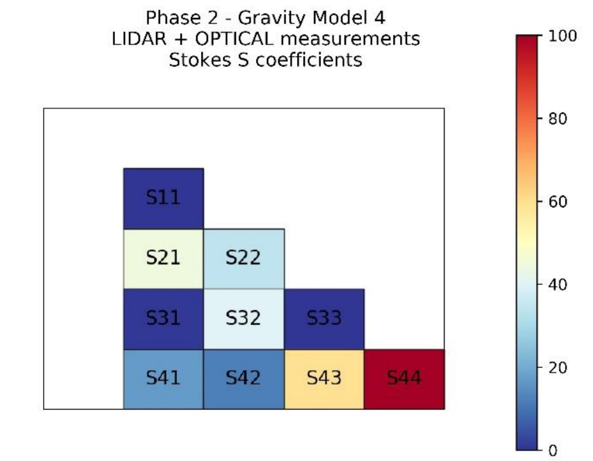

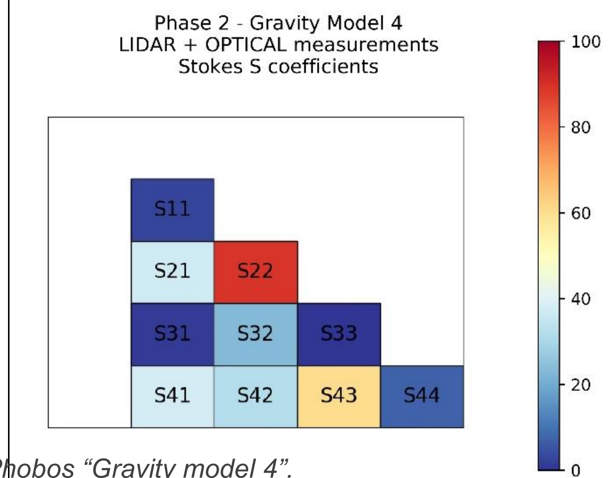

Figure 58.b *– a priori Phobos "Gravity model 4".*

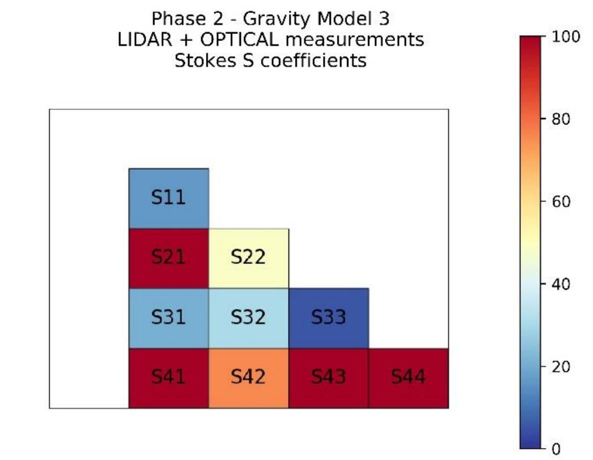

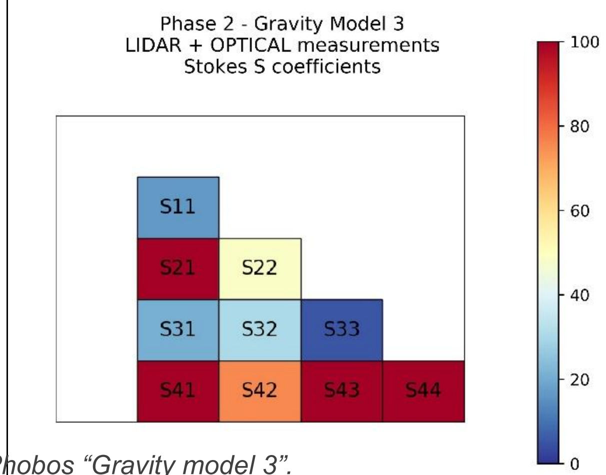

Figure 58.c *– a priori Phobos "Gravity model 3".*

Figure 58 *- Phobos gravity $\overline{S}_{lm}$ coefficient adjustment at the end of the second nominal and alternative MMX Phobos phase, considering the LIDAR and Optical measurement combination.*

$\overline{C}_{lm}$ – Lower inclination (A1,B1)	$\overline{C}_{lm}$ – Higher inclination (A5,B5)

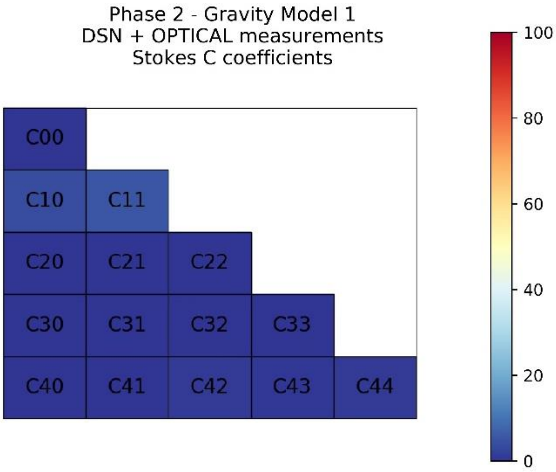

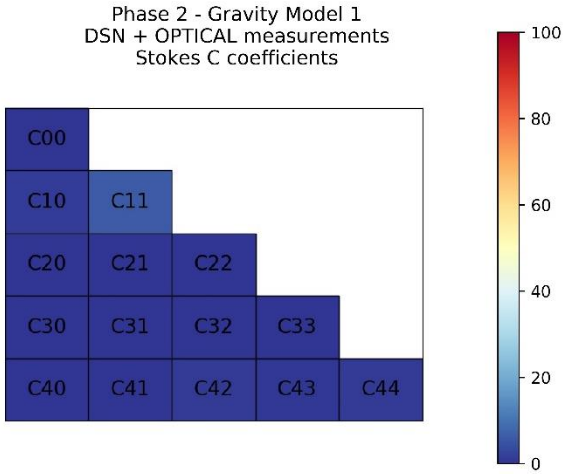

***Figure 59.a** – End of the second mission phase.*

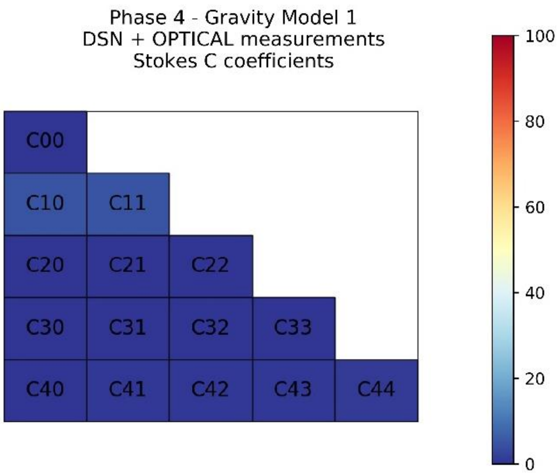

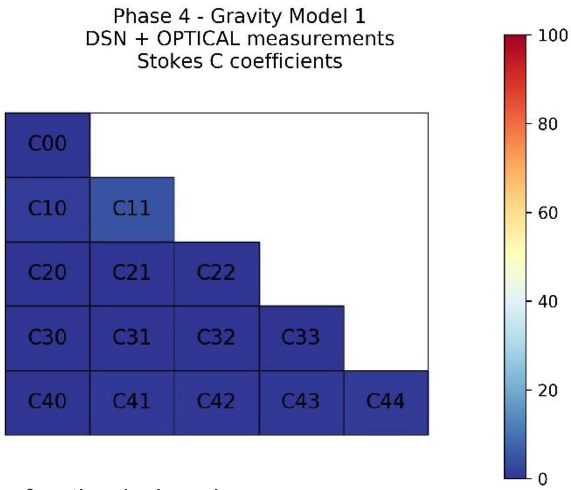

***Figure 59.b** – End of the fourth mission phase.*

***Figure 59** - $\overline{C}_{lm}$ adjustment from "Gravity model 1" at the end of the second and fourth phases, considering the DSN-Optical measure combination, along the least and the most inclined 3D orbits.*

$\overline{C}_{lm}$ – Lower inclination (A1,B1)	$\overline{C}_{lm}$ – Higher inclination (A5,B5)

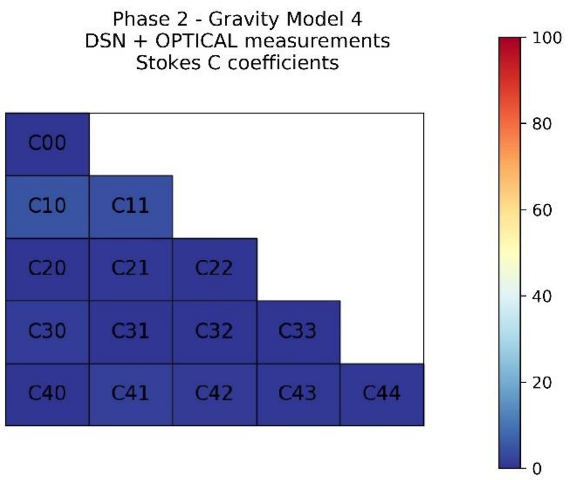

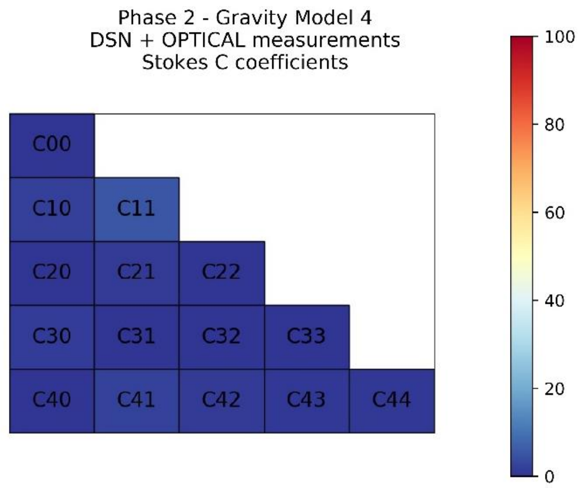

Figure 60.a *– End of the second mission phase.*

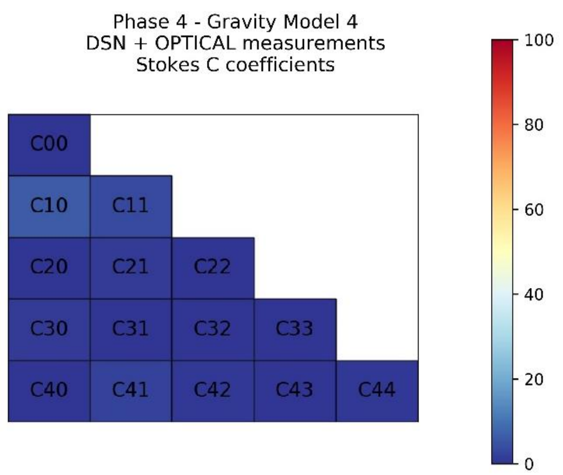

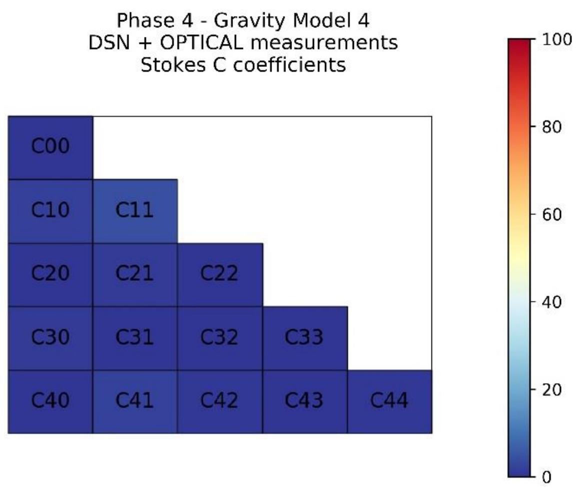

Figure 60.b *– End of the fourth mission phase.*

Figure 60 *- $\overline{C}_{lm}$ adjustment from "Gravity model 4" at the end of the second and fourth phases, considering the DSN-Optical measure combination, along the least and the most inclined 3D orbits.*

$\overline{S}_{lm}$ – Lower inclination (A1,B1)	$\overline{S}_{lm}$– Higher inclination (A5,B5)
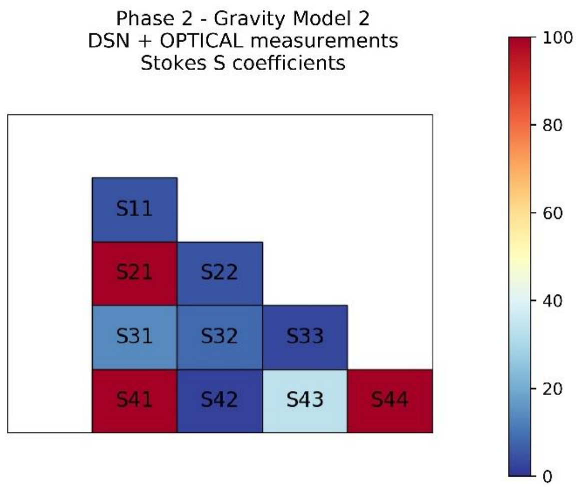	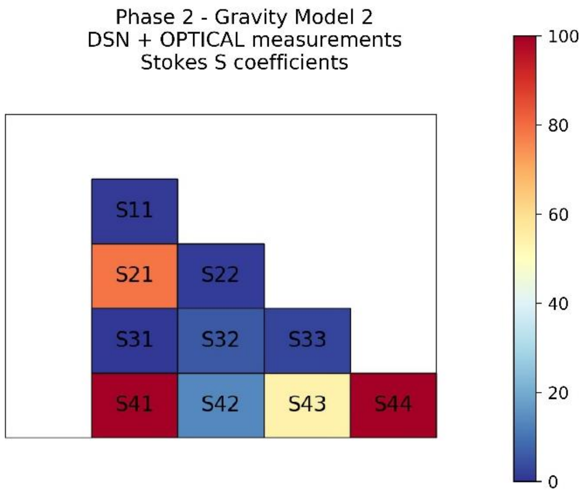
Figure 61.a *– End of the second mission phase.*	
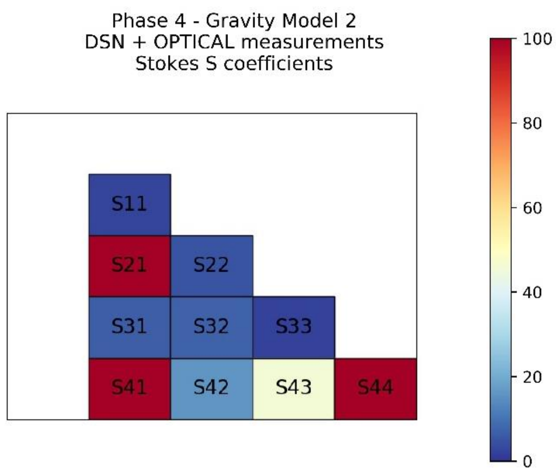	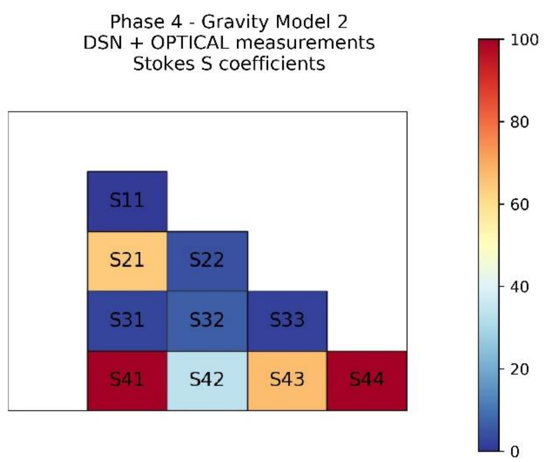
Figure 61.b *– End of the fourth mission phase.*	

Figure 61 *- $\overline{S}_{lm}$ adjustment from "Gravity model 2" at the end of the second and fourth phases, considering the DSN-Optical measure combination, along the least and the most inclined 3D orbits.*

Bibliography

[1] X. W. K. O. J. e. a. Shi, “Working Models for the Gravity Field of Phobos,” *Science China Physics, Mechanics & Astronomy,* vol. 55 (2), 2012.

[2] Y. T. Y. T. H. I. ,. S. T. a. Y. K. Naoko OGAWA, “Orbit Design for Martian Moons Explorer,” 2017.

[3] P. a. S. J. Gil, “Simulations of Quasi-Satellite Orbits,” *Journal of Guidance, Control and Dynamics,* Vols. Vol. 33, No. 3, p. 901–914, 2010.

[4] C. Elisabet, “QUASI-SATELLITE ORBITS (QSO). APPLICATION IN THE MARSPHOBOS,” Toulouse , 2020.

[5] B. a. R. D. Chao, “The gravitational field of Phobos.,” in *Geophysical research letters, Vol. 16*, 1989, pp. No. 8, pp. 859–862.

[6] M. Zamaro, “Natural and artificial orbits around the Martian moon Phobos.,” Department of Mechanical and Aerospace Engineering, University of Strathclyde, 2014-2015.

[7] F. a. G. P. Cabral, “On the Stability of Quasi-Satellite Orbits in the Elliptic Restricted Three-Body Problem.,” Lisbone, Master Thesis at the Universidade T´ecnica de Lisboa, 2011.

[8] G. Balmino, “Gravitationl potential harmonics from the shape on an homogeneus body,” Toulouse, 1994.

[9] “ALGORITHMIC DOCUMENTATION OF THE GINS SOFTWARE,” Toulouse.

[10] G. Bourda, “Rotation terrestre et Variations du champ de gravité : Etude et apport des missions CHAMP et GRACE,” Sciences de la Terre. Observatoire de Paris, Paris, 2004.

[11] “OBELIX (VALIDE_17_1),” Toulouse, 2017.

[12] I. M. Longman, “Computation of Love Numbers and Load Deformation Coefficients for a Model Earth,” *Geophysical Journal International,* vol. Volume 11, p. 133–137, September 1966.

[13] J. LAURENT-VARIN, “Preliminary gravity study for MMX mission,” Toulouse, 2018.

[14] “pds-geosciences.wustl.edu,” [Online]. Available: http://pds-geosciences.wustl.edu/mro/mro-m-rss-5-sdp-v1/mrors_1xxx/data/shadr/.

[15] C. E. MMX Team, “MMX REFERENCE FRAMES DEFINITION FOR MMX MISSION ANALYSIS,” Toulouse, 2019.

[16] “MMX - Marsian Moon eXploration,” JAXA, [Online]. Available: http://mmx.isas.jaxa.jp/en/.

[17] H. K. N. O. M. O. K. E. T. K. H. S. H. M. a. A. Y. S. Kameda, “TELESCOPIC CAMERA (TENGOO) AND WIDE-ANGLE MULTIBAND CAMERA (OROCHI) ONBOARD MARTIAN MOONS EXPLORATION (MMX) SPACECRAFT,” in *50th Lunar and Planetary Science Conference* , The Woodlands, Texas,, 2019.